

Andreia Fernandes Jorge

DNA-POLYETHYLENIMINE-Fe(III) COMPLEXES FOR GENE DELIVERY. A COMBINED MONTE CARLO AND EXPERIMENTAL STUDY

Tese de Doutoramento em Química ramo de Química Macromolecular, orientada por Professor Doutor Alberto Canelas Pais e Doutora Rita de Sousa Dias e apresentada à Faculdade de Ciências e Tecnologia da Universidade de Coimbra

Coimbra, 2013



UNIVERSIDADE DE COIMBRA

DNA-Polyethylenimine-Fe(III) complexes for gene delivery.

A combined Monte Carlo and experimental study

Andreia Fernandes Jorge



Faculdade de Ciências e Tecnologia, Universidade de Coimbra 2013

Tese apresentada à Universidade de Coimbra para apreciação nas provas de Doutoramento em Química, ramo de Química Macromolecular.

Trabalho desenvolvido no Departamento de Química da Faculdade de Ciências e Tecnologia da Universidade de Coimbra, sob orientação científica do Professor Doutor Alberto António Caria Canelas Pais e da Doutora Rita de Sousa Dias.

Aos meus pais e irmão,

“Não é o trabalho, mas o saber trabalhar, que é o segredo do êxito no trabalho. Saber trabalhar quer dizer: não fazer um esforço inútil, persistir no esforço até ao fim, e saber reconstruir uma orientação quando se verificou que ela era, ou se tornou, errada.”

Fernando Pessoa, in *'Teoria e Prática do Comércio'*

Acknowledgments

I would like to start by acknowledging Professor Alberto Canelas Pais, from Department of Chemistry of FCTUC for giving me this opportunity and for sharing his broad scientific knowledge that help me through this work. I would also like to thank for all the conditions conceded, including the establishment of collaborations, scientific guidance, design of the work, and for never neglecting the personal part.

I would like to extend my acknowledgments to Dr. Rita de Sousa Dias, formerly at the Department of Chemistry of FCTUC, for her valuable guidance during this journey and to all the knowledge transmitted in the polymers field. Thanks for introducing me to Monte Carlo simulations and to some experimental techniques relevant to this work, and for the revision of the scientific reports.

I also want to express my gratitude to those who gave me the possibility of pursue my research in collaboration: to Professor M. Pilar Vinardell from Department de Fisiologia, Facultat de Farmàcia, Universitat de Barcelona, for kindly providing me all the conditions to pursue my work in toxicity assays; to Dr. Carmen Morán also from Department de Fisiologia, Facultat de Farmàcia, Universitat de Barcelona, thanks for the precious help in lab, for all the critical and fruitful discussions, and for the friendship since we met (it was a great pleasure to work with you); I also want to extend my acknowledgments to Professor Ernst Wagner, from Pharmaceutical Biotechnology, Center for System-Based Drug Research, and Center for Nanoscience (CeNS), Ludwig-Maximilians-Universität München for giving me the opportunity to work in his lab, for sharing his broad scientific knowledge and to introduce me on the challenges in formulating pDNA; to PhD students, Petra Kos and Ruth Röder, from Ludwig-Maximilians-Universität München, for instructing me in the cell culture room, for ready availability and kindness, and for the positive attitude to research; to Dr. Joana Viola, from Ludwig-Maximilians-Universität München for her kindly help that made my stay in Munich easier and to all scientific knowledge that transmitted me; Professor Jorge Costa Pereira from the Department of Chemistry of FCTUC for providing me all the conditions to conduct the potentiometric assays and for his valuable analyses of data; to Professor Artur Valente, from Department of Chemistry of FCTUC for conceding the lab facilities to perform conductimetric and potentiometric assays and for his help in the discussion of work; to Dr. Rui Pereira for his helpful contribution to this work, for his solid scientific knowledge, for his friendship and for the pleasant times that we spend in the lab that made this journey easier; and to Dr. Sandra Nunes for her kindly help in Monte Carlo simulations and for our stimulating discussions, valuable comments and for the revision of some parts of this work.

I must also mention other people that in many ways have participated in this work: Professor Hugh Burrows, from Department of Chemistry of FCTUC, for kindly giving me helpful comments; Professor Rui Brito, from Department of Chemistry of FCTUC for allowing me to carried out circular dichroism assays; Professor Graça Rasteiro from Department of Chemical Engineering of FCTUC for allowing me to perform zeta potential and size measurements; Professor Francisco Veiga and Professor João José Sousa from Faculty of Pharmacy of UC for kindly allowing me to perform zeta potential and size measurements; Ana Lapinha from Department of Chemistry FCTUC, for her help in conducting atomic absorption spectroscopy assays.

The work presented was carried out in the Photochemistry and Molecular Spectroscopy group coordinated by Professor Sebastião Formosinho, whom I thank for all the conditions provided, and supported by a grant (SFRH/BD/66748/2009) from Fundação para a Ciência e Tecnologia (FCT, Portugal) through the POPH/FSE (QREN), COMPETE program - Programa Operacional Factores de Competitividade (FCOMP-01-0124-FEDER-010831) and under the project PTDC/QUI-QUI/101442/2008.

Gostaria de deixar um agradecimento especial a todos os meus amigos com quem partilhei bons momentos no laboratório, no gabinete, nos almoços e jantares, e pelas boas gargalhadas que facilitaram o dia-a-dia: Bruno Medronho, Carla Vitorino (pelas semanas e fins-de-semana no DQ), Cláudia Duarte, Fátima Pinto, Filipe Antunes, João Almeida, Jorge Sarraguça, Luís Alves, Rachel Evans, Raquel Teixeira, Rui Pereira, Sandra Nunes, Sérgio Silva, Tânia Firmino, Telma Encarnação e Tiago Santos. Agradeço ainda a amigas especiais que me acompanham há mais tempo em Coimbra e que me ajudaram bastante neste percurso: Ana Sofia Lourenço, Rita Figueiras e Verónica Oliveira.

A ti, Oscar, gracias por la paciencia y apoyo y por creer que cerca y lejos tienen el mismo significado.

Uma última palavra de apreço vai para a minha família, meus pais, irmão, cunhada e sobrinha, um enorme obrigada pelo apoio que sempre me deram e por todos os valores que me ensinaram, e à Amália, peço desculpa por fazê-la sentir constantes saudades da tia.



Contents

Abstract	ix
Resumo	xi
CHAPTER 1	
General aspects.....	1
1.1 Basic concepts	1
1.2 DNA.....	3
1.2.1 Structure and properties.....	3
1.2.2 Condensation	5
1.2.3 Gene delivery	8
1.3 Polyethylenimine	15
1.3.1 Structure and properties.....	15
1.3.2 PEI-mediated gene delivery.....	17
1.4 Metal ions as a candidate supporting agents for gene delivery	20
CHAPTER 2	
Methods and techniques for DNA complexes characterization	25
2.1 Introduction	25
2.2 Computer simulation.....	25
2.2.1 Statistical mechanics	25
2.2.2 Monte Carlo: Concepts.....	27
2.2.3 Sampling.....	28
2.2.4 Spherical boundary conditions.....	29
2.2.5 Monte Carlo trial moves	29
2.2.6 Single particle moves	30
2.2.7 Chain moves	30
2.2.8 Cluster moves	31
2.2.9 Simulation convergence	32

2.3	Experimental.....	32
	<i>Physicochemical characterization</i>	32
2.3.1	Circular dichroism (CD).....	32
2.3.2	Size.....	33
2.3.3	Zeta potential (ZP).....	34
2.3.4	Agarose gel electrophoresis (GE).....	35
2.3.5	Fluorescence microscopy (FM).....	36
	<i>In vitro characterization</i>	36
2.3.6	MTT assay	36
2.3.7	LDH assay.....	37
2.3.8	ATP assay	38
2.3.9	Hemolysis	38
2.3.10	Fluorescence-activated cell sorting (FACS)	39
2.3.11	Transfection	40
2.3.12	Other techniques.....	40

CHAPTER 3

	DNA-PEI complexes	41
3.1	Introduction	41
3.2	Materials and methods.....	42
3.2.1	Materials	42
3.2.2	Sample preparation.....	42
3.2.3	Potentiometric titration	43
3.2.4	Circular dichroism.....	43
3.2.5	Precipitation assay.....	43
3.2.6	Agarose gel electrophoresis assay.....	44
3.2.7	Size analysis	44
3.2.8	Zeta potential analysis	44
3.3	Results and discussion.....	44
3.3.1	Acid/base behavior of PEI	44

3.3.2	Assessment of DNA conformation at different pH values	47
3.3.3	Characteristics of the complexes.....	48
3.3.4	Average size values with non-monotonic trends.....	51
3.3.5	Surface charge with a global minimum.....	53
3.4	Conclusion.....	54
 CHAPTER 4		
DNA-PEI-Fe(III) complexes: Condensation and decondensation		57
4.1	Introduction	57
4.2	Materials and methods	58
4.2.1	Materials	58
4.2.2	Sample preparation.....	58
4.2.3	Precipitation assay.....	59
4.2.4	Agarose gel electrophoresis assay.....	59
4.2.5	Fluorescence microscopy	59
4.2.6	Model and simulation details	60
4.3	Results and discussion	63
4.3.1	Experimental approach.....	63
4.3.2	Complexes in solution and precipitates	63
4.3.3	Electrophoretic motion of complexes.....	65
4.3.4	Conformational behavior of single DNA molecules	66
4.4	Theoretical approach.....	70
4.4.1	Compaction.....	70
4.4.2	Decompaction	77
4.5	Conclusion.....	78
 CHAPTER 5		
Effect of PEI architecture		81
5.1	Introduction	81
5.2	Materials and methods	82
5.2.1	Materials	82

5.2.2	Sample preparation.....	82
5.2.3	Precipitation assay.....	82
5.2.4	Agarose gel electrophoresis assay.....	82
5.2.5	Size and zeta potential analysis.....	83
5.3	Results and discussion.....	83
5.3.1	DNA–bPEI and DNA–lPEI complexes.....	83
5.3.2	DNA–bPEI and DNA–lPEI complexes: addition of Fe(III) ions.....	84
5.3.3	Characterization of complexes.....	88
5.4	Conclusions.....	90
 CHAPTER 6		
Cytotoxicity.....		93
6.1	Introduction.....	93
6.2	Materials and Methods.....	94
6.2.1	Materials.....	94
6.2.2	Sample preparation.....	94
6.2.3	Hemolysis assay.....	94
6.2.4	Polyplex stability assay.....	95
6.2.5	Cell Culture.....	95
6.2.6	MTT assay.....	95
6.2.7	LDH assay.....	95
6.3	Results and Discussion.....	96
6.3.1	Determination of hemolytic activity.....	96
6.3.2	Determination of in vitro cytotoxicity: Isolated products.....	97
6.3.3	Determination of in vitro cytotoxicity: Polyplexes.....	99
	<i>i. Polyplex stability.....</i>	<i>100</i>
	<i>ii. Polyplex cytotoxicity.....</i>	<i>101</i>
6.4	Conclusions.....	103
 CHAPTER 7		
PEI-Fe(III) chelation.....		105

7.1	Introduction	105
7.2	Materials and Method	106
7.2.1	Materials	106
7.2.3	Conductance measurements.....	106
7.2.4	Polyplex formation.....	107
7.2.5	Precipitation assays	107
7.2.6	Agarose gel electrophoresis (GE)	107
7.2.7	Size analysis.....	107
7.2.8	Quantification of Fe(III) ions in solution.....	107
7.2.9	Monte Carlo simulation.....	107
7.3	Results and Discussion.....	110
7.3.1	Interaction bPEI1.2-Fe(III)	111
7.3.2	DNA condensation: influence of the mixing sequence	113
	<i>i. Quantification of DNA by UV-VIS spectrophotometry</i>	113
	<i>ii. Charge and size of complexes</i>	115
	<i>iii. Determination of Fe(III) by AAS</i>	116
7.4	Theoretical approach.....	119
7.4.1	Effect of PC-mi chelation on PA compaction.....	119
7.4.2	Quantification of mi in PA-PC-mi complex	120
7.4.3	Disposition of mi and PC in PA-PC-mi complexes	123
7.5	Overview	128
7.6	Conclusions	130

CHAPTER 8

PEI and Fe(III) mediating transfection

8.1	Introduction	131
8.2	Materials and Methods.....	132
8.2.1	Materials	132
8.2.2	Complex formation	132
8.2.3	Gel shift assay.....	133

8.2.4	Particle size and zeta-potential.....	133
8.2.5	Cell culture.....	133
8.2.6	Cell transfection	133
8.2.7	Fluorescence activated cell sorting (FACS).....	134
8.2.8	Metabolic activity assay.....	134
8.3	Results	135
8.3.1	Gel shift assay	135
8.3.2	DLS measurements.....	136
8.3.3	Gene expression of DNA-PEI-Fe(III)	139
8.3.4	Effect of Fe(III) on DNA-PEI-Fe(III) cytotoxicity	145
8.3.5	Effect of Fe(III) in endosome release and cellular association	145
8.4	Discussion.....	148
8.5	Conclusions	151

CHAPTER 9

Concluding remarks	153
Bibliography	157

Abbreviations & Symbols

Ac30	Acetate buffer 30 mM
Ac50	Acetate buffer 50 mM
Ac100	Acetate buffer 100 mM
ATP	Adenosine triphosphate
β	Polycation/DNA charge mixing ratio
bPEI	Branched polyethylenimine
CD	Circular dichroism
Cys-5	Indodicarbocyanine
DAPI	(4', 6-Diamino-2-Phenylindole)
DLS	Dynamic light scattering
DMEM	Dulbecco's modified Eagle's medium
DNA	Deoxyribonucleic acid
EDL	Electric double layer
FACS	Fluorescence-activated cell sorting
Fe(III)/P	Fe(III)/phosphate groups molar concentration ratio
FM	Fluorescence microscopy
N/P	Amine/phosphate groups molar concentration ratio
GE	Gel agarose electrophoresis
HBG	Hepes buffered 5% glucose
HBS	Hepes buffered 150 mM NaCl
Hepes	4-(2-hydroxyethyl)-1-piperazineethanesulfonic acid
LDH	Lactate dehydrogenase
IPEI	Linear polyethylenimine
MC	Monte Carlo simulations
mi	Multivalent ion
MTT	(3-(4,5-Dimethyl-2-thiazolyl)-2,5-diphenyl-2H-tetrazolium bromide)
PA	Polyanion
PB	Poisson-Boltzmann theory
PC	Polycation
pDNA	Plasmid deoxyribonucleic acid
PEI	Polyethylenimine
UV	Ultraviolet-visible spectrophotometry
ZP	Zeta potential

Abstract

Gene therapy offers promising opportunities for the medical treatment of numerous severe diseases, including cancer. In recent decades, a great deal of effort has been made to develop non-viral biocompatible vectors that enable to overcome several biological barriers. This task becomes very demanding, since this vector has to be sufficiently versatile to adapt to adverse and sometimes contradictory conditions along its trafficking through the cell. Natural and synthetic polymers have been widely used and recognized as efficient vectors for gene administration. Among all, the polyethylenimine (PEI) has been renowned for its high performance. However, the use of this polycation has to be moderate due to its acute toxicity.

This work aimed at studying the parameters that modulate the efficiency of gene delivery DNA-PEI complexes, and assessing the effect of the addition of a second condensing agent upon their physicochemical and biological properties. The selected metal was Fe(III) due to their crucial role in living organisms, which consequently makes it a relatively inert compound in biological environment and may present interesting properties for a therapeutic application.

In the first phase of this work, efforts have been directed towards a better understanding of the fundamental mechanisms of DNA compaction after addition of PEI, imposing changes in the pH of solutions. Later, under selected conditions based on the previous study, the metal was added and analyzed its action on the condensation and decondensation of DNA using several experimental techniques. In parallel, the Monte Carlo simulation in the framework of a primitive model was used to construct a polyanion (simulating DNA) and to monitor changes in the respective structure imposed by the presence of positively charged ions (simulating Fe(III)) and polycations (simulating PEI). Experimental versus theoretical analyses were carried out throughout the work in order to strengthen the interpretations and proposed mechanisms.

In the second part of this work, in order to understand which properties model the interactions in the ternary complex DNA-PEI-Fe(III) were induced changes in parameters such as, the size and architecture of PEI, and in the order of addition of each component to the mixture. In general, a consistent theory arises in which Fe(III) ions compensates PEI, probably modulating their respective overall charge. Through experimental and theoretical data, it is evident that chelation between the amine groups of PEI and metal proves to be a crucial parameter for the promotion of the condensation of DNA, and consequently, in reducing the complex size of the final complexes.

In the final phase, *in vitro* studies were conducted to test the toxicity and biological activity of ternary complexes. In general, the Fe(III) attenuates the toxicity of the complex, either by replacing PEI molecules or by reducing the harmful potential of PEI to the cells. Transfection studies revealed a non-trivial behavior of ternary polyplexes with a clear reduction of transfection

efficiency for small particles, while this fact is less evident for complexes with larger sizes. Complexes prepared under high ionic strength and at a particular charge ratio show that the presence of Fe(III) increases 5.3-fold the transfection efficiency. In conclusion, the Fe(III) acts as a good supporter condensing agent with capacity to modulate the properties of DNA-PEI complexes, including condensation, decondensation and toxicity, without great penalty on the transfection efficiency.

Keywords: DNA condensation, DNA decondensation, polyplexes, Monte Carlo simulation, cytotoxicity, transfection

Resumo

A terapia génica apresenta excelentes oportunidades médicas para o tratamento de várias doenças graves, incluindo o cancro. Nas últimas décadas, um grande esforço tem sido realizado para desenvolver vetores não-virais biocompatíveis com capacidade de superar as diversas barreiras biológicas. Esta tarefa torna-se bastante exigente, na medida em que o vetor tem de ser suficientemente versátil para se adaptar às condições adversas, e por vezes contraditórias que encontrará ao longo do seu percurso através da célula. Polímeros naturais e sintéticos têm sido amplamente utilizados e são reconhecidos como vetores eficientes para a administração de genes. Entre todos, a polietilenimina (PEI) tem-se destacado pelo seu elevado desempenho. No entanto, a utilização deste polímero tem que ser moderada devido a sua elevada toxicidade.

O principal objetivo do presente trabalho consiste num estudo aprofundado dos mecanismos fundamentais que influenciam a eficiência dos complexos de ADN-PEI, bem como, o efeito resultante da adição de um segundo agente compactante na modulação das propriedades físico-químicas e biológicas destes complexos. O Fe(III) foi o metal selecionado devido ao seu papel crucial em organismos vivos o que faz com que seja um composto relativamente inerte em meio biológico e que poderá apresentar propriedades interessantes para uma aplicação terapêutica.

Numa primeira fase deste trabalho, os esforços foram dirigidos no sentido de uma maior compreensão dos mecanismos fundamentais da compactação do ADN após adição de PEI, impondo variações de pH durante a sua preparação. Mais tarde, sob condições selecionadas com base no estudo anterior, o metal foi adicionado, e analisada a sua acção na compactação e descompactação de ADN com recurso a várias técnicas experimentais. Em paralelo, a simulação por Monte Carlo foi utilizada para construir polianiões (simulando ADN) e monitorar modificações na respetiva estrutura, impostas pela presença de iões carregados positivamente (simulando o Fe(III)) e policatiões (simulando o PEI). Análises experimentais e teóricas correspondentes foram sempre realizadas ao longo do trabalho, a fim de fortalecer as interpretações e os mecanismos propostos.

Na segunda parte deste trabalho, com o objetivo de compreender quais as propriedades que regulam as interações no complexo ternário ADN-PEI-Fe(III) foram induzidas alterações em parâmetros tais como, o massa molecular e a arquitetura do PEI, assim como a ordem de adição de cada componente na mistura. Em geral, uma teoria consistente surge em que Fe(III) compensa a redução da quantidade de PEI, provavelmente modulando a sua respetiva carga global. Através de dados experimentais e teóricos torna-se evidente que a quelação entre os grupos amina de PEI e o metal demonstra ser um parâmetro crucial para a promoção da condensação de ADN e, conseqüentemente, tem efeitos na redução do tamanho do complexo final. Numa última fase,

estudos *in vitro* foram realizados para testar a toxicidade e a atividade biológica dos complexos ternários. Em geral, o Fe(III) atenua a toxicidade do complexo, quer pela substituição de moléculas de PEI ou pela diminuição do potencial prejudicial do PEI para as células. Estudos de transfecção revelaram um comportamento não-trivial dos poliplexos ternários, com uma evidente redução da eficiência de transfecção para partículas pequenas, sendo esta menos evidente para complexos de tamanhos superiores. Em complexos formados num meio com elevada força iónica e sob determinadas condições, a adição de Fe(III) aumenta 5.3 vezes a transfecção do ADN. Em suma, o Fe(III), surge como um bom agente auxiliar de condensação com capacidade de modular as propriedades dos complexos de ADN-PEI, incluindo a condensação, descondensação e toxicidade, sem grande penalização da eficiência de transfecção.

Palavras-chave: condensação de ADN, descondensação de ADN, poliplexos, simulação de Monte Carlo, citotoxicidade, transfecção

CHAPTER 1

General aspects

This thesis focuses on the behaviour of oppositely charged polymers in aqueous solution, in the absence and in the presence of a third component, a metal cation. In this first chapter, the general concepts and properties of each component are described, stressing the interest of their combination and the respective practical application.

1.1 Basic concepts

A polymer is a large molecule, a macromolecule, composed of a repetition of smaller units, the monomers. Synthetic polymers are synthesized by polymerization of monomers generating linear, branched or cross-linked structures. This synthesis can be performed with only one kind of monomer or with more than one kind, obtaining homopolymers and heteropolymers, respectively. This latter distribution is commonly found in biopolymers such as, proteins and nucleic acids. In the cases in which monomer units carry a charge, the polymer is denoted as polyelectrolyte. The properties of the monomers and how they are arranged in the chain, dictate the conformation of the polymer in diluted solution.

A polyelectrolyte solution contains the salt of a polyion commonly neutralized by small ions, the counterions. The effective electrical forces that arise from the distribution of these charged species around the polyion, and from the surface charges of the polyion is of extreme importance in colloidal systems and is known as electric double layer (EDL). This ionic structure plays an important role in the stability of colloidal systems. A central theory in the description of the EDL is the Poisson-Boltzmann (PB) theory. The PB equation is obtained by relating the

charge density, $\rho(r)$, in the diffuse part of the double layer to the electrostatic potential, $\psi(r)$, through the Poisson equation,

$$\Delta\psi(r) = -\frac{\rho(r)}{\varepsilon_r\varepsilon_0} \quad (1.1)$$

where ε_0 and ε_r are the dielectric permittivity in vacuum and in the solvent under consideration, and assuming that the ionic density around an oppositely charged ion are Boltzmann distributed,

$$\rho(r) = Zec_0 \exp\left(-\frac{Ze\psi(r)}{k_B T}\right) \quad (1.2)$$

where Z is the ion valence, e is the elementary charge, c_0 the ionic concentration at infinity and k_B the Boltzmann constant. Adding eqs. (1.1) and (1.2), the final Poisson-Boltzmann equation can be represented as

$$\Delta\psi(r) = -\frac{\sum Z_i e c_{0,i}}{\varepsilon_r\varepsilon_0} \exp\left(-\frac{Z_i e \psi(r)}{k_B T}\right) \quad (1.3)$$

This is a non-linear equation and usually difficult to solve, but by linearizing the exponential it can be obtained a tractable equation,

$$\Delta\psi(r) = k^2\psi(r) \quad (1.4)$$

in which k^2 is the Debye-Hückel parameter given by

$$k^2 = \frac{8\pi q^2 I}{\varepsilon k_B T} \quad (1.5)$$

and I is the ionic strength of the electrolyte solution, q is the magnitude of the charge of the electrolyte ions and ε is the dielectric constant of the medium. The final expression for the potential is given by the following,

$$\psi(r) = \left[\frac{Ze}{4\pi\varepsilon_r\varepsilon_0(1+2kR)} \right] \left\{ \frac{\exp[k(2R-r)]}{r} \right\} \quad (1.6)$$

where R is the ionic radius and r is the separation. The inverse of k is called the Debye length. Note that k^{-1} has the unit of length and is considered the measure of the range of the electrostatic interactions after the ion atmosphere has been taken in account, and is also often referred to as the screening length. According to Equation (1.6), the potential around an ion in a salt solution does not decay as r^{-1} , which is typically found for charge-charge electrostatic interactions, but instead with $\exp(-kr)/r$ due to the screening caused by the ionic atmosphere around each charge. This reflects in electrostatic interactions with a shorter range, and dependent on the valence of the ions and on the ion concentration. Despite the great importance of PB theory in the description of EDL, this mean field approximation fails under several conditions. In the mean field approximation, an ion does not interact explicitly with other ions, but merely with the average field created by the ions. It also ignores the fact that two ions cannot come closer than the sum of their radii. These correlation effects, particularly the electrostatic ion-ion correlation, can lead to

an effective attraction between like-charged particles in the presence of multivalent ions. This behavior has been reported experimentally [1-5] and is usually explained in terms of ion-ion correlations, which are neglected by the PB theory. Computer simulations, such as Monte Carlo and molecular dynamics simulations have been a useful tool to predict the colloidal forces [6, 7]. In fact, they show that between like charged particles can be attractive in the presence of divalent ions, corroborating experimental data.

In this chapter, the properties of the two polyelectrolytes of interest to the present work, DNA and polyethylenimine (PEI) are presented in different sections. Some of these introduced concepts will be further detailed when considered relevant from the application standpoint.

1.2 DNA

Deoxyribonucleic acid (DNA) is a molecule that contains biological information required for the synthesis of a functional biological product, whether protein or RNA, and is essential for the development of all known forms of life. This huge relevance may anticipate the enormous complexity and the number of properties that should be addressed when focusing in this biological molecule. Here, an overview is provided on aspects that are relevant within the contents of this thesis.

1.2.1 Structure and properties

DNA consists of a long polymer chain composed of two strands coiled around an axis in a double-stranded helical structure [8]. A DNA strand consists of a repetition of nucleotides with alternating pentose and phosphate groups, with one nitrogenous base attached to a sugar molecule as represented in Figure 1.1.

The two strands are partially held together by hydrogen bonds between the internally located complementary bases. The nitrogenous bases are derivatives of two parent compounds, pyrimidine and purine, and in the double helix are linked specifically, i.e., adenine (A) links to thymine (T) forming two hydrogen bonds and cytosine (C) binds to guanine (G) forming three hydrogen bonds. The sequence of the bases along the polynucleotide chain is not restricted, and the precise sequence of bases carries the genetic information. The hydroxyl groups of the sugar residues form hydrogen bonds with water and thus, the covalent backbones are hydrophilic. The phosphate groups, with a pK_a close to 1.5 [10], are completely ionized at pH 7, carrying two negative elementary charges per 3.4 Å. Typically, in the cell, this rigid and long polyelectrolyte presents a persistence length of around 50 nm and a contour length of 2 m [11]. However, purine and pyrimidine bases are hydrophobic and relatively insoluble in water in the pH conditions of the cells. This makes DNA an amphiphilic polymer adopting a helix configuration to expose the hydrophilic charged backbone and hide the hydrophobic interior. Hydrophobic stacking

interactions in which two or more bases are positioned with the planes of their rings parallel stacking are one of the two modes of interaction between bases. Secondly, are also existent a combination of van der Waals interactions between the bases. A balance between these attractive interactions and repulsions of the phosphate backbone are very important in the stabilization of the three dimensional structure of DNA.

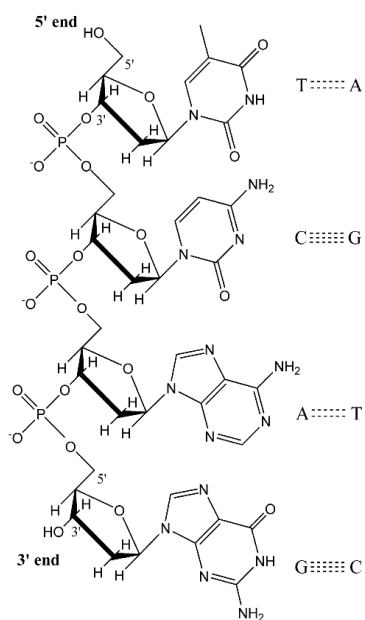


Figure 1.1. Backbone structure of DNA. (Reprinted from reference [9])

The conformation of the molecule in solution depends on the balance between interaction of the nucleotides with the solvent, and the interaction of the nucleotides with each other (Figure 1.2).

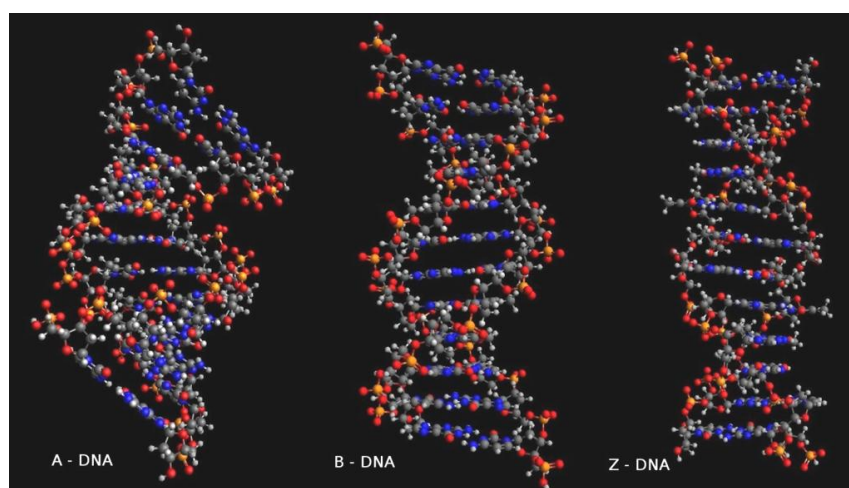


Figure 1.2. Secondary structures of DNA at different conformations, A, B and Z-DNA. Graphical representations were produced with the Avogadro package, an open-source molecular builder and visualization tool (Version 1.0.0.).

Under physiological conditions, B-DNA is the most stable conformation. The general observation is that the A-DNA conformation is favored upon dehydration and when the electrostatic repulsions along the helix are reduced [12]. Z-DNA presents the “left handed” helix, in contrast with the right handed sense of B-DNA and A-DNA. This conformation appears to be relevant in binding of proteins and transcriptional activity [13].

1.2.2 Condensation

To introduce the long molecule of DNA within the tiny micrometre-sized nucleus of the cells an efficient process of compaction is required. If free in solution DNA would form a swollen coil of 100 μm , which would be too large to fit into the nucleus (10-20 μm). The densely packed genome forms a structure of around 2 μm when compacted in the cell. Mandatory compaction of the genome is obtained via complexation of the DNA with small, strongly positively charged proteins, the histones, combined with monovalent and divalent ions into a large nucleoprotein complex that is referred to as the chromatin [14]. More precisely, some studies have reported that only 50% of the DNA charge in chromatin is neutralized by histones, and the remaining charge is neutralized by divalent metallic ions [15, 16]. Motivated by the finding that DNA is condensed inside the cell by the action of positive condensing agents, studies of DNA compaction *in vitro* started in the 1970s [17, 18] and represent an important model to understand DNA functioning *in vivo* and also to modulate systems to obtain efficient controlled drug delivery in gene therapy. This latter theme will be further discussed in detail later in the chapter. Due to the large electrostatic repulsion between negatively charged phosphates, DNA is dispersed in aqueous solution in an elongated coiled state. Hitherto, a number of agents that are able to condense DNA have been identified, such as multivalent ions, alcohol, cationic surfactants, cationic polymers and neutral polymers at high concentration [19-23].

In the present work, we are particularly interested in DNA condensation by cationic agents. According to Bloomfield [20, 24], the transition from an elongated coil state to a compact state is achieved only when the negative charge of the polyelectrolyte is reduced by 89–90% with the positive counterions. Following this theory, it was concluded that divalent cations alone cannot induce DNA compaction because the maximum charge neutralization possible does not exceed 88% [20], and therefore DNA condensation requires counterions with charge +3 or higher [25, 26]. A multitude of cationic species have been investigated as condensing agents, inorganic cations such as $\text{Co}(\text{NH}_3)_6^{3+}$, ferric ions [27-30], polyamines [31, 32], protamines and the histone octamer [33, 34], natural and synthetic peptides [35, 36], lipids and liposomes [37, 38]. Single molecule microscopy has suggested that DNA compaction with multivalent cations is observed as a discrete all-or-none type for individual DNA molecules, in the sense that each macromolecule assumes either the coil or globule conformation, and as a continuous transition when an ensemble

of DNA molecules is considered [39]. This latter transition corresponds to the coexistence of unfolded and compact DNA conformations. When this coexistence occurs in a single DNA chain it is called “intrachain segregation” [32], in a different perspective from that of the all-or-none interpretation. Some of the separate steps of DNA compaction are represented in Figure 1.3, in good agreement with conformations acquired in Monte Carlo simulations [40, 41]. Besides globules, partially compacted structures with one or two collapsed parts edging a single chain are observed as intermediate forms. The formation of these intermediate structures are known to be dependent on salt concentration in solution [42, 43]. At low salt concentration, the collapse proceeds via the formation of an intermediate necklace structure stabilized by Coulomb repulsion between the uncompensated charges of DNA chains.

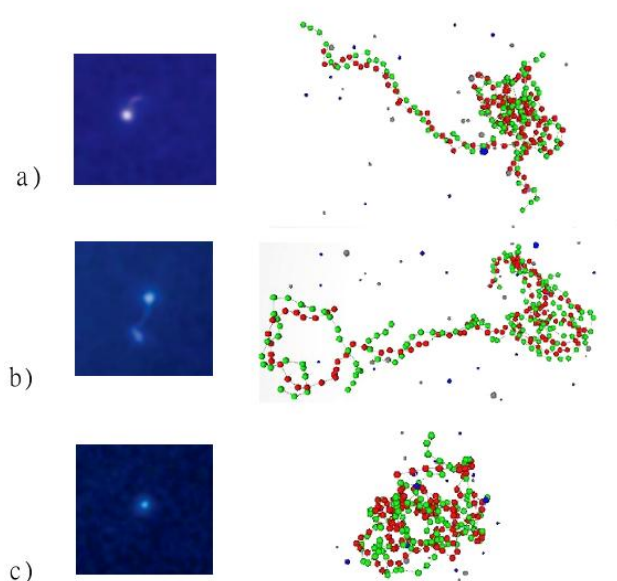


Figure 1.3. Fluorescence images and comparable snapshots from Monte Carlo simulations of a) and b) partially unfolded, and c) compacted configurations of DNA. In the experimental images, T4DNA compaction was induced by protamine (from reference [44]), whilst theoretical snapshots represent the compaction of a long chain of polycation with shorter polycation chains (from reference [40]).

Conversely, at high salt concentration, when the electrostatic repulsion is sufficiently screened, the collapse proceeds between the coil and globule states without any intermediate structures. The onset of the DNA compaction is dependent on the multication valence, occurring for values beyond electroneutrality for low charge cations, while for higher charged cationic agents, condensation takes place typically at an equivalent number of oppositely charges (or slightly less). With the increase of the multication charge, the DNA compaction mechanism tends to a continuous transition scenario [42]. Additionally, it was observed that more efficient DNA condensation is attained if there is a geometrical match between the negative charges of DNA and the positive charges of multication [45, 46]. A high concentration of highly charged cations leads

to overcharging, i.e, the overall net charge of the complex becomes opposite to that of DNA [47]. In the range where DNA should be optimally overcharged, large cations must overcome a Coulomb barrier to collapse the overcharged complexes. This fact, in practice, leads to reduced aggregation between these highly charged complexes.

Fluorescence microscopy does not have sufficient resolution to reveal conformation details of the condensed DNA structures, but techniques such as atomic force microscopy (AFM), dynamic light scattering (DLS), scanning electron microscopy (SEM), cryo-transmission electron microscopy (cryo-TEM) have helped to shed information about condensed structures. Upon compaction, the DNA chain is generally organized into globules, toroids or rods in the nanoscale size (see in Figure 1.4). DNA condensation may occur either as a monomolecular collapse [48] or comprising a small number of aggregated molecules [49]. It should be noted that the term “condensation” is generally considered for the aggregation of several chains in an orderly morphology [20], while compaction often refers to the collapse of one single chain. Several researchers have devoted their attention to the mechanisms behind the formation of these different structures. The formation of DNA condensates has been shown to be the result of a nucleation-growth process [50]. However, studies confirmed that the size of the structure is dependent on the interactions between topological defects, which allows for circumferentially wound DNA strands in toroids [51]. A significant number of theoretical models have attempted to establish which conditions govern toroid formation, and generally agree that both DNA length and flexibility are important factors in complex organization [52-54]. The length and diameter of the rods are found to be similar to the circumference and thickness of the toroids, respectively, but there is no evidence of interconversion between these two structures [55]. The well-defined toroids or rods are not the most frequent morphology, being inhibited in kinetically trapped states. Hence, the mechanism of their formation is of interest as a model of DNA condensation within biological organisms.

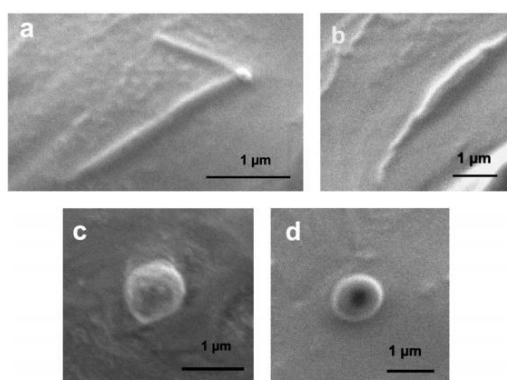


Figure 1.4. Scanning electron micrographs of different morphologies of T4 DNA condensed with protamine sulfate salt; (a) V-shaped, (b) rod-like, (c) globular and (d) toroidal. (Taken from reference [44])

The compaction of DNA has received a significant attention, but, it should be noted that DNA decompaction is not less important, being fundamental for the transcriptional activation in cells. Contrarily to what was found for compaction, the unfolding of the DNA chain is accelerated and continuous, in which intermediate structures have not been identified [50]. Various compounds and methods have been tested so far, showing the ability for reversing DNA compaction induced by multication agents, including the addition of simple salt [56], polyanions [57], cyclodextrins [58], pH increase [59] or simple dilution [50]. Heparin, for example, is a very efficient decompacting agent for DNA condensed with multications due to the respective high charge density and, of utmost importance is the fact that they heparin ions are much more flexible than the DNA molecules, with a persistence length of approximately 5 nm [60]. Thus, DNA decompaction results from a competition of heparin for the multications with subsequent DNA-multication complex dissociation.

Furthermore, the properties of the media in which the DNA and multication are dissolved affect significantly complex formation. The interactions are not purely electrostatic and each charged colloid or macromolecule is surrounded by a diffuse electrical double layer that results in an entropic contribution upon release of counterions. The evaluation of thermodynamic parameters of DNA condensation has been extensively pursued by isothermal titration calorimetry [61]. It has been observed that the driving force for polyelectrolyte complexation tends to decrease with salt concentration, not only due to the screening of electrostatic interactions between the polyelectrolytes, but also due to a large entropic effect [62-64]. Reports further show also the dependence of DNA-multication interaction on pH of the media and buffer protonation enthalpy [63, 65, 66]. DNA condensation was found to be dependent on the proton transfer from the buffer to chitosan, and additionally, this transfer occurs in larger extent at higher pH values [67].

1.2.3 Gene delivery

Since the discovery of the basic structure and function of the human genome, the manipulation of genes as a therapy for both cancer and genetic disorders has been an important goal for medical research. An imperative requisite for the therapeutic application of any type of nucleic acid is the successful delivery into the host cell followed by the release in the target compartment, cytoplasm or nucleus, whether RNA or DNA are used, respectively. Naked nucleic acids are unable to induce relevant therapeutic effect when administered systemically *in vivo*, being easily degraded by nucleases and hampered by cross biological membranes. Therefore, there is a need for a vector that improves the overcome of biological barriers by presenting properties that include (i) stability in the extracellular environment, (ii) interaction with target cell surface and cell uptake, (iii) release from endo/lysosomal vesicles, and (iv) vector unpacking followed by DNA translocation

into the nucleus, when required [68]. These extracellular and intracellular traffic barriers are schematically represented in Figure 1.5. Depending on the vectors used, gene delivery is broadly divided in two main classes, viral and non-viral. Viral vectors, in which therapeutic nucleic acid substitutes most of the virus genome, are natural masterpieces of nucleic acid delivery being programmed to be dynamic and bioresponsive in their infection process and have proven to be clinically efficient [69, 70]. However, viral vectors are limited by their small cargo loading capacity, and more importantly, due to the propensity to trigger immune reactions. In this context, non-viral vectors have gained special attention in the past decades, being considered as non-immunogenic, easy to produce and not oncogenic. The major challenge for non-viral gene delivery is to accomplish an efficient targeting of the genes, and natural and synthetic carriers need to be carefully designed by modulating chemical and physical properties, in order to cross all extracellular and intracellular hurdles.

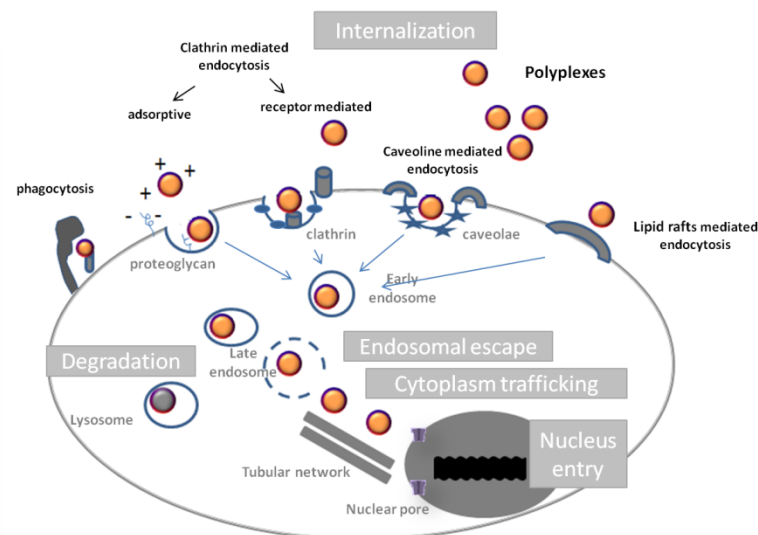


Figure 1.5. Schematic representation of extracellular and intracellular barriers to the delivery of gene into cell nucleus. (Adapted from reference [71])

The most common non-viral vectors used are natural and synthetic cationic lipids (lipoplexes), polymers (polyplexes) and peptides. Alternative inorganic materials are also used, such as gold nanoparticles, carbon nanotubes, silica and superparamagnetic iron oxide nanoparticles [72]. Several newly designed and synthesized materials use a combination of organic and inorganic compounds in one delivery system, and are denoted as “hybrids” [73], having shown to provide better opportunities for non-viral vectors. The development process of a newly synthesized delivery system, consists firstly in an analysis and optimization by *in vitro* techniques. In case these show promising characteristics, it is thereafter analyzed *in vivo*. From the body of literature, it is evident that the majority of studies are performed *in vitro*, and often with a large variability

among them, in what concerns the different experimental conditions, in terms of buffers, compounds concentration, and cell line types. Moreover, the correlation between *in vitro* and *in vivo* experiments is still poor and some reports point to contradictory characteristics required for an efficient delivery system [74, 75]. Firstly, it was found that the DNA condensation efficiency and the stability of the resulting complex required for an efficient transfection *in vitro* is correlated to the *in vivo* results, whereas requirements for size and zeta potential do not show any correlation. Secondly, the prediction of cytotoxicity and transfection efficiency *in vitro* has shown to be overrated in comparison to *in vivo* [76]. A possible explanation is that *in vitro* studies of non-viral vectors are usually not performed at physiological conditions, and thus do not provide meaningful results *in vivo*. This gap between *in vitro* and *in vivo* approaches should be circumvented by using a multitude of complementary tests with maximal reproduction of bloodstream conditions for a better risk assessment [77, 78]. In what follows the relevant properties of the non-viral vector needed to overcome each trafficking step, and simultaneously, the recent strategies used to solve it, as well as the contradictions reported between *in vivo* and *in vitro* experiments, if any, are reported in detail.

As already stated, the first prerequisite for the transport of the nucleic acid into the cell is the respective complexation with positively charged species into nano-sized complexes. The complexation with polycations should confer protection to the nucleic acid, and be strong enough for the DNA to remain complexed in the presence of physiologic competitors (e.g. serum proteins) and, afterwards, allow DNA release when within the target compartment. *In vitro* studies showed that an excess of polycation titrated against DNA with a charge ratio superior to 1 generated optimal values of gene transfer in HeLa cells, while lower charge ratios yielded a low efficiency [79]. Therefore, polyplexes are conventionally prepared so that the number of positive charges of the polycation exceeds that of the negative charges of polyanion, and the physicochemical properties of the complex may be modulated by the charge ratio of the polyplexes. Thus, the success of gene delivery is dependent on both size and surface charge (zeta potential), since these properties influence the circulation time, cellular binding and uptake, and intracellular trafficking of polyplexes [80]. However, a close look at the literature shows that variations of these parameters often present diverging results between the *in vitro* and *in vivo* approaches, and even between different studies with apparently similar conditions. Regarding the size of particles, Prabha et al [81] have shown that smaller particles exhibit higher transfection efficiency than the larger particles, when tested *in vitro* in COS-7 and HEK293 cell lines. Similarly, Rejman et al. [82] have observed that an increase in the size of the particles reduces the internalization of the silica particles. On the other hand, Ogris et al. [83] reported that large polyplexes prepared under physiological salt conditions display a 100-fold higher transfection efficiency in comparison to small polyplexes prepared in low salt conditions. Results from other authors also corroborate that larger lipoplexes, likely give rise to higher levels of transfection in

COS-7 cells [84, 85]. Size-dependent internalization, additionally reported for non-phagocytic tumor cells (B16 cells), in which small particles (<200 nm) internalize via clathrin-mediated endocytosis, whilst large particles (500 nm) internalize via caveolae-mediated endocytosis [82]. Particles following the latter internalization route did not reach the lysosomal compartment, which leads to the degradation of complexes, thus suggesting the possible advantage of the larger particles.

Conversely, in the case of *in vivo* studies, the systemic delivery of gene systems is often a long and cumbersome process, and larger aggregates can be easily retained in the small diameter capillaries and vascular vessels, inducing immune response or embolism [86]. The aggregation phenomenon is very common in physiological salt conditions due to the presence of highly positively charged species and the screening of electrostatic repulsive interactions promoted by the high ionic strength [87]. Some strategies have been conducted to avoid aggregation. A possible one resorts to the use of sugars during the preparation of the complex. These, owing to the high content of hydroxyl groups helps to stabilize the complexes by steric hindrance [83]. However, intravenous administration of positively charged polyplex leads to the activation of the innate immune system, and consequent agglomeration of erythrocytes [88] and/or serum proteins [89], which may cause acute cytotoxicity. The shielding of the particles by attaching neutral hydrophilic moieties such as poly(ethylene glycol) PEG or poly(N-(2-hydroxypropyl-methacrylamide) (pHPMA), have been shown to increase solubility and extend circulation time, presumably due to the reduction of undesired interactions between the complexes and blood components and also due to the reduction of complex surface charge [88, 90]. It should be noted that this method allows to reduce the aggregation between complexes in physiological conditions and also to reduce positive charge of polyplexes, which are required features for *in vivo* administration.

The first obstacle to the entrance of the particle in the cell is the selective cell membrane. Unless there exists a specific target ligand added to the polyplexes, the binding to the cell surface is the result of the electrostatic interactions between the positively charged polyplex and the negative sulfated proteoglycans embedded in the cell surface [91]. Also, it has been suggested that the simple precipitation of larger complexes onto the cell surface is sufficient for nonspecific endocytic uptake [83]. Using *in vitro* assays, these latter mentioned aspects, positive surface charge and precipitation, seem to be crucial parameters to attain efficient cell binding. Thus, to achieve a therapeutic response *in vivo* and concomitantly, a selective gene delivery, the addition of cell-specific ligands or antibodies attached to gene vector is compulsory. Cationic polymers have been modified with ligand moieties that can be chemically attached or physically adsorbed to the delivery system. Numerous ligands, e.g., folic acid [92], sugars [93], synthetic peptides [94], proteins, such as transferrin [88], growth factors or antibodies [95] have been tested. The addition of these compounds to the complexes show a marked enhancement of internalization in

some specific cells [96]. Recently, it was demonstrated that a dual-targeted approach, i.e., the use of two kinds of ligands, promotes a synergistic effect in transfection efficiency [97].

Particles are engulfed by the cell membrane and consequently, penetrate the cell through vesicle formation, namely endosome, by a variety of pathways such as phagocytosis, clathrin/caveolin-dependent endocytosis, cell adhesion molecule mediated endocytosis and macropinocytosis [98, 99]. Although, the contribution of each cellular pathway to the internalization of the non-viral vectors is not yet fully understood, a number of physicochemical characteristics of polyplexes are shown to influence internalization. For instance, Rejman and co-authors [100] used several specific inhibitors of endocytic pathways to show that dodecyl trimethyl ammonium bromide (DOTAB) lipoplexes are internalized via clathrin-mediated endocytosis, while polyethylenimine (PEI) polyplexes do so via two mechanisms, caveolae and clathrin-coated pits. On the other hand, Gersdorff et al.[101] described that the internalization pathway mediating successful transfection is dependent on cell line, type of PEI applied and polyplex formulation used. It should be recalled that the endocytic pathway followed by complexes is also dependent on their size, as aforementioned. Once inside the endocytic vesicles, the trapped non-viral vectors suffer a decrease in pH from neutral to value of ca. 6. In this stage, called early endosome, two mechanisms may occur in which, the internalized content is transported out of the cell or, most often, the vectors are trafficked to late endosomes which are acidified to pH 5-6. The last step consists in the fusion of late endosome with lysosomes leading to a further pH reduction to 4.5 and degradative processes including enzymes. Therefore, if the nucleic acid is entrapped into these acidic vesicles at this stage, it gets degraded and the process of gene delivery fails. This step is currently considered the major obstacle for gene delivery.

The success of the escape from the endosome on time to prevent the degradation of the nucleic acid strongly depends on the selected cationic vector. Many mechanisms have been proposed to explain the easy release attained by cationic polymers with ionizable amino groups, such as PEI and polyamidoamine (PAMAM) dendrimers, but the more accepted is the so-called “proton-sponge” hypothesis (Figure 1.6) [102-104]. Endosomal membranes possess the ATPase enzyme that regulates the acidification of the compartment by transporting protons from the cytosol. The proton sponge hypothesis postulates that, upon introduction of ionizable polymers into the endosome, the pH of the compartment decreases and, consequently, ATPase actively transports more protons to reach the desired pH. The accumulation of protons in the compartment leads to an influx of counter ions and water, as well as an expansion of the polycation due to internal charge repulsion, resulting in osmotic swelling and rupture of the endosomal membrane [105, 106]. This hypothesis is not yet fully proved yet but several works evidence its validity. For instance, Sonawane et al. [107] systematically followed the concentration of chloride ions, pH and volume of endosomes after internalization with polyplexes prepared with PEI, PAMAM and poly-L-lysine (PLL). Contrarily to what was observed with PLL, variations of ion accumulation,

volume expansion and membrane lysis were found in the presence of PEI and PAMAM, corroborating the suggested “proton sponge effect”. In contrast to PEI and PAMAM, PLL does not possess the required buffering capacity due to the presence of strongly charged amino groups [108]. Moreover, the N-quaternization of ionizable groups in PEI decreases the transfection efficiency by roughly 2-fold [109]. The underlying protonation character of PEI is highlighted in detail later in this chapter. A classical method used to enhance the vector escape from the endosome to some degree, is the addition of exogenous additives, namely chloroquine and inactivated adenovirus, during the transfection assay. Chloroquine is a weak base that can rapidly cross the plasma membrane, accumulate in endosome and increase the pH of the acidic medium. Additionally, the presence of chloroquine causes swelling and rupture of the endosomal vesicle, hindering lysosomal formation [110, 111].

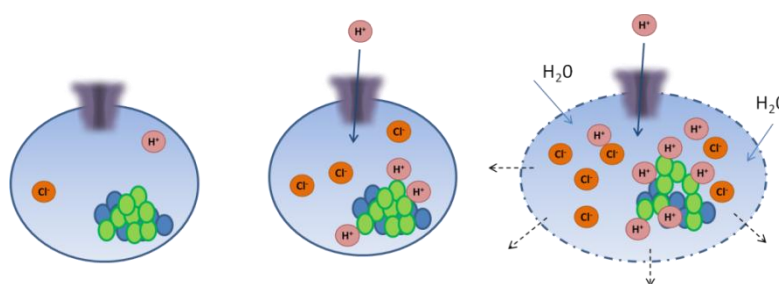


Figure 1.6. Schematic representation of proton sponge effect. The segments in green and blue represent polycation and polyanion, respectively.

A number of studies have investigated the influence of chloroquine in transfection efficiency, but different results were reported. For instance, in combination with PEI-transferrin-DNA [83] and PLL-transferrin-DNA [112] polyplexes, or with DOTMA-DOPE-DNA liposomes [113], it showed an improvement of transfection efficiency, but combined with PAMAM [114] no positive effect was observed. The effect of chloroquine seems, thus, to be dictated by the type of cationic vector and cell line used, showing a particularly strong effect on K562 cells which may be explained by the low pH in early endosomes attained in this cell line [112]. However, the application of chloroquine is limited by safety concerns. Although it is approved by Food and Drug Administration (FDA) as an anti-malaria medication, it can induce undesirable side effects when administered in high doses.

Recent strategies used to enhance the escape of nucleic acids from the endosome comprise the design of vectors with buffering capacity. A widely used buffering moiety is the imidazole ring of histidine that is a weak base with ability to acquire cationic charge when the pH of the environment drops below 6. The attachment of these histidine moieties to polymers, lipids or peptides has been shown to enhance their transfection efficiency, often reducing their cytotoxicity [115, 116]. Another method used is the functionalization of polymers with peptides that facilitate the internalization and include the ability to enhance the escape from endosome, the so-called

cell-penetration peptides (CPPs) [117]. Typically, these peptides are constituted by a sequence of 10-30 residues which are able to complex with nucleic acids or can be incorporated in polymeric or lipidic vectors. Firstly, CPPs were originally derived from viruses and after the discovery of the sequences, a number of new synthetic analogues were synthesized to mimic the endosomal disruptive properties of fusogenic sequences of viral fusion proteins. Wagner et al. introduced haemagglutinin subunit HA2 of influenza virus in conjunction with transferrin-PLL-DNA polyplexes resulting in an increase of the delivery efficiency [118].

Other bottlenecks in the gene delivery trafficking are diffusion through the cytoplasm and vector dissociation. It is not well established in which stage DNA should dissociate from the vector. The major problem in this stage is the potential degradation of the unprotected nucleic acids by cytoplasmic nucleases with a half-time of 50-90 minutes. Suh et al. [119] found an unexpected parallel between nature most efficient viruses and PEI-DNA complexes, using both the cytoplasmic tubular network to diffuse through the cytoplasm towards the nucleus. Hence, in designing the vector, it should be taken into account that a low diffusion leads to low transfection, and furthermore an easy disassembly of the nucleic acid from the vector promotes better gene delivery results [120]. Several strategies have been envisaged to facilitate the disassembly of polyplexes, by taking advantage of the different conditions experienced during the cellular trafficking, such as differences in pH and redox potential gradient. It is important to note that a number of other stimuli-responsive polymers have been designed and they are well described in several reviews [121-123]. Bioreducible polymers possessing disulfide bonds are stable extracellularly providing stability to the complex before entering the cell, while the reducing environment of the intracellular medium leads to polymer breakdown and nucleic acid release [124-126]. The degradation of the disulfide bonds proceeds mainly in cytosol or in the nucleus. However, some other studies indicate the possibility that degradation occurs in other compartments of the cell [127]. Results show that the integration of disulfide bonds on the polymer backbone leads to a gain in transfection efficiency [128, 129]. The incorporation of acid-labile linkages is another helpful alternative to enhance endosomal escape and release of nucleic acids, taking the advantage of the acidification of the endosome [130].

The final barrier for transfection is the nucleus. The nuclear compartment is surrounded by the nuclear envelope, which consists of a double membrane interrupted by large protein structures, the nuclear pore complexes (NPC). Resorting to electron microscopy and gold nanoparticles, Panté et al. [131] found that the largest rigid particle to achieve nuclear entry through NPCs is roughly 39 nm in diameter. Hence, a DNA molecule is too large to pass through this nuclear pore and reasonable amount of studies evidence that the actual nuclear translocation of DNA occurs during mitosis [132-134]. This fact may justify the higher values of transfection found for *in vitro* experiments when compared to *in vivo*, since in cell culture the multiplication of cells is faster.

1.3 Polyethylenimine

1.3.1 Structure and properties

Polyethylenimine is a synthetic polymer widely used in a number of applications. In 1995, PEI was used as gene vector, attaining high levels of *in vivo* gene transfection with values comparable to those obtained with viral vectors [102]. Since then, PEI has been largely studied, and is considered the most efficient polycation used in gene therapy. The basic monomer of PEI possesses a backbone of two carbons followed by one nitrogen atom, and may be synthesized in the branched or linear forms, as depicted in Figure 1.7. The syntheses from ethyleneimine (aziridine) or oxazoline monomers lead to branched or linear polymeric backbones, respectively. The branched structure of PEI contains a 1:2:1 ratio of primary/secondary/tertiary amines. The linear PEI form is composed almost exclusively of secondary amines. PEI is available in a wide range of molecular weights (Mw) from <1000 Da to 1.6×10^3 kDa [135].

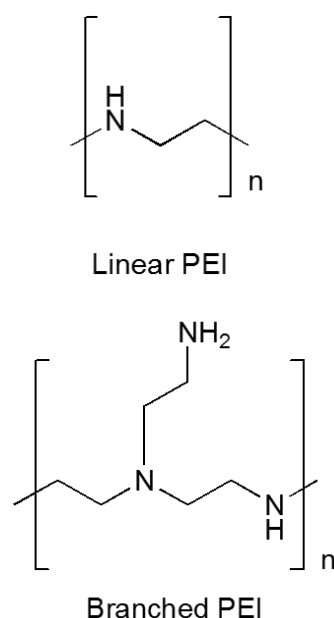


Figure 1.7. Chemical structures of PEI in linear and branched forms.

The study of PEI protonation is essential to characterize the electrostatic binding to negatively charged DNA. A number of studies have been made to determine the protonation constants mainly through potentiometric measurement and nuclear magnetic resonance (NMR) spectroscopy [136]. Some experimental difficulties are encountered, namely for potentiometric studies because linear PEI (IPEI) is insoluble at room temperature, being the usual practice to dissolve PEI in an acidic solution, and then back-titrate the solution with a base. But precipitation may occur again during titration, at high pH values. The study of these polybases is particularly difficult because the basicities of the nitrogen atoms in monomers can be very similar, but different in different parts of the long molecules. In Figure 1.8, some examples of monoamines

and diamines with the respective pK_a value for each amine group are represented. The values are shown to be dependent on the neighboring atoms of amines and on the nature of the binding groups, aliphatic or aromatic [136, 137]. Therefore, the titration of a polyamine shows a marked different profile when compared with the corresponding monomer, methylamine [138, 139]. The electrostatic repulsion between charged ammonium sites plays a predominant role in determining the values of the protonation constants and the location of protonation in the compound. Regarding this, the protonation behavior was found to be different in branched and linear forms [140, 141]. Several successful theoretical models have been proposed to estimate the acid-base behavior of the different forms of polyamines, and the influence of the ionic strength of the medium [142-144], and showed good agreement with experimental data. In theory, a typical titration curve of a branched PEI (bPEI) comprises the first protonation step occurring at pH around 9.5 corresponding to the protonation of the primary amine groups on the side chains, followed by a second step at pH around 4.5 in which secondary amines protonate. Finally, the last step corresponds to the protonation of tertiary amines, that is suspected to occur at a pH value close to 0 [140]. Due to this, titration curves show incomplete hydrolysis because tertiary amine groups start to significantly protonate only in very acidic conditions due to the repulsion promoted by the surrounding protonated sites [140].

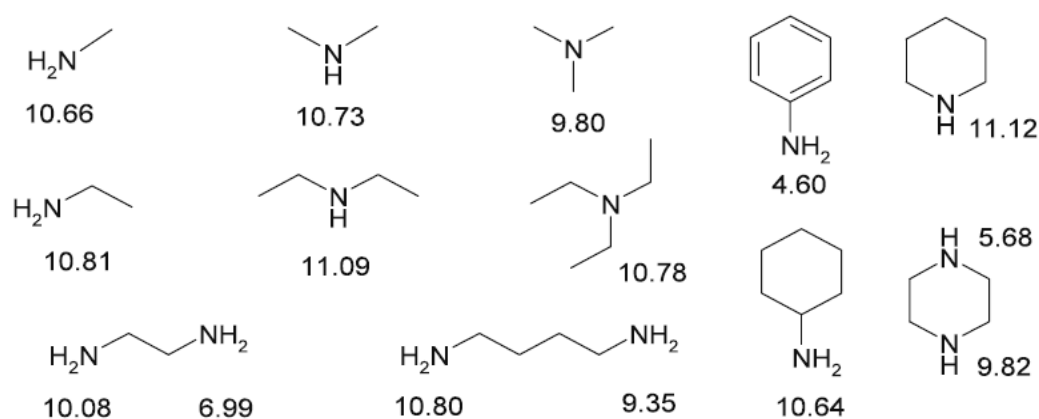


Figure 1.8. The pK_a values of different monoamines and diamines. (Reprinted from reference [145])

On the other hand, the protonation of IPEI can be seen as two separate protonation steps [146, 147]. The bPEI polymer in solution does not change considerably its conformation upon protonation and accumulation of positive charge, contrarily to what is observed in IPEI [148, 149]. Hence, different values of the protonation constants of PEI have been reported in the literature. Some studies produced only one or two pK_a values and show a great discrepancy on the percentage of amine groups protonated, in the range of 10% to 90% at physiological conditions and, pH 7.4 [150-153]. Other studies identified 2-6 protonable sites for polyamines similar to PEI,

and typically possessing at least 50% of the amine groups protonated at physiological pH [136, 137, 154]. The values of pK_a were found to decrease with increasing bPEI molecular weight [152], and also with the decrease of the ionic strength [146]. The latter effect is probably due to the increase in the electrostatic interactions between the charged amine groups on the PEI chain. Additionally, in the presence of a polyanion such as DNA, there is an increase in proton transfer from the buffer to the polycation and, consequently, a raise in the degree of protonation of the PEI in the bound state, when compared with its free form [67]. Comparable results were obtained by theoretical methods [142]. This interesting pH behavior is definitely the key factor of the high efficiency of this polyamine as gene carrier. Nevertheless, the lack of assurance of the actual PEI protonation state causes some difficulties in the estimation of the overall charge of PEI-DNA complexes, which is an important feature for the gene delivery uptake. Moreover, as polyamines are bases in aqueous solution there will be a competition between protonation and complexation reactions. This latter topic will be discussed later in this chapter.

1.3.2 PEI-mediated gene delivery

Hundreds, if not thousands, of synthetic polymers and copolymers have been synthesized in the past decades to circumvent the low efficiency of non-viral vectors. Nonetheless, PEI is still regarded as the most efficient non-viral vector used [102]. In numerous *in vitro* and *in vivo* studies, either linear or branched PEIs with molecular weights ranging from 800 Da to 800 kDa have been used. PEI is a nondegradable polymer in which the molecular weight correlates with both, inherent cytotoxicity and transfer activity. It is documented [155, 156] that long PEI chains lead to higher transfection efficiencies, but simultaneously show higher values of cytotoxicity due to pronounced cell membrane perturbation by the high charge density of the chains [157]. Results show that the most suitable size should be equal or below 25 kDa owing to safety concerns. However, PEI with a lower charge density, as well as a lower molecular weight, might impair the transfection efficiency. Therefore, PEI of Mw 25 kDa is considered one of the best transfection agents and is often referred as the “golden standard” of gene delivery. However, the molecular weight is not the only important factor and a few other properties that influence the efficiency of this polycation in acid nucleic delivery and should be enumerated.

In a comparative study, *in vitro* transfection efficiency and physicochemical properties of polyplexes made with either DNA or small interfering RNA (siRNA), and different PEI (bPEI 25 kDa and lPEI 22 kDa) were analyzed [158]. Using DNA, lPEI polyplexes yielded 5-fold higher transfection efficiency than bPEI. Polyplexes prepared with lPEI showed smaller sizes, low positive surface charge and easier decondensation when submitted to heparin than their bPEI analogs, and this latter property seems to be the most significant to attain good results. The

authors suggested that the lower level of IPEI-DNA polyplex stability may facilitate displacement from DNA, thus, promoting higher levels of transcription. In another work, IPEI was shown as the most efficient carrier for DNA in many applications [159]. Interestingly, bPEI-siRNA polyplexes showed superior condensation degree and better transfection results compared to IPEI-siRNA, presumably due to the fact that the flexible branched structure of bPEI provides better three dimensional folding to siRNA resulting in a more stable complex. IPEI-DNA and bPEI-siRNA polyplexes displayed a comparable stability, as siRNA is a very small molecule and limits the electrostatic interaction with PEI. This results in the formation of weaker complexes, compared with those of the bPEI-DNA system [160]. Previously, complex stability and transfection efficiency have been correlated with the increase in PEI primary amine content [161, 162]. Additional studies have been conducted to evaluate *in vitro* and *in vivo* transfection efficiencies of polyplexes formed with linear (PEI 22 kDa) and branched (PEI 25 or 800 kDa) at different salt conditions [159]. Under physiological salt conditions IPEI was considered the most efficient whilst in salt-free conditions IPEI and bPEI displayed equally low transfection abilities. On the other hand, polyplexes formed with IPEI 22 kDa in salt-free conditions were more effective than bPEI 25 kDa *in vivo*, in good agreement with other results [162]. The higher efficiency of IPEI was attributed to its propensity to associate with the cell membrane which has not been observed for bPEI.

As mentioned before, the ionic strength of the medium of complexation is an important factor for the resulting polyplex size, which has shown to be a time dependent property. Complexes of DNA-IPEI 22 kDa acquired a large size (~750 nm) after 20 min of complex formation, growing to larger aggregates after 3 hours, under salt conditions Hepes buffer saline (HBS) with a ionic strength of 75 mM [159]. In comparison, complexes of bPEI25-DNA prepared in the same conditions reached sizes of about 120 to 370 nm after 3 hours, remaining stable thereafter [159]. At physiological conditions (150 mM NaCl), the tendency of polyplexes to aggregate increases and bPEI 25 kDa complexes after incubated for 30 min display with size values of roughly 600 nm [163]. A strikingly smaller size is observed when polyplexes are prepared under low salt condition, using for instance 10 mM NaCl or Hepes buffer saline 20 mM plus 5% glucose (HBG). These present sizes generally below 300 nm for a long period of time, irrespective of the PEI used [83, 135, 163]. Another important property which influences the final size of the polyplex is the N/P charge ratio. Polyplexes prepared at high N/P ratios (overcharged polyplexes) show a reduced aggregation tendency as a result of the electrostatic repulsion between the, now, positively surface charged complexes, an effect which seems to stabilize polyplexes even under physiological conditions [83]. It has been found, using fluorescence correlation spectroscopy, that each polyplex contain an average of 3.5 plasmid and 30 PEI 25 kDa molecules when prepared at N/P ratios of 6 and 10, values commonly used in transfection assays [164]. This study assumes the complete complexation of DNA and additionally the existence of a

high proportion of PEI in the free form, also confirmed by other authors [165]. It has also been shown that the PEI chains that remain free in solution are more toxic than those bound to DNA [165, 166]. However, the removal of free PEI chains by size exclusion chromatography significantly reduced the gene transfection efficiency, being this recovered if free PEI chains were added to the transfection medium 4 hours after initiation [165]. According to this procedure, the post addition of free PEI chains with Mw 2.5 or 25 kDa, contributed in the same extend to the improvement of transfection efficiency [167]. Resorting to flow cytometry, it was confirmed that the presence of free PEI chains induces a faster and more efficient cellular internalization of the polyplex but, most importantly, they contribute to polyplex endosomal escape. In contrast, PEI bounded to acid nucleic molecule mainly confers condensation and protection [168].

Due to the many advantages of PEI over other polycations, a great deal of effort has been made to improve PEI-mediated transfection and, simultaneously, mitigate the respective cytotoxicity. Herein, some of the used strategies will be enumerated. As aforementioned, one of the strategies broadly used to improve PEI cytotoxicity is the covalent attachment of non-ionic polymer, such as PEG. PEGylated PEI tends to be less toxic than the native PEI, both *in vitro* and *in vivo* approaches [169, 170]. It has been previously observed that PEGylation of PEI prior to the mixing of DNA, appears to hinder DNA condensation and particle formation [163, 171, 172]. On the other hand, post-PEGylation, i.e., PEGylation after DNA complex formation does not interfere with DNA condensation [173]. Therefore, the post-PEGylation does not modify the size of complexes but reduces the surface charge of the particles, and at the same time, it confers a reduction in transfection activity [99, 163]. More detailed examination of the internalization of particles by cells has show that the unmodified DNA-PEI polyplexes enter in cells as large aggregates while PEGylated polyplexes remain small and discrete, both outside and within cells [99]. According with these results, the steric effect provided by PEG is a two edged sword, i.e., the better particles are shielded from aggregation, and presumably the less cytotoxic, the lower is the efficiency of the vector in the following cellular uptake process and intracellular release.

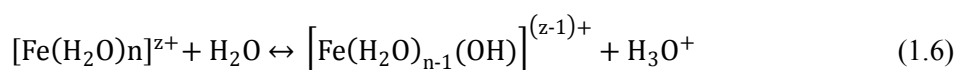
As mentioned above, low Mw PEI exhibits a reduced toxicity. However, it does not provide sufficient polyplex stability for an efficient gene transfer. Based on this, many studies have been performed to minimize cytotoxicity and improve transfection efficiency by synthesizing new polymers composed of low molecular weight oligoamines bound with different biodegradable crosslinkers [174, 175]. A large library of oligoethylenimine (800 Da) was analyzed and the results demonstrated that a high gene transfection comparable to that obtained with the “golden standard”, could be obtained while a remarkable gain in terms toxicity profile was achieved. In an analogous work, with different requisites in the PEI synthesis, the biocompatibility of these new compounds was confirmed, showing a 2-10 fold increase in gene transfer when compared to both the “golden standard” PEI 25 kDa and the commercially PEI widely used, Lipofectamine 2000 [176].

Furthermore, hybrid systems combining both electrostatic interaction and self-assembly properties were synthesized using low Mw PEI (10 kDa) with hydrophobic modifications without reduction of primary amines content. These compounds showed an improvement in the transfection efficiency of the PEI 10 kDa, reaching comparable values to PEI 25 kDa, while maintaining a low toxicity [177]. Also, the incorporation of alanine in PEI 25 kDa doubled the transfection efficiency and decreased the cytotoxicity [178].

Overall, the modulation of PEI properties by addition or incorporation of different compounds able to mitigate some of its drawbacks is a recommended approach. Imperative is that the polyions interaction should be balanced to offer protection and at the same time allow vector unpackaging. Likewise, all the critical parameters such as size, charge, stability and cytotoxicity must be controlled. An ideal non-viral vector gathering all these properties is still missing and requires further investigation.

1.4 Metal ions as a candidate supporting agents for gene delivery

Biological systems benefit from the versatile chemical properties of metal ions, which execute several fundamental functional roles. In the specific case of DNA condensation in nucleus monovalent and divalent metal ions are involved, to aid the frequent processes of partial decondensation and condensation of the long molecule during for instance, processes of transcription [15, 16]. This has prompted a series of experiments where the combination of condensing agents, PEI and a metallic ion Fe(III) is used to induce and control DNA condensation. Fe(III) was chosen due to its essential role in life. One of the most multitasking metals in cellular environment is iron which is involved in a number of specific functions. The dependence of life upon this metal is due to the fact that iron acts as a cofactor within the active site of enzymes. The high versatility of iron chemistry in aqueous medium comes from the occurrence of two stable oxidation states, Fe(III) and Fe(II), which allows it to act as an electron donor and acceptor, and from the high reactivity of iron complexes within acid – base phenomena [179]. In aqueous solution Fe(III) suffers a process of hydrolysis, in which Fe(III) behaves as an Brønsted acid with ability to donate protons following the equation,



and often terminates in aggregation as metal hydroxides or hydrated metal oxides. It is well known that Fe(III) ions in solution condensate into small polycationic species on very distinct ranges of pH (see Figure 1.9) [180, 181].

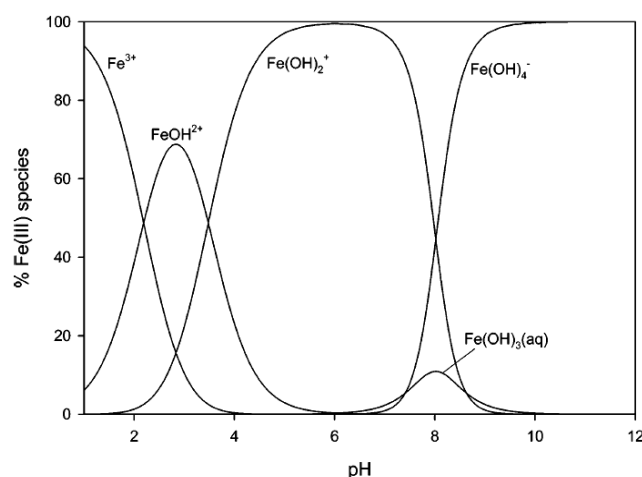


Figure 1.9. Speciation of Fe(III) in solution as a function of pH. (Taken from reference [182])

Thus, an ion such as $[\text{Fe}(\text{H}_2\text{O})_6]^{3+}$ is a fairly strong acid with a pK_a value of 2.2 [183]. General studies on the hydrolytic oligomerization on Fe(III) confirmed that it is a slow process and practically irreversible [184].

This lack of solubility presents a great challenge to cells to accumulate iron. Both excess and deficiency of iron are damaging, and cells have been forced to develop mechanisms to control this situation. To do so, low molecular weight aggregates of iron are targeted to iron storage protein, ferritin [185], when iron is not required for immediate metabolic needs. In this way, the stored iron is neither available for producing damaging radicals, nor for allowing the viability of pathogen microorganisms. If required, iron can be released from the storage to participate in cell metabolism. Moreover, Fe(III) is transported in the serum by glycoprotein transferrin, that binds to 2 atoms of Fe(III) with high affinity. Iron-loaded transferrin binds to the cell surface through transferrin receptor (TfR) and undergoes endocytosis with subsequently metal release accomplished by acidification of endosome [186]. The pathological consequences outcome from the participation of Fe(III) in the redox process is considered within the Haber-Weiss reaction [187]. The products of this reaction are reactive oxygen species (ROS), such as the hydroxyl radical (OH^\cdot) and the hydroxide anion (OH^-). The hydroxyl radical (OH^\cdot) is able to induce cell death that may result in DNA oxidation, mitochondrial damage and peroxidation of membrane lipids [188]. However, under physiological conditions most iron is bounded to proteins, and the presence of free Fe(III) is only significant in patients with iron overload disease.

The iron chelating therapy involves the use of chelating drugs that are able to chelate with iron, and expel it from the organism. These iron-chelating agents possess oxygen and nitrogen donor atoms that are able to coordinate with iron [189, 190]. The chelation between iron species and ligands, for instance therapeutic iron chelator molecules or iron-sulfur proteins, is governed by the fact that iron is a Lewis acid in solution that can easily interact with Lewis bases. The free electron doublet on the nitrogen chelates iron at neutral pH, or conversely, the anionic character

of oxygen may attract electrostatically the metal cation. Additionally, another therapeutic effect was established for iron chelators, anti-tumoral effect. Controversial studies have shown that a depletion or an overload of iron in the cell results in cancer cells arrest [191]. The inactivation of iron in tumor cells, by chelators, has been shown to effectively reduce the growth of some tumors [190], but, curiously, an overload of tumor cells with iron also showed promising results [192].

Apart from therapeutic treatments, metal complexes hold excellent properties for diagnostic applications. It is possible to form under specific conditions nanoparticles with range of technological applications, such as superparamagnetic iron oxide nanoparticle (SPIO) [193, 194]. These superparamagnetic agents are highly effective in magnetic resonance imaging (MRI) and were recently applied as gene carrier [195-197]. At present, SPIOs nanoparticles are considered to be biocompatible and inert because their metabolite Fe exists in living organisms. Two divergent results have been reported, several studies declare SPIOs as no cytotoxic [198-200] but other works have reported issues associated with their use [201, 202].

The Fe(III) inherent chemical versatility and its potential use in medical application may anticipate the potentialities of the combination of this metal with the efficient gene vector DNA-PEI, in a ternary complex.

Motivation and scope

In this first chapter, an extensive overview of the insights from the literature in the theme of gene delivery was presented. From this large number of documented data, it is observed that some concerns, which restrict an efficient gene transfer, are still far from being solved and further knowledge of the fundamental processes is extremely required.

The central scope of this thesis is to investigate all the potential effects that the addition of a third component in the mixture, specifically Fe(III), may determine in crucial aspects for gene transfer, namely condensation and decondensation of DNA, size and charge of complexes, toxicity of complexes, and in the ultimate stages of transfection.

The use of a manifold of methodologies represents an advantage in the study of these complex systems. Theoretical and experimental studies were conducted in parallel, in order to compensate the existent limitations recognized in both approaches. In Chapter 2, the techniques used in this work are described in terms of their fundamentals and applicability.

In Chapter 3, an extended study is presented on the properties of DNA-PEI complexes, when subject to different pH media. The influence of this variation in the complexes formation is analyzed, in terms of DNA condensation efficiency and resultant physicochemical properties.

In Chapter 4, the third component, Fe(III), is added to the DNA-PEI mixture and analyzed its repercussion. In this chapter, condensation and decondensation assays are conducted using both experimental and Monte Carlo simulations. A rationale for the effect of the third component in the mixture was proposed.

The effect of the architecture of PEI chains on the ternary mixtures is studied in Chapter 5. Different PEI molecules, with branched and linear configurations, at different lengths were analyzed. Measurements of physicochemical parameters of the formed complexes were made.

The work presented in Chapter 6 is an extension of the study of complexes formed in the latter Chapter but resorting to hemolysis and cytotoxicity effects. The potential toxic effect of each condensing agent in separate and in conjunction is evaluated. Moreover, the toxic effect of optimized polyplexes to the cells is investigated and compared with reference systems.

In Chapter 7, the binary interaction between PEI-Fe(III) is assessed in a fundamental study. Further assays on ternary mixtures show the importance of PEI-Fe(III) interaction on ternary complexes. Monte Carlo simulations are carried out to shed light on this aspect.

In Chapter 8, the effect of Fe(III) in the transfection efficiencies of DNA-PEI complexes is assessed. Again, physicochemical properties of complexes formed in different media are analyzed, as well as, the effect of iron in some particular stages of transfection, such as cell uptake and endosomal release.

In Chapter 9, are gathered some concluding remarks.

CHAPTER 2

Methods and techniques for DNA complexes characterization

2.1 Introduction

In this chapter is provided a brief introduction to the theoretical and experimental techniques used throughout the present work. In the former approach, some general concepts of statistical mechanics are initially inserted to facilitate the understanding of Monte Carlo simulations. For convenience, the experimental techniques are divided in two main sets, physicochemical and *in vitro* characterization techniques, that encompasses the analysis used to follow the processes undergone by DNA, from condensation to the last step, the deliver in the cell. A general description of the methods is presented here, while specific information about the actual procedures carried out for each system will be presented along the results and discussion sections.

2.2 Computer simulation

2.2.1 Statistical mechanics

Statistical mechanics allows the connection between the microscopic properties of a substance and its bulk properties. The basic question in statistical mechanics is: how can we explain the macroscopic properties of matter, like pressure, entropy, etc., in terms of the microscopic properties of atoms and molecules, such as molecular energy levels or bond distances. The aim is

thus to predict macroscopic phenomena and calculate macroscopic properties from the properties of the individual particles that constitute the system. This is done not by focusing on the motion and interactions between the components of the system, as in a classical mechanics and quantum mechanics, but by determining the average behaviour of the system. Such an average over all possible quantum states of a system is called an ensemble average. An ensemble is a collection of a large number, N_{sys} , of configurations all having the same defining parameters. The systems in an ensemble are macroscopically identical, but they are not equal at the microscopic level. The first postulate of statistical mechanics states:

The time average, over a long time period, of a mechanical variable M of a thermodynamic system is equal to the ensemble average as $N_{\text{sys}} \rightarrow \infty$.

The time average on the actual system may be replaced by an instantaneous average over a large number of configurations “representative” of the system, i.e. an ensemble average. Note that the ensemble average of M as $N_{\text{sys}} \rightarrow \infty$ must be time independent. Otherwise, the original system that the ensemble represents is not in equilibrium. We clearly cannot hope to extend the calculation to an infinite time, but might be satisfied to average over a long finite time. The average ensemble can also be regarded as a large collection of points in phase space. They are distributed according to a probability density. This function is determined by the chosen fixed macroscopic parameters. The three most important cases are (i) a microcanonical ensemble where the number of particles, energy and volume are the same for all ensemble members (NVE), (ii) a canonical ensemble, where N , V and T are fixed and (iii) a grand-canonical ensemble that keeps the same chemical potential, volume and temperature (μVT). Since the work presented in this thesis was carried out in the canonical ensemble, that is an example of a representation of a closed isothermal system in equilibrium, this will be explained in more detail.

In a canonical ensemble, all values of the energy are allowed, while the temperature is fixed. The weight of each state depends on its energy and is proportional to the respective Boltzmann weight, $\exp(-\beta E_i)$, where $\beta = 1/k_B T$. From the latter factor, it is possible to conclude that low energy configurations have higher probabilities. The configuration weight, with the constraints that the total energy of the ensemble is constant and the total number of particles is fixed, is given by the *canonical distribution function*, Q ,

$$\frac{n_i}{N} = \frac{e^{-\beta E_i}}{Q}, \text{ where } Q = \sum_i e^{-\beta E_i} \quad (2.1)$$

in which n_i is the most probable distribution of energies in the canonical ensemble and N the total number of particles, and $p_{i=n_i/N}$ is the fraction of molecules in configuration i . If a number of states possess the same energy and contribute in the same extent to the sum, a new term is added to the *canonical distribution function*

$$Q = \sum_i g_i e^{-\beta E_i} \quad (2.2)$$

where g_i is the degeneracy factor and the sum comprises now all the levels of energy (set of states with the same energy) and not just states. The canonical partition function carries all the thermodynamic information about a system. The average of a mechanical property M is generally defined as

$$\langle M \rangle = \sum_i M_i p_i \quad (2.3)$$

where the sum is taken over all possible configurations attainable for the system in a given ensemble. For example, the average energy in the canonical ensemble is given by

$$\langle E \rangle = \frac{\sum_i^{N_{total}} E_i g_i e^{-\beta E_i}}{\sum_i^{N_{total}} g_i e^{-\beta E_i}} \quad (2.4)$$

In theory, it is possible to make a large number of steps and calculate the upper and lower sums in Equation (2.4), but in practice it is not feasible for many-particle systems due to the fact that many states are possible, and many of them have a very low Boltzmann weight. Therefore, completely random sampling is very inefficient for thermodynamic problems, wasting too much effort away from the very small region of most probable configurations determined by the Boltzmann weight.

2.2.2 Monte Carlo: Concepts

Monte Carlo (MC) simulation is a stochastic method, which enables us to solve multi-dimensional integrals. Suppose that we want to solve numerically the following integral

$$I = \int_a^b f(x) dx \quad \langle f(x) \rangle \quad (2.5)$$

where $\langle f(x) \rangle$ denotes the unweighted average of $f(x)$ over the interval $[a, b]$. With Monte Carlo, this average is determined by evaluating $f(x)$ at a large number of x values randomly distributed over the interval $[a, b]$. This integration will converge very slowly because most randomly chosen points will possess a negligible Boltzmann factor. The computational effort of the sampling can be significantly reduced by attributing, a priori, a statistical weight to each point of phase space. It would be preferable to sample many points in the region where the Boltzmann factor is large.

The most significant advance in Monte Carlo modeling took place when Metropolis et al. [203] described an approach, in which, instead of choosing configurations randomly, then weighting them with $\exp(-E/k_B T)$, they were chosen with a probability $\exp(-E/k_B T)$ and evenly weighted". This means that the space phase is sampled in such a way that configurations which contribute significantly to the configurational integral are visited more frequently than those that

only contribute less to it. The typical approach of Metropolis algorithm is implemented by the following steps (Figure 2.1):

i. Perform a *trial move* by randomly changing the configuration, and calculate the energy difference, $\Delta U_{\text{trial}} = U_{\text{new}} - U_{\text{old}}$ between the old and the new configuration.

ii. Accept or reject the newly generated configuration according to:

If $\Delta U_{\text{trial}} \leq 0$, i.e. the energy of the new configuration is not higher than that of the old configuration, the point is always accepted. If $\Delta U_{\text{trial}} > 0$, the energy of the new configuration is higher than the first, p is compared to a random number z between 0 and 1, and the move is accepted if $\exp(-\Delta U/k_B T) \geq z$.

Accepting the new configuration means that the value of M is calculated for that point and that the value is added to the overall sum, and the data for the averages is accumulated. The entire process is repeated. If the next point is rejected, then the previous point “repeats”, i.e., the old configuration is taken as the new configuration and a new, random perturbation is attempted.

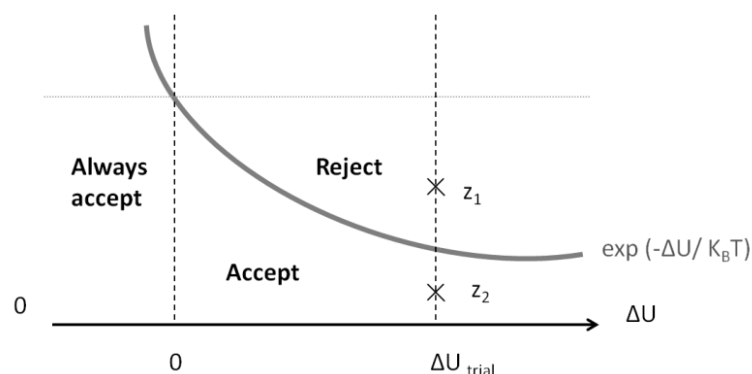


Figure 2.1. Scheme of accepting and rejecting trial moves in the Metropolis algorithm. (Adapted from reference [204])

The probability of accepting a new configuration can also be written as,

$$p = \min \left[1, \exp \left(-\frac{\Delta U_{\text{trial}}}{k_B T} \right) \right] \quad (2.6)$$

and is illustrated in Figure 2.1. Such a sequence of phase points, in which each new point depends only on the immediately preceding point, is called a *Markov chain*.

2.2.3 Sampling

The characterization of the conformations and energetic of polyions in solution has been vastly studied from theoretical approaches [205-207]. The inherent structural complexity of a macromolecule requires a wide range of computational effort for attaining an accurate description of the molecule behavior. Therefore, most theoretical and simulation studies of polyelectrolytes

are based on coarse-grained models within the so-called primitive model. This approach implies a simpler description that reduces the complexity of the system. In the coarse-grained model, the chemical details are ignored by merging a set of atoms in a single particle, reflecting only the essential properties of this set. Figure 2.2 represents the difference between an atomistic description of a polymer molecule and the coarse-grained approach.

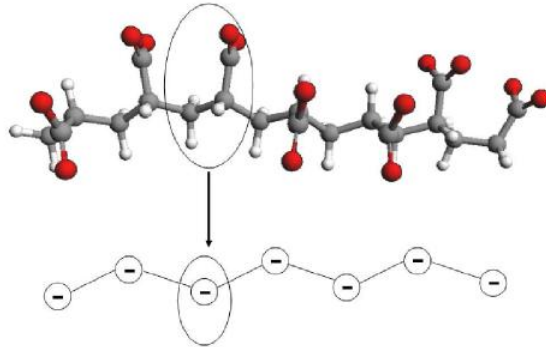


Figure 2.2. Atomistic and coarse grain model of a polymer segment. Taken from reference [208]

In this description, particles are modeled as charged hard spheres at different charge and size interacting through a Coulomb potential attenuated by the dielectric permittivity of the solvent, which represents a statistical average over all solvent degrees of freedom at thermal equilibrium. The structural properties of the modeled systems and conditions applied are given in the following chapters.

2.2.4 Spherical boundary conditions

In order to simulate bulk phases it is of major importance to choose boundary conditions that mimic an infinite bulk surrounding the particles that constitute the model system. The spherical cell approach is based on a hypothetical subdivision of the colloidal solution in electroneutral subvolumes, each including the polyions with the corresponding amount of counterions and the solvent. With the introduction of a hard wall that constitutes the sphere, some configurations may be rejected. Nevertheless, the effects of the curved geometry will decrease as the system size increases, and it is a useful approach for the simulation of diluted systems. This boundary condition is frequently used to examine simple colloidal systems.

2.2.5 Monte Carlo trial moves

The success of running a MC calculation resides in defining the perturbation steps. There are two situations that are not desirable: if the steps are very small, then the volume of phase space sampled will increase slowly over time and the computational cost will be high. On the other hand, if the steps are too large, again computational resources will be wasted because the rejection rate will be high.

The easiest way to generate a new configuration of a molecule is induce random changes in Cartesian coordinates of individual atoms in conjunction with translations and rotations of whole molecule. The possible values for these various perturbations will be adjusted so that 20-50% of attempted moves are accepted. Each perturbation allowed is described in more detail in the following sections.

2.2.6 Single particle moves

The most frequently used type of MC move is a separate move of each particle. This move is applied to all elements present in the system. An acceptable method to create a translational displacement is to add random numbers between $-\Delta/2$ and $\Delta/2$ to the Cartesian components of the coordinates of the particle:

$$\begin{aligned}x'_i &\rightarrow x_i + \Delta(\text{Ranf} - 0.5) \\y'_i &\rightarrow y_i + \Delta(\text{Ranf} - 0.5) \\z'_i &\rightarrow z_i + \Delta(\text{Ranf} - 0.5),\end{aligned}\tag{2.7}$$

where *Ranf* are random numbers uniformly distributed between 0 and 1. The single-particle move for an ion and a chain bead is depicted in the Figure 2.3.

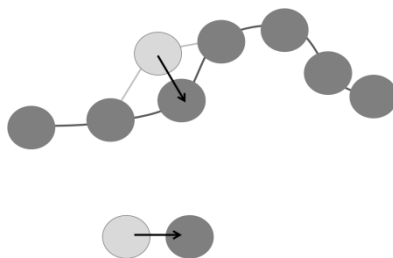


Figure 2.3. The single-particle move for a chain bead and a single ion.

2.2.7 Chain moves

In the presence of non rigid molecules, like the ones sampled in the present study, one must also consider MC trial moves that are able to change the internal degrees of freedom of the molecule. The sampling of the configurational space of such model chains is hardly achieved by moving the elements each at a time. A typical change in chain conformation corresponds to a mutually contrived move of a group of elements. In order to assess all the possible conformations, a given polymer model can be explored using a variety of different MC algorithms which involve different types of moves [209]. These different kinds of moves are useful for avoiding different kinds of “trapped” configurations. Three examples are given in what follows.

i. End pivot rotation

A segment of the polymer is randomly selected and rotated by a random amount, α , as illustrated in Figure 2.4.

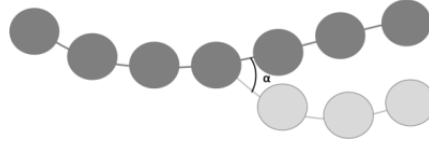


Figure 2.4. Illustration of a pivot rotation.

ii. Slithering

The move resembles the sliding of a snake. One of the end beads is displaced as bond distance from the previous position. The second bead places to the old position of the first one, the third bead took the old position of the old position of the second one, and this procedure is repeated for the rest of the chain. At the end of this procedure the chain is separated in two fragments, and the end fragment is translated into the other extreme and becomes the new beginning [210] (Figure 2.5).

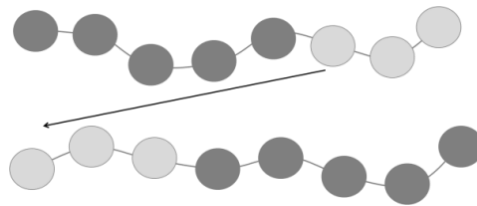


Figure 2.5. Illustration of slithering move. The beads in light grey are those moved from one extremity to the other.

iii. Chain translational move

The chain translation is similar to the one described single particle move, but in this case the displacement is considered to all components of the chain.

2.2.8 Cluster moves

In the presence of strong coupling interactions imposed between particles in the modeled systems, there is an obvious need to use more advanced displacement procedures [211]. The simulation efficiency can be improved considerably by applying a displacement procedure in which strongly coupled particles are moved in consonance, the “cluster move”. A cluster is composed of a central

particle and the neighboring particles, within a cut-off defined distance, that move simultaneously, as depicted in Figure 2.6.

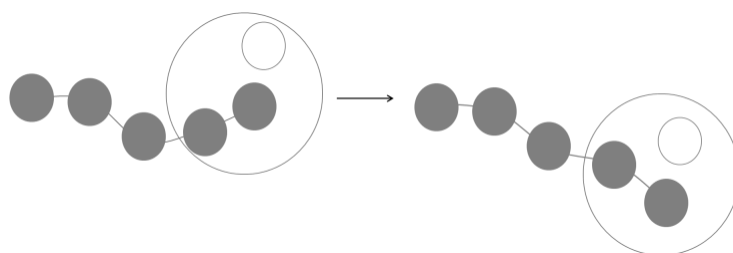


Figure 2.6. Schematic illustration of a cluster trial move. Polyion (grey) and a neighbor counterion (white), moving simultaneously.

2.2.9 Simulation convergence

Convergence is defined as the acquisition of a satisfactory number of phase points, allowing to consider the sampling as ergodic. MC simulations require an initial equilibration step to guarantee that the initial property average is not biased by poor initial values. As a common procedure, various properties are used to monitor if the simulation appears to attain a reasonable level of convergence, prior to proceeding to the production statistics. We have used energy, conformation and contact analyses to control the convergence of our simulations and these analyses are further described when relevant.

2.3 Experimental

Physicochemical characterization

2.3.1 Circular dichroism (CD)

Circular dichroism is used to measure the optical activity of asymmetric molecules in solution. It is a form of spectroscopy used to determine the optical isomerism and secondary structure of molecules. This technique gives the information about the unequal absorption of left-(L) and right-handed (R) circularly-polarized light by optically active molecules. Circular dichroism consists on the difference between the absorption of these two components. In Figure 2.7 the two possible situations in a CD analysis are schematically represented. In case I, the L and R components are, after passing through the sample, not absorbed or absorbed to equal extents. In the case of recombination of L and R results in the generation of radiation polarized in the original plane. On the other hand, in case II, the components R and L are absorbed to different extents and, therefore, the resulting radiation is said to possess elliptical polarization. The quantity used to

describe this phenomenon is called ellipticity, Θ , and is expressed in degrees. The molar ellipticity ($\text{deg cm}^2 \text{ dmol}^{-1}$), $[\Theta]$ is calculated from the measured Θ using the expression

$$[\Theta] = \frac{\Theta \times 100 \times M}{c \times l} \quad (2.7)$$

where Θ is the measured ellipticity in degrees, c is the DNA concentration in mg mL^{-1} , and l is pathlength in cm, and M is the DNA molecular weight. The application of this technique to study DNA conformations has stemmed from the sensitivity and ease of measurements, and its non-destructive nature.

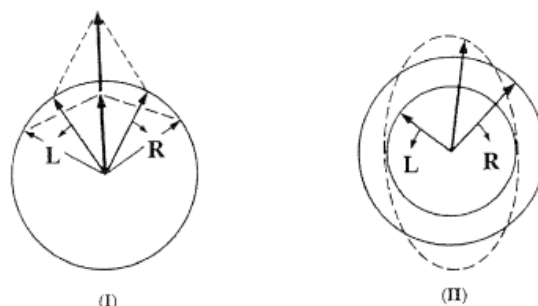


Figure 2.7. Schematic representation of CD effect. Considering the left (L) and right (R) circularly polarized components of plane polarized radiation: (I) both components have the same extent and when combined generate plane polarized radiation; (II) the two components are of different magnitude and the resultant (dashed line) is elliptically polarized. (Adapted from reference [212])

2.3.2 Size

Dynamic light scattering (DLS, also known as photon correlation spectroscopy or quasi-elastic light scattering, QELS) is a technique for measuring the size of particles comprised in the submicron region suspended in solution, ranging from 0.3 nm to 10 μm in the case of Zetasizer Nano ZS (Malvern) [213]. DLS measures the fluctuation of the intensity of the scattered light of a laser beam caused by particle Brownian motion and relates this to the size of the particles. The larger the particle, the slower the Brownian motion will be. Thus, larger particles will diffuse more slowly than the smaller ones. The velocity of the particle Brownian motion is defined by a property known as the translational diffusion coefficient (usually given by the symbol, D). The size of a particle is then calculated from the translational diffusion coefficient by using the Stokes-Einstein equation,

$$d(H) = \frac{k_B T}{3\pi\eta D} \quad (2.8)$$

where $d(H)$ corresponds to the hydrodynamic diameter, T the absolute temperature, η the viscosity and D stands for the translational diffusion coefficient. It should be noted that the diameter obtained by this technique is a value that corresponds to how a particle diffuses in the medium, and as such is referred to as a hydrodynamic diameter. The value $d(H)$ is dependent on factors that affect the diffusion speed of the particles such as ionic strength. A high concentration of ions in the medium affects the particle diffusion by changing the thickness of the electric double layer, i.e. the Debye length (k^{-1}).

Size is obtained from the correlation function, which describes the decay of the intensity of scattered light as a function of time, and contains the diffusion coefficient information required to be entered into the Stokes-Einstein equation. The diffusion coefficient is obtained by fitting the correlation function with a suitable algorithm, such as the cumulants analysis, which determines a mean size and polydispersity index (PI). In the case of polydisperse samples, which are more challenging, an algorithm like non-negatively constrained least squares (NNLS) should be used to deconvolute the measured intensity autocorrelation function of the sample into a number of intensity values each associated with a discrete size band. The guidelines ISO 13321 and more recently ISO 22412 contain important information to warrant high quality results.

2.3.3 Zeta potential (ZP)

Zeta potential is a physical property which is exhibited by any particle in suspension, being related to its surface charge. It measures the magnitude of the electrostatic or charge repulsion or attraction between particles, and is one of the fundamental parameters known to affect particles stability. The existence of a net charge at the particle surface rules the distribution of ions in the surrounding interfacial region, resulting in an increased concentration of counter ions close to the surface. Thus, an electrical double layer exists around each particle. Specifically, the liquid layer surrounding the particle exists as two parts: an inner region where the ions are strongly bound, the Stern layer, and an outer region where they are less firmly associated, the diffuse layer. Within the latter, there is a theoretical boundary inside which the ions and particles form a stable entity, so that, when a particle moves, ions within the boundary move with it. In turn, those ions beyond the boundary remain with the bulk dispersant. Zeta potential is considered the potential at this boundary, that is, at the slipping plane (Figure 2.8).

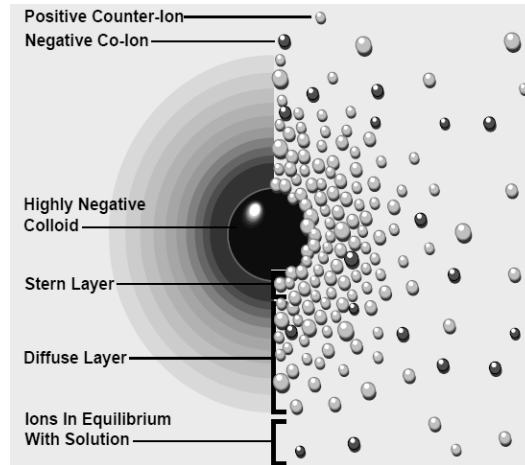


Figure 2.8 Schematic representation of the ionic distribution around colloid. Taken from reference [214].

The magnitude of the zeta potential gives an indication of the potential stability of the colloidal system, which is determined by the sum of attractive and repulsive forces which particles experience as they approach one another. If the zeta potential is high, the particles are stable due to high electrostatic repulsion. Conversely, a low zeta potential value, near neutrality, increases the probability of particles colliding and consequently forming aggregates.

The value of the zeta potential is calculated by determining the electrophoretic mobility and then applying the Henry equation. Under an electric field, charged particles suspended are attracted towards the electrode of opposite charge with a given velocity or, in other words, electrophoretic mobility. Electrophoretic light scattering (ELS) is a technique used to measure the electrophoretic mobility of particles in dispersion, based on the fundamental physical principle of electrophoresis. The zeta potential, z , is related to the electrophoretic mobility, U_E , by the latter equation

$$U_E = \frac{2 \varepsilon z f(ka)}{3 \eta} \quad (2.9)$$

where ε is the dielectric constant, η the viscosity, and $f(ka)$ Henry's function. In many aqueous solutions containing an electrolyte, the zeta potential can be calculated from the Smoluchowski equation, for which a value of 1.5 for $f(ka)$ is considered.

2.3.4 Agarose gel electrophoresis (GE)

Gel Electrophoresis is a technique used to separate macromolecules that differ in size, charge or conformation. Charged molecules or particles when are placed in an electric field, they migrate either the positive or negative pole according to their charge. Several different buffers have been recommended to use in electrophoresis of DNA, but the most common are TAE (Tris-acetate-EDTA) and TBE (Tris-borate-EDTA). Buffers not only establish pH, but also provide ions to support conductivity. When samples are introduced in the wells of the gel, typically, a loading buffer is added, which contains something dense (e.g. glycerol) to allow the sample to "fall" into

the sample wells. Also, one or two tracking dyes are used, which migrate in the gel and allow visual monitoring and follow how far the electrophoresis has proceeded. GelStar[®] is a nucleic acid binding fluorescent dye, whose spectra shows an excitation peak at 493 nm and an emission peak at 527 nm (green), and 532 nm for ssDNA and RNA. Maximum sensitivity detected as low as 20 pg of dsDNA [215].

2.3.5 Fluorescence microscopy (FM)

A popular technique of optical microscopy that relies on the excitation of fluorescent molecules within a specific wavelength region with production of an image generated by the secondary fluorescence emission at longer wavelengths has been largely used to study compaction and decompaction of DNA [27, 39, 44]. The fundamental feature of such a microscope is to provide a mechanism for excitation of the probe with selectively filtered illumination and subsequent isolation of the much weaker fluorescence emission using a second filter to enable image formation with a maximum sensitivity [216]. DAPI (4',6-Diamino-2-Phenylindole) is a fluorescent probe useful for DNA staining [217]. It is believed that DAPI associates with the minor groove of double stranded DNA with a preference for the adenine-thymine basepair. DAPI fluorescence increases 20-fold when is bounded to DNA [218]. The excitation maximum for DAPI bound to dsDNA is 358 nm and the emission maximum at 461 nm. DAPI is excited with a xenon or mercury-arc lamp or with a UV laser.

***In vitro* characterization**

In a first approach, characterization of the *in vitro* physicochemical properties is essential to the development of gene vectors in order to ascertain consistent formulation. Secondly the evaluation of toxicity and efficiency of the gene vector must be assessed. Cell culture assays are used to assess the biocompatibility of the condensing agents, PEIs and Fe(III) whether alone or complexed with DNA in isolated cells *in vitro*, and also to analyze the gene transfection. These techniques are useful in evaluating and optimizing parameters of interest prior to the *in vivo* tests.

2.3.6 MTT assay

The most widely used cell viability tests are based on conservation of mitochondrial integrity and activity. Loss of mitochondrial activity is one of the crucial steps during necrosis and apoptosis of cells. The MTT assay is based on the protocol first described by Mosmann [219]. Chemicals such as MTT (3-(4,5-Dimethyl-2-thiazolyl)-2,5-diphenyl-2H-tetrazolium bromide) are converted by the succinate dehydrogenase in the mitochondrion in an insoluble colored dye. The crystals are solubilized by the addition of dimethylsulfoxide (DMSO) and the results measured by

spectrophotometry. Because the cellular reduction is only catalyzed by living cells, it is possible to quantify the percentage of living cells in a solution. Additionally, the MTT can be performed on 96-well microplates in a standard reader allowing the fast screening of multiple samples.

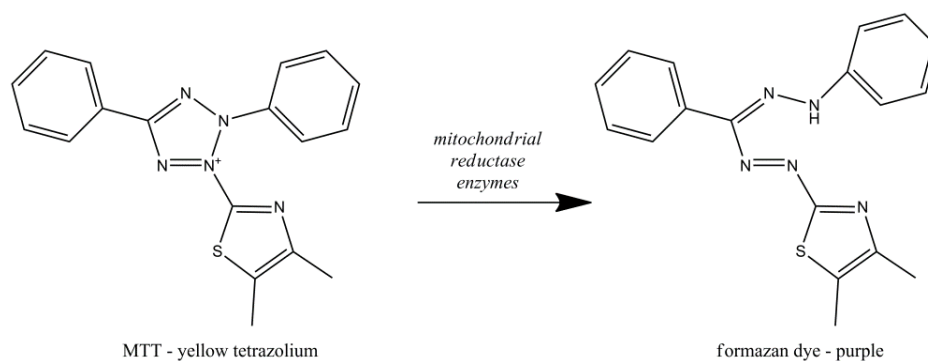


Figure 2.9. MTT is reduced a formazan by mitochondrial reductase.

The treatment of the samples with proteins, i.e. a medium including serum, may be of importance since protein adsorption might dramatically change the interaction of the cells with surfaces. In the *in vivo* situation, this also occurs, and thus it is advisable to mimic the *in vivo* situation as closely as possible. These conditions are used in the following assays.

The screening of the cytotoxicity over several condensing agents concentrations was performed and the response curves fitted with a 4-parameter logistic model (4PL) according to the guidelines [220, 221]. Model fits were carried out using Prism software (Version 6.02).

2.3.7 LDH assay

LDH is a cytoplasmic enzyme that is released into the cytoplasm upon plasma membrane damage or rupture. The LDH assay, therefore, is a measure of membrane integrity and of cell viability because LDH release into the media is a marker of cell dead. The essential principle behind the assay is that LDH released into the growth medium, from the damaged cells, catalyzes the conversion of lactate to pyruvate, and additionally converts nicotinamide adenine dinucleotide NAD^+ to NADH. In a second step, the catalyst (diaphorase) transfers H/H^+ from NADH/H^+ to the yellow tetrazolium salt 2-(*p*-iodophenyl)-3-(*p*-nitrophenyl)-5-phenyltetrazolium chloride (INT) which is reduced to red formazan [222] (see Figure 2.10).

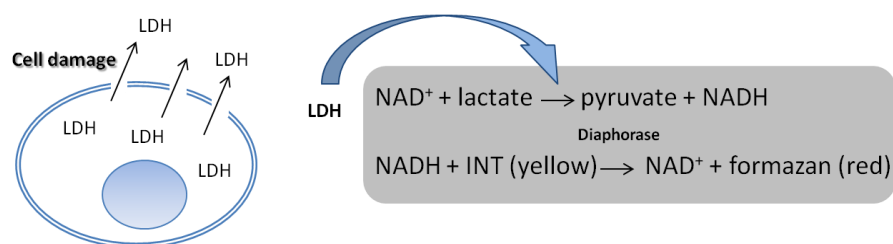


Figure 2.10. Schematic representation of the chemical reaction in the LDH assay.

The increase of the LDH enzyme activity in the supernatant directly correlates with the amount of formazan formed. The formazan dye formed is water soluble and the maximum absorption at 492 nm, while the tetrazolium salt INT shows no significant absorption around this wavelength.

2.3.8 ATP assay

This method relies on the measurement of adenosine triphosphate (ATP) by luminescence using the luciferase-luciferin system [223]. ATP plays an important role in energy exchange in biological systems. It is the principal immediate donor of energy and fundamental in all metabolically active cells. ATP has been used as a tool for the functional integrity of living cells since all cells require ATP to remain alive and perform their specialized function. Since ATP degrades rapidly after cell death, its concentration is related with cell viability. Cell injury or oxygen / substrate depletion results in a rapid reduction of cytoplasmic ATP. The reaction is catalyzed by the enzyme luciferase obtained from the firefly. The $Mg \cdot ATP_2$ converts the luciferin into a form which is capable of being catalytically oxidized by the luciferase in a high quantum yield chemiluminescent reaction [224], in Figure 2.11.

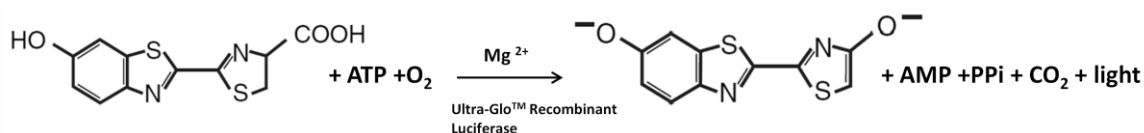


Figure 2.11. The mono-oxygenation of luciferin is catalyzed by luciferase in the presence of Mg^{2+} , ATP and molecular oxygen [225].

The luminescence obtained is based on the interaction of the enzyme, luciferase, with the luminescent substrate, luciferin. Under optimum conditions, light intensity is linearly related to ATP concentration. Cellular ATP can be measured by direct lysis of the cells, and therefore, the released ATP is then free to react with the luciferin-luciferase and leading to light emission at 562 nm. This method has shown to be more sensitive than MTT assay [226, 227].

2.3.9 Hemolysis

Interactions with blood components, namely erythrocytes, may occur after injection of complexes into the bloodstream. Hemolysis is the damage of red blood cells (RBCs) leading to the release of iron containing protein hemoglobin into plasma. The hemolytic activity of condensing agents and the tendency to form aggregates with freshly purified erythrocytes *in vitro* is recommended by FDA [228]. In this assay the condensing agents are incubated with RBCs and hemoglobin released by damaged cells. Thereafter, condensing agents and undamaged RBCs are removed from

solution by centrifugation, and the amount of hemoglobin in the supernatant measured by visible light spectrophotometry.

2.3.10 Fluorescence-activated cell sorting (FACS)

Interaction of colloidal particles and cells is of fundamental interest for gene delivery. FACS is a high-throughput method that allows the automated quantification of fluorescent or fluorescence labeled particles internalized by cells [229, 230]. As it was already mentioned diverse mechanisms of cellular internalization are recognized and the properties of polyplexes influence this step of gene transfer (see Section 1.2.3, Chapter 1). In a simplified scheme the cell suspension is pumped through a very thin capillary, whereby cells pass through detector one by one, and are sequentially probed by a light source to excite the attached fluorescent dyes (Figure 2.12).

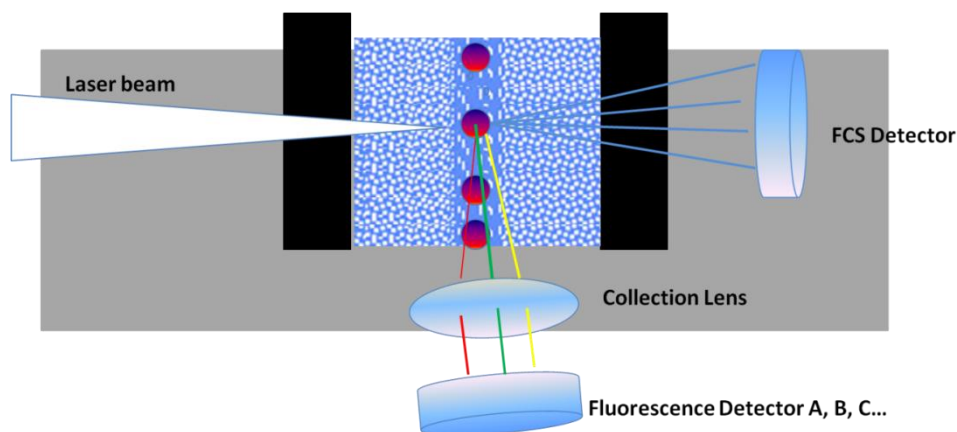


Figure 2.12. Representation of flow cytometry apparatus.

Flow cytometers possess an extra detector for forward scattered light. The forward-scattering signal permits the separation of events when a cell is passing through detectors from those in which only fragments of free particles are detected. For optimal illumination, the stream transporting the cell should be positioned in the center of the laser beam. To attain this, the sample is introduced into a stream of sheath fluid within the flow chamber. The flow of sheath fluid accelerates the cell and restricts them to the centre of the sample core, in a process deemed hydrodynamic focusing.

The amount of fluorescent signal detected is proportional to the number of fluorochrome molecules in the cell, leading to higher signal cells with more fluorescent particles. A cyanine dye, Indodicarbocyanine (Cy-5) is used to detect DNA, with excitation maximum at 649 nm and emission maximum at 670 nm. The most common type of quantitative analysis using FACS data is the creation of a histogram of fluorescence events to count the number of cells with the attached probe. Usually in this histogram, data is displayed logarithmically, and normally, contain two major populations of events denoting stained and unstained samples [231]. In order to measure

only internalized particles, cells are commonly treated chemically before FACS measurement to complete removal of membrane cellular adherent complexes.

2.3.11 Transfection

Transfection consists in the introduction of foreign DNA in to the nucleus of a cell. The analysis of transfection efficiency *in vitro* is used as a rather general descriptor of a transfected cell line, so that, higher transfection efficiency results in higher expression levels of a plasmid. Typically, a reporter gene is cloned with a DNA sequence of interest into an expression vector that is subsequently transferred to the cells. Reporter vectors allow functional identification and characterization of promoter and enhancer elements because expression of the reporter protein correlates with transcriptional activity of the reporter gene. In our study, luciferase from firefly (*Photinus pyralis*) [232] was used as the reporter gene. The vast popularity of this luminescent gene is due to its high sensitivity and convenience of the enzyme assay. This gene does not require any post-translational modifications and it is available as a mature enzyme directly upon translation of its mRNA (see Figure 2.13).

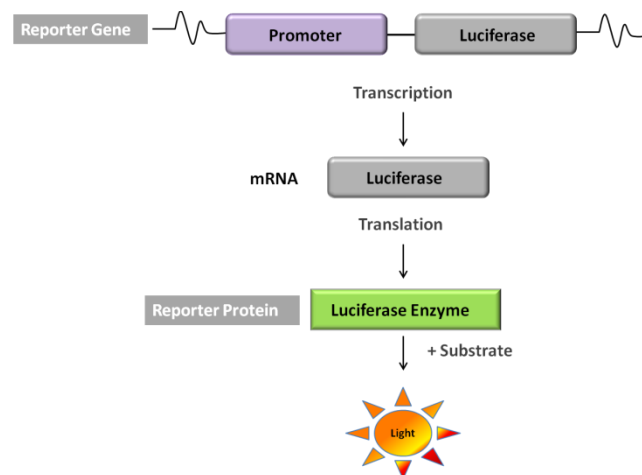


Figure 2.13. Schematic representation of the transfection steps in the cell.

Upon mixing with substrates (see Figure 2.11), firefly luciferase produces an initial burst of light that decays over about 15 seconds to a low level of sustained luminescence.

2.3.12 Other techniques

A number of other techniques, including precipitation assays and potentiometry, will be detailed in subsequent chapters.

CHAPTER 3

DNA-PEI complexes

3.1 Introduction

This chapter provides the assessment, at a fundamental level, of the impact of pH variation on the physicochemical characteristics of the resulting DNA-PEI complexes. In the literature, some works reported the effect of varying the polycation charge density, either by changing the degree of polymerization [233, 234] or the pH of the medium [66, 235]. The main findings indicate that the interaction between a highly charged polycation and DNA is stronger than with a polycation with low charge density, consolidated from both experimental [235, 236] and theoretical evidences [40, 237]. However, most of the studies usually look into similar systems but do not directly compare systems with equivalent effective charge ratio between polycations and DNA. The understanding of how the complexes react to these variations and the influence of the polycation charge density on the polyplex formation is of extreme importance, due to the stabilizing effects that may arise from a privileged interaction. Consequently, in systems in which linear charge density of the PEI molecules is varied, while keeping the charge ratio between polycation and polyanion constant, leads inevitably to a difference in the number of PEI molecules in solution. This adjustment of the charges is of fundamental importance, and should be accounted in complex formation. Therefore, a preliminary study of the optimum conditions to

generate DNA-PEI polyplexes is crucial to the aftermost development of the ternary of complexes.

In this chapter, a complete potentiometric study is preformed to obtain a fully characterization of the pH behavior of PEI. Based on these data, a precise calculation of charge ratios between PEI and DNA is possible in each pH under study, and allows performing a reliable comparison between systems. Here, polyplexes will be prepared at pH 4, 6 and 8, with a constant ionic strength of 150 mM, analogous to physiological conditions.

3.2 Materials and methods

3.2.1 Materials

Salmon testes DNA (~2000 base pairs) was purchased from Sigma, UK, and used as received. Polyethylenimine, $M_n \sim 1200 \text{ g mol}^{-1}$ and $M_w \sim 1300 \text{ g mol}^{-1}$, 50 wt % in H₂O was received from Sigma, UK. Sodium chloride, sodium acetate, disodium tetraborate, Tris acetate, and EDTA were purchased from Sigma, UK, and chloride acid and acetic acid from Riedel-de Haens. All chemicals and reagents were of analytical grade. Agarose and the dyes used in electrophoresis were obtained from Lonza, Switzerland, and Fermentas, Germany, respectively. All experiments were performed in solutions prepared with Millipore Milli-Q deionized water (18.2 M Ω /cm resistivity).

3.2.2 Sample preparation

DNA stock solutions were prepared by dissolution in each of the three different buffers, pH 4 (85 mM CH₃COOH, 15 mM NaCH₃COO·3H₂O, 46 mM NaCl), 6 (5 mM CH₃COOH, 95 mM NaCH₃COO·3H₂O, 46 mM NaCl), and 8 (18 mM Na₂B₄O₇·10H₂O, 29 mM HCl) with equal ionic strength (150 mM). These buffers were chosen so as to avoid the presence of trivalent ions which, even for relatively low amounts, are known to induce DNA condensation. The concentration of DNA in solution was determined by the respective UV absorbance at 260 nm, considering a molar extinction coefficient of 6600 M⁻¹ cm⁻¹. A solution of 50 $\mu\text{g mL}^{-1}$ of double-stranded DNA possesses an absorbance of 1 [238]. PEI stock solutions were prepared by dilution in the same buffers as DNA. Besides the variations in pH already described, we have also varied, throughout the chapter, the polycation/DNA charge mixing ratio, β , which is defined according to

$$\beta = \frac{C_{PEI}}{C_{DNA}} \quad (3.1)$$

where C_{PEI} and C_{DNA} are the molar concentrations of positive charge, present in the protonated amine groups of PEI, and negative charge of the phosphate groups of DNA, established for each pH. The average percentage of ionizable amine groups in the PEI for each pH value was

obtained from potentiometric studies (see below). The DNA-PEI complexes were prepared as described in what follows. A fixed volume of PEI solution (600 μL) of variable concentration was added to a solution containing DNA (2400 μL). The final concentration of DNA was equal to 20 $\mu\text{g mL}^{-1}$ (60.6 μM) and was kept constant in all techniques used for the characterization of the DNA-PEI complexes. The samples were subsequently left for equilibration at room temperature for 120 min on a mixing board. Test experiments were conducted after 5 min to 24 h after mixing without variations in the results.

3.2.3 Potentiometric titration

Solutions with a concentration of 0.16 mg mL^{-1} of PEI were basified by adding enough 0.5 M NaOH. The solutions were then titrated with standardized 0.1 M HCl in a Metrohm AG (Herisau, Switzerland) water jacketed titration vessel, thermostatted at 25.0 (\pm 0.1) $^{\circ}\text{C}$, with a microburet in the presence of an inert atmosphere (N_2). Potentiometric titrations were conducted with a 665 DOSIMATE (Metrohm AG, Herisau, Switzerland) microburet with minimal volume increments of 0.001 mL, recorded with a pHM 95 potentiometer (\pm 0.1 mV; Radiometer Analytical SAS, Lyon, France). Potentiometric titration end-point was estimated by the inflection of the titration curve, and the overall ionization constant using the highest buffering capacity of the respective solutions. The pH values were obtained via three standard buffers (50 mM KHP; 25 mM KH_2PO_4 ; 25 mM NaHCO_3 /25 mM Na_2CO_3) calibration (pH 4.005, 6.865, and 10.012) [239] under similar experimental conditions.

3.2.4 Circular dichroism

Circular dichroism (CD) was used to monitor the DNA double-helix conformation when subjected to the different pH values. CD measurements were performed with an Olis, model DMS20. Spectra were acquired using a 0.5 cm path length quartz cuvette at the constant temperature of 25 $^{\circ}\text{C}$, maintained using a Peltier device, and with DNA concentrations of 50 $\mu\text{g mL}^{-1}$. Two scans were obtained and averaged per spectrum, operating from 220 to 320 nm at a scan speed of 10 nm min^{-1} and a bandwidth of 1 nm. All measurements were conducted under a constant gas flow, to purge the ozone generated by the light source of the instrument.

3.2.5 Precipitation assay

The interaction of DNA with the condensing agent, as the concentration of the latter increases, was studied by UV spectrophotometry (Shimadzu, UV-2450). After equilibration, the samples were centrifuged for 1 h at 3800 g and the concentration of DNA remaining in the supernatant was analyzed spectrophotometrically at 260 nm. Three repetitions of this procedure were performed for each system.

3.2.6 Agarose gel electrophoresis assay

Agarose (0.7 g) was dissolved in 100 mL of TBE buffer (pH 8.2) by heating until boiling and subsequently allowed to cool down. A total of 5 μL of a 10000 \times solution of Gelstar[®] were added to the agarose solution, which was then poured into a 10 \times 20 cm gel tank. Potential air bubbles were removed with a pipet tip, and a gel comb was added to the gel which, in turn, was allowed to set. The DNA-PEI samples (25 μL) were prepared following the previously indicated procedure, and loaded into each sample well. The electrophoresis was carried out in a horizontal tank containing TBE buffer and run at 90 V for 1 h. Gels were imaged using a UV transilluminator.

3.2.7 Size analysis

The size of the DNA-PEI complexes was assessed by dynamic light scattering (photon correlation spectroscopy, PCS) using an N5 Particle Analyzer (Beckman Coulter Inc., U.S.A.). Samples were prepared as described for the precipitation assays, and measured in triplicate at 25 $^{\circ}\text{C}$ with a detection angle of 90 $^{\circ}$. The time-averaged autocorrelation functions were transformed into intensity-weighted distributions of the apparent hydrodynamic diameter using the available software. The standard error of the mean was calculated from the three measurements.

3.2.8 Zeta potential analysis

Zeta potential measurements were performed by laser Doppler electrophoresis using a Zetasizer Nano ZS (Malvern Instruments Ltd., U.K.). Samples were prepared as described in the general procedure. Measurements were carried out in a folded capillary electrophoresis cell (Malvern Instruments) at 25 $^{\circ}\text{C}$. The average values of zeta potential were calculated with the data obtained from three runs.

3.3 Results and discussion

3.3.1 Acid/base behavior of PEI

We started by investigating the pK_a values at 25 $^{\circ}\text{C}$ for the amine groups of PEI through potentiometric studies in acidified solutions ($\text{pH} \approx 2.5$). The buffer capacity of PEI, BC, is obtained from the slope $d[A]/d\text{pH}$, where $[A]$ is the analytical concentration of acid species added to solution. Values of pK_a are extracted from the maxima of these buffer capacity curves, the latter modeled using

$$BC = -\frac{d[A]}{d[\text{pH}]} = 2.303 \left[(H^+) + \frac{K'_w}{(H^+)} + \sum_i \left(\frac{C_i \left(\frac{V_0}{V_0 + V_i} \right) K_{ai}(H^+)}{(K_{ai} + (H^+)^2)} \right) \right] \quad (3.2)$$

where (H^+) is the H^+ activity, K'_w is the conditional ionic product of water, and C_i , V_0 , V_i , and K_{ai} are the analytical concentration, the volume of the initial solution, the added titrant volume, and the ionization constant of the reactive species i , respectively. This equation enables us to fit the buffer capacity of the solutions and accurately estimate the contributions of each ionizable species. It was analyzed the potentiometric data obtained in three different media (no salt added, and NaCl and NaBr at the same ionic strength, 150 mM). The values found for the different pK_a are compiled in Table 3.1. It should be noted that, in the absence of salt, and due to polyelectrolyte interaction with small ions, the calculated polyelectrolyte charge density versus pH functions may be incorrect.

Table 3.1. Averaged pK_a and the concentration of ionizable species (expressed as pC_i) estimated from the fitting of four titrations of PEI 1.2 kDa to solutions with no salt added, 150 mM of NaCl and 150 mM NaBr, respectively.

	No salt		NaCl		NaBr	
	pK_a	pC_i	pK_a	pC_i	pK_a	pC_i
1	3.72±0.02	2.84±0.01	3.51±0.33	2.91±0.11	2.87±0.54	2.88±0.12
2	5.04±0.14	2.83±0.11	4.81±0.58	3.05±0.13	4.26±0.31	2.92±0.17
3	5.95±0.18	2.80±0.07	6.28±0.07	2.61±0.03	6.22±0.03	2.59±0.02
4	7.45±0.08	2.67±0.02	7.94±0.13	2.75±0.07	7.79±0.06	2.85±0.02
5	8.57±0.06	2.49±0.01	9.02±0.13	2.46±0.03	8.92±0.05	2.49±0.02
6	9.70±0.03	2.40±0.01	9.92±0.05	2.40±0.05	9.91±0.03	2.33±0.02

Applying a statistical treatment using Mandel's test, it is possible to discern six ionizable species in the PEI under study (Figure 3.1), whereas data obtained from the literature attributes only two [152] or four [240] for similar derivatives of PEI. Additionally, the model allows us to distinguish three different regions: acidic region (2.5-3.3), weakly acid region (4.9-6.1), and alkaline region (7.4-9.7), see Figure 3.2. We are now able to analyze the total amount of ionizable species of the PEI solution. The differential plots of pH ($-\text{d}(\text{pH})/\text{dV}_a$) as function of the number of equivalents of acid, C_a (in mM), added during the titration (not shown) allow the determination of the number of total equivalents per weight of polymer solution. In the present experimental conditions, the global average value estimated for the (50%) solution of PEI in 150 mM NaCl is 8.72 ± 0.18 mequiv g^{-1} . Based on the structure and M_w of the PEI used, we calculate $11.61 (\pm 0.27)$ mequiv g^{-1} of amines in solution.

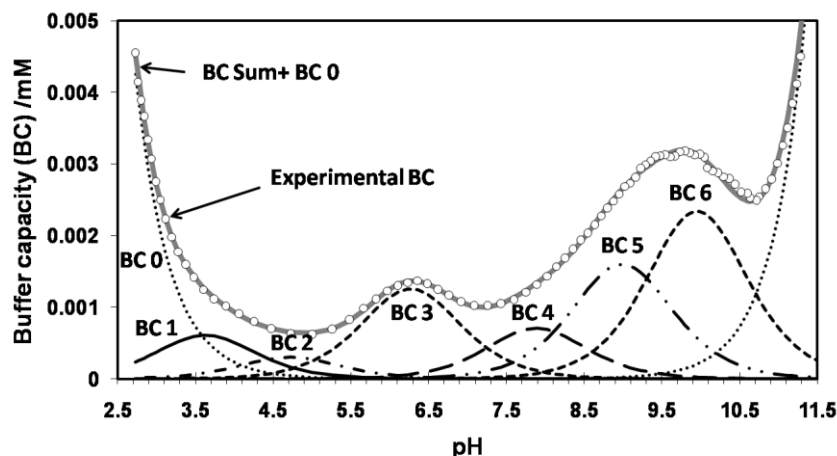


Figure 3.1. Modeling of the buffer capacity curve of PEI using six different protonation contributions (BC 1-6), while BC 0 depicts the buffering capacity of the 150 mM NaCl solution. The open circles correspond to the experimental data, to which the fitting using Equation (Eq. 3.2) is superimposed.

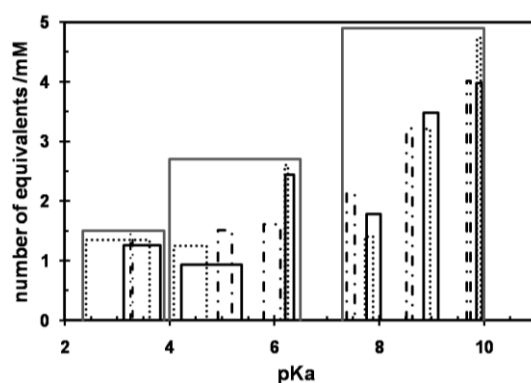


Figure 3.2. Graphic representation of the number of equivalents of each contribution (C1 to C6) vs the respective ionization constant estimated (pK_1 to pK_6): PEI (dotted-dashed line), PEI + NaCl (dotted line), PEI + NaBr (solid line).

The percentage of protonated amines in PEI at pH 2.5 is, thus, 75.1 (± 1.8) %, in agreement with previous work on a similar system [138]. The percentage of ionized groups at each pH (comparatively to the total number of charges obtained at our experimental limit, pH 2.5), which is of paramount importance in this study, can now be easily calculated for each different solution using

$$I_g = 100 \times \frac{\sum_{i=1}^6 \left(C_i \frac{(H^+)}{(H^+) + K_{ai}} \right)}{\sum_{i=1}^6 C_i} \quad (3.3)$$

This information allows us to prepare DNA-PEI complexes with full control of the ratio of negative (phosphate groups) to positive (charged amine groups) charges. The results are summarized in Table 3.2, for PEI in 150 mM NaCl solutions.

Table 3.2. Estimated values for the percentage of ionized groups (I_g) of PEI, relatively to that obtained at pH 2.5, and estimated average number of charges per PEI molecule (z_{PEI}) at 150 mM NaCl as a function of the pH of the medium.

pH	I_g	z_{PEI}
4	92.3	20
6	78.8	17
8	57.8	13

This salt content is compatible with the ionic strength used throughout the present chapter. Note that although some variations are discernible from the solution without salt to the other two, those containing NaBr and NaCl are equal within the uncertainty of the determination.

3.3.2 Assessment of DNA conformation at different pH values

The conformational stability of DNA molecules in the different buffer solutions was assessed using CD. The CD spectra of the DNA solutions at pH values of 6 and 8 are very similar and show characteristic features of the double-stranded B-form DNA (Figure 3.3). These consist of a positive band around 275 nm, a negative signal, with approximately the same intensity, at 245 nm, a high intensity band at about 220 nm, and a maximum in absorbance, reflected by the crossover point, near 258 nm [241].

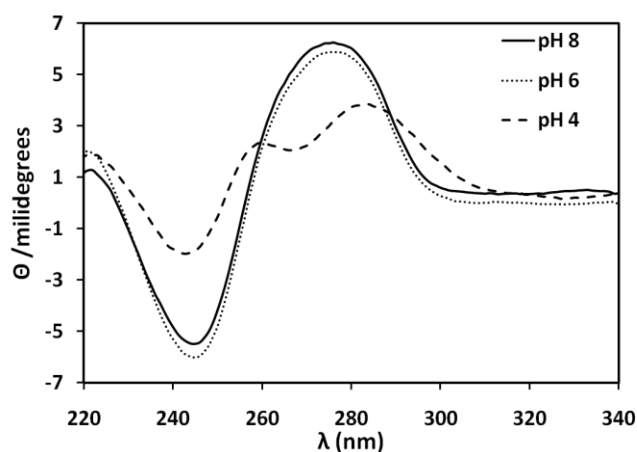


Figure 3.3. CD spectra of salmon test DNA in the three different buffers under study.

For DNA at pH 4, however, we observe a decrease in the intensity of the negative peak (275 nm) and the splitting of the positive peak into two: one at approximately 258 nm and the other at 288 nm. From the results, it can be concluded that the conformation of DNA is changed at lower pH. However, there is no consensus on the precise nature of the changes that occur in the DNA

conformation when the pH is lowered. Previous work [242], addressed structural changes of calf thymus DNA, induced by pH treatment, and large differences were observed in the Raman spectra at pH 3.8. These changes were attributed to adenine protonation (disruption of AT base pairs), GC base pair protonation, adenine, thymine, and cytosine unstacking, and DNA backbone conformational changes. The described changes found for pH values close to 4 may explain the uncommon CD profile found for the lowest pH under study.

3.3.3 Characteristics of the complexes

i. Species in bulk vs precipitates

Precipitation studies were performed to follow the binding of PEI to DNA and assess the differences induced by the different pH values of the solutions. The mixing of PEI with DNA at different β values results in the formation of DNA-PEI particles that can be sedimented by centrifugation. The percentage of DNA remaining in the supernatant is plotted versus β (Figure 3.4). The shape of the curve is similar for all pH values under study. The profiles present a sigmoidal shape, indicating a cooperative binding between PEI and DNA. It is interesting to note that, for all the systems considered, the second plateau of the curve is reached for $\beta < 1$. This has been observed for other sufficiently charged polyamines [243].

Comparing the results obtained at the different pH values, it should be emphasized that the transition does not occur at the same β values, as it would be expected from a crude electrostatic viewpoint. Furthermore, full precipitation occurs in the order pH 4, 8, and 6. A smaller amount of positive charge is thus needed to induce the condensation of DNA for pH 4. This is not surprising because polycations with a higher charge density are known to promote stronger binding to DNA [66, 244]. However, the CD results must also be taken into consideration. It is seen that the conformation of DNA is altered and it is possible that the new conformation interacts more favorably with PEI. The differences between the solutions prepared at pH 6 and pH 8 are smaller, but it is, nevertheless, possible to observe that the condensation of DNA occurs for lower β values at pH 8 than at pH 6, which is somewhat unexpected. It is also observed (Figure 3.4a) that only the DNA-PEI complexes prepared at pH 6 display some degree of redissolution for high β values. These results will be now compared with those obtained from agarose gel electrophoresis.

ii. Electrophoretic motion of complexes and overcharging

Figure 3.5 gathers the behavior of DNA-PEI polyplexes prepared at pH 4, 6, and 8, when subjected to agarose gel electrophoresis. For all systems, it is observed that the complexation of DNA starts for $\beta < 1$, as shown by the presence of DNA in the wells (neutralized DNA). There is an intermediate region where most of the DNA molecules are partially condensed, followed by

complete condensation of DNA for sufficiently large concentrations of PEI. A careful look at the band profiles reveals, however, subtle differences in the condensation path for low β values.

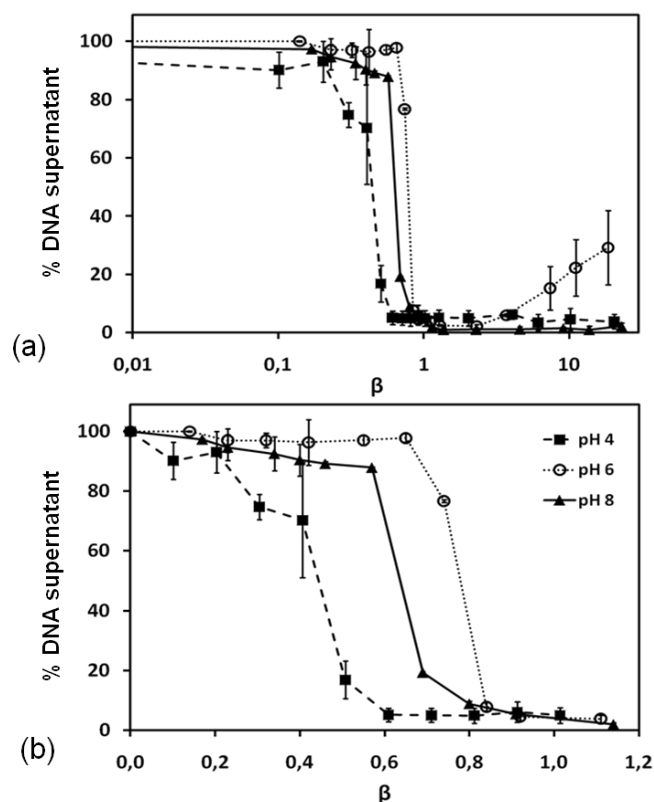


Figure 3.4. Percentage of DNA remaining in the supernatant after DNA-PEI complex formation and separation by centrifugation, measured from UV absorbance, (a) with β ranging from 0 to 20 and (b) a closer look into the condensation region.

For both pH 4 and 6, the samples at $\beta > 0.1$ show the presence of DNA in the wells whereas the DNA band maintains its shape to around $\beta = 0.6$, which suggests that the PEI chains interact strongly with some DNA molecules inducing their condensation, while some others remain free in solution. On the other hand, samples prepared at pH 8 suggest a more progressive condensation with a gradual decrease in the charge of the DNA molecules. At pH 4, DNA is mostly retained for charge ratios around 0.6. However, at β in the 0.9-1.0 region, a small quantity of free DNA is still visible, in contrast to what is observed in the precipitation assays.

Two factors can contribute to this result: (i) gel electrophoresis is expected to have a higher sensitivity to DNA detection than UV spectrophotometry [215], and (ii) the agarose gel is submerged in a buffer with pH 8.2, which can explain the shift to larger values of β . At pH 8.2 the acetate buffers are no longer effective. As such, under these conditions, the samples might behave more closely to those prepared at higher pH values. Multiple attempts were done to perform electrophoresis in buffer solutions with the same pH values as those used for

preparation of the DNA-PEI complexes. We were, however, not successful because the solutions presented different and generally too low conductivities.

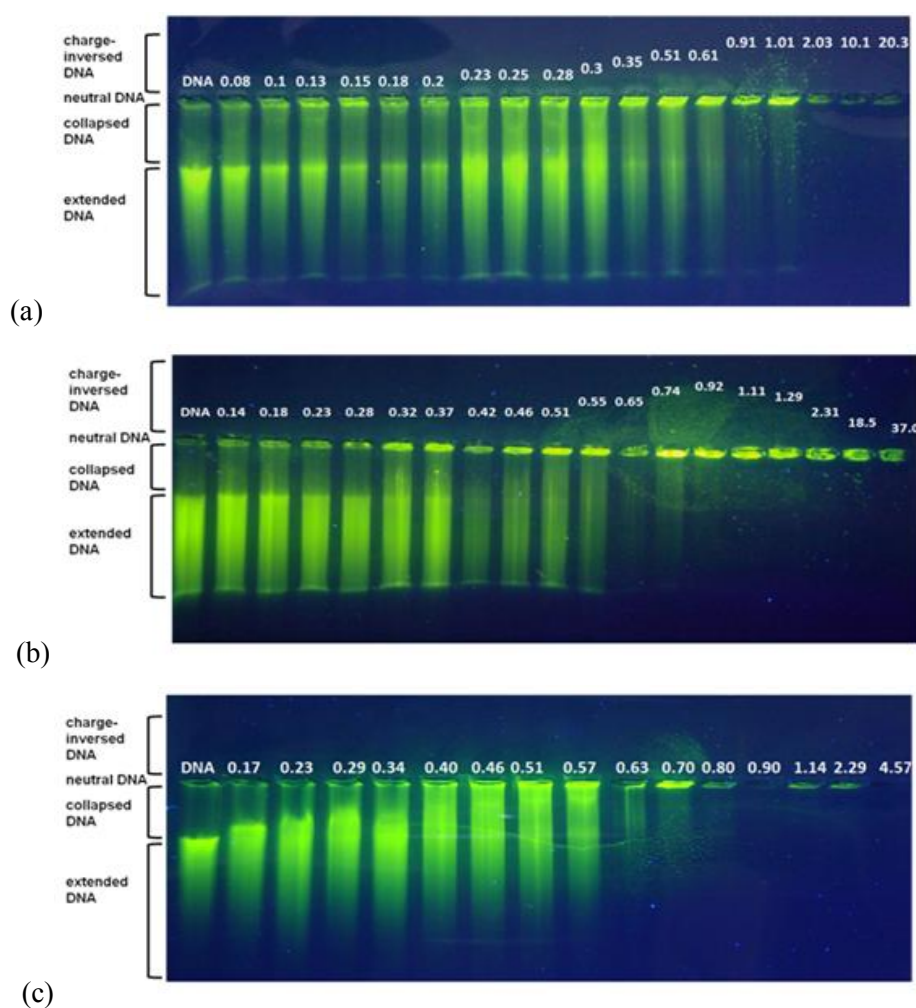


Figure 3.5. Effect of pH on DNA-PEI complexes using agarose gel electrophoresis. Samples prepared at pH values 4 (a), 6 (b), and 8 (c) and analyzed under the same conditions. The first lane of the gel corresponds to DNA in the absence of PEI. The β values are indicated in each lane taking into account the degree of protonation of the PEI for each pH. The DNA concentration is $20 \mu\text{g mL}^{-1}$.

This leads, among other effects, to the degradation of the gels. Results obtained at pH 6 and 8 are in close agreement with those obtained in the precipitation assays. DNA complexation starts at very low β values, as seen by the shift of the band and the presence of DNA in the wells. More visible condensation starts at around $\beta = 0.65$, for pH 6, and at $\beta = 0.92$ most DNA molecules are complexed as attested by the drastic decrease in intensity of the band that corresponds to free DNA. In solutions with pH 8, strong DNA condensation starts at β around 0.63 and is practically

complete at β equal to 0.80. Once again, a slightly larger number of positive charges is needed to induce the condensation of DNA at pH 6 as compared to that of DNA at pH 8.

These observations can be rationalized in terms of charge density and number of chains. At pH 8, PEI presents the lowest of the studied charge densities and, at the same time, the sample contains the largest number of PEI chains for a particular β . This can lead to two effects. First, a more uniform distribution of the PEI chains on the DNA molecule, which would explain the more continuous transition observed in gel electrophoresis at low β values. A similar phenomena has been reported for the polyethylene glycol-PEI copolymer, which was suggested to be evenly distributed among the DNA molecules at pH 7, but showed disproportionation (uneven distribution) at pH 5 [245]. Some of us have also shown, using Monte Carlo simulations, that for $\beta = 0.75$ a polyanion complexed with a larger number of polycation chains of low charge density is further condensed than a polyanion complexed with less polycation chains of higher charge density, probably due to the balance between the enthalpic gain and entropic loss of condensation [40]. Additionally, it should not be ruled out that the decrease in the charge density of the PEI may enhance nonelectrostatic interactions that are otherwise masked. In spite of the experimental difficulties described above, electrophoresis is known to be a relevant tool in the study of the complexation of DNA and condensing agents. For these particular systems it provides additional, and very useful, information on the charge of the complexes in the region of condensation. It can be clearly observed in the gels of Figure 3.5 that, in this region, some DNA particles move in the direction of the anode, that is, some DNA particles present an excess of positive charge. The presence of overcharged complexes is mainly detected for pH 6, which is also in good agreement with the precipitation assays. The mixing procedure used in this study was identical to the specific method developed by Pinto et al [44], where overcharged DNA complexes were also detected.

The efficiency of the condensation of a polyelectrolyte and the charge distribution inside the polyplex is known to depend on the distance between the charges in the multication condensing agent [46]. We suggest thus that, at pH 6, the distance between the charges of PEI is the most favorable for the formation of overcharged complexes. It is interesting to note that, contrary to what has been predicted using simulations [237], the coexistence of neutral, negative, and positively charged complexes is observed in solution, probably due to the diluted nature of the solution that prompts a single-chain behavior rather than an equilibrium situation.

3.3.4 Average size values with non-monotonic trends

The size of the DNA-PEI complexes at different β values was evaluated by PCS. The size of salmon testes DNA, in the absence of PEI, is similar in the three different buffers roughly 467 nm in diameter. This result is substantially different from that obtained by other groups using the

same DNA source (214 nm) [246]. Differences may be ascribed to variation in the experimental conditions and determination technique. We note that for DNA solutions in the absence of PEI, the increase in the concentration of the former from 25 to 150 $\mu\text{g mL}^{-1}$ reduces the respective diameter by a factor of 2.5 (data not shown). Samples with different pH and β values were analyzed and the results are depicted in Figure 3.6.

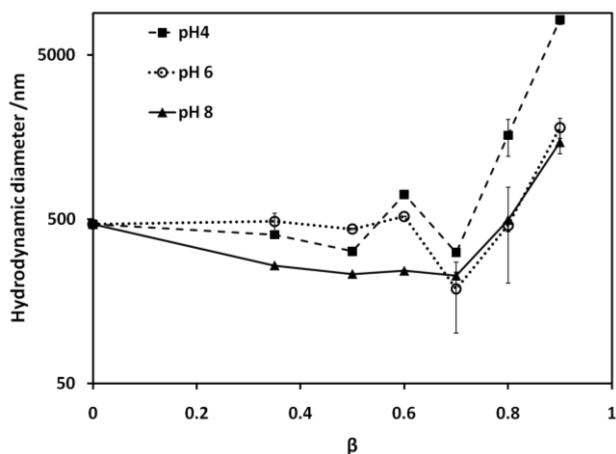


Figure 3.6. Sizes of complexes formed by DNA and PEI at different charge ratios, β , prepared at the various pH values.

The trends are similar for the three pH values under study. There is an initial decrease in the size of the DNA, to a minimum at $\beta = 0.7$, followed by a drastic increase that will eventually lead to the precipitation of the complexes, as seen in the precipitation assays. It is interesting to note that, comparing now the samples prepared at different values of pH, the order is again unexpected. DNA complexes at pH 8 are smaller than those prepared at pH 4 or 6. In fact, it would be likely for the samples at pH 4 to show the strongest condensation and, thus, smaller sizes. However, it should be recalled that this technique measures the mean size of all particles in solution. The highly charged polycations interact strongly with the DNA molecules. As such, and due to the sample preparation procedure, the PEI chains in the DNA solution bind and fully condense those DNA chains that are in their vicinity. However, and because the system is deficient in polycation charge, not all the DNA molecules will condense. This can be clearly seen in the electrophoresis gel in Figure 3.5a. The size that is measured is thus the result of a mixture of DNA-PEI complexes and free DNA molecules. As the concentration of PEI is increased, the measured size presents a nontrivial behavior, which was also observed in precipitation assays. This seems to indicate some balance between condensation and precipitation of the DNA complexes. At pH 6, we observe the same general behavior as for pH 4, also in good agreement with the gel electrophoresis observations. The size remains approximately constant (presumably due to free DNA molecules in solution) up to $\beta = 0.6$, after which it decreases for $\beta = 0.7$, where only a small amount of free DNA is detected. Solutions at

pH 8 present a slightly different trend. The initial decrease in the sizes of the complexes, as compared to the free DNA, seems to be more gradual, in accordance with the gel electrophoresis results. Generally, lower sizes were obtained for the complexes prepared at this pH, especially for the lower values of β . It should be noted that the number of PEI chains at this pH is the highest for each charge ratio.

Clear aggregation starts for $\beta > 0.7$ for all systems under study. The size of the aggregates is especially high for the complexes formed with the highest charge density polycations (pH 4). Initially, upon the addition of some polycation to the DNA solution some complexes are formed, due to the strong interaction between DNA and PEI. The PEI chains that are subsequently added can interact with free DNA (or undercharged complexes) but also promote overcharging. The binding of these positively charged complexes with the remaining DNA molecules or undercharged complexes will be facilitated, leading to higher values of aggregation. This behavior has been previously reported [247].

3.3.5 Surface charge with a global minimum

Zeta potential measurements were conducted to assess the overall charge of the DNA-PEI complexes (Figure 3.7). The relative positioning of the curves, corresponding to the various pH values under study, is similar to that observed in the determination of the sizes of the complexes. The overall trend comprises an initial decrease in the charge of the complexes, for all systems, upon the addition of PEI, followed by an increase. The initial decrease can be explained by a moderate degree of folding in the DNA molecules, induced by the compacting agent, which has the effect of concentrate the negative charge. Note that, in the absence of PEI, the different values of the zeta potential are induced by the use of different buffers. Analyzing in more detail, we see that, at the lower values of β , DNA complexes prepared at pH 6 are slightly less negative, but when the PEI concentration is increased, it converges with the systems at pH 8, which indicates that the addition of a larger number of chains of polycation compensates the lower charge density. This is compatible with the PCS results. Surprisingly, and contrary to the results obtained with the precipitation assays and the gel electrophoresis technique, no positive complexes were detected using this technique at those values of pH. Samples prepared at pH 8 and low β values display the most negative charges. This is expected, because (i) the PEI chains at this pH present a lower charge density, promoting a lower degree of neutralization of DNA charges than that of those prepared at lower pH, and (ii) the weakly charged and larger amount of PEI chains condense DNA more evenly, which decreases the amount of free DNA molecules and concentrates the negative charge in a similar phenomena as the decrease in charge when the first PEI molecules are added. The larger charge of the complexes prepared at pH 8 and for low β values explains the larger stability toward aggregation, resulting in complexes with smaller

sizes. Considering now the samples prepared at pH 4, it is observed that, for low β values, the surface charge of the component in the sample is lower than that of systems at pH 6, which might be a consequence of using different buffers, as mentioned above. When the PEI concentration is increased, it is observed that the neutralization of the DNA charges is more efficient for pH 4. The complexes prepared in these conditions attain neutralization for lower β values and are the only ones that clearly display overcharging using this technique. This is not in agreement with the gel electrophoresis studies, where positively charged DNA-PEI complexes could be observed for all studied pH values.

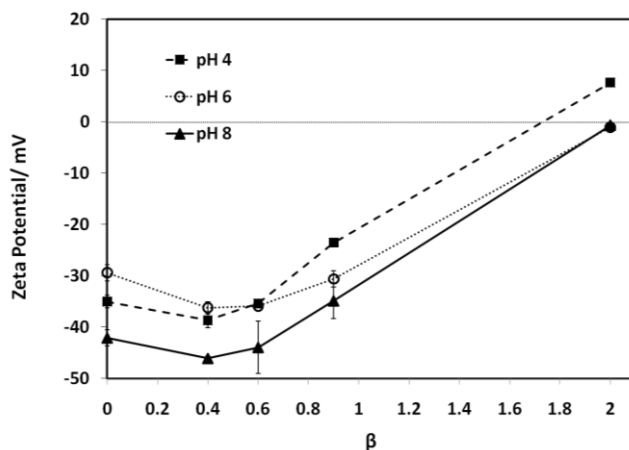


Figure 3.7. Zeta potential vs β of solutions prepared at different pH values.

Finally, it is worthwhile remarking that the agreement between the different techniques used in this study was not always evident, even though special care was taken to ensure the same concentration ranges and similar experimental conditions. The different techniques have different detection methods and, as such, may pinpoint different aspects of the systems and thus emphasize apparently contradictory results. For example, gel electrophoresis is not sensitive to the cancellation of charges due to the presence of positive and negative species. For this reason, neutral, positive, and negatively charged species could be detected in these assays. PCS and zeta potential measurements, on the other hand, tend to average values of size and charge, respectively, and, as such, are more prone for cancellations.

3.4 Conclusion

It is important to focus on the benefits of our study in the experimental application of interest, gene therapy. Properties such as DNA complexes charge, size, and condensation degree play paramount roles in gene expression. The present study shows how such parameters can be modulated by using pH responsive polycations. It was observed that variations in the pH, while keeping the polycation/polyanion charge ratio constant, leads to nonmonotonic and nontrivial trends in the precipitation behavior, electrophoretic mobility, and size of the complexes. At

lower pH values, DNA and PEI interact more strongly and form complexes with larger mean sizes, which suggest disproportionation. On the other hand, complexes prepared at pH 8 show a weaker binding between DNA and PEI, smaller aggregates, and possibly a more uniform population. All systems showed some degree of overcharging even at $\beta < 1.0$, with the complexes prepared at pH 6 presenting the more marked effect. This reflects the fact that both linear charge density and the relative number of chains of the condensing agent are important factors in the condensation behavior.

These findings confirm that DNA changes the overall conformation at pH 4 and indicates that complexes prepared at these lower values of pH are polydisperse and strongly bound. This corroborates, as speculated [40], that polyplexes prepared at intermediate or higher pH values are the most appropriate for gene delivery, either used directly (in the form of polyplexes) or for the precondensation of DNA.

CHAPTER 4

DNA-PEI-Fe(III) complexes: Condensation and decondensation

4.1 Introduction

The effect of the addition of a second condensing agent, Fe(III), in the previously studied DNA-PEI complexes is followed in detail throughout this chapter. As mentioned in Chapter 1, during the trafficking through the cell, two crucial aspects are required to warrant a successful gene delivery, the efficient compaction of DNA to ensure enough protection along the route, and afterwards, the respective decompaction when the appropriate cellular compartment is reached. Regarding this, a commitment between the compactness/stability of the polyplexes and ability to release their cargo should be taken in consideration [248, 249].

The body of this chapter is divided in two main parts. Initially, experimental techniques are conducted to elucidate on the mechanisms of condensation and decondensation of DNA, and in the second part, MC simulations are used to simulate the same phenomena. Experimentally, different concentrations of PEI were tested with increasing concentrations of Fe(III), and focus was directed to optimizing the compaction and decompaction of DNA. The same designed experiments were performed in parallel resorting to MC simulations using a coarse-grained model that enables to rationalize the experimental results.

4.2 Materials and methods

4.2.1 Materials

Bacteriophage T4 DNA (165.6 kilobase pairs, contour length of 57 μm) and Salmon testes DNA (~2000 base pairs) were purchased from Wako Nippon Gene and Sigma, respectively. The fluorescence dye 4,6-diamidino-2 phenylindole (DAPI; excitation/emission = 360/460 nm) and the antioxidant, 2-mercaptoethanol (ME) were also purchased from Sigma. Polyethylenimine (average $M_n \sim 1,200$, average $M_w \sim 1,300$ by LS, 50 wt.% in aqueous solution) and ferric chloride hex-ahydrate were received from Sigma. Buffer reagents including sodium chloride, sodium acetate, Trizma base, Tris acetate and EDTA were purchased from Sigma, and chloride acid and acetic acid were obtained from Riedel-de Haen. Heparin (8000-25000 g mol^{-1}) was purchased from Applichem. All chemicals and reagents were of analytical grade and used as received. Agarose and the dyes used in electrophoresis were obtained from Lonza, Switzerland and Fermentas, respectively. All experiments were performed in solutions prepared with Millipore Milli-Q deionized water (18.2 $\text{M}\Omega/\text{cm}$ resistivity).

4.2.2 Sample preparation

For the precipitation assay and agarose gel electrophoresis, the DNA-PEI-Fe(III) complexes were prepared according to the procedure that follows. A fixed volume of PEI solution (600 μL) and trivalent salt solution (50 μL) of variable concentrations were added to a solution containing DNA (2400 μL). The final concentration of DNA was equal to 20 $\mu\text{g mL}^{-1}$ (60.6 μM in phosphate groups) and was determined by the respective UV absorbance at 260 nm, considering an average molar extinction coefficient of 6600 $\text{M}^{-1}\text{cm}^{-1}$. A solution of 50 $\mu\text{g}\cdot\text{mL}^{-1}$ of double-stranded DNA possesses an absorbance of 1 [238]. All solutions were prepared in acetate buffer solution at pH 6 (5 mM CH_3COOH , 95 mM $\text{NaCH}_3\text{COO}\cdot 3\text{H}_2\text{O}$, 46 mM NaCl). The samples were subsequently left for equilibration at room temperature for 120 minutes on a mixing board. For the fluorescence microscopy experiments a different procedure was used. T4 DNA was diluted with 10 mM Tris HCl buffer at pH 7.6 containing 4% (v/v) ME and DAPI (0.25 μM). Again, constant volumes of PEI and Fe(III) with variable concentrations were added to the solution containing the DNA (final DNA concentration was 0.25 μM in terms of nucleotide units). In all mixtures, the final volume was 500 μL . An aliquot (6 μL) of each solution was placed onto the glass microscope slide, covered with a coverslip, sealed, and observed immediately. The polycation/DNA charge mixing ratio, $\beta_{\text{PEI/DNA}}$, is defined according to

$$\beta_{\text{PEI/DNA}} = \frac{C_{\text{PEI}}}{C_{\text{DNA}}} \quad (4.1)$$

where C_{PEI} and C_{DNA} are the molar concentrations of the protonated amine groups of PEI and the phosphate groups of DNA, respectively. The number of ionizable amine groups in the PEI was established for each pH value (6.0 and 7.6) from potentiometric studies, as determined in previous Chapter. The trivalent/DNA charge mixing ratio, is defined by

$$\beta_{Fe(III)/DNA} = \frac{3C_{Fe(III)}}{C_{DNA}} \quad (4.2)$$

where $C_{Fe(III)}$ is the molar concentration of Fe(III) ions. Systems will be denoted according to both charge ratios, $\beta_{PEI/DNA}$: $\beta_{Fe(III)/DNA}$ throughout the text.

4.2.3 Precipitation assay

The procedure is described in Section 3.2.5..

4.2.4 Agarose gel electrophoresis assay

Agarose (0.7 g) was dissolved in 100 mL 1 x TBE buffer (pH 8.2) by heating until boiling and subsequently allowed to cool. 5 μ L of a 10,000x solution of Gelstar[®] was added to the agarose solution which was then poured into a 10x20 cm gel tank. Potential air bubbles were removed with a pipette tip, and a gel comb was added to the gel which, in turn, was allowed to set. The pore radii of the agarose gel at concentration 0.7% (w/v) is 163.7 Å [250]. The DNA-PEI-Fe(III) samples (25 μ L), prepared according to the previously indicated procedure, were loaded into each sample well. The electrophoresis was carried out in a horizontal tank containing TBE buffer and run at 90 V for 1 h. The images of the gels were acquired using a UV transilluminator.

4.2.5 Fluorescence microscopy

Fluorescence images of DNA molecules were obtained using an Olympus BX51 M microscope, equipped with a UplanFL N 100x/1.30 oil immersed objective lens ($\infty/0.17/FN/26.5$), a filter set type U-MNU2 (360-370 nm excitation and 400 nm dichromatic mirror) and an UV-mercury lamp (100 W Ushio Olympus). Images were digitized on a computer through a video camera (Olympus digital camera DP70) and were analyzed with an image processor (Olympus DP Controller 2.1.1.176, Olympus DP Manager 2.1.1.158). Special care was taken to clean the glass microscope slides (Marienfeld) and coverslips with ethanol thoroughly before each observation to prevent DNA degradation and precipitation onto the glass surface. The observations were carried out at room temperature (≈ 25 °C). Representative images of the different systems were recorded, mostly consisting of 5 s long movies (ca.23 frames). Analyses of the images were performed using the public domain Image J, version 1.44p program (<http://rsb.info.nih.gov/ij/>). The average

values of the long axis length were calculated from measurements of 50-100 molecules. All the fluorescence microscopy images shown in this chapter were digitally enhanced.

4.2.6 Model and simulation details

Systems comprising one polyanion (DNA) titrated with shorter oppositely charged polyions (PEI), and multivalent ions (Fe(III)) have been studied using the primitive model. A polyion consists of a sequence of segments connected by harmonic bonds, with the chain flexibility regulated by angular force terms. In the primitive model, ions and chain segments are considered as hard-spheres, with point charges in the center, differing in charge and size. The solvent is considered as a continuum with a dielectric permittivity corresponding to that of water $\epsilon_r = 78.4$ at the simulation temperature, $T = 298.15$ K. The model consists of four different types of charged particles: i) connected negatively charged spheres, representing the polyanion, ii) connected positively charged spheres, representing the polycation, iii) positively charged spheres representing the multivalent ions, and iv) positive or negatively charged spheres that represent the counterions. All interactions are assumed to be pairwise additive. The total potential energy, U , is expressed as a sum of three contributions

$$U = U_{nonbond} + U_{bond} + U_{ang} \quad (4.3)$$

The nonbonded potential energy, $U_{nonbond}$, is given by

$$U_{nonbond} = \sum_{i < j} u_{ij}(r_{ij}) \quad (4.4)$$

where the summation extends over all chain segments, multivalent ions and simple ions with u_{ij} representing the electrostatic potential plus hard-sphere repulsion according to

$$u_{ij}(r_{ij}) = \begin{cases} \infty, & r_{ij} < R_i + R_j \\ \frac{z_i z_j e^2}{4\pi\epsilon_0\epsilon_r r_{ij}}, & r_{ij} \geq R_i + R_j \end{cases} \quad (4.5)$$

being z_i the valence of particle i , while e denotes the elementary charge, r_{ij} the distance between particle i and particle j , and R_i the corresponding hard-sphere radii of each particle i . The values $R_i = 2.7$ Å and $z_i = -1$ were imposed to the polyanion segments, $R_i = 2.0$ Å and $z_i = +1$ to the polycation segments, $R_i = 2.0$ Å and $z_i = +1$ or -1 to the counterions, and finally, $R_i = 3.5$ Å and $z_i = +3$ to the multivalent ions. These values were chosen considering the radius of hydration of phosphate and iron (III) ions [251]. Contiguous hard-spheres belonging to the chains also interact through a harmonic potential, U_{bond} , given by

$$U_{bond} = \sum_{c=1}^{N_c} \sum_{i=1}^{N_{seg,c}-1} \frac{k_{bond}}{2} (r_{c,i,i+1} - r_0)^2 \quad (4.6)$$

where N_c is the number of chains and $N_{seg,c}$ the number of segments of chain c . Furthermore, $r_{c,i,i+1}$ is the distance between two connected segments of chain c , $k_{bond} = 0.4 \text{ N m}^{-1}$ the bond force constant, and r_0 the equilibrium separation of a bond. We have used $r_0 = 6.0 \text{ \AA}$ for the polyanion and $r_0 = 5.6 \text{ \AA}$ typical for polyamines, for the polycations. The intrinsic, i.e. non-electrostatic, chain stiffness is incorporated by defining the desired value for the angular force constant, k_{ang} , in the angular potential, U_{ang} , defined as

$$U_{ang} = \sum_{c=1}^{N_c} \sum_{i=2}^{N_{seg,c}-1} \frac{k_{ang}}{2} (\alpha_{c,i} - \alpha_0)^2 \quad (4.7)$$

where $\alpha_{c,i}$ is the angle formed by the vectors $r_{c,i+1} - r_{c,i}$ and $r_{c,i-1} - r_{c,i}$ of chain c , $\alpha_0 = 180^\circ$ the equilibrium angle, and $k_{ang} = 1.7 \times 10^{-24} \text{ J deg}^{-2}$. All particles are enclosed and free to move in a spherical cell of radius 400 \AA . All values mentioned so far were kept constant for all studied systems. The charge ratio, β , between the polyanion (indicated by the subscript ‘‘PA’’) and polycations (subscript ‘‘PC’’), and that between the polyanion and multivalent ions (subscript ‘‘mi’’) are defined as

$$\beta_{PC/PA} = \frac{z_{seg,PC} N_{seg,PC} N_{PC}}{z_{seg,PA} N_{seg,PA}} ; \beta_{mi/PA} = \frac{z_{mi} N_{mi}}{z_{seg,PA} N_{seg,PA}} \quad (4.8)$$

where z_{seg} and N_{seg} are the charge and number of segments in the chains, respectively, and N_{PC} is the number of polycation chains in the system. Note that some of these values were above described with the subscript ‘‘i’’. In the study it was modeled the action of a different number of 30-segment long polycations, $N_{seg,PC}$, mixed with an increasing concentration of trivalent ions, upon an oppositely charged polyion, $N_{seg,PA} = 120$. In an initial approach, it was looked into systems where the total charge ratio ($\beta_{PC/PA} + \beta_{mi/PA}$) is 1 and polycations are gradually replaced by trivalent ions. Additionally, we have looked upon three different sets of systems where $\beta_{PC/PA}$ is kept constant at 0.25, 0.5, and 0.75, and the concentration of multivalent ions is varied ($\beta_{mi/PA}$ between 0.2 and 10). With the latter approach, it is followed the methodology used in the experimental part of this chapter. The distinctive characteristics of the different systems studied are summarized in Table 4.1. The notation $\beta_{PC/PA} : \beta_{mi/PA}$ will be used throughout the text to identify the systems under study.

The addition of negatively charged chains (decompacting agent) to systems with a mixture of PA-PC and PA-PC-mi was also looked upon. These studies intend to follow the decompaction of the polyanion chain. For this, four short chains with 40 beads ($z_i = -2$, $R_i = 2.0$) were added to the equilibrated PA-PC or PA-PC-mi systems. The corresponding counterions had $z_i = +1$ and $R_i = 2.0$.

Table 4.1. Summary of the systems under study.

Systems	N_{PC}	N_{mi}	$\beta_{PC/PA}$	$\beta_{mi/PA}$
0:1	0	40	0	1
0.25:0	1	0	0.25	0
0.25:0.2		8		0.2
0.25:0.3		12		0.3
0.25:0.7		28		0.7
0.25:0.75		30		0.75
0.25:2		80		2
0.25:10		400		10
0.50:0	2	0	0.50	0
0.50:0.2		8		0.2
0.50:0.3		12		0.3
0.50:0.5		20		0.5
0.50:0.7		28		0.7
0.50:2		80		2
0.50:10		400		10
0.75:0	3	0	0.75	0
0.75:0.2		8		0.2
0.75:0.25		10		0.25
0.75:0.3		12		0.3
0.75:0.7		28		0.7
0.75:2		80		2
0.75:10		400		10
1:0	4	0	1	0

For each system, Metropolis MC simulations were performed in the canonical ensemble using the Molsim package [252]. The efficiency of the simulations was improved by taking concerted moves in the chain particles. These included translation, end pivot rotation, and slithering [253]. Equilibration was performed with no less than 5×10^6 Monte Carlo steps and production runs comprised, typically, 5×10^6 steps or more, each step corresponding to a trial move for every particle.

4.3 Results and discussion

4.3.1 Experimental approach

A number of experimental techniques was used to study the influence of mixtures of condensing agents, PEI and Fe(III), on condensation or compaction of DNA. Throughout the text, we will use condensation when referring to complexes involving multiple DNA chains and compaction in single DNA chain studies (FM and Monte Carlo simulations).

4.3.2 Complexes in solution and precipitates

Precipitation studies were conducted to assess the degree of binding between DNA and a mixture of PEI and Fe(III). Upon mixing of the three components, the formation of a precipitate is observed. The precipitate is sedimented by centrifugation and DNA that remains in the supernatant is quantified using UV spectrophotometry. The approach was as follows: variations in both $\beta_{\text{PEI/DNA}}$ and $\beta_{\text{Fe(III)/DNA}}$ were imposed. The results are summarized in the color map of Figure 4.1. Two distinct regions are observed: the onset of condensation for low concentrations of PEI and full condensation at high PEI charge ratios. It is clear, however, that, as the concentration of PEI is increased, the amount of Fe(III) needed to induce condensation of DNA decreases. Also, when the concentration of Fe(III) is increased, DNA condensation is attained for decreasing values of $\beta_{\text{PEI/DNA}}$.

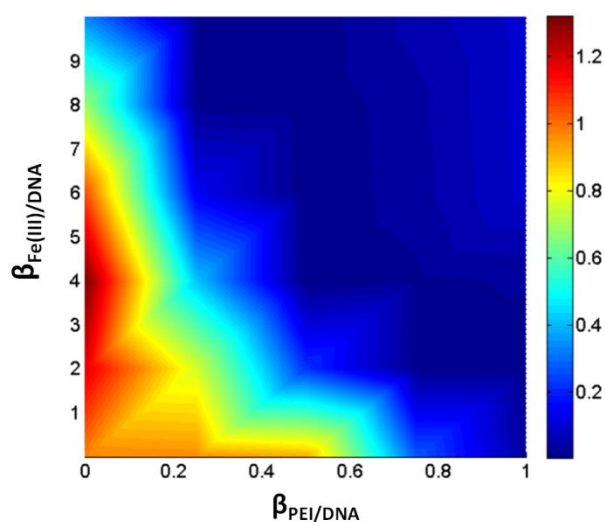


Figure 4.1. Color gradient maps for UV absorbance, measured at 260 nm, after DNA-PEI-Fe(III) complex formation and separation by centrifugation at varying concentrations of PEI and Fe(III). All values are normalized to the values of free DNA. The DNA concentration is $20 \mu\text{g mL}^{-1}$ ($60.6 \mu\text{M}$).

For a clearer assessment of the combined effect of PEI and Fe(III) in DNA condensation, we have focused on systems where values of $\beta_{\text{PEI/DNA}} = 0, 0.35, 0.5, \text{ and } 0.7$ were imposed, Figure 4.2a. As described above, for all considered systems, the increase in Fe(III) concentration leads to the precipitation of DNA. The system in the absence of PEI requires a large concentration of Fe(III)

to induce DNA condensation. In fact, we have observed no decrease in the absorbance values within the studied range. On the contrary, an increase was found instead, a consequence of that the Fe(III) ions present some absorbance at 260 nm. As the concentration of PEI is increased, full DNA condensation is obtained with smaller quantities of Fe(III). Note that even for the lower PEI concentration ($\beta_{\text{PEI/DNA}} = 0.35$), DNA condensation is significantly enhanced by the presence of trivalent ions. It is interesting to note that in all systems where PEI is present A_{260} almost reaches 0 values, which is lower than the absorbance of DNA-Fe(III) ions systems at the same Fe(III) concentration, suggesting that the majority of Fe(III) ions is uptake by the DNA-PEI complexes even for $\beta_{\text{PEI/DNA}} + \beta_{\text{Fe(III)/DNA}} > 1$. The ability of PEI to bind to divalent and trivalent ions has been described [148, 254]. This will be explored further in the next chapter.

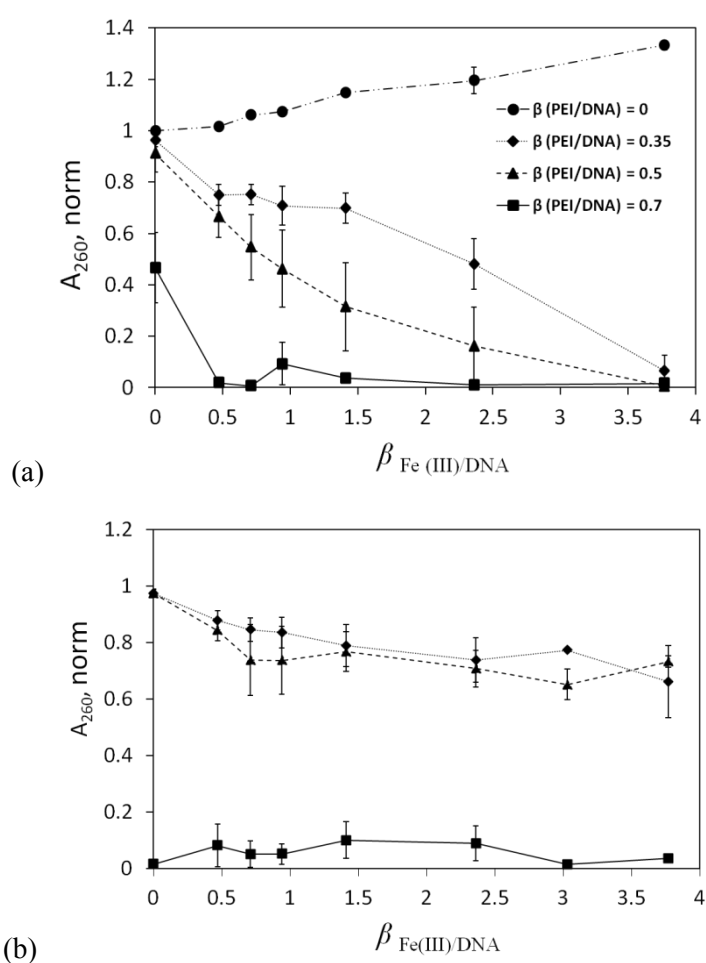


Figure 4.2. UV absorbance, measured at 260 nm, (a) after DNA-PEI-Fe(III) complex formation and separation by centrifugation, and (b) after addition of heparin ($3.1 \mu\text{M}$) to DNA-PEI-Fe(III) complexes, eventual DNA release, and separation by centrifugation. All values are normalized to the values of free DNA. The DNA concentration is $20 \mu\text{g mL}^{-1}$ ($60.6 \mu\text{M}$).

Another reason behind using mixed condensing agents in DNA compaction is to facilitate the decompaction process. We have investigated this possibility by assessing the decompaction of DNA-PEI-Fe(III) complexes using heparin, a flexible and highly negatively charged polyelectrolyte, with an average of 71 to 223 negative charges per chain, considering four charges per monomer at pH 6. In this essay, a constant concentration of heparin, 3.1 μM , was added to three sets of samples with different PEI concentrations and increasing concentration of Fe(III), Figure 4.2b. For the set of systems with the larger PEI concentration, $\beta_{\text{PEI/DNA}} = 0.7$, it is clear that the addition of heparin does not affect DNA condensation and the plot is coincident with that in the absence of heparin (squares and solid line, panel (a) vs. panel (b) in Figure 4.2). The series of samples with lower concentrations of PEI, on the other hand, show very different results. Upon the addition of heparin a substantial delay in the precipitation of DNA-PEI-Fe(III) complexes is observed, even for large Fe(III) concentrations. For example, both (0.35:3.7 and 0.5:3.7 systems) show a concentration of DNA in the supernatant very close to 0; however, the addition of heparin has regained about 70% of the absorbance.

4.3.3 Electrophoretic motion of complexes

The complexation of DNA induced by PEI at three different concentrations and increasing concentrations of Fe(III) was also monitored using agarose gel electrophoresis. Figure 4.3 gathers the three sets of systems studied at pH 6. The results show that, for all considered PEI concentrations, as the concentration of Fe(III) is increased a retention of the DNA in the wells is more visible. Panel (a) shows DNA migration for system with $\beta_{\text{PEI/DNA}} = 0.5$ and increasing concentrations of Fe(III). Full retention is achieved at $\beta_{\text{Fe(III)/DNA}} = 11.8$. For $\beta_{\text{PEI/DNA}} = 0.6$, panel (b), this is obtained around $\beta_{\text{PEI/DNA}} = 4.5$, as attested by the drastic decrease of the intensity of the band that corresponds to free DNA. This result is consistent with that obtained with UV spectrophotometry, considering that in electrophoresis the solutions are immersed in a buffer at higher pH. Similarly, when the concentration of PEI is raised to a charge ratio equal to 0.7, panel (c), full DNA retention occurs at $\beta_{\text{PEI/DNA}}$ around 2.3. As it was observed for UV experiments, the electrophoresis results show that at a constant concentration of PEI, the addition of Fe(III) enhances the neutralization of DNA.

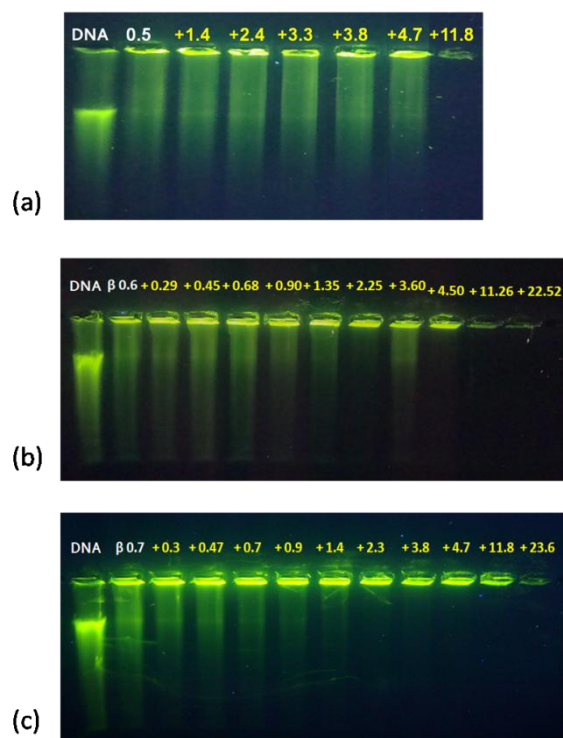


Figure 4.3. The effect of Fe(III) on DNA-PEI complexes probed using agarose gel electrophoresis. Samples were prepared at $\beta_{\text{PEI/DNA}} = 0.5$ (a), 0.6 (b), and 0.7 (c), as indicated in the second lane, and increasing $\beta_{\text{Fe(III)/DNA}}$ values, as noted in each lane. The first lane of the gel corresponds to DNA in the absence of PEI and Fe(III). The DNA concentration is $20 \mu\text{g mL}^{-1}$ ($60.6 \mu\text{M}$).

4.3.4 Conformational behavior of single DNA molecules

Fluorescence microscopy has been used to monitor DNA conformational changes upon the addition of cationic species. It has been described that individual DNA chains exhibit, in the presence of multivalent ions, a conformational change from elongated coil to an intrachain segregated molecule and, finally, to the fully collapsed state in a stepwise manner [27]. In the same study it has been shown that at intermediate Fe(III) concentrations, $\beta_{\text{Fe(III)/DNA}}$ ranging from 16 to 42, DNA coils and globules coexist in solution, whereas, at lower Fe(III) concentrations only coils were observed. We examine here the combination of Fe(III) and PEI on the conformation of T4 DNA molecules and, at a later step, the effect of adding heparin to such mixtures. Once again, we have used the approach of keeping $\beta_{\text{PEI/DNA}}$ constant at two different values, 0.5 and 0.75, and increased the amount of Fe(III) ions (Figure 4.4 and Figure 4.5). Resorting to fluorescence images, the distribution of long-axis length of T4 DNA, L , was measured for the different systems. The probability shown in each figure is normalized so that the total area is unitary.

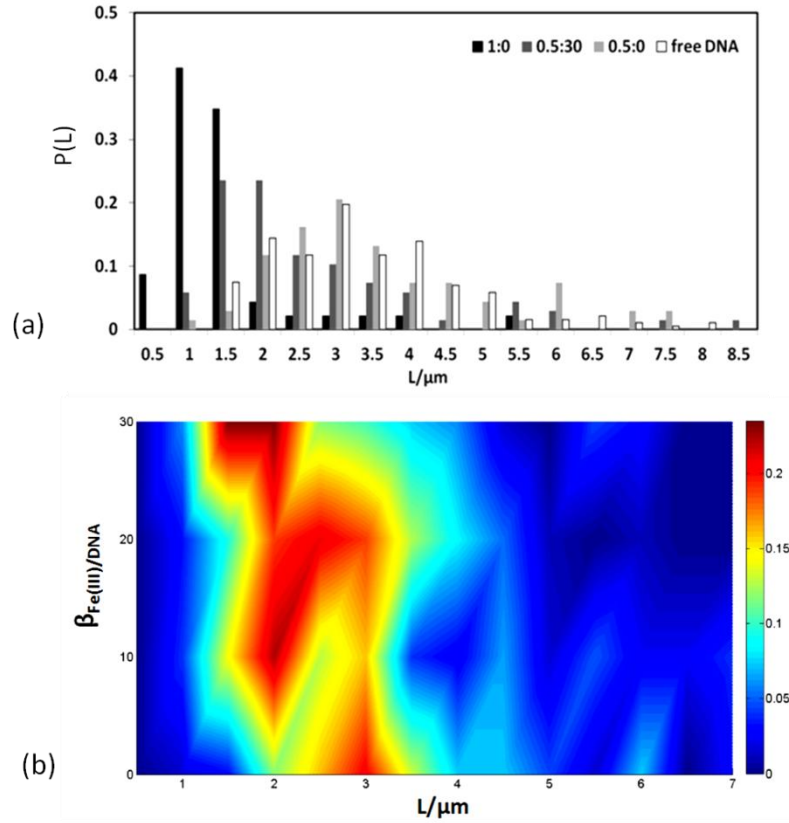


Figure 4.4. Probability distribution of the longest axis of T4 DNA molecules, L , measured for system 0.5:30. (a) Histogram of systems 0.5:0, 0.5:30, and 1:0. (b) Color gradient maps for all used concentrations of compacting agents.

Firstly is considered the system 0.5:0. This system shows a broad distribution of sizes, with a maximum of probability around 3 μm (light grey bars in Figure 4.4a). There is no significant population of molecules with an extension below 2 μm and there are some molecules that show an extended configuration with $L \geq 4$ μm , typical of free DNA molecules, ca. 4.4 μm (data not shown) and also in good agreement with the literature [30]. However, the average size indicates that there is some degree of compaction of the DNA molecules, compatible with some intrachain segregation. It is interesting to note that the addition of trivalent ions to system 0.5:0 (0.5:30, dark grey bars) induces a significant compaction of the DNA molecules, as seen by the shift in the maximum probability for lower L values, now around 1.5 and 2 μm , and a general decrease of the number of very extended molecules. If we compare these results with those of system 1:0, that in what follows will be considered the reference system, it is seen that the latter is characterized by more compact structures. Figure 4.4b collects the probability distributions of DNA extension observed for a range of $\beta_{\text{PEI/DNA}}$ values. In the absence of Fe(III), and as described above, the DNA-PEI solution possesses DNA molecules displaying some extension. At low concentrations of trivalent ions ($\beta_{\text{Fe(III)/DNA}} \sim 10$), a coexistence regime is obtained, as can be seen by the two maxima in the size distribution. Further addition of trivalent ions leads, initially, to an expansion of DNA extension and, afterwards, for $\beta_{\text{Fe(III)/DNA}} = 30$, to a compaction of the DNA, as seen by

the narrowing of the size distribution peak and shift to lower sizes. Also for comparison, the average extension of DNA molecule in the presence of Fe(III) in the higher value of $\beta_{\text{Fe(III)/DNA}} = 30$ added, is $3.4 \mu\text{m}$, which shows a weak effect of trivalent ion as condensing agent alone. Figure 4.5a shows the probability distribution of the extension of DNA molecules, obtained for systems 0.75:0 and 0.75:20. As expected, system 0.75:0 is characterized by more compact DNA molecules than system 0.5:0, shown in Figure 4.4a, due to the larger concentration of PEI. This is clear from the almost complete absence of DNA molecules with an extension exceeding $3 \mu\text{m}$ and the shift in the probability maximum to $1.5 \mu\text{m}$. When Fe(III) is added to this system (0.75:20, dark grey bars), the compaction of the DNA is further improved; the probability distribution becomes narrower and shifts towards lower values of L , with a maximum at ca. $1 \mu\text{m}$, consistent with the presence of compact DNA molecules. Looking now at the reference system (1:0), depicted in the same figure, the degree of compaction obtained from the mixture is larger than that of the reference system, which corresponds to a larger PEI concentration. It should be kept in mind, however, that the reference system might not be the system that shows maximum compaction. Often, in such dilute DNA solutions, an excess of the condensing agent is required to induce full compaction [30].

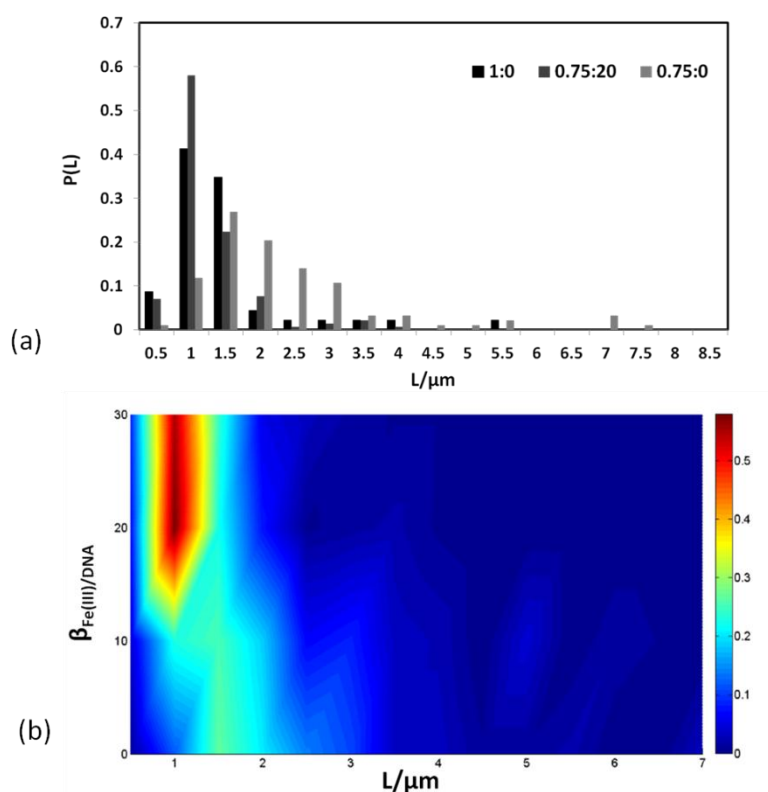


Figure 4.5. Probability distribution of the longest axis of T4 DNA molecules, L , measured for system 0.75:20. (a) Histogram of systems 0.75:0, 0.75:20, and 1:0. (b) Color gradient maps for all used concentrations of compacting agents.

A wider range of Fe(III) concentrations was additionally looked upon, as shown in Figure 4.5b. It is clear for the set of systems with $\beta_{\text{PEI/DNA}} = 0.75$ (Figure 4.5b) that the degree of compaction of the DNA molecules is larger than the corresponding systems with $\beta_{\text{PEI/DNA}} = 0.5$ (Figure 4.4b) as should be expected. Also, lower concentrations of Fe(III) are needed to achieve very compact states. This is in excellent agreement with the gel electrophoresis and precipitation studies. Next, the decompaction of the DNA-PEI-Fe(III) complexes by the addition of heparin was assessed. We have used the same approach as in the precipitate assays i.e., a constant concentration of heparin (1.8 nM) was added to two different systems, (1:0 and 0.75:20).

Figure 4.6 shows the distribution of the probabilities for the long axis of DNA systems 1:0 (a) and 0.75:20 (b) before and after the addition of heparin. It is clear that the addition of heparin leads to some decompaction of the DNA molecules. It is interesting to note that, although system 1:0 in the absence of heparin shows DNA molecules with a lower degree of compaction, when compared to 0.75:20, the addition of heparin leads to slightly more compact DNA structures than those obtained for system 0.75:20:hep.

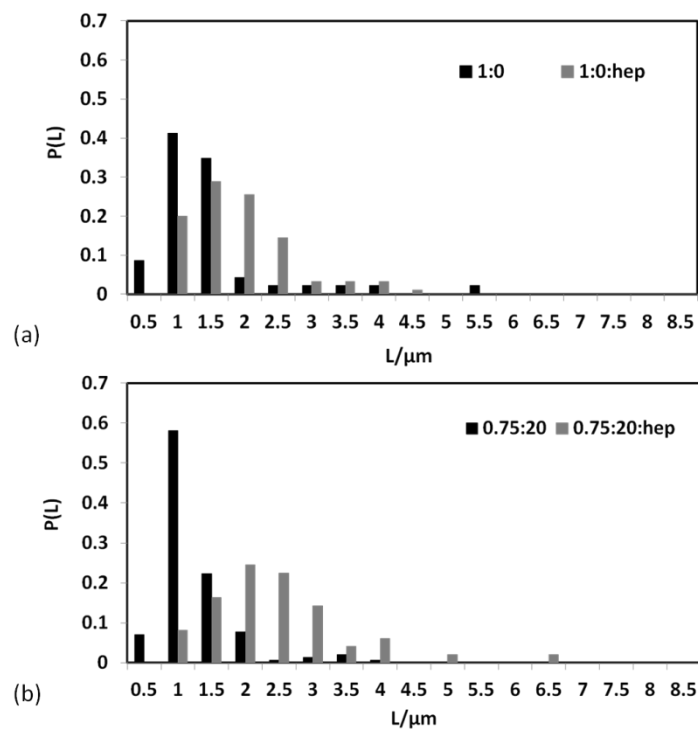


Figure 4.6. Probability distribution of the longest axis of T4 DNA molecules, L , measured for systems (a) 1:0 and (b) 0.75:20, in the absence and in the presence of the decompacting agent, heparin 1.8 nM.

Figure 4.7 shows some representative fluorescence microscopy images of T4 DNA molecules in systems 1:0 and 0.75:20, in the absence and presence of heparin. In systems 1:0 and 0.75:20 (Figure 4.7a and Figure 4.7c), globular structures are observed; these are easily recognized due to their faster diffusion and stronger fluorescence. In Figure 4.7b and Figure 4.7c we show the effect

of the addition of heparin. Whereas system 1:0 shows no significant differences in the absence and presence of heparin, system 0.75:20:hep displays a relatively large number of partially decompacted DNA molecules. This is a significant result that can be summarized as follows. The addition of Fe(III) ions to an intermediate PEI concentration induces a DNA compaction degree nearly as high as that obtained at larger PEI concentrations and facilitates DNA decompaction upon the addition of moderated concentrations of a decompacting agent.

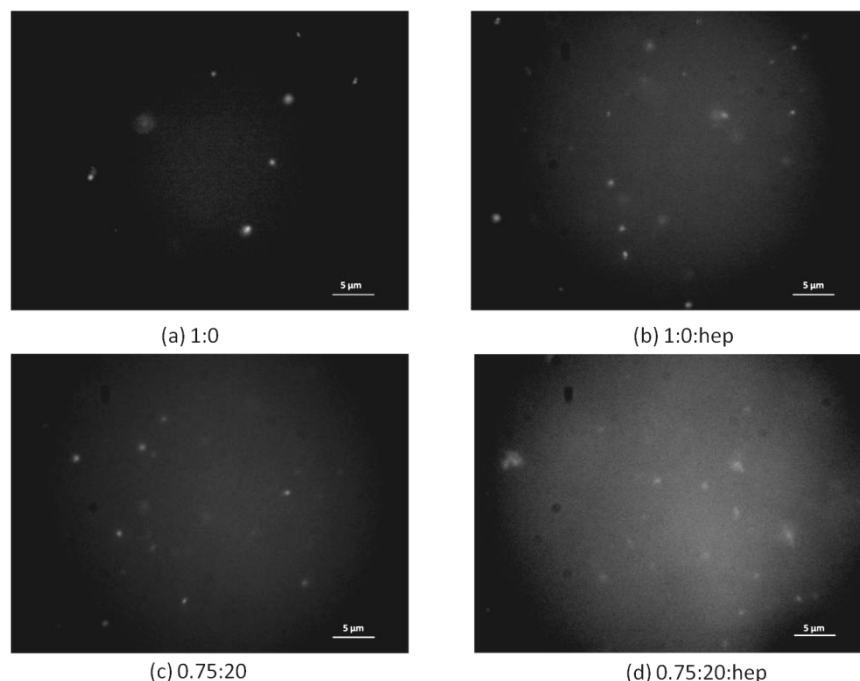


Figure 4.7. Fluorescence images of T4 DNA molecules showing the different conformations that can be observed in the different systems, 1:0 and 0.75:20, in the absence (a) and (c) and, in the presence (b) and (d) of heparin. A constant concentration of heparin, 1.8 nM, was added to all solutions.

4.4 Theoretical approach

MC simulations have additionally been performed to elucidate the results obtained experimentally. In this section, the complexity of the systems is reduced and all particles are modeled as hard spheres carrying a certain charge. The polymers, DNA and PEI are described as a segment of particles (120 and 30 monomers, respectively) and Fe(III) ions are considered as individual particles.

4.4.1 Compaction

We have started by analyzing the impact, on the compaction degree of the long polyanion (DNA), of replacing 30-segment long polycation (PEI) chains by 10 trivalent (Fe(III)) ions each (systems 1:0; 0.75:0.25; 0.5:0.5; 0.25:0.75; 0:1). For this purpose we have analyzed the radius of gyration of the polyanion, formally defined as

$$\langle R_{gyr}^2 \rangle^{1/2} = \left\langle \frac{1}{N_{seg,PA}} \sum_{i=1}^{N_{seg,PA}} (r_i - r_{CM})^2 \right\rangle^{1/2} \quad (4.9)$$

where r_i the position of segment i , and r_{CM} denotes the position of the center of mass of the polyanion chain. This quantity is a measure of extension of the chain. The probability distributions of the radius of gyration, $P(R_{gyr})$ are depicted in Figure 4.8a. As expected, a very narrow distribution centered at small values of the radius of gyration is observed for the system with four polycation chains (1:0), which is compatible with a significant lack of conformational freedom, i.e., compact PEC conformations. In the other extreme, when only trivalent ions are present (system 0:1), the distribution is very broad and shifted to the right, towards larger values of the radius of gyration. Considering the intermediate systems, it is shown that, as the polycation chains are replaced by trivalent ions, the distributions become broader and the polyanion adopt more extended conformations.

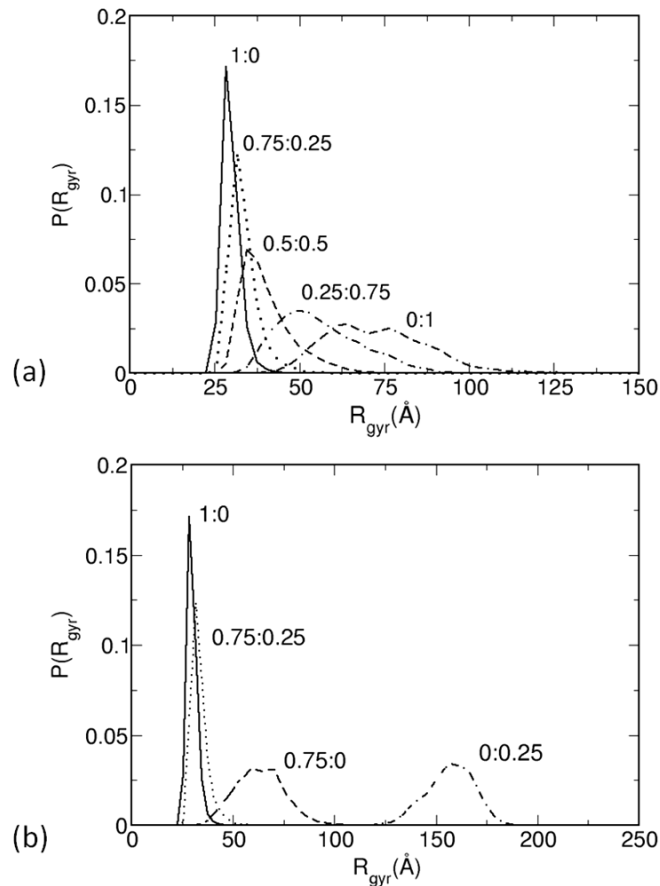


Figure 4.8. Probability distribution of the radius of gyration, $P(R_{gyr})$, for a polyanion in the presence of a varying concentration of polycations and multivalent ions, as indicated in each curve using the notation $\beta_{PC/PA} : \beta_{mi/PA}$. In panel (a) all the systems with $\beta_{PC/PA} : \beta_{mi/PA} = 1$ are compared and in panel (b) the system 0.75:0.25 is compared to the reference system and also with the systems with condensing agent separately.

However, it is interesting to note that the combination of the two different types of compacting agents promote a larger degree of compaction when compared to systems where only one of the agents was used, at the same concentration. This is, of course, not so obvious when the trivalent ions are in excess but becomes very noticeable as the number of polycations is increased. System 0.5:0.5, for example, shows some probability of finding very compact structures, particularly when compared to system 0.5:0 (not shown). System 0.75:0.25 was the mixed system among those studied, that showed the larger compaction and is also depicted in more detail in Figure 4.8b, which shows the respective $P(R_{\text{gyr}})$, as well as that of systems 0.75:0 and 0:0.25. It can be seen that, the combination of the two compacting agents largely increases the compaction of the polyanion, even though not to as large an extent as that of the chosen reference system, 1:0, also depicted in that panel. It is relevant to compare Figure 4.8b with Figure 4.4a that shows the $P(L)$ of T4 DNA molecules, measured using fluorescence microscopy. Clearly, the behavior is qualitatively very similar. A different approach has also been used: three sets of systems with different polycation concentrations and an increasing number of trivalent ions were calculated, mimicking the experimental procedures. Figure 4.9, that shows the root mean square (rms) radius of gyration, $\langle R_{\text{gyr}}^2 \rangle^{1/2}$, of the polyanions in the presence of different polycation concentrations versus $\beta_{\text{mi/PA}}$, summarizes the results.

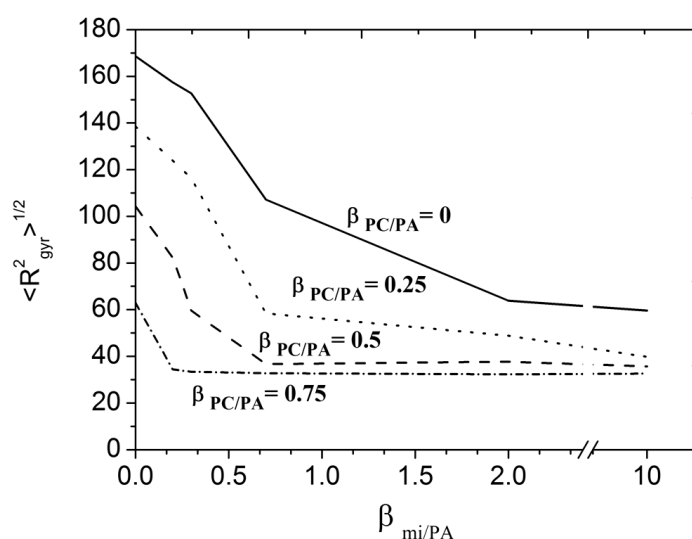


Figure 4.9. Rms radius of gyration, $\langle R_{\text{gyr}}^2 \rangle^{1/2}$, for the polyanion in the presence of a constant concentration of polycation chains, $\beta_{\text{PC/PA}} = 0, 0.25, 0.5,$ and 0.75 , as indicated in the respective curves, and an increasing concentration of trivalent ions.

As observed experimentally, the systems with larger concentration of polycations show a larger compaction (smaller sizes) in the absence of multivalent ions. It is also shown that the addition of trivalent ions progressively increases the degree of compaction of the polyanion for all systems.

As expected, systems with a higher $\beta_{PC/PA}$ require a smaller number of trivalent ions to reach full compaction of the polyanion. For $\beta_{PC/PA} = 0.75$, a small concentration of trivalent ions ($\beta_{PC/PA} = 0.2$) promotes an average radius of gyration for polyanion of 34 Å, similar to that obtained for the reference system, 1:0 (30 Å). This value remains constant with further addition of trivalent ions. For $\beta_{PC/PA} = 0.5$, the $\langle R_{gyr}^2 \rangle^{1/2}$ of the polyanion decreases as trivalent ions are added to the system, until it reaches the lowest value for $\beta_{mi/PA} = 0.7$. Again, the degree of compaction of the polyanion reaches values that are very close to those obtained for systems 1:0 and 0.75:0.25. When the number of polycations is further decreased ($\beta_{PC/PA} = 0.25$) it is observed that the addition of trivalent ions leads to a significant reduction of the polyanion extension, particularly at $\beta_{mi/PA} = 0.7$; however, it does not reach the degree of compaction of the previously mentioned systems. The trivalent ions alone with polyanion were simulated and the lowest value of polycation radius of gyration was 60 Å, obtained for $\beta_{mi/PA} = 10$ (Figure 4.9). It should be noted that Figure 4.9 is qualitatively very similar to Figure 4.2a, that roughly describes the % of DNA present in the supernatant. It was now established that the model chosen is able to reproduce the most significant characteristics of the DNA-PEI-Fe(III) systems. A more complete description of the polyplexes, desirable for a better understanding of the systems at study, will now be performed, resorting to two different analyses. One shows the preferential positioning of the compacting agents along the polyanion chain (contact analysis), while the other calculates the number of sequential segments of the polyanion that are linked to each polycation chain (linking analysis).

Figure 4.10 shows the results from the contact analysis, looking individually at the polycation segments, panel (a), and the trivalent ions, panel (b). It can be seen that the number of polycation segments and trivalent ions, in the vicinity of the polyanion, increases as their respective concentration increases. Another common feature is the decrease on the number of compacting agents towards the ends of the polyanion, which can be attributed to a weaker electrostatic attraction to the polyanion. In the previous work [40], focused solely on polyanion-polycation mixtures, it has been observed that when only one polycation chain is present, it tends to reside in the central part of the longer chain. For two and three chains, there is some repulsion between them and the distribution shows one and two minima, respectively. Finally, when four chains are present, these are evenly distributed along the polyanion chain, showing no preferential positioning along the long chain. In the presence of trivalent ions, the polycations show a larger range of action along the polyanion, as noted by the wider distribution of segments. Additionally, the degree of compaction is such that the average positioning of different polycation chains can no longer visible be discerned. Figure 4.10b indicates the contacts of the trivalent ions along the polyanion and clearly shows that the trivalent ions tend to occupy the regions of the polyanion that are less populated by the polycation chains, such as the polyanion extremities.

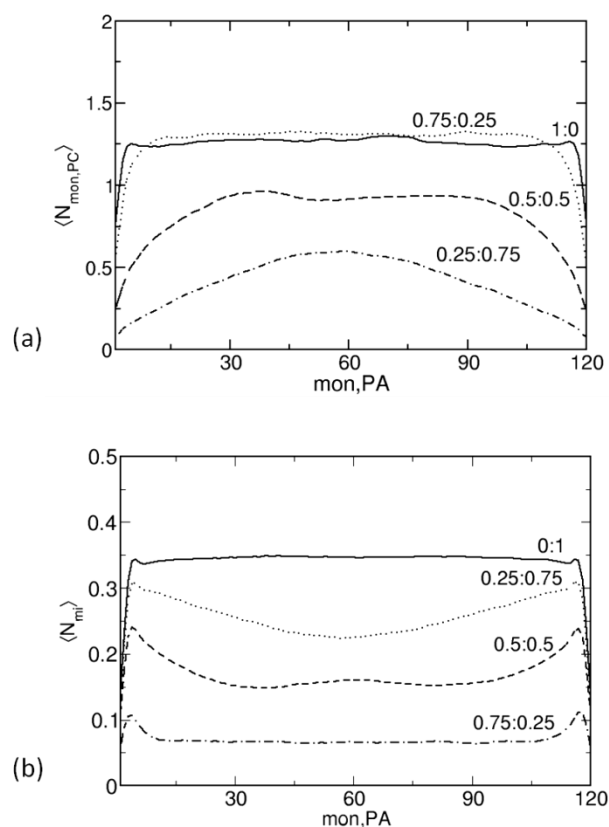


Figure 4.10. Contact analysis, displaying the preferential positioning of polycations and trivalent ions along the polyanion. Averaged number of (a) polycation segments and (b) trivalent ions, at a distance not exceeding 8 \AA from each polyanion segment.

This provides a clue on the potential mechanism of the enhanced compaction of the polyanion in the presence of multivalent ions. Polyplexes often show intrachain disproportionation, in which the longer polyion adopts a partially compacted configuration. This is especially so for systems with relatively long condensing agents close to charge neutralization [255].

The preferential positioning of the trivalent ions between the polycation chains suggests that the multivalent ions induce some local folding, enhancing the probability of the polycation chains to bridge (link) parts of the polyanion chains that are significantly far apart, and reducing the probability of finding very extended conformations. To elucidate this we have resorted to a linking analysis. This, together with the contact analysis, can provide valuable information regarding the topology of the polyplexes [255]. In the linking analysis, the segments in the longer chain that are in contact with segments of the shorter one are identified, and those two that are further apart along the chain selected. The number of segments between (and including) these two, corresponds to the indicator L_{Link} . For example, one polycation chain that is simultaneously in contact with the two end segments of the polycation chain will result in $L_{\text{Link}} = N_{\text{seg,PA}}$. Contact is considered for a distance between segments in different chains not exceeding 8 \AA . The results are depicted in Figure 4.11.

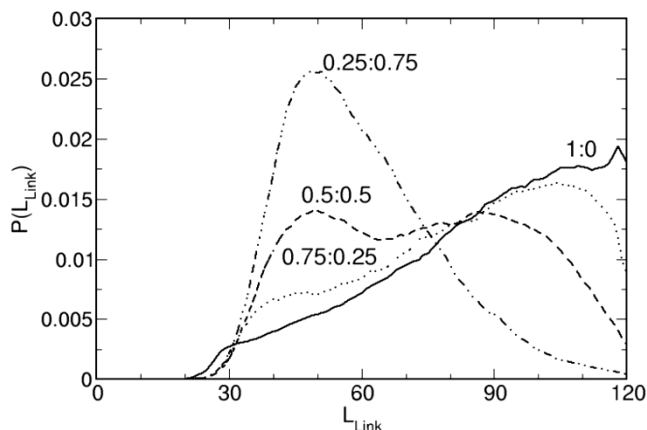


Figure 4.11. Probability distribution of L_{Link} (see text for detail).

Let us, first, consider system 1:0, the one that shows the most compact conformation. The maximum probability occurs for about 120 segments, indicating that in a large number of configurations the polycations are in contact with both ends of the polyanion simultaneously.

With 3 polycations and trivalent ions (0.75:0.25), the topology of the polyplexes remains very compact, but a convoluted maximum appears at approximately one third of the polyanion chain, indicating that while most of the polycations are able to reach segments of the polyanion that are significantly far apart (large values of L_{Link}), some polycation chains are in an extended conformation along the polyanion, and only interact with a third of the latter. This is a strong indication of intrachain disproportionation. Snapshots in Figure 4.12 show the two main conformations adopted by this system. This situation is significantly different from that observed for system 0.75:0 (not shown).

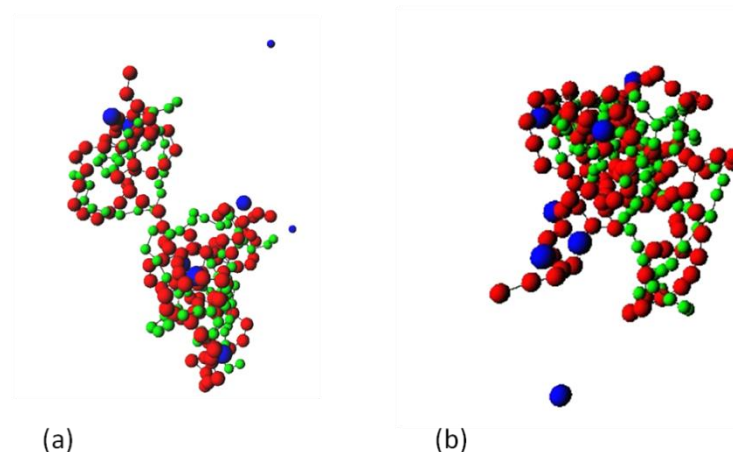


Figure 4.12. Representative snapshots showing distinct conformations of the polyanion in the presence of polycations and trivalent ions (system 0.75:0.25). The polyanion and polycations segments are represented in red and green, respectively, and the trivalent ions in blue.

In the latter case, two maxima are obtained, suggesting, again, partially folded polyanion conformations, but the maximum that corresponds to polycations linking about one third of the chain shows the largest probability, indicating a much larger probability of finding extended conformations. This can be seen in the $P(R_{\text{gyr}})$ in Figure 4.8, where system 0.75:0.25 shows a much narrower distribution of sizes than the neat 0.75:0 system. For system 0.5:0.5, two very distinct maxima are found, at lengths of approximately 40 and 90 segments. Also, there is some probability, although small, for the 2 polycation chains, in the presence of trivalents, to be in contact with all segments along the polyanion chain, which was not observed in the absence of trivalent ions. In fact, for system 0.5:0, polycations are fully stretched onto an equally extended polyanion chain (data not shown). Figure 4.13 provides snapshots showing three different polyplexes topologies obtained for system 0.5:0.5. Finally, for system 0.25:0.75, the distribution indicates that the polycation is stretched along the polyanion chain. However, it should be noted that the distribution is skewed to the right, indicating some degree of compaction of the polyanion already in this system.

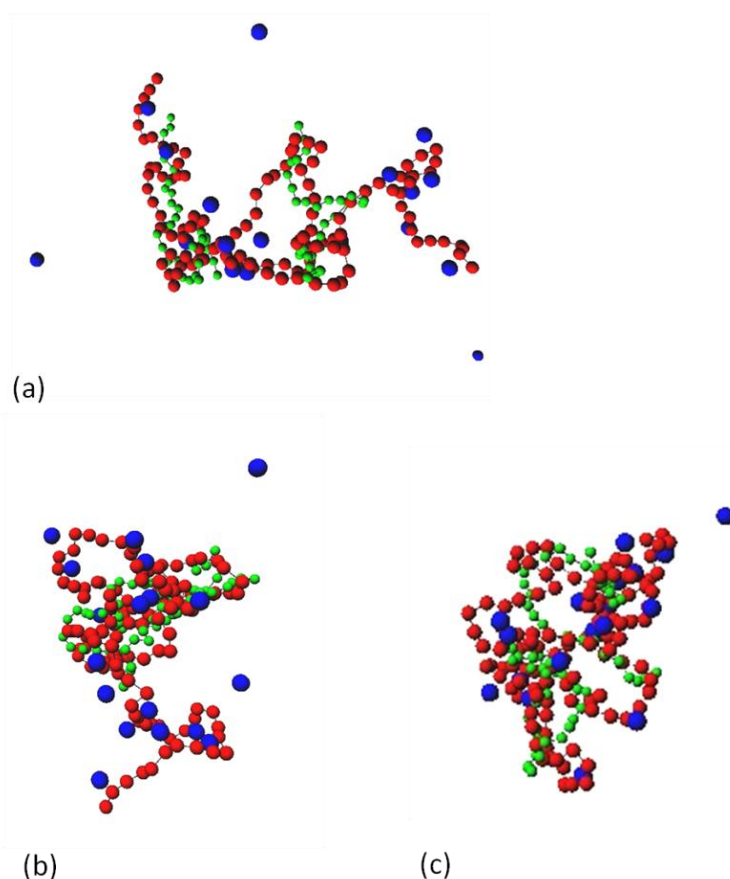


Figure 4.13. Representative snapshots showing distinct conformations of the polyanion in the presence of polycations and trivalent ions (system 0.5:0.5). The polyanion and polycations segments are represented in red and green, respectively, and the trivalent ions in blue.

In summary, the contact analysis show that the trivalent ions occupy, preferentially, areas of the polyanion less populated by the polycation chains, which suggests that the ions induce a local folding. Such folding seems to be enough to allow a longer range of the polycation over the polyanion, as shown by the linking analysis, and the narrowing of the size distribution of the polyanion, by drastically reducing the probability of finding very extended configurations. The mechanism partially explain the high efficiency obtained for combining both agents, but it should be noted that chelation between PEI and Fe(III) may play some role in this action.

4.4.2 Decompaction

The decompaction of PA-PC-mi complexes was, following the experimental approach, investigated using MC simulations. This was accomplished by adding three 40-segment long negatively charged polyelectrolyte chains, inspired in heparins, to selected PA-PC-mi systems. The results are depicted in Figure 4.14. The addition of heparin-like molecules induces some degree of decompaction for all systems, as observed by the broadening of the size distribution and their shift towards larger sizes. It is also observed that systems with mixed compacting agents are able to achieve more extended conformations upon the addition of the decompacting agents.

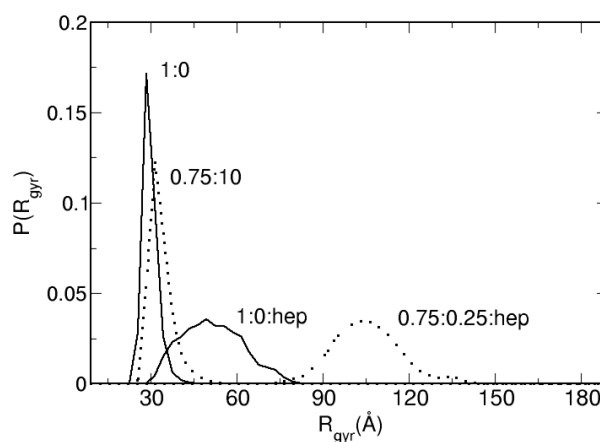


Figure 4.14. Probability distribution of the radius of gyration, $P(R_{\text{gyr}})$, for the polyanion in different systems in the presence (:hep) and absence of the decompacting agent, as indicated for each curve.

System 1:0, the most compact, shows, upon the addition of the decompacting agent (1:0:hep), a $P(R_{\text{gyr}})$ distribution centered at around 60 Å. A comparison with the distributions obtained for the pure PA-PC systems (not shown), as well as visual inspections of the snapshots, indicate that the most probable conformation is one in which three polycation chains remain in contact with the polyanion. As for system 0.75:0.25, the same occurs but in this case only 2 chains are left in contact with the polyanion, with a $P(R_{\text{gyr}})$ distribution centered around 109 Å. These final conformations are observed in representative snapshots in Figure 4.15. It can be seen that some of

the polycation chains have left the longer polyanion, which is associated with the remaining polycation chains and some trivalent ions. Replacing one polycation chain by 10 trivalent ions did facilitate, to a large extent, the decompaction of the polyanion. It should be noted that these are very coupled systems and the probability of slightly different situations cannot be completely ruled out.

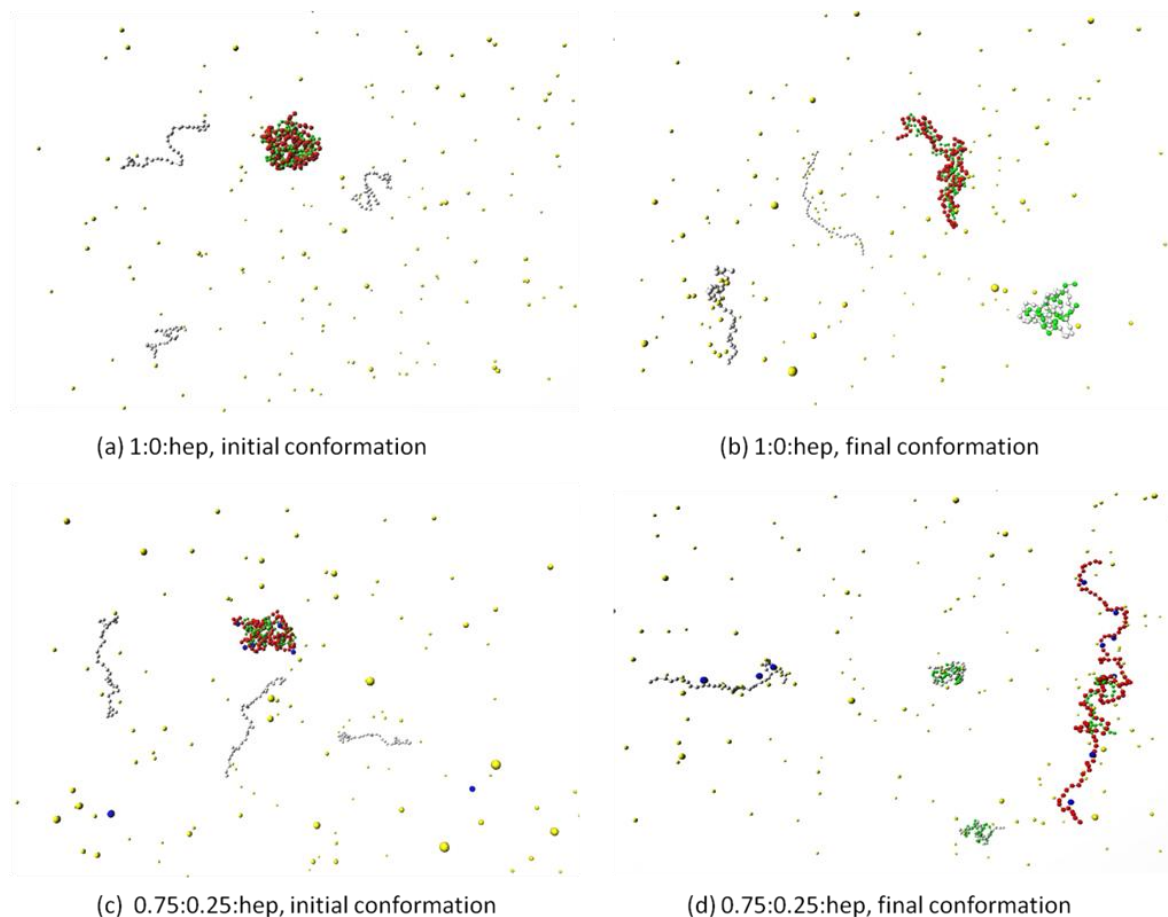


Figure 4.15. Representative snapshots showing the different conformational states of the polyanion (red) upon the addition of a decompacting agent, for systems 1:0 (panels a and b) and 0.75:0.25 (panels c and d). The initial configurations, in the panels to the left, show the free heparins and the compact polyplexes, while the final configurations, in the panels to the right, correspond to various degrees of polycation release. The polyanion, polycation, and heparin segments are represented in red, green, and white, respectively, the trivalent ions in blue, and the counterions of the heparins are displayed in yellow.

4.5 Conclusion

In this chapter was investigated the influence of mixtures of polycations and trivalent ions on DNA condensation and precipitation using experimental techniques and MC simulations. It was found that the presence of Fe(III) ions enhances the condensation of DNA in DNA-PEI mixtures. The larger the concentration of PEI, the lower is the amount of Fe(III) ions necessary to induce

reasonable degrees of condensation. It was also shown that combining both agents for $\beta_{\text{PEI/DNA}} < 1$, it is possible to obtain a degree of condensation, higher than that for $\beta_{\text{PEI/DNA}} = 1$, in the absence of Fe(III). The macroscopic behavior, monitored using UV spectrophotometry and gel electrophoresis, was qualitatively the same as that observed for single-molecule experiments, via fluorescence microscopy. Although coherent, complementary aspects have been pointed out by the different experimental techniques. The experimental results were rationalized using MC simulations. These have shown the same qualitative behavior as that observed in the experimental part. In addition, it could be found that the trivalent ions occupy, preferentially, the areas of the polyanion that are less populated by the polycation chains, which suggests that the trivalent ions enhance the degree of compaction by inducing a local folding of the longer chain, allowing, thus, a longer range of action of the polycations, and a narrowing of the size distribution. One of the reasons behind using a mixture of cationic agents is to facilitate the decondensation of the DNA complexes using a decondensing agent. This hypothesis has been tested experimentally and resorting to simulations. It was shown that the addition of a small concentration of heparin induced the, at least partial, release of DNA from the complexes when a lower concentration of PEI was present, while keeping intact the complexes formed at larger concentrations of PEI, even though the degree of condensation of DNA in both systems, prior to the addition of heparin, was very similar.

CHAPTER 5

Effect of PEI architecture

5.1 Introduction

Beyond the electrostatic forces in the DNA-PEI-Fe(III) ternary system, well characterized in the last chapter, it is known that metal cations may bind to PEI via the lone electron pairs of the nitrogen atoms. In the literature, it is reported the metal chelation efficiencies of both bPEI and lPEI [148, 256-258] and differences emerged when different architected PEI structures are employed. The results showed that the branched structure presents a chelating capacity 10 times higher than that of lPEI [148], and it is argued that the presence of neighboring donor atoms in the chain tends to control the strengths of the interaction.

Motivated by these dissimilarities, this chapter aims at studying the influence of PEIs structures, bPEI and lPEI, in a range of molecular weights, on the formation of the ternary complexes. Herein is included an overview of the physicochemical properties of the polyplexes, in terms of degree of condensation, size and surface charge. Due to difficulties encountered to analyze in detail the pH behavior of lPEI, from now on the complexes are prepared in terms of the molar ratio concentration between positive and negative charges, considered as the N/P ratio. Moreover, after a detailed description of the condensation and decondensation of DNA in previous chapters, henceforth our focus involves the study of complexes suitable for gene delivery that generally are generated at high values of N/P ratio, and the advantages introducing Fe(III) as a condensing agent discussed.

5.2 Materials and methods

5.2.1 Materials

Salmon testes DNA (~2000 base pairs) was purchased from Sigma, UK and used as received. Commercial branched polyethylenimines with average Mw 1.2 (bPEI1.2) and 10 kDa (bPEI10) were purchased from Polysciences, Inc (USA) and Alfa Aesar (UK), respectively. Commercial linear polyethylenimines with average Mw 2.5 (lPEI2.5) and 25 kDa (lPEI25) were purchased from Polysciences, Inc (USA). Ferric chloride hexahydrate and buffer reagents, sodium chloride, sodium acetate, Trizma base, boric acid and EDTA were purchased from Sigma (UK), and acetic acid was from Riedel-de Haens (Germany). Agarose and the dyes used in electrophoresis were obtained from Lonza, Switzerland and Fermentas, Germany. All chemicals and reagents used were of analytical grade.

5.2.2 Sample preparation

DNA-PEI-Fe(III) complexes were prepared according to the following procedure: to a fixed volume of DNA solution (2400 μL) were added variable concentrations of PEI solution (600 μL) and trivalent salt solution (50 μL). Firstly, PEI is added to DNA and left to equilibrate for 20 minutes and, subsequently, the Fe(III) solution is added to the mixture. The trivalent salt solutions were always freshly prepared just prior to the addition to the DNA-PEI mixture. The final concentration of DNA was equal to 20 $\mu\text{g mL}^{-1}$ (60.6 μM in phosphate charges) as determined by the respective UV absorbance at 260 nm. A solution of 50 $\mu\text{g mL}^{-1}$ of double-stranded DNA possesses an absorbance of 1 [238]. All solutions were prepared in acetate buffer solution pH 6 (5 mM CH_3COOH , 95 mM $\text{NaCH}_3\text{COO}\cdot 3\text{H}_2\text{O}$, 46 mM NaCl). The samples were subsequently left for equilibration at room temperature for 120 minutes on a mixing board. Throughout the study, specific N/P ratio was determined considering that the mass of 330 g mol^{-1} corresponds to one phosphate group (base) on DNA and, in PEIs, the mass of 43 g mol^{-1} corresponds to one amine group ($-\text{CH}_2\text{CH}_2\text{NH}-$). The same calculation was performed considering now the molar concentration of positive charges for the Fe(III) in solution and represented as the Fe(III)/P ratio. It should be noted that both N/P and Fe(III)/P ratios were established on the basis of the amounts of PEI/DNA and Fe(III)/DNA added to the solution. They do not necessarily reflect actual charge ratios.

5.2.3 Precipitation assay

The procedure is described in section 4.2.3.

5.2.4 Agarose gel electrophoresis assay

The procedure is described in section 4.2.4.

5.2.5 Size and zeta potential analysis

The hydrodynamic radius and the zeta potential of the DNA-PEI-Fe(III) complexes were assessed by dynamic light scattering in a Delsa Nano C Submicron (Beckman Coulter, Krefeld, Germany). Samples were prepared, equilibrated and measured in triplicate at 25 °C with a detection angle of 160°. The standard error of the mean was calculated from the three independent measurements.

5.3 Results and discussion

Next, the results of the physicochemical characterization of the DNA complexes, prepared using PEIs of different architectures and Mw, in terms of stability, size and charge will be discussed. The effect of the addition of trivalent ions to these mixtures is, subsequently, assessed using the same methodologies. In what follows, condensation will be used in general when referring to complexes involving, in most cases, multiple (compacted) DNA chains. Precipitation and aggregation will be used for the formation of insoluble and large complexes, respectively.

5.3.1 DNA–bPEI and DNA–lPEI complexes

The DNA condensation ability of the different PEIs, bPEI (1.2 and 10 kDa) and lPEI (2.5 and 25 kDa), was analyzed using UV spectrophotometry (UV) and agarose gel electrophoresis assays (GE), see Figure 5.1. Panels (a) and (c) show the percentage of DNA in the supernatant after PEI was added to the DNA solution, left to equilibrate for 2 hours, and then centrifuged, as described in the experimental part. PEI and DNA alone are soluble but, their interaction leads to the neutralization of the components and, the polyplexes formed become insoluble as their charge approaches zero. Using UV combined with centrifugation, it is possible to follow the condensation of DNA as it precipitates out of solution. For all different systems, it is seen that the increase in the concentration of the condensing agent (PEI) results in a decrease of the absorbance at 260 nm (UV) and of the intensity of the DNA band (GE), both indications of DNA condensation. Figure 5.1a shows the DNA condensation profile in the presence of branched PEI molecules. Surprisingly, the shortest bPEI (bPEI1.2) neutralizes and, consequently, precipitates the DNA for lower N/P ratios than the larger bPEI (bPEI10). For bPEI1.2, DNA absorbance in the supernatant mainly disappears at N/P = 1.2, in agreement with gel electrophoresis results, Figure 5.1b. In the presence of bPEI10, DNA reaches neutralization at N/P value of 2.5. In this system, a near complete retention of DNA is observed at N/P = 1.8 (GE), which is lower than in the UV assays. It should be noted, however, that faint bands are still perceivable in the gel for N/P values of 6 for both systems, indicating the presence of a low concentration of small negatively charged DNA complexes. System bPEI1.2 shows migration of DNA complexes towards the anode for N/P = 10, Figure 5.1b, indicating the presence of positive polyplexes, whereas for bPEI10, DNA

overcharging is not observed. Note, however, that such phenomenon is not easily monitored using gel electrophoresis. For IPEI25 at $N/P = 2$ no significant amount of DNA is detected in the supernatant, while for IPEI2.5 a N/P value of 2.5 is needed to completely precipitate DNA, see Figure 5.1c. In this case, the longer PEI chains condense DNA more efficiently. This trend was also confirmed using GE. Figure 5.1d shows that the majority of the DNA molecules are retained in the wells for N/P values above 1.4 and 2 for IPEI25 and IPEI2.5, respectively, in good agreement with the precipitation assays. Again, light bands are still visible in the gels for higher N/P values. Also, overcharging was now observed for the two systems, at $N/P = 10$ for IPEI2.5 and at $N/P = 6$ and 10 for IPEI25, with complexes sufficiently small to be mobile. In general, the trend indicated by the UV and GE assays is consistent. However, the values of the N/P ratio where electrophoretic mobility ceases do not exactly correspond to those where the presence of DNA in the supernatant is practically null. This discrepancy can be ascribed to the size of complexes and to the different conditions found in bulk solution and in the electrophoresis gels. The unexpected ordering found for the bPEIs can, at least partially, be ascribed to the fact that a higher percentage of protonated amine groups is present in bPEI1.2, at pH 6. Following a potentiometric procedure used in the Chapter 3, it was calculated that at pH 6, 63.9% of the groups in bPEI10 are protonated, a value lower than that found for bPEI1.2, 78.8%. However, this moves the onset of condensation for a N/P ratio of ca. 0.9 for bPEI1.2 and 1.5 for bPEI10, which is not sufficient to reverse the order of effectiveness. Moreover, to ensure the stability of the complexes, UV analyses were performed for samples that were left to equilibrate for 24 hours before centrifugation (data not shown). The results are similar to those found when the samples are equilibrated for 2 hours.

5.3.2 DNA–bPEI and DNA–IPEI complexes: addition of Fe(III) ions

To study the influence of PEI chain length and architecture on the formation of the DNA-PEI-Fe(III) ternary complex, the different PEI chains were inspected again. For a clear assessment of the effect of Fe(III) on DNA condensation, N/P values were selected before the onset of condensation, according to the results in the previous section. The addition of Fe(III) ions is represented in Figure 5.2 as Fe(III)/P values.

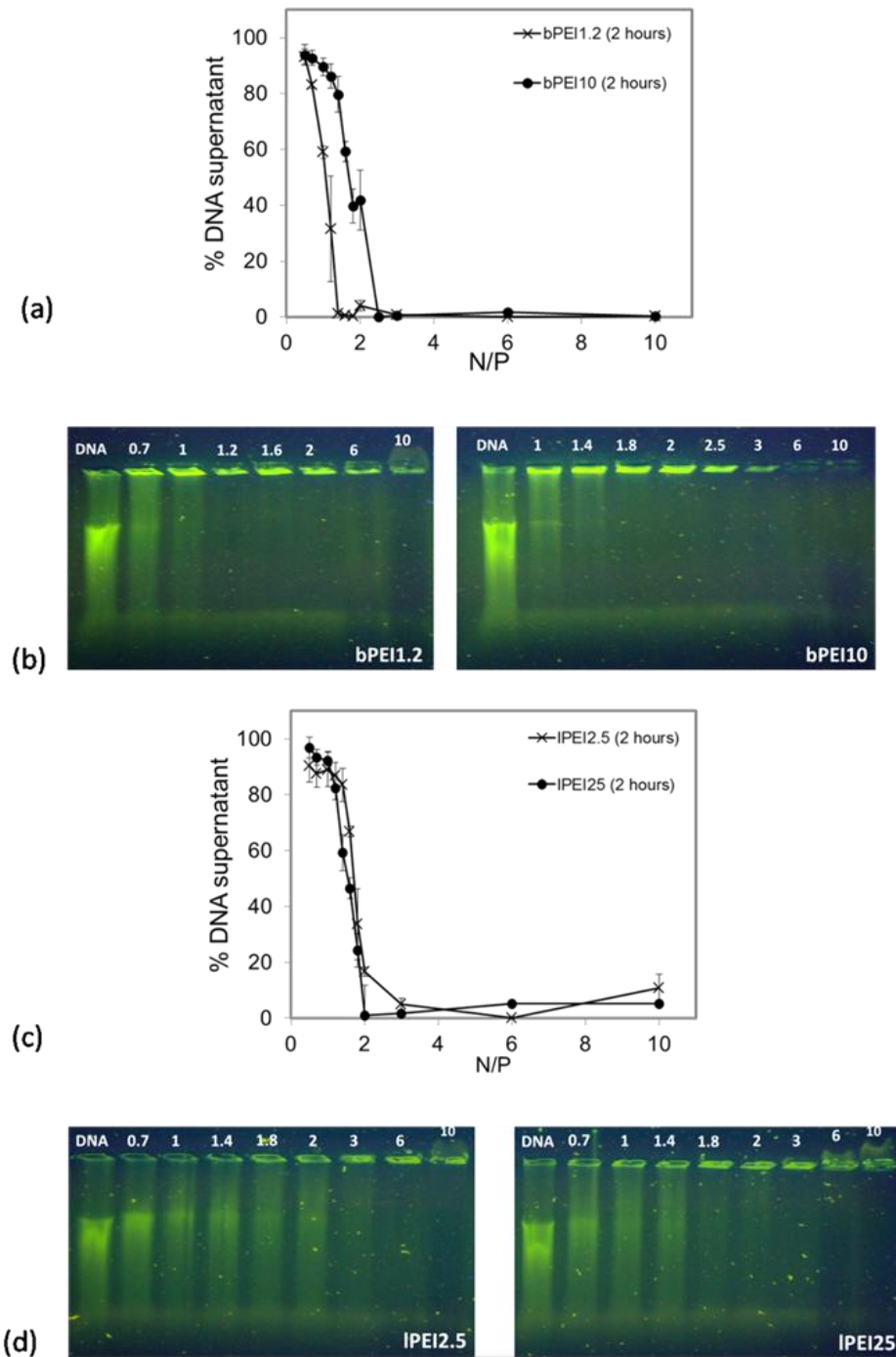


Figure 5.1. UV absorbance, measured at 260 nm, and agarose gel electrophoresis (GE) for DNA-bPEI are represented in panels (a) and (b), respectively. The corresponding results for DNA-IPEI complexes are shown in panels (c) and (d). In GE, the first lane of the gel corresponds to DNA in the absence of PEI and the next lanes correspond to increasing N/P values, as noted in each lane. The DNA concentration is $20 \mu\text{g.mL}^{-1}$ ($60.6 \mu\text{M}$).

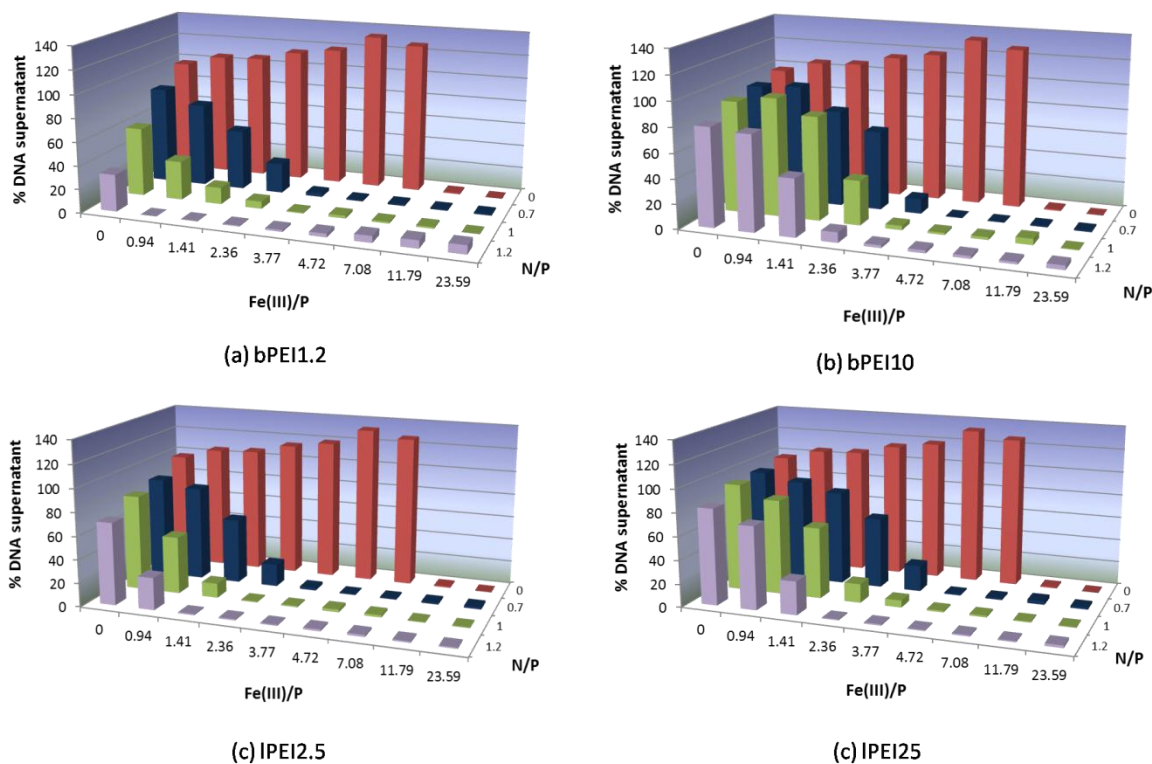


Figure 5.2. UV absorbance, measured at 260 nm, after DNA-PEI-Fe(III) complex formation, equilibration for 2 hours, and separation by centrifugation. Panels correspond to (a) bPEI1.2, (b) bPEI10, (c) IPEI2.5, and (d) IPEI25, respectively.

The results reveal that the addition of Fe(III) to the DNA-PEI complex enhances the condensation of DNA, in agreement with previous chapter. At $N/P = 0.7$, for all PEIs in the absence of Fe(III) ($Fe(III)/P = 0$), the percentage of DNA in the supernatant is close to 100%. The addition of $Fe(III)/P = 3.7$ promotes a nearly complete condensation of DNA, irrespective of the type of PEI that is used. Figure 5.3 shows GE results of the same systems. Again, at $N/P = 0.7$ and with increasing concentrations of Fe(III) all the DNA complexes are neutralized at ca. $Fe(III)/P = 4.7$, with the exception of bPEI1.2 that neutralized at a lower $Fe(III)/P$ value, corroborating the results in the absence of Fe(III). Considering bPEIs, Figure 5.2a and b, it is seen that the addition of Fe(III) maintains the previously observed trend in which the shorter polycation is more efficient. Interestingly, IPEI now follows the same trend, Figure 5.2c and d. In fact, the presence of Fe(III) makes IPEI2.5 a more efficient condensing agent than IPEI25, thus reversing the order found in the absence of Fe(III). This result is compatible with a previously suggested mechanism (Chapter 4) for DNA condensation in the presence of these mixed condensing agents, that suggests the positioning of Fe(III) ions in the empty spaces between polycation chains. Note that a larger number of shorter chains allows more frequent alternation between PEI and trivalent ions. The addition of Fe(III) ions to these systems seems to reinforce the positive charge in the systems

where the less efficient PEIs are present, IPEI2.5 and bPEI10, equalizing their ability for DNA condensation.

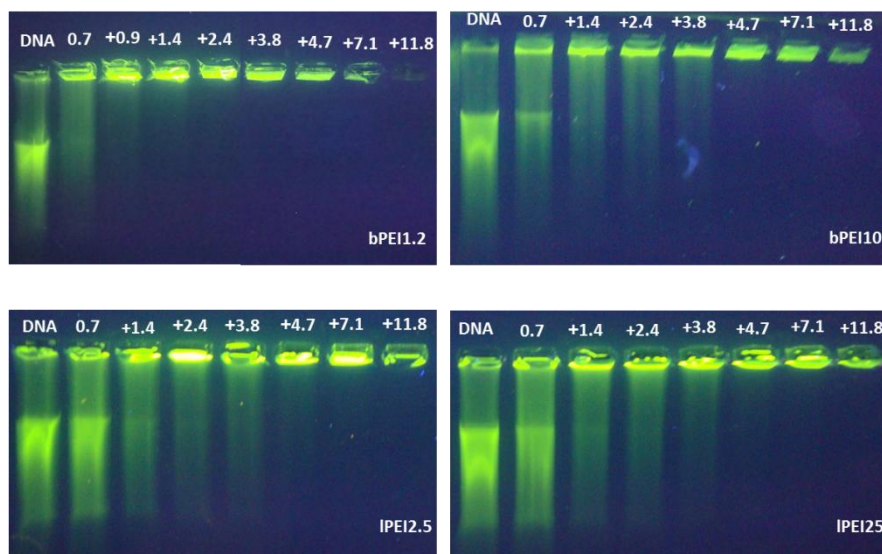


Figure 5.3. Binding efficiency of DNA-PEI-Fe(III) polyplexes at various Fe(III)/P. The upper panels correspond to bPEI1.2 (left) and bPEI10 (right) and the lower panels to IPEI2.5 (left) and IPEI25 (right). The first lane of the gels correspond to free DNA, the second to DNA-PEI, N/P = 0.7. The numbers in each of the remaining lanes, preceded by (+), indicate the Fe(III)/P values.

As for the DNA-PEI complexes, the equilibration and stability of DNA-PEI-Fe(III) complexes were checked by evaluating the DNA concentration in the supernatant after 2 and 24 hours of equilibration (Figure 5.4).

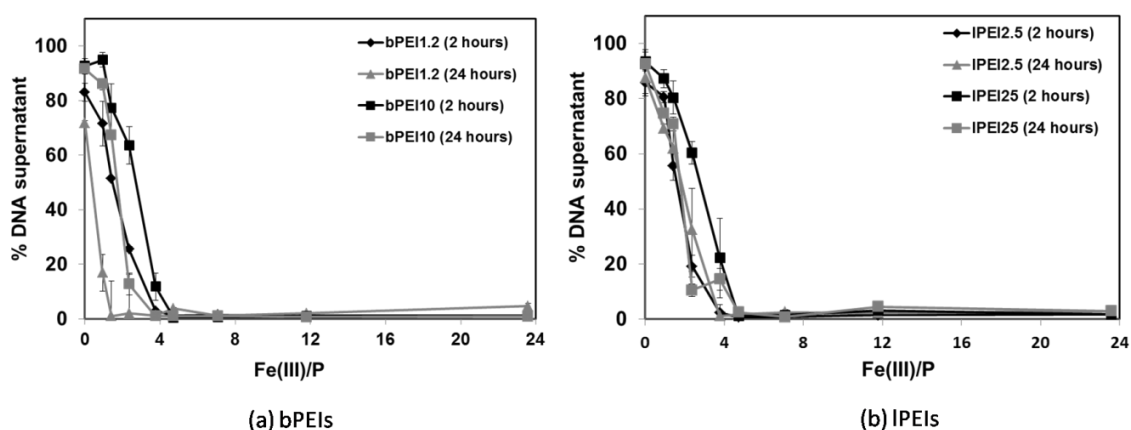


Figure 5.4. UV absorbance, measured at 260 nm, after (a) DNA-bPEI-Fe(III) and (b) DNA-IPEI-Fe(III) complex formation and separation by centrifugation, after 2 and 24 hours of equilibration. The value of N/P = 0.7 was kept for all polyplexes represented.

The differences in the precipitation profiles with time are more significant for bPEI. The precipitation profiles for both IPEIs become very similar after 24 hours, reducing thus the differences observed with chain length upon the addition of Fe(III). For bPEI, on the other hand, there was a decrease in the concentration of DNA detected in the supernatant after 24 hours equilibration, which affected equally bPEI1.2 and bPEI10. We can conclude from here that the presence of Fe(III) seems to favor the interaction between polyplexes and concomitantly, DNA aggregation and precipitation, the effect being more pronounced for the bPEIs. Some studies indicate that the chelation metal–amine is more pronounced for bPEIs than for IPEIs [148]. As such, the aggregation may be more significant in the case of bPEI polyplexes.

5.3.3 Characterization of complexes

i. Size

The average size of the polyplexes formed by the addition of increasing amounts of PEI and Fe(III) to a mixed concentration of DNA is shown in Figure 5.5. Both DNA-PEI and DNA-PEI-Fe(III) systems are represented in each plot for an easier comparison. In a first stage, the presence of PEIs reduces the size of the DNA molecules. When a certain N/P value is reached, around N/P 1.2 to bPEI1.2, N/P 2 to IPEI2.5 and IPEI25, and N/P 2.5 to bPEI10, polyplex aggregation takes place, similar to what was observed in precipitation assays. Polyplex aggregation is a consequence of the neutralization of DNA negative charges, and also it is well documented that, at a high ionic strength, these systems tend to aggregate at N/P values in the range of 2 to 5, after which they are stable in the form of small complexes [83, 135]. The addition of Fe(III) was performed to selected N/P values, as before. Some PEI architectures seem to be more sensitive to the presence of the trivalent ions. The complexes formed with branched PEIs show a more pronounced ability to aggregate than those with IPEIs (Figure 5.5a and b vs. 5.5c and d), presenting a considerable aggregation for N/P values below 1.0. This tendency is also confirmed by the low stability of bPEI polyplexes during longer periods (Figure 5.4a). The IPEI, on the other hand and for N/P = 0.7, allows the addition of up to a Fe(III)/P = 7.1 without a significant increase in the size of the complexes. In these systems, there is no significant amount of free DNA present in the supernatant (see Figure 5.4b), indicating DNA condensation in relatively small polyplexes, ~ 250 to 300 nm. Additionally, for some N/P ratios and upon the addition of Fe(III) a decrease in the size of the complexes is first observed, followed by an increase (see N/P : Fe(III)/P = 0.7 : 3.7 for IPEI2.5, for example), which indicates an initial DNA condensation promoted by Fe(III), followed by neutralization and aggregation.

This behavior was also observed using fluorescence microscopy, in the previous Chapter. The trivalent ions are more mobile species than the PEI, since they are smaller and less charged, and it is likely that they contribute to minimize the charge of the complexes (either positive or negative), and thus the respective repulsion. Moreover, they may correlate with negative polyplexes and

promote a higher degree of aggregation, as previously observed in macroion interactions mediated by trivalent ions [259].

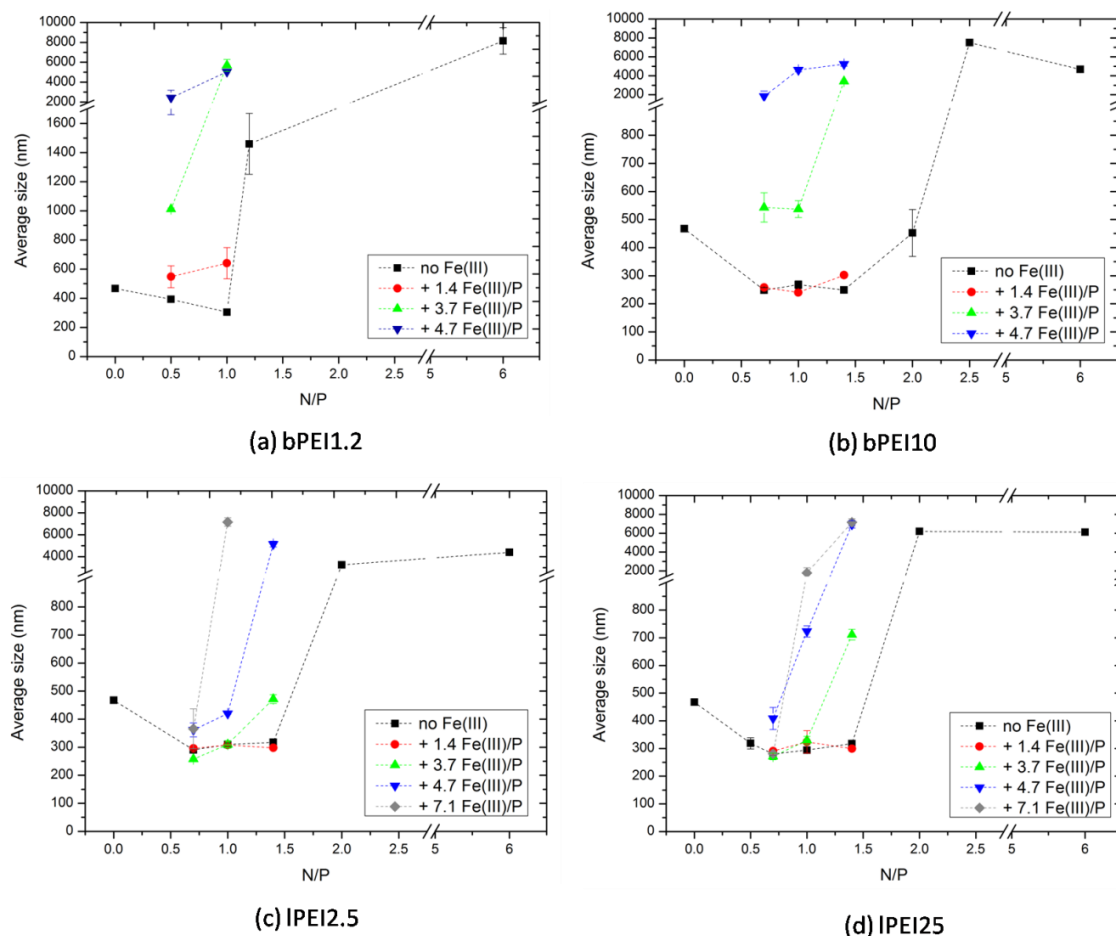


Figure 5.5. Size of DNA-PEI-Fe(III) complexes as a function of the N/P ratio and the Fe(III)/P ratio. The upper panels show the sizes of polyplexes prepared with (a) bPEI1.2, (b) bPEI10 and the lower panels with (c) IPEI2.5 and (d) IPEI25.

ii. Zeta potential

Besides particle size, the surface charge of DNA-PEI and DNA-PEI-Fe(III) complexes is also an important parameter in the interaction of the complexes with cell membranes. The zeta potential values for complexes prepared with bPEI10 and IPEI25 are presented in Figure 5.6. Only these two polycations were chosen for this study, since they are considered more promising for use in gene transfection [260]. The values of zeta potential obtained for DNA-PEI complexes (black bars in Figure 5.6) show that, in both cases, electrical neutralization occurs at relatively high values of N/P, 4.5 for bPEI10 and 3.5 for IPEI25. These N/P values are in agreement with the GE results that show that negatively charged DNA complexes are still present in solution for N/P = 3, for both PEI (Figure 5.1b and d). Also, the values obtained for IPEI25 in the N/P range from 3 to 6 are in agreement with those reported in the literature for DNA-bPEI25 [261]. The preparation of

polyplexes at higher concentrations of PEI leads to the formation of more charged complexes, of about +25 mV, as it was also observed using GE. The consequence of replacing PEI with Fe(III) on the zeta potential of the polyplexes was evaluated in the Fe(III)/P range of 7.1 to 23. Interestingly, the addition of increasing concentrations of Fe(III) allows formation of polyplexes with positive zeta potentials ($\sim +10$ mV) with low concentrations of PEI, N/P = 2.5 vs. 3 for bPEI10 and N/P = 1.5 vs. 2.5 for IPEI25. However, further addition of Fe(III) does not lead to a noticeable increase of the positive charge of the polyplex.

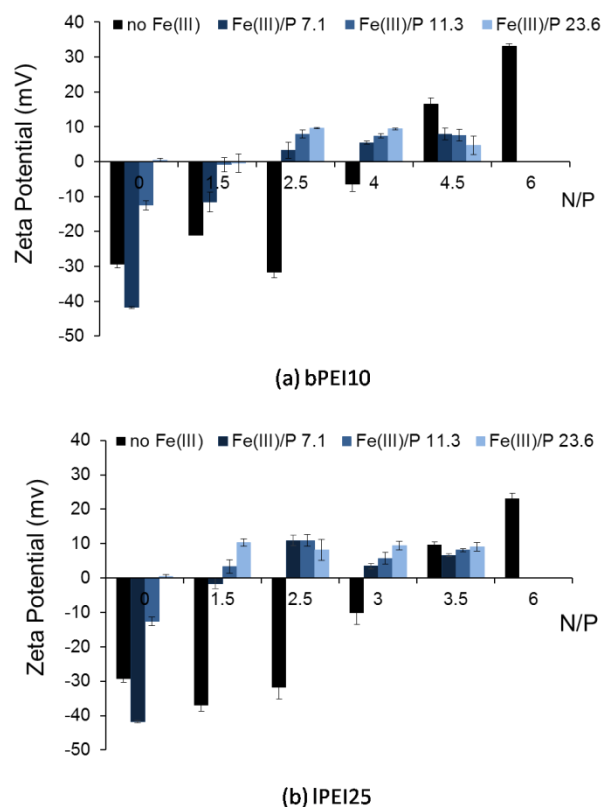


Figure 5.6. Zeta potential (mV) of polyplexes formed with (a) bPEI10 and (b) IPEI25 as a function of the N/P and Fe(III)/P ratios.

5.4 Conclusions

Two different architectures of PEI (branched and linear) in conjunction with Fe(III) were used to prepare DNA ternary complexes. The degree of DNA condensation, size and surface charge of DNA–PEI–Fe(III) were studied as a function of N/P and Fe(III)/P ratios. It was observed that the different PEIs, on their own, possess different efficiencies as condensing agents. However, the addition of Fe(III) to DNA–PEI systems tended to equalize the action of these different agents. The shorter chain PEIs (bPEI1.2 and IPEI2.5) are, notwithstanding, the most efficient in the presence of Fe(III). This result is compatible with a previously suggested mechanism that places

the metal ions in the empty spaces left by PEI. The addition of Fe(III) to the negative DNA–PEI polyplexes produced charge reversal, which favors their interaction with the cell membranes. Additionally, polyplexes in solution at low N/P ratios were smaller in the presence of Fe(III), but their neutralization promotes aggregation, which is enhanced by high ionic strength conditions.

CHAPTER 6

Cytotoxicity

6.1 Introduction

This chapter is in sequence with the preceding chapter using the same systems, but now focusing on biological effects. The knowledge of the interactions of the DNA based particles with cells is fundamental for improving their behavior *in vitro* and *in vivo*. A current problem with PEI mediated gene delivery is the associated toxicity, owing to the strong positive surface charge that can interact with blood components, such as erythrocytes, leading to hemolysis, or else, interact with cellular membranes and, again, inducing undesirable effects [165]. It has been established that higher molecular weights lead to an increased cytotoxicity but, in turn, low molecular weight PEI have demonstrated low cytotoxicity but also a lower transfection efficiency [156]. Some concerns about the presence of free Fe(III) ions in the cells have been raised, despite the general accepted concept of its biocompatibility. This issue is inspected to the present system.

Therefore, a set of experiments is made to investigate the individual harmful potential of the each PEI (bPEI1.2, bPEI10, IPEI2.5 and IPEI25) and Fe(III). In addition, a possible strategy to reduce the number of PEI molecules in the polyplex, while maintaining the DNA condensation and positive surface charge, is tested. The underlying mechanism for the beneficial activity of the addition of Fe(III) to PEI-DNA complexes is also discussed.

6.2 Materials and Methods

6.2.1 Materials

Salmon testes DNA (~2000 base pairs) was purchased from Sigma, UK and used as received. Commercial branched polyethylenimines with average Mw 1.2 (bPEI1.2) and 10 kDa (bPEI10) were purchased from Polysciences, Inc (USA) and Alfa Aesar (UK), respectively. Commercial linear polyethylenimines with average Mw 2.5 (lPEI2.5) and 25 kDa (lPEI25) were purchased from Polysciences, Inc (USA). Ferric chloride hexahydrate and buffer reagents, sodium chloride, sodium acetate, Trizma base, boric acid and EDTA were purchased from Sigma (UK), and acetic acid was from Riedel-de Haens (Germany). Agarose and the dyes used in electrophoresis were obtained from Lonza, Switzerland and Fermentas, Germany. Dulbecco's Modified Eagle's Medium (DMEM), fetal bovine serum (FBS), 2,5-diphenyl-3-(4,5-dimethyl-2-thiazolyl) tetrazolium bromide (MTT), dimethylsulphoxide (DMSO), phosphate buffered saline (PBS), trypsin–EDTA solution (170 000 U L⁻¹ trypsin and 0.2 g L⁻¹ EDTA), and penicillin–streptomycin solution (10 000 U mL⁻¹ penicillin and 10 mg mL⁻¹ streptomycin) were purchased from Lonza (Switzerland). All chemicals and reagents used were of analytical grade. The 75 cm² flasks and 96-well plates were obtained from TPP (Switzerland).

6.2.2 Sample preparation

The procedure is described in Section 5.2.2.

6.2.3 Hemolysis assay

Rat blood was obtained from anesthetized animals by cardiac puncture and drawn into tubes containing EDTA. This procedure was approved by the Ethical Committee for Animal Research of the University of Barcelona. Isotonic saline PBS solution, containing 22.2 mmol L⁻¹ Na₂HPO₄, 5.6 mmol L⁻¹ KH₂PO₄, and 123.3 mmol L⁻¹ NaCl in distilled water (pH 7.4), was added into the blood sample, and the supernatant was removed after centrifugation at 3000 rpm (Megafuge 2.0 R Heraeus Instruments) at 4 °C for 10 min. The erythrocyte pellets at the bottom of the centrifuge tube were washed four times with the PBS solution. After that, the cells were diluted to 1/2 of their volume with isotonic phosphate buffer solution (PBS) (cell density of 8 x10⁹ cells per mL). Thus, a series of different volumes of PEI and Fe(III) solutions (1 and 10 mg mL⁻¹), ranging from 10 to 100 µL, were added to 25 µL of erythrocyte suspension in the presence of PBS, and incubated at room temperature for 10 min under constant shaking. The final volume of each solution is 1 mL. Following incubation, the tubes were centrifuged (5 min at 10 000 rpm). PBS was used as a negative control and distilled water was used as the positive control. The degree of hemolysis was determined by comparing absorbance (540 nm) (Shimadzu UV-160A) of the supernatant of each sample with the positive control.

6.2.4 Polyplex stability assay

The complexes DNA-PEI-Fe(III) and DNA-PEI were individually mixed in the different media, acetate buffer, DMEM or DMEM with 5% FBS, and incubated at 37 °C with 5% CO₂ for 24 h, reproducing the same conditions of the cell culture. The stability of the polyplexes was monitored through agarose gel electrophoresis.

6.2.5 Cell Culture

The murine Swiss albino 3T3 fibroblast cell line and the human epithelial carcinoma HeLa cell line were grown in DMEM medium (4.5 g L⁻¹ glucose) supplemented with 10% (v/v) FBS, 2 mM L-glutamine, 100 U mL⁻¹ penicillin and 100 µg mL⁻¹ streptomycin at 37 °C and 5% CO₂. The 3T3 and HeLa cells were routinely cultured in 75 cm² culture flasks and were trypsinized using trypsin-EDTA when the cells reached approximately 80% confluence.

6.2.6 MTT assay

The cytotoxicity of different PEIs and Fe(III), and DNA-PEI-Fe(III) complexes was evaluated using the MTT assay. 3T3 and HeLa cells were seeded into the central 60 wells of a 96-well plate at a density of 1x10⁵ and 5x10⁴ cells per mL, respectively. After incubation for 24 h under 5% CO₂ at 37 °C, two different procedures were conducted: (1) the spent medium was replaced in the wells with 100 µL of fresh medium supplemented with 5% FBS or (2) the spent medium was replaced with a mixture of (1:1) DMEM-acetate buffer supplemented with 5% FBS, and in these distinct cell culture media, free PEI chains and Fe(III) in concentrations ranging from 2.5 to 2000 µg mL⁻¹ were dissolved. The DNA-PEI and DNA-PEI-Fe(III) complexes, previously prepared in acetate buffer, were diluted with DMEM with 10% FBS (1:1) and added to the cells. Each sample was tested in triplicate and the control cells were exposed only to the media, DMEM with 5% FBS or (1:1) DMEM–acetate with 5% FBS.

6.2.7 LDH assay

The degree of membrane destabilization was examined by lactate dehydrogenase (LDH) activity liberated from the cytoplasm. Using the same conditions as described for the MTT assays, the 96-well plate was centrifuged at 1200 rpm for 8 min and 50 µL per well supernatant of the treated cells was carefully transferred into a new 96-well plate. To determine the LDH activity in these supernatants, a 100 µL reaction mixture of commercial kit (Takara Bio Inc, Otsu, Japan) was added to each well, according to the manufacturer's protocol, and incubated for 30 min. Absorption was measured at 492 nm with a background correction at 620 nm using an ELISA reader 492. The percentage of cytotoxicity was calculated as

$$\text{Cytotoxicity (\%)} = \frac{(A_{\text{treated}} - A_{\text{control}})}{(A_{\text{maximum}} - A_{\text{control}})} \quad (6.1)$$

Where A_{treated} and A_{control} refer to the absorbance of the cells in the absence and presence of PEI (or polyplexes), respectively. Control experiments were performed with 0.1% (w/v) Triton X-100 and set as 100% cytotoxicity (A_{maximum}). Each experimental condition was carried out in triplicate. Data are shown as the mean value plus a standard deviation of the mean (\pm SEM).

6.3 Results and Discussion

One of the main concerns in the use of PEI is the respective toxicity. A number of recent reports collected in the literature confirm that PEI-mediated cytotoxicity may be a result of two effects, direct interaction with mitochondria [262] and/or interaction with the cell membrane leading to perturbation in the structure and pore formation [157, 262, 263]. Despite the large number of studies using different types of cationic particles differing in size and surface charge, there is still a lack of studies and methods in which a complete analysis of their overall toxicity is performed. Results show the relevance of using a variety of complementary tests to a comprehensive risk assessment [77, 227].

The hemocompatibility of the condensing agents is also a factor of large importance that indicates their suitability for introduction into the systemic circulation. In the present study, we investigate the potential hemolytic and cytotoxic effect of PEI and Fe(III) separately. Also, the cytotoxicity of the polyplexes, in the presence and absence of Fe(III), was analyzed and compared. To this end, two in vitro complementary methods to measure changes in cell viability, MTT and LDH assays, were conducted. The former allows determination of the metabolic activity of the mitochondria of viable cells, and the latter determines the integrity of the cell membrane.

6.3.1 Determination of hemolytic activity

The administration of DNA complexes to the blood can lead to their dissociation when in contact with erythrocytes or plasma proteins, inducing the release of the genetic material and the condensing agents [264-266]. As a consequence, the free positively charged components may interact with erythrocytes, cell membranes and extracellular matrix proteins, resulting in undesired effects. To assess this problem more clearly, the interaction of the different PEIs and Fe(III) with erythrocytes was performed separately. The release of hemoglobin was used to quantify the erythrocyte membrane-damaging properties of the condensing agents. The dependence of hemolysis on the concentration of the polycations and Fe(III) in two different pH media is shown in Figure 6.1. The percentage of hemolysis due to the presence of PEIs and

Fe(III) was not significant (below 5%) [267, 268] at pH 7.4, revealing no hemolytic activity (Figure 6.1a). At pH 6, the values were below 5% within the working concentration (from around $1 \mu\text{g mL}^{-1}$ to $100 \mu\text{g mL}^{-1}$), except for bPEI10 that presented a slightly larger value (Figure 6.1b). This result indicates that, in the worst case scenario, if total release of condensing agents from the polyplexes takes place, there is no harmful effect to the erythrocyte membrane integrity. At an even higher concentration, $1000 \mu\text{g mL}^{-1}$, hemolysis can reach values of 12% and 9%, for bPEI10 and IPEI25, respectively. Such an effect of pH on cytotoxicity has already been observed in related systems [269, 270]. In addition, Fe(III) revealed no hemolytic activity in all the concentrations and in both media tested, which indicates high compatibility of this component towards biological membranes.

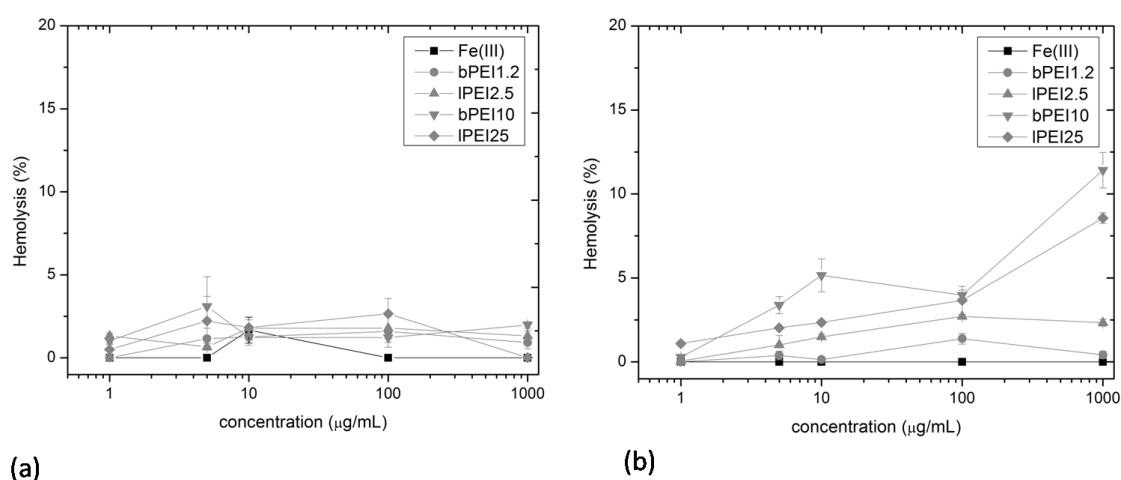


Figure 6.1. Hemoglobin release from rat erythrocytes as a function of PEIs and Fe(III) concentration. Erythrocytes were incubated at room temperature in the presence of the condensing agents in two media, (a) PBS buffer, pH 7.4 and (b) acetate buffer, pH 6.

6.3.2 Determination of in vitro cytotoxicity: Isolated products

Subsequently, the influence of the condensing agents individually and that of the polyplexes on 3T3 and HeLa cell lines were analyzed using MTT and LDH assays. In what concerns MTT results, the cell viability was measured and expressed as the half maximal metabolic inhibitory concentration, IC_{50} , for each compacting agent individually and for the condensing agent mixture (PEI-Fe(III)) in two different media, DMEM with 5% FBS and (1:1) DMEM– acetate buffer with 5% FBS. Two different procedures have been described in the literature. In one, the preparation of polyplexes is performed directly in the culture medium [271], and, in the other, the polyplexes are firstly prepared in a buffer and then added in a considerable dilution to the medium of the assay [272]. However, it has been observed that variations in the medium can influence the interactions and, in some cases, even hamper DNA condensation [40, 235]. In the present study, the polyplexes were initially prepared in acetate buffer and subsequently diluted with DMEM

containing 10% FBS, in order to minimize the possible perturbation on DNA condensation. Cells treated with each of the media were considered control cells. The presence of the acetate buffer did not induce a pronounced toxic effect on cells.

The values of IC_{50} obtained for the four PEIs and Fe(III) individually are gathered in Table 1. In DMEM, the presence of Fe(III) does not change cell viability. However, the PEIs can induce a decline in cell viability which depends on the respective molecular weight and architecture. The presence of the acetate buffer in the medium leads, in general, to a larger toxicity of the condensing agents, as seen by the sharp decrease in all the values of IC_{50} , especially in 3T3 cells. For HeLa cells, only bPEI1.2 shows no sign of cytotoxicity and Fe(III) displays a very moderate decrease in cell viability. This result agrees well with the generally accepted view that Fe(III) is inert, biocompatible and capable of being metabolized [273, 274]. Additionally, the effect of the largest Mw condensing agents bPEI10 and IPEI25, plus a constant concentration of ferric chloride hexahydrate equal to $61.5 \mu\text{g mL}^{-1}$ (equivalent to $\text{Fe(III)/P} = 12$), was tested in DMEM-acetate buffer. The PEI- Fe(III) mixture still promotes a large cell cytotoxicity, but is considerably lower than in the absence of Fe(III). The saturation of amine groups, known to be responsible for the PEI cytotoxicity, by chelation with Fe(III) ions, may explain this result.

Table 6.1. $IC_{50}(\text{mg}\cdot\text{mL}^{-1})$ values for the pure compounds, PEIs and Fe(III) ions separately and in conjunction, dissolved in both media, DMEM and DMEM-acetate buffer.

Products	$IC_{50}(\mu\text{g mL}^{-1})^a$			
	DMEM		DMEM-Ac buffer	
	HeLa	3T3	HeLa	3T3
Ferric chloride	>2000	>2000	1186 ± 1	1108 ± 1
bPEI1.2	>2000	>2000	>2000	58.3 ± 1.082
IPEI2.5	216 ± 1	98.9 ± 1.006	12.3 ± 1.283	8.64 ± 1.042
bPEI10	29.3 ± 1.362	28.1 ± 1.949	21.8 ± 1.176	15.0 ± 1.629
IPEI25	158 ± 1.362	20.5 ± 1.057	<1.25	3.95 ± 1.218
bPEI10 + Fe(III)			19.5 ± 1.146	>20
IPEI25 + Fe(III)			12.9 ± 1.091	14.4 ± 1.102

^a The curves were fitted with a mathematical model, 4-parameter logistic model (4PL) that describes the sigmoid-shaped response curve using GraphPad Prism 6.02 (GraphPad Software Inc, San Diego, CA).

In LDH studies, the extracellular concentration of the cytoplasmatic enzyme was quantified for three different concentrations of each PEI. Solutions of bPEI1.2 and Fe(III) were also tested, and have shown no significant cytotoxicity (data not presented). Considering first DMEM as the medium (Figure 6.2 a and c), it is seen that the linear PEIs (IPEI2.5 and IPEI25) cause little or no damage to the membrane of 3T3 and HeLa cells. The bPEI10, on the other hand, produces a significant damage for both cell lines. The addition of acetate buffer to the medium reflects in an

increase in the degree of membrane damage for the linear PEIs, Figure 6.2b and d, similar to MTT results. Interestingly, bPEI10 presents the same degree of interaction with the 3T3 cell membrane, independently of the used medium, but it does not seem to interact to a large extent with the HeLa cell membranes when DMEM–acetate buffer was used. In general, and as observed with the MTT assay, the degree of protonation, the molecular weight and the degree of branching of the polycation seem to influence the cytotoxicity, as previously reported in the literature [156, 271, 275, 276].

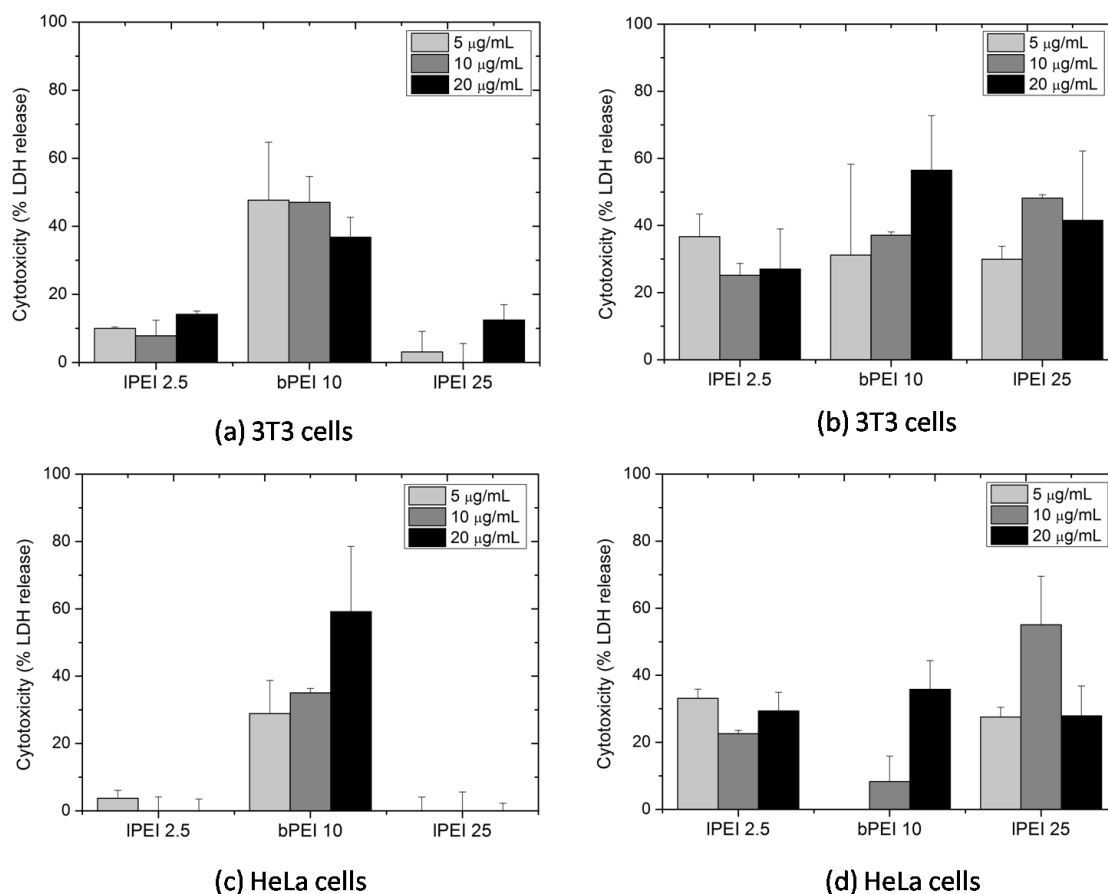


Figure 6.2. The cytotoxic effect of the polycations IPEI2.5, bPEI10, and IPEI25 on 3T3 and HeLa cells. The extent of membrane damage induced by the polycations was evaluated at three different concentrations (5, 10 and 20 $\mu\text{g}\cdot\text{mL}^{-1}$) and in two different media. Panels (a) DMEM, 5% FBS, (b) (1:1) DMEM–acetate buffer, 5% FBS in 3T3 cells, (c) DMEM, 5% FBS, and (d) (1:1) DMEM–acetate buffer, 5% FBS in HeLa cells gather the results of quantification of the release of the cytosolic enzyme LDH.

6.3.3 Determination of in vitro cytotoxicity: Polyplexes

A concern that has been raised in the literature is the understanding of the underlying mechanisms in PEI polyplexes-induced cytotoxicity [277]. It has been suggested that the free polycations damage the cell but when associated with DNA in a polyplex their cytotoxic effect is attenuated [156]. On the other hand, it was also demonstrated that the cytotoxicity of the polyplexes is equal

to or in some cases higher than that of the equivalent concentrations of free polycations [271]. The cytotoxicity of the previously optimized DNA-PEI-Fe(III) complexes is now determined and compared to the DNA-IPEI25 and DNA-bPEI10 of higher N/P ratios, using MTT and LDH assays. It should be recalled that only these polycations were used due to their high cytotoxicity and their larger potential for use in gene transfection. The values of N/P and Fe(III)/P were chosen according to the results obtained in the DNA binding studies (UV and GE) and zeta potential values depicted in Chapter 5. As such, we have used samples that show (i) complete DNA condensation and polyplexes close to charge neutrality (N/P = 4.5 for bPEI10 and N/P = 3.5 for IPEI25), (ii) complete DNA condensation and an overall positive zeta potential (N/P = 6 for bPEI10 and N/P = 4.5 for IPEI25), and (iii) N/P > 6, the most used conditions in transfection studies.

i. Polyplex stability

To guarantee that the comparison between systems is done without perturbations of the polyplex integrity during the experiments, studies of polyplex stability were conducted. The total solutions of DNA-PEI-Fe(III) and DNA-PEI complexes were run in gel electrophoresis under three different conditions: acetate buffer, DMEM-acetate buffer (1:1) and DMEM-acetate buffer (1:1) containing 5% FBS, in which in vitro cell experiments were carried out. Results in Figure 6.3 indicate that there is no migration of DNA through the gel for any of the polyplexes studied, except for a discrete DNA migration from the complex of bPEI10 at N/P : Fe(III)/P = 1.5 : 12 in DMEM-acetate buffer plus 5% of serum. The serum conditioned stability is a predictive evaluation of the polyplex stability under physiological conditions [278, 279], and the results show good stability of the DNA-PEI-Fe(III) polyplexes under these conditions.

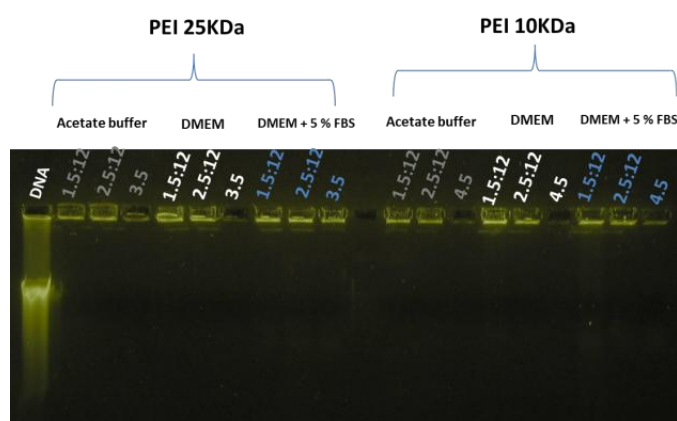


Figure 6.3. Agarose gel electrophoresis of total solutions DNA-PEI-Fe(III) and DNA-PEI incubated with acetate buffer, DMEM-acetate buffer and DMEM-acetate buffer plus 5% of serum. The respective N/P ratios and Fe(III)/P ratios are indicated.

ii. Polyplex cytotoxicity

In the present study, three different portions of the polyplex mixture are analyzed: total, supernatant and pellet. The total corresponds to the entire sample of the polyplex solution, which is added directly to the culture medium. The other two portions result from the centrifugation of the sample; the supernatant is separated and added to the culture medium, while the pellet is resuspended in acetate buffer prior to addition to the culture medium. This methodology allows us to distinguish the cytotoxicity of the polyplexes and that of the free polycation present in the supernatant, if any. The results of MTT assays are depicted in Figure 6.4.

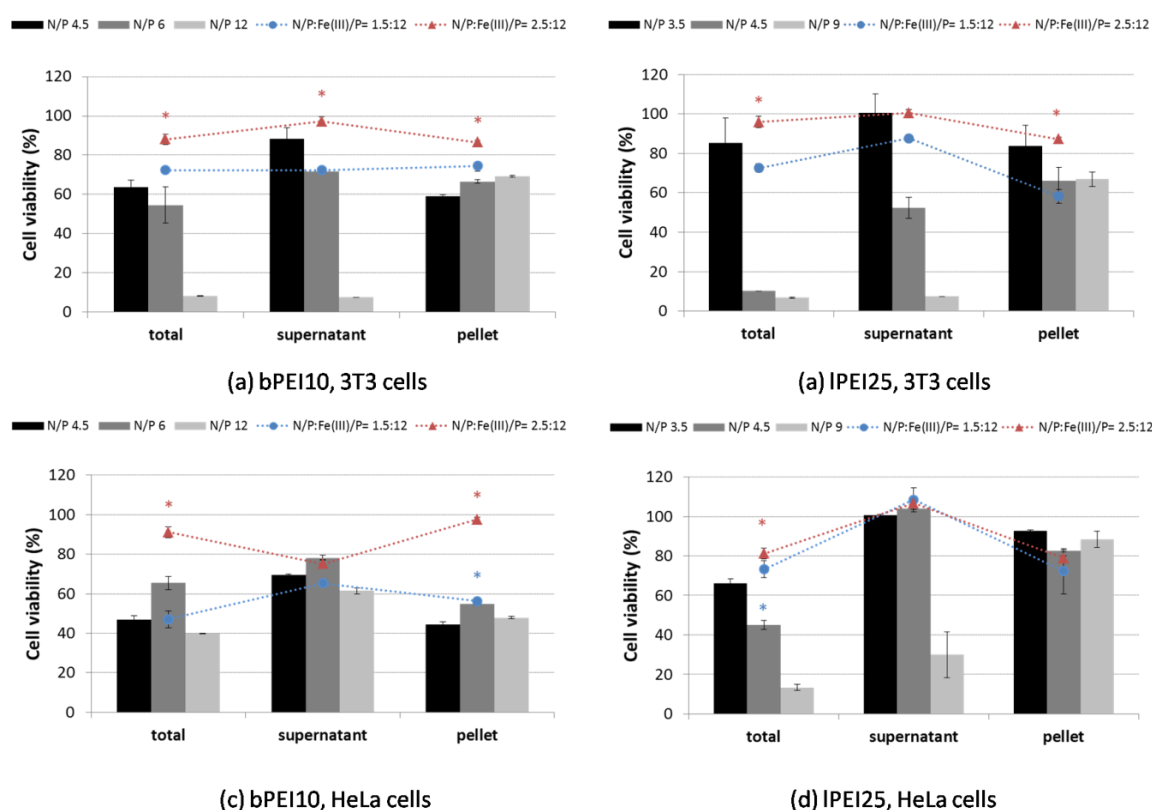


Figure 6.4. Effect of polyplexes DNA-PEI and DNA-PEI-Fe(III) with (a) bPEI10 and (b) IPEI25 on viability of 3T3 cells, and the corresponding (c) bPEI10 and (d) IPEI25 on HeLa cells, measured by the MTT assay. Ternary mixtures of DNA-PEI-Fe(III) are indicated in the plot in blue (N/P : Fe(III)/P = 1.5:12) and red (N/P : Fe(III)/P = 2.5:12), all solutions possess Fe(III) at a Fe(III)/P value of 12. The N/P values correspond to polycation concentrations: N/P 1.5 to 2.0 $\mu\text{g mL}^{-1}$; N/P 2.5 to 3.3 $\mu\text{g mL}^{-1}$; N/P 3.5 to 4.6 $\mu\text{g mL}^{-1}$; N/P 4.5 to 5.9 $\mu\text{g mL}^{-1}$; N/P 6 to 7.8 $\mu\text{g mL}^{-1}$; N/P 9 to 11.7 $\mu\text{g mL}^{-1}$ and N/P 12 to 15.6 $\mu\text{g mL}^{-1}$, considering the dilution (1:1) DMEM-acetate buffer. Each point represents the mean \pm SD of six measurements (* $p < 0.05$: ternary mixtures are significantly different compared to the corresponding samples without Fe(III), at the same zeta potential and degree of condensation, N/P 4.5 for bPEI10 and N/P 3.5 for IPEI25). The samples were compared by Student's t-test using GraphPad Prism 6.02 (GraphPad Software Inc., San Diego, CA).

Focusing on the pellet that should comprise only the neutralized DNA complexes, the results show similar trends of cell viability for both PEIs, in both cell lines, with approximately constant values in the range of N/P values studied. This result shows that increasing the N/P values does not alter the pellet constitution, as documented in the literature [165]. The supernatant should mainly comprise polycation molecules that remain free after DNA condensation. The cell viability is high at the lowest and intermediate N/P values, whilst at the higher N/P value, however, a sharp decrease in cell viability is found for the majority of the tested systems due to the highest concentration of free PEI chains in this portion. In HeLa cells, bPEI10 shows a different behavior with the supernatant being the portion of the sample that presents the lowest cytotoxicity in all cases. The total is more toxic than the parts, showing, in all cases, a decrease of cell viability as the N/P ratio increases, as a result of the polycation concentration increment. The agreement in the results of total and supernatant stresses the importance of free PEI molecules for cytotoxicity of PEI-DNA complexes, as stated in the literature [165, 280].

Interestingly, the pellet and the supernatant for lPEI25 at N/P 3.5 attain approximately the same values of cell viability, in both cell lines, but the total solution is more toxic than each one individually. The sum of both contributions seems to promote a higher toxicity, especially, and as expected, in the 3T3 cell line. However, it should be recalled that the IC_{50} value of lPEI25 is drastically low. A clear exception is detected for bPEI10 in HeLa cells. In particular, it is observed that the total and the pellet show similar trends, with lower values of cellular viability, pointing out the dependence of the cell viability on the polyplexes. In addition, the supernatant at high N/P values does not induce a high cell death as that observed for the other complexes. This fact may be related to the low interaction of bPEI10 with the cell membrane obtained in LDH studies (Figure 6.2d).

The results of cytotoxicity assays for DNA-PEI-Fe(III) complexes are also presented in Figure 6.4, for comparison. Two different sets were chosen, one of approximately neutral polyplexes (N/P : Fe(III)/P = 1.5 : 12) and the other of slightly overcharged complexes (N/P : Fe(III)/P = 2.5 : 12), see Figure 5.6. These ternary mixtures, when compared with iron free samples, at the same zeta potential and degree of condensation, N/P 4.5 (bPEI10) and N/P 3.5 (lPEI25), display an equal or higher cell viability, but it should be noted that the highest viability is observed for N/P : Fe(III)/P = 2.5 : 12. This observation stems probably from some destabilization of the polyplexes, in the presence of a lower amount of PEI. Although this is not observed in the stability assays, it may happen in the proximity of the cells. The enhancement of cell viability is mainly seen for the total and pellet, since the concentration of free PEI molecules in the corresponding samples is low. As expected, when the N/P value is increased, a larger difference in cell viability of the different parts of the sample is discerned. Moreover, it should be mentioned here that, in the worst case scenario, if the polyplexes fully dissociate and all

polycation molecules are free in the cell, the total PEI concentration ($3.3 \mu\text{g mL}^{-1}$, $N/P = 2.5$) is still below that of the IC_{50} , calculated at ca. $4.0 \mu\text{g mL}^{-1}$ (see Table 6.1).

Complementary studies of LDH were also performed with the same samples and the results are shown in Figure 6.5. The complexes based on bPEI10 did not induce LDH release (data not shown). Also, for polyplexes with low N/P ratios in conjunction with Fe(III), a reduced cell toxicity was detected. For IPEI25 and an intermediate N/P ratio in 3T3 cells, the total sample presents the highest cytotoxicity, in agreement with the MTT results. At high N/P values, the supernatant presents a significant cytotoxicity, but the total does not. It is clear that varying the N/P ratio, from 3.5 to 9, results in two distinct mechanisms of membrane induced cytotoxicity. In the intermediate N/P, the cytotoxicity arises from both the polyplexes and possible free chains of PEI. In the case of $N/P = 9$, the damage to the cells is only a consequence of free PEI chains. Studies of flow cytometry have shown that purified polyplexes are more prone to cellular association than those in the presence of competing free PEI [165] which may suggest the less interaction of the total with the cell membrane in the latter case. In HeLa cells, the same trend is observed with, generally, lower levels of cytotoxicity. However, the action of the polyplex with Fe(III) on the cell membrane is more visible for the HeLa cells than for the 3T3 ones. Results of the complementary cytotoxicity assays indicate that both the mechanisms involving direct interaction with the mitochondria and membrane cell damage play a definite role in polyplex cytotoxicity.

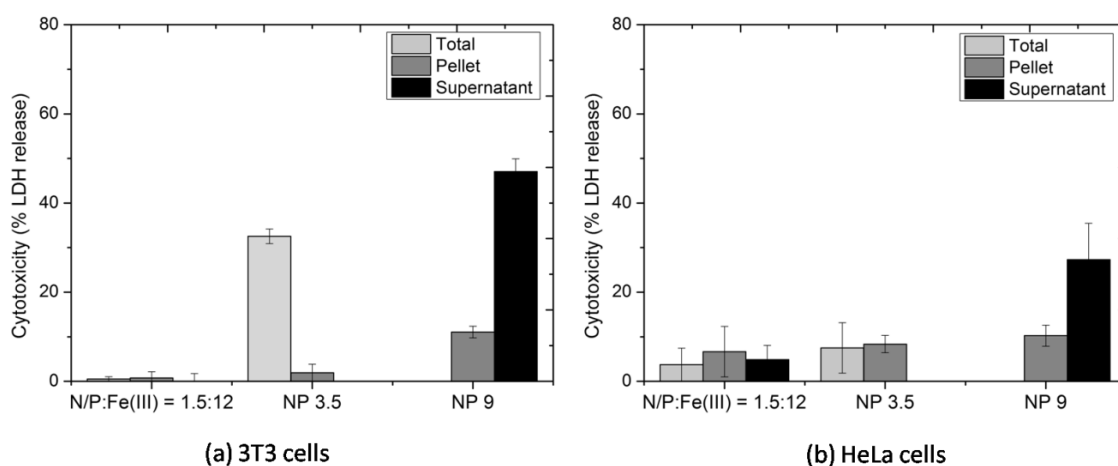


Figure 6.5. The extent of membrane damage induced by DNA-IPEI25-Fe(III) complexes quantified by the release of the cytosolic enzyme LDH in (a) 3T3 and (b) HeLa cells. The polyplexes DNA-bPEI10-Fe(III) did not induce loss of cell viability when added to both cell lines (data not shown).

6.4 Conclusions

The cytotoxicity and hemolysis studies revealed a clear dependence on PEI concentration, and the respective molecular weight and degree of branching. Dependence was also found on the pH of

the medium, leading to a high toxicity at lower pH. Results of MTT and LDH assays indicated that these features influence directly the interaction with the mitochondria and cell membrane damage. The saturation of PEI amine groups by Fe(III) ions reduced the PEI harmful effects upon the cells. In polyplexes, the substitution of PEI molecules by Fe(III) resulted in an enhancement of biocompatibility, when compared to DNA–PEI complexes with the same degree of condensation and surface charge. These results reinforce the possibility of producing polyplexes with a high degree of condensation and stability, and low cytotoxicity, which are desirable features for cell administration.

CHAPTER 7

PEI-Fe(III) chelation

7.1 Introduction

Due to the relevance of chelation, both in living cells and in technological applications, the interaction between polyamines and metal ions was addressed in several contributions in the last decades [148, 256, 281-285], usually, without detailing the mechanism of interaction. The lack of detail arises, probably, because it is hard to overcome some experimental difficulties faced when working with PEIs and metal ions in aqueous solutions, such as the pH-dependency of the polycation structure and of the metal ion species [286, 287], the low solubility of both compounds (metal ions and PEIs) [288, 289], and the difference between architectures of PEI (linear, branched) which may lead to completely different behaviors in solution [148]. Ternary polymer-metal (PAA-PEI-Cu(II)) complexes have also been studied for the development of selective ion exchange resins [290]. However, to our knowledge, the number of studies on these ternary mixtures is low.

The work presented in this chapter displays a characterization of the binary PEI-Fe(III) and ternary DNA-PEI-Fe(III) mixtures. In the first part, the interactions between bPEI1.2 and Fe(III) ions through potentiometric and conductance measurements were assessed. Secondly, studies on the ternary mixture DNA-PEI-Fe(III) using again different PEIs are also conducted by UV spectrophotometry and atomic absorption spectroscopy (AAS). Thirdly, Monte Carlo simulations are carried out, to interpret the main findings of the experimental part. It should be stressed here that this experimental part looked for (and ultimately provided) new insights on the nature of the interaction between PEI-Fe(III), complementing the one presented in Chapter 4. Again, a coherent picture of the system is drawn resorting to experimental and theoretical data.

7.2 Materials and Method

7.2.1 Materials

Salmon testes DNA (~2000 base pairs) was purchased from Sigma (UK) and used as received. Commercial branched polyethylenimines with average Mw 1.2 (bPEI1.2) and 10 kDa (bPEI10) were purchased from Polysciences, Inc (USA) and Alfa Aesar (UK), respectively. Commercial linear polyethylenimines with average Mw 2.5 (lPEI2.5) and 25 kDa (lPEI25) were purchased from Polysciences, Inc (USA). Ferric chloride hexahydrate and buffer reagents, sodium chloride, potassium chloride, sodium acetate, Trizma base, boric acid and ethylenediamine tetraacetic acid (EDTA) were purchased from Sigma (UK), and chloride acid, acetic acid and nitric acid were obtained from Riedel-de Haen, (UK). Agarose and the dyes used in electrophoresis were obtained from Lonza, Switzerland and Fermentas (Germany). Multi-element standard for Atomic Absorption Spectroscopy was purchased from Sigma (UK). All chemicals and reagents used were of analytical grade. Experiments were performed in solutions prepared with Millipore-Q water (18.2 M Ω /cm resistivity).

7.2.2 pH measurements

Potentiometric measurements were carried out with a pH Radiometer PHM 240. The pH was measured on fresh solutions with an Ingold U457-K7 pH conjugated electrode and was calibrated immediately before each set of measurements using IUPAC-recommended pH 4 and 7 buffer solutions. In a typical experiment, using a Gilson Pipetman micropipette, aliquots of titrant solution were added to 20 mL of titrated solution. All measurements were carried out at 25.00 °C (\pm 0.02 °C) under a nitrogen atmosphere, and the electrode potential was recorded after signal stabilization. In these experiments, no control was made on the pH, which was the natural value for each solution.

7.2.3 Conductance measurements

Electrical conductance measurements were carried out with a Wayne-Kerr model 4265 automatic LCR meter at 1 kHz, through the recording of solution electrical resistances, measured by a conductivity cell with a constant of 0.1178 cm⁻¹, uncertainty 0.02 % [291]. The cell constant was determined from electrical resistance measurements with KCl (reagent grade, recrystallized, and dried) using the procedure and data of Barthel et al [292]. Measurements were taken at 25.00 °C (\pm 0.02 °C) in a Thermo Scientific Phoenix II B5 thermostat bath under a nitrogen atmosphere. In a typical experiment, 20 mL of metal ion solution was placed in the conductivity cell. Subsequently, aliquots of the PEI solution were added in a stepwise manner using a Gilson Pipetman micropipette. The specific conductance of the solution was measured after each

addition, and corresponds to the average of three ionic conductance measurements (uncertainty less than 0.2%), determined using homemade software. The specific electrical conductance of the solutions, κ , is calculated from the experimental specific conductance, κ_{exp} , corrected for the specific conductance of water, κ_0 : $\kappa = \kappa_{\text{exp}} - \kappa_0$. In these experiments, no control was made on the pH, which presented the natural value for each solution.

7.2.4 Polyplex formation

The DNA-PEI-Fe(III) complexes were prepared according with the procedure described in Section 5.2.2, but in this Chapter, two other mixing alternatives were tested. In one, the condensing agents were pre-mixed and, after 20 minutes, added to the DNA solution. In the other alternative, the Fe(III) solution was added to the DNA solution, equilibrated for 20 minutes and, finally, the PEI solution was added.

7.2.5 Precipitation assays

The procedure is described in Section 4.2.3.

7.2.6 Agarose gel electrophoresis (GE)

The procedure is described in Section 4.2.4.

7.2.7 Size analysis

The procedure is described in Section 5.2.5.

7.2.8 Quantification of Fe(III) ions in solution

The quantification of Fe(III) present in the supernatant after polyplex formation and centrifugation was carried out by atomic absorption spectroscopy. The polyplexes were prepared as described above, and centrifuged after 2 hours of incubation. The supernatant was collected and diluted in a mixture (1:1) HNO₃ (2.5%) (w/w). The calibration curve was performed using solutions with increasing concentration of Fe(III) in the same mixture of (1:1) acetate buffer/HNO₃ to minimize matrix effects and reproduce the same conditions of samples. The blanks, DNA-Fe(III), acetate buffer-Fe(III) and PEI-Fe(III) were prepared following the same procedure. All samples were fortified with 1 ppm of Fe(III) using the standard AAS solution. Absorption measurements were made in a Unicam AAS Solar 939 equipped with a hollow cathode lamp for iron, as well as a deuterium lamp for background correction, under the following conditions: wavelength: 248.3 nm; slit width: 0.2 nm; lamp current: 75%; flame: air/acetylene.

7.2.9 Monte Carlo simulation

Systems involving one polyanion (DNA), different architected shorter polycations (PEI) and trivalent ions (Fe(III)) were modeled within the primitive model. In the primitive model, a polyion is defined as a semi-flexible sequence of hard-spheres with point charges (when applicable)

residing in a solvent described as a continuum with a dielectric permittivity corresponding to that of water, $\epsilon_r = 78.4$, at the simulation temperature, $T = 298.15$ K. In the simulation, particles were enclosed in a spherical cell with a radius of 400 \AA . The model consists of four different types of charged particles: (i) connected negatively charged spheres, representing the polyanion, (ii) connected neutral and positively charged spheres, representing the polycations, (iii) positively charged spheres representing the trivalent ions, and (iv) positively or negatively charged spheres representing the counterions present to ensure the system electroneutrality. The total potential energy, U_{tot} , was obtained assuming that interactions are pairwise additive and can be divided in three terms according to Equation (4.3). The nonbonded energy is divided into the Coulomb potential energy plus the hard-sphere potential energy, U_{nb} , and the chelation potential energy, $U_{chelation}$, given by the Lennard-Jones potential according to

$$U_{nonbond} = U_{nb} + U_{chelation} = \sum_i \sum_{j>i} u_{ij}^{nb} + \sum_i \sum_j 4\epsilon_{ij} \left[\left(\frac{\sigma_{ij}}{r_{ij}} \right)^{12} - \left(\frac{\sigma_{ij}}{r_{ij}} \right)^6 \right] \quad (7.2)$$

with

$$u_{ij}^{nb} = \begin{cases} \infty, & r_{ij} < R_i + R_j \\ \frac{z_i z_j e^2}{4\pi\epsilon_0\epsilon_r} \frac{1}{r_{ij}}, & r_{ij} \geq R_i + R_j \end{cases} \quad (7.3)$$

where z_i is the valency of particle i , e denotes the elementary charge, ϵ_0 the permittivity of vacuum, r_{ij} is the distance between particle i and particle j , and R the corresponding hard-sphere radii of each particle, $R = 2 \text{ \AA}$ for chain segments and monovalent ions, and $R = 3.5 \text{ \AA}$ for trivalent ions, according to the hydrated radius of Fe(III) ions [293].

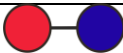

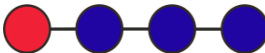
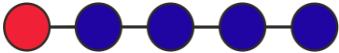
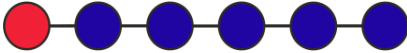

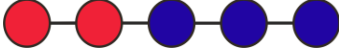


The summation of the first term in Eq. (7.2) extends over all particles in the system, whereas the chelation potential (second term) extends only over the neutral segments of the polycation (PC) chain and multivalent ions (mi). The chelating interaction corresponds to an attractive potential of $3.2 kT$ ($\epsilon_{ij} = 8 \text{ kJ mol}^{-1}$) at a distance, $\sigma_{ij} = 5 \text{ \AA}$. As a starting point a value close to that corresponding to the ΔG of formation of the Fe(III)-EDTA hexachelate was used ($\Delta_r G = -143 \text{ kJ mol}^{-1}$), which corresponds of an average value of $-23.8 \text{ kJ mol}^{-1}$ per N-Fe(III) [294]. However in these simulations, an excessively high value for the interaction between PC-mi affects the displacement of single particles and chains, and thus the evolution and equilibration of the systems. The value imposed to this term allowed an acceptable rate of convergence, while being suitable to simulate the chelation effect.

The contiguous hard-spheres that compose the chains are connected by an harmonic potential U_{bond} , according to Equation (4.6). A bond force constant, $k_{bond} = 0.4 \text{ N m}^{-1}$ was

imposed. In the polyanion (PA) chain, a bead–bead reference distance of $r_0 = 5 \text{ \AA}$ was imposed, whereas for the polycations a slightly larger value, $r_0 = 5.6 \text{ \AA}$, typical of polyamines was used. With other interactions included the typical root-mean-square (rms) bead-bead separation becomes $\langle R_{bead,bead}^2 \rangle^{1/2} \approx 5.8 \text{ \AA}$ for PA and $\langle R_{bead,bead}^2 \rangle^{1/2} \approx 6.1 \text{ \AA}$ for PC. The intrinsic rigidity was introduced by an angular potential, U_{ang} , as depicted in Equation (4.7) with a $k_{ang} = 1.7 \times 10^{-24} \text{ J deg}^{-2}$.

In the present study, the architecture and charge density of the short polycations (30 beads) (see Table 7.1), as well as the number of Fe(III) ions were varied in order to assess the importance of these factors on PA compaction, which in turn, is defined as a negatively charged chain with 120 beads and $z = 1$. The number of polycation chains was kept constant, using 2 chains of PC per system. The modeled systems are summarized in Table 7.2.

Table 7.1. Summary of charge density, α , and architecture of the monomers of polycations under study. Indicated in the second column of the table is the repetition unit of each polycations containing a total of 30 beads, except when state otherwise. Positive and neutral beads are represented in red and blue, respectively. The parameter α is calculated by the ratio between the number of positive and total number of beads of the polycation chain.

Polycation	Polycation chain monomer	α
PN		0.50
PN2		0.33
*PN3		0.25
PN4		0.20
PN5		0.17
*P2N2		0.53
P2N3		0.40
P3N2		0.60
P3N3		0.50

(*) System possessing two additional beads per chain to allow the correct chain architecture.

The model was solved by Monte Carlo (MC) simulation in the canonical ensemble using the Molsim package [252]. The efficiency of the simulations was improved by taking concerted moves in the chain particles. These included slithering, pivot rotation and chain translation.

Table 7.2. Systems studied in this Chapter. Indicated is the number of neutral, $N_{0,PC}$, and positive, $N_{+,PC}$, beads of each PC chains. Three values for the number of multivalent ions, N_{mi} , were used in each system. PC/PA refers to the fraction of the PA charge balanced by the PCs in each system, $N_{PC}N_{+,PC}/N_{-,PA}$, where N_{PC} is the number of PC chains. The counterions with negative (-) and positive (+) signs added to each system are presented in the same order of the number of multivalent ions, N_{mi}

Systems	PC	$N_{0,PC}$	$N_{+,PC}$	N_{mi}	Counterions	PC/PA
PN:N_{mi}	PN	15	15	20, 30, 40	() 0, 0, ()30	0.25
PN2:N_{mi}	PN2	20	10	20, 30, 40	(+)40, () 10, ()20	0.17
*PN3:N_{mi}	PN2	24	8	20, 30, 40	() 44, () 14, ()16	0.13
PN4:N_{mi}	PN4	24	6	20, 30, 40	() 48, () 18, ()12	0.10
PN5:N_{mi}	PN5	25	5	20, 30, 40	() 50, () 20, ()10	0.08
*P2N2:N_{mi}	P2N2	14	16	20, 30, 40	() 28, ()2, ()32	0.27
P2N3:N_{mi}	P2N3	18	12	20, 30, 40	() 6, () 6, ()24	0.20
P3N2:N_{mi}	P3N2	12	18	20, 30, 40	() 24, ()6, ()36	0.30
P3N3:N_{mi}	P3N3	15	15	20, 30, 40	() 0, 0, ()30	0.25

(*) System with two additional beads per chain to allow the correct chain architecture.

Additionally, a cluster-move [295] was employed, which was found to be crucial for achieving a better sampling efficiency, especially in systems in which trivalent salt is present [296]. Equilibration was performed with no less than 5×10^6 MC steps, and production runs comprised, typically, 5×10^6 steps or more, each step corresponding to a trial move for every particle.

7.3 Results and Discussion

Although studies on interactions between PEIs and metal ions have been reported throughout the last decades [148, 256, 282-285], the mechanism of those interactions has not been unveiled. There are several factors that make such a system a challenge even at the present date. The hydrolysis of both metal ions and PEI significantly differs on the solubility of both components and contributes for a wide range of, e.g., stability constants values for PEI-metal ion interaction [284, 285]. Firstly, the results from the potentiometric study are presented to provide a better assessment of the acid-base behavior of both metal ion and PEI, and how it affects the interaction between both components. However, due to experimental limitations related with PEI properties, such as solubility and stability in solution, mainly for lPEI, only bPEI1.2 was used in the experiments described in what follows.

7.3.1 Interaction bPEI1.2-Fe(III)

Metal ions in aqueous solution behave as Lewis acids [287], and in the concentration range studied the initial values of pH for the iron chloride solutions range from 2.5 to 3.5. On the other hand, bPEI1.2 possesses a strong polybase character, and shows a different behavior when compared to the corresponding monomers or other polybases, even at high ionic strength [256]. The conformation of the polymer in aqueous solution is pH-dependent: at low pH values, charge repulsion leads to expansion of the polyion and, at higher pH values, the polymer contracts, due to hydrogen bonding [148, 256, 282]. Also, an increase in the solution pH leads to the deprotonation of bPEI1.2 and, consequently, favors the complexation of the PEI with a metal ion [256, 297].

The addition of PEI aqueous solution to iron(III) chloride aqueous solutions, at different initial concentrations (0.25, 0.41, 0.63, 0.91 and 1.27 mM) of the latter, leads to an increase of the solution pH in a strong acid-weak base-like titration, with a pH, at the inflexion point of $\text{pH}=f([\text{bPEI1.2}])$, equal to $5.3 (\pm 0.3)$. Representative titration profiles are shown in Figure 7.1.

The analysis of Figure 7.1 shows that by increasing the amount of Fe(III) the number of moles of bPEI1.2 needed to reach the equivalence point increases in a linear relation ($R^2=0.9963$). From the slope of the fitting of $d^2\text{pH}/d[\text{bPEI1.2}]^2=0$, the following equation was determined

$$n_{(\text{PEI})_{\text{eq}}} = 4.8 \pm 0.1 n_{(\text{Fe}^{3+})_{\text{eq}}} \quad (7.6)$$

In order to check the reliability of Eq. (7.6), electrical conductance measurements were carried out to evaluate the effect of adding aqueous solutions of Fe(III) with different initial concentrations (0.25, 0.65 and 1.27 mM) to bPEI1.2 solutions (Figure 7.2).

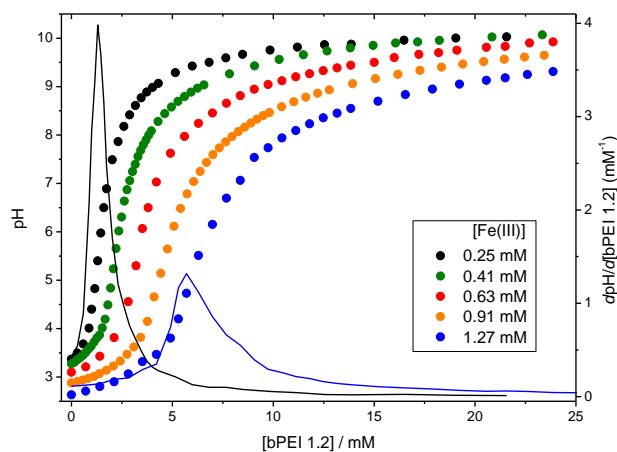


Figure 7.1. Potentiometric titration of aqueous iron(III) chloride solutions with bPEI1.2, at 25 °C. Different initial concentrations of metal solutions were used: 0.25, 0.41, 0.63, 0.91 and 1.27 mM. Solid lines represent the first derivative of pH values for the lower and higher concentration of metal ion.

It is possible to distinguish two different regions of specific electrical conductance (κ) as a function of the concentration ratio, $r = [\text{bPEI1.2}]/[\text{Fe(III)}]$. Upon addition of bPEI1.2, a sharp decrease in the electrical conductivity of the solution is observed until an inflexion point is reached. Such inflexion points occur at $r = 5.1(\pm 0.2)$, $5.5(\pm 0.3)$ and $5.4(\pm 0.3)$, for the increasing Fe(III) concentrations. At a bPEI1.2 concentration above r a slight increase of k is observed upon further addition of bPEI1.2. This suggests that Fe(III) is not available to interact with bPEI1.2 and, consequently, will be in excess in bulk solution. From these data it is worth noting that a) the molar ratio at which the maximum interaction between bPEI1.2 and Fe(III) occurs, is located around 5, as determined by two different techniques, and b) the sharp decrease of k at r values below ca. 5 cannot be explained just by a simple acid-base like titration, suggesting the formation of species with a lower charge density [298-300].

In order to check the latter hypothesis, separated titrations of Fe(III) and bPEI1.2 solutions were carried out using NaOH and HCl, respectively. The titration curves show well-defined inflexion points at

$$n_{(\text{OH}^-)_{\text{eq}}} = 2.60 \pm 0.02 n_{(\text{Fe}^{3+})_{\text{eq}}} \quad (7.7)$$

$$n_{(\text{H}^+)_{\text{eq}}} = 1.92 \pm 0.04 n_{(\text{PEI})_{\text{eq}}} \quad (7.8)$$

respectively. From simple grounds, and assuming that an acid-base neutralization takes place, the amount of bPEI1.2 necessary to neutralize 1 mol of Fe(III) should be equal to 1.35 mol. This value is 3.5 times lower than that obtained by direct titration of Fe(III) solution with bPEI, indicating that Fe(III) plays an additional role, beyond that of an acid.

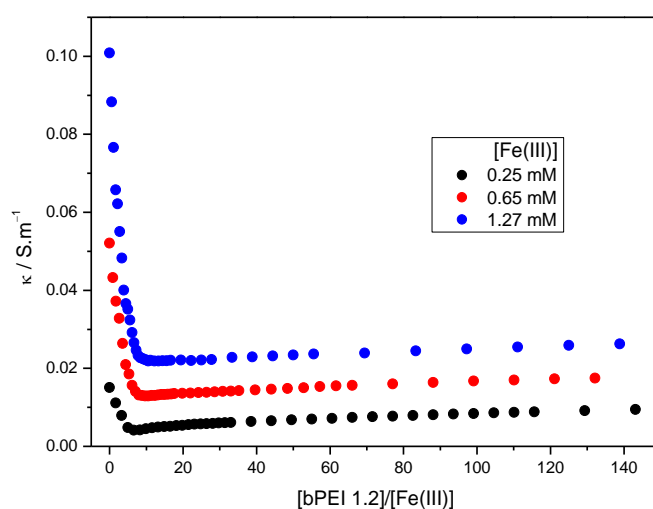


Figure 7.2. Effect of bPEI1.2 on the specific conductance of aqueous iron(III) chloride (0.25, 0.65 and 1.27 mM), expressed as a function of the $[\text{bPEI1.2}]/[\text{Fe(III)}]$ ratio, at 25 °C.

The results from the electrical conductivity measurements pointing to a complexation between PEI and Fe(III) (Figure 7.2) are in good agreement with other studies reporting the interaction between divalent and trivalent metals with amine groups of polyions [281, 297, 301, 302].

7.3.2 DNA condensation: influence of the mixing sequence

It is well described in the literature that polyplex formation depends on the solution characteristics, including ionic strength and solvent properties [303, 304], on the properties of the condensing agents, such as charge density [247, 305, 306] and chain length [307], and on the preparation procedure [44]. Simply manipulating the way DNA comes in contact with the condensing agent leads to a variety of polyplex morphologies, with different degrees of compaction and aggregation [44].

The now well-established chelation between PEI and Fe(III) ions is likely to influence further the formation and characteristics of ternary DNA-PEI-Fe(III) complexes. Bearing this in mind, the next sections are focused on the characterization of the ternary mixtures. Thus, studies were carried out in which the order of addition of the condensing agents to DNA was varied. Three distinct sequences were used: a) PEI was added to DNA, followed by the addition of the Fe(III) solution, denoted in what follows as (DNA+PEI)Fe, b) Fe(III) was added to DNA, followed by the addition of the PEI solution, (DNA+Fe)PEI, and finally c) Fe(III) was added to PEI, and subsequently the DNA solution was added to this mixture, DNA(PEI+Fe).

i. Quantification of DNA by UV-VIS spectrophotometry

UV spectrophotometry was used to analyse the influence of the distinct sequences of addition on DNA condensation. Herein, four different PEIs with varying chain architecture, linear and branched, and chain length were used and compared, as present in Chapter 5. The N/P ratio was maintained at 0.7 for all PEIs, and a range of Fe(III)/P ratios was assessed for each mixing protocol. After equilibration, the solutions were centrifuged to remove insoluble polyplexes (DNA complexes), as well as, Fe(III) either complexed or insoluble.

The results are presented in Figure 7.3. Panel (a) shows the percentage of DNA in the supernatant in the presence of bPEI1.2 and increasing concentration of Fe(III). It is observed that if one condensing agent is added to DNA followed by the other, (DNA+PEI)Fe or (DNA+Fe)PEI, the obtained trend is similar independently of which is added first. Some differences arise for the longer lPEI that presents a steeper decrease in DNA concentration in the supernatant, when the mixture (DNA+Fe)PEI is analyzed.

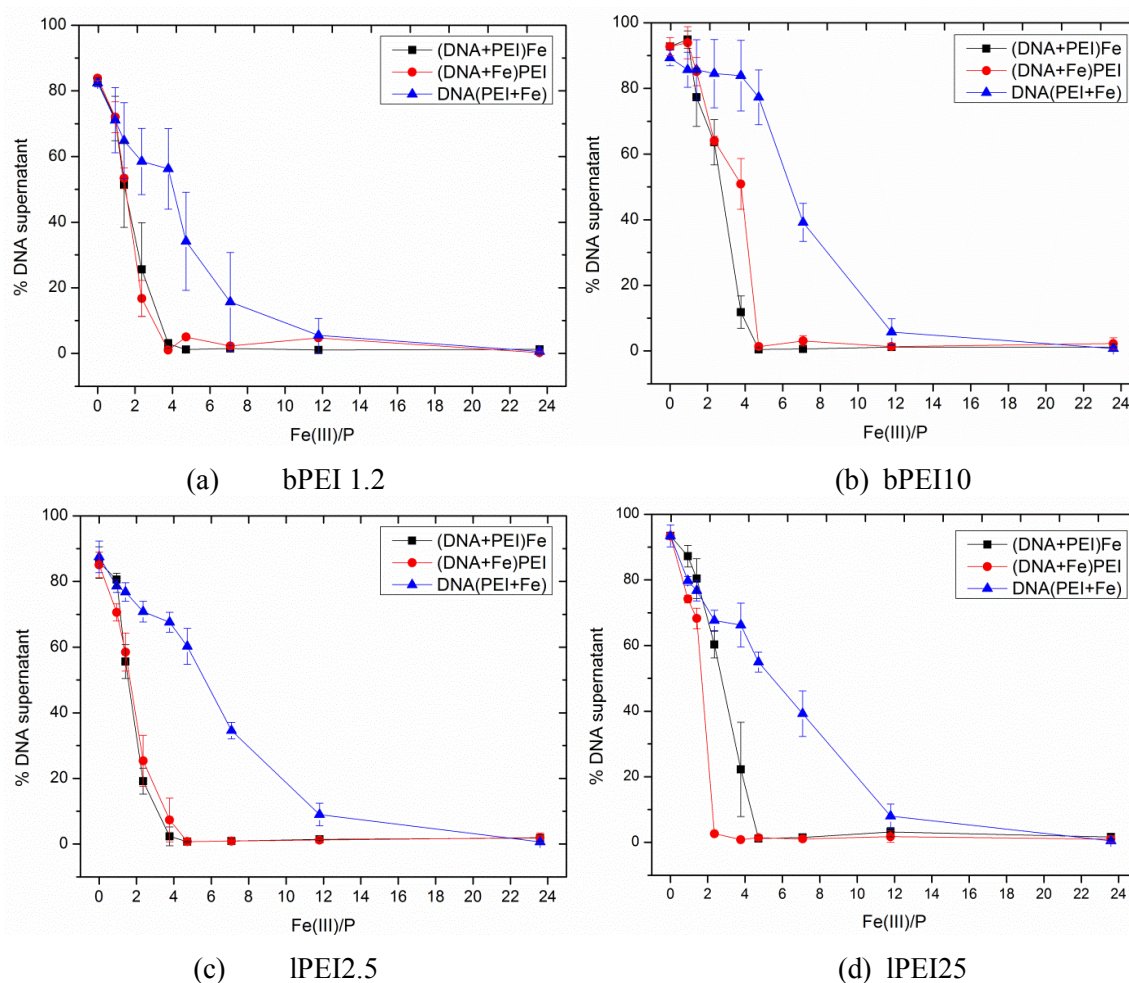


Figure 7.3. Percentage of DNA in the supernatant of the ternary mixtures as a function of Fe(III)/P ratios, determined by UV at 260 nm, using three different mixing procedures. The DNA-bPEI-Fe(III) complexes generated with (a) bPEI1.2 and (b) bPEI10, and DNA-IPEI-Fe(III) complexes using (c) IPEI2.5 and (d) IPEI25. The measurements were made after 2 hours of equilibration and centrifugation. $[DNA] = 20 \mu\text{g mL}^{-1}$ and $N/P=0.7$ were used in all samples. Solid lines are guides to the eyes.

When the condensing agents are pre-mixed, a marked discrepancy is visible for all studied systems (panels a-d). The premix of the condensing agents hampers DNA condensation, which clearly takes place at a higher Fe(III)/P ratio, which indicates that the interaction between Fe(III) and the amine groups of PEI reduces the ability of either or both to complex with DNA. This fact may be attributed to the formation of less charged species as indicated by the electrical conductance measurements. Although the profiles of the four different systems are not exactly equal, there is a general slow decrease of the concentration of DNA in the supernatant for Fe(III)/P values up to around 4, followed by a steeper decrease. It is interesting to note that this inflection in the curves roughly coincide with the full condensation of DNA for systems prepared with the other mixing protocols. Moreover, the total disappearance of DNA from solution occurs

approximately at the same Fe(III)/P ratio for all PEIs, at Fe(III)/P = 12, which is the same value observed for DNA condensation alone with Fe(III) [308].

ii. Charge and size of complexes

Gel electrophoresis assays were conducted for polyplexes prepared with IPEI25 for two different orders of mixing as depicted in Figure 7.4. For the (DNA+Fe)PEI sequence, panel (a), the full DNA neutralization is visible at Fe(III)/P = 4.7. In the case of (PEI +Fe)DNA protocol, panel (b), the migration of DNA through the gel is observed at lower Fe(III)/P ratios, and a fully DNA neutralization is attained at Fe(III)/P = 11.4. These results corroborate the trends observed in the DNA precipitation assays, depicted in Figure 7.3d. Note that, the decrease in the charge of DNA-PEI complexes by the addition of Fe(III) and their full neutralization had already been proved previously using the (DNA+PEI)+Fe mixing protocol, in Chapter 5.

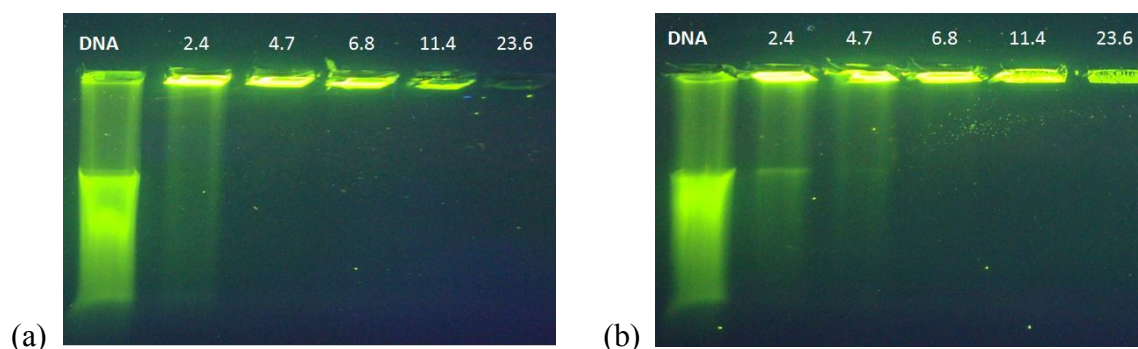


Figure 7.4. Electrophoresis of DNA-IPEI25-Fe(III) complexes obtained using two different mixing sequences, (DNA+Fe)PEI (a) and (PEI+Fe)DNA (b). The first lane of gel corresponds to DNA in the absence of compacting agents. The other lanes correspond to the samples prepared at constant (DNA+PEI) N/P = 0.7 and increasing values of Fe(III)/P. The DNA concentration is 20 $\mu\text{g mL}^{-1}$.

The influence of three different mixing protocols in the size of ternary complexes was also evaluated by DLS. The N/P:Fe(III)/P ratios in which complexes were formed correspond, in each case, to the values where DNA condensation is attained, in accordance with results shown in Figure 7.3d. The average size of complexes is depicted in Table 7.3. Results show a high dependency of the size of the complexes on the order of the mixing of the components. The mixing protocol (DNA+Fe)PEI gives rise to complexes with smaller sizes than those obtained with the other two mixing orders. This fact seems to be correlated with the higher efficiency of this protocol to induce DNA precipitation and neutralization (Figures 7.3d and 7.4a). On the other hand, the premix of both condensing agents before addition to DNA, (PEI+Fe)DNA, reveals to be comparatively less efficient to neutralize and compact DNA giving rise to larger particles, suggesting higher tendency of aggregation.

Table 7.3. Average size of DNA-PEI-Fe(III) complexes formed using IPEI25 by the three different mixing protocols. The standard error of the mean (SEM) was calculated from three independent samples measured in triplicate.

Order of mixing	N/P:Fe(III)/P	Z-average (nm) \pm SEM
(DNA+PEI)Fe	0.7:4.7	408.3 \pm 39.6
(DNA+Fe)+PEI	0.7:3.8	267.0 \pm 15.4
(PEI+Fe)+DNA	0.7:11.4	921.1 \pm 52.5

iii. Determination of Fe(III) by AAS

To assess the inclusion ability of Fe(III) into the polyplexes, the residual concentration of Fe(III) in solution was evaluated using AAS. Following previous methodologies, in Chapter 5, complexes prepared with bPEI10 and IPEI25 were further analyzed to assess the difference in polymer architecture, while working with molecules with the higher potential in gene delivery. Simple mixtures of DNA-Fe(III), bPEI10-Fe(III), IPEI25-Fe(III), and Fe(III) in acetate buffer, as control samples, were also assessed. The concentration of DNA and PEI was, as previously, kept constant at a N/P ratio of 0.7. Four Fe(III)/P ratios, 1.4, 3.8, 6.8 and 11.4, were evaluated for each system.

The results obtained for the control samples are shown in Figure 7.5a. The concentration of Fe(III) in acetate buffer increases up to approximately $2.5 \mu\text{g mL}^{-1}$ for a Fe(III)/P ratio of 3.8, which corresponds to $4 \mu\text{g mL}^{-1}$ of added Fe(III), reaching a plateau at the largest Fe(III)/P ratios studied. It is clear that a part of Fe(III) is not solubilized, even when present at low concentrations. The plateau indicates the maximum solubility of the metal in the buffer. The remaining portion of Fe(III), not solubilized, is separated by centrifugation. The addition of PEI to the Fe(III) solution promotes an increase in the solubility of the metal ion, again highlighting the interaction between these components. It is seen that bPEI10 displays a higher ability to solubilize Fe(III) than IPEI25, which is consistent with previous results reported in the literature [148]. On the other hand, the addition of Fe(III) to a solution containing DNA leads to a very moderate increase in the metal ion concentration in solution, when compared with the other systems. A possible explanation is the interaction of Fe(III) ions with the negatively charged DNA also through chelation via guanine N-7 atom and the phosphate group, as previously suggested [309, 310]. This induces condensation of some DNA molecules that are separated by centrifugation, reducing the amount of Fe(III) in solution. At a higher concentration, the metal ion disappears, to a large extent, from solution, as a result of DNA condensation and precipitation.

The metal concentration in the supernatant measured on the ternary mixtures is depicted in Figures 7.5b and c for the three different mixing protocols and different PEI architectures. The

results show that, when Fe(III) is added in advance to DNA, the concentration of Fe(III) in solution is always lower than in the other two mixing protocols, independently of the PEI architecture. Moreover, the profile is similar to that of the control sample, DNA+Fe(III). In this case, Fe(III) precipitates together with DNA in accordance to the results depicted in Figure 7.5c and d.

On the other hand, when both condensing agents are pre-mixed, the concentration of Fe(III) in the maximum of the curves is higher than for the two other mixing protocols. This occurs, since at this point the DNA is not fully condensed. Complete condensation only takes place at a Fe(III)/P ratio close to 12. For Fe(III)/P ratios corresponding to the maximum of the curves, the concentration of Fe(III) in solution is higher for bPEI10 than for lPEI25, in agreement with the trends found in the respective control solutions, and corroborating the higher chelating ability of branched PEI and consequent solubilizing effect. However, it should be stressed that the difference in the solubilizing effect between both PEIs in the control solutions is not as pronounced as that evidenced in the ternary mixtures. This seems to indicate that although the percentage of DNA in the supernatant is similar in both samples, the higher affinity between bPEI10 and Fe(III) promotes a higher solubilization of the trivalent ion. This effect also explains the higher Fe(III) concentration found for bPEI10 at Fe(III)/P = 6.8 in the mixing protocol where Fe(III) is added to DNA in advance.

Furthermore, it can be seen that the mixing protocol in which the PEI architecture has a lower influence, giving rise to profiles with similar shapes, corresponds to (DNA+PEI)Fe. Note, however, that the Fe(III) content is different in the two curves. In this case, for example at Fe(III)/P = 1.4 and when 80% of condensation of DNA is attained in both systems, the concentration of Fe(III) in the supernatant is $0.46 \mu\text{g mL}^{-1}$ for bPEI10 and $0.91 \mu\text{g mL}^{-1}$ for lPEI25. This suggests that bPEI10, being less efficient to condense DNA alone [311], removes more Fe(III) from the solution when complexed with DNA. On the contrary, the low ability of lPEI25 to chelate Fe(III) dictates that most trivalent ion added before full DNA condensation remains free in solution. These results suggest that both charge and architecture of PEI affects the uptake of Fe(III) by the ternary mixtures.

The data shows that, independently of the mixing protocol, the concentration of Fe(III) in solution diminishes with DNA condensation (Figure 7.3), clearly indicating that trivalent ions are an active agent in the condensation of these ternary mixtures.

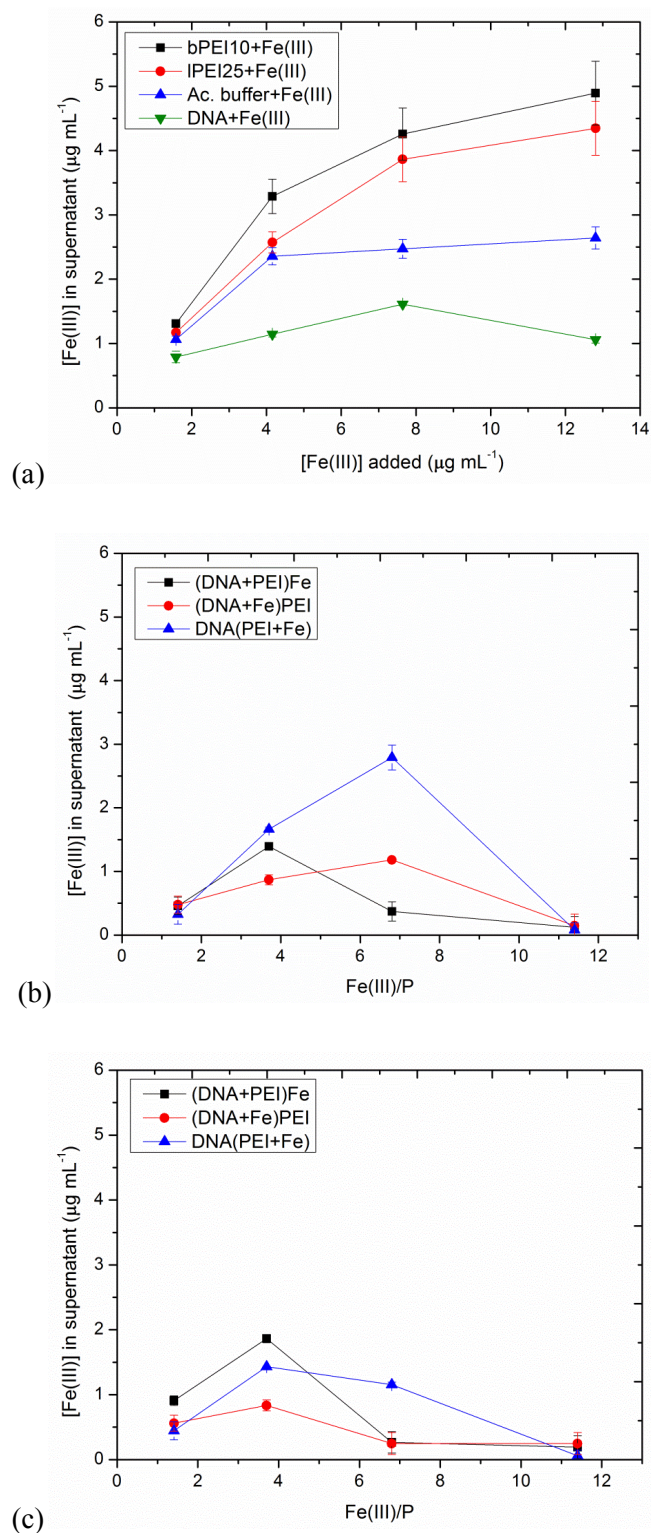


Figure 7.5. Concentration of Fe(III) in the supernatant measured by AAS after centrifugation, in control samples (a) PEI-Fe(III), DNA-Fe(III) and Fe(III) in acetate buffer, and in the ternary mixtures (b) DNA-bPEI10-Fe(III), and (c) DNA-IPEI25-Fe(III). The ternary mixtures were prepared using three different mixing protocols (see text). Two independent repetitions of this measurement were carried out in triplicate. The lines are guides to the eyes.

7.4 Theoretical approach

In an effort to rationalize some of the points of the experimental part, Monte Carlo (MC) simulations were performed. Taking into consideration the limitations concerning the characterization of some of the polycations, herein, it is not intended to reproduce the actual charge densities and structural properties of the species involved in the experimental section nor their relative proportions (DNA charge or dimension vs. PC charge and dimension). Instead, it is proposed to clarify the influence of two characteristics of the polycations: how their ability to chelate Fe(III) affect condensation of DNA, and how their inherent condensation efficiency influences fixation of Fe(III) and subsequently DNA condensation. To this end, systems considered include both the presence and the absence of chelation (PC-Fe(III)) and concomitantly, variations in the polycations linear charge density, from more efficient PCs (highly charged) to less efficient ones (low charged). From here on, the term compaction is used since the study entails solely one polyanion chain. The charge density was controlled by varying the ratio of charged monomers in the PC chains (see Table 7.1 in Section 7.2.9).

In addition, the ability of PEI to interact with Fe(III) was controlled by using different sequences of neutral and positive monomers in the PC chains, since the chelation potential acts between the neutral monomers and the trivalent ions. It should be remarked here that chelation should be favored when positive charges are further away, thus minimizing repulsion, according to experimental evidences [256, 281, 297, 312]. This feature will be mentioned along the text as capacity of chelation. A PC chain is more prone to chelate as it possesses a higher number of consecutive neutral beads. The simulations comprising systems with no interaction between PC-mi ($\epsilon = 0 \text{ kJ mol}^{-1}$) are considered as references. In this theoretical model, the DNA is described, as mentioned above, as a sequence of 120 negatively charged beads. Two PC chains were considered in each systems, containing each 30 beads. The number of multivalent ions N_{mi} , was varied between 20, 30 and 40.

7.4.1 Effect of PC-mi chelation on PA compaction

The degree of compaction of the PA is analyzed resorting to the radius of gyration, a measure of the extension of the polymer, formally described in Equation 4.9.

Figure 7.6 shows the root mean square (rms) of the radius of gyration obtained for the PA as a function of the PC architecture and the number of mi. Panel (a) shows the systems of PA-PC-mi in the absence of PC-mi interaction ($\epsilon = 0 \text{ kJ mol}^{-1}$). The presence of PC with increasing linear charge density, analogous to higher N/P ratios in the experimental part, leads to a more efficient PA compaction, as seen by the decrease in $\langle R_{gyr}^2 \rangle^{1/2}$. The addition of trivalent ions leads to a more pronounced compaction of DNA, beyond the effect of PC alone, as shown in previous work [308]. However, systems with a high concentration of cations ($N_{mi} = 40$), do not promote further

DNA compaction in the presence of highly charged PCs, showing values of the radius of gyration similar to those obtained for $N_{mi} = 30$. This does not occur when the metal ion is added in conjunction with the less charged PC backbones, where a condensation enhancement is still observed.

When a chelating interaction (PC-mi) is considered, Figure 7.6b, a decrease in the extension of the PA chain is visible for all systems. Again, as for systems in the absence of the chelation, this effect reaches a saturation for $N_{mi} = 30$, and only systems with PCs with a lower charge density show a slight decrease in the $\langle R_{gyr}^2 \rangle^{1/2}$ with $N_{mi} = 40$. It is interesting to note that for systems with a chelating interaction and $N_{mi} = 40$ a nearly constant radius of gyration is obtained, independently of the architecture of the PC.

In Figure 7.6c two sets of systems are presented, for clarity, together with reference systems. It is seen that the chelation clearly favors the formation of more compact structures. The differences between both sets are significant, especially at low charged PC. For $\epsilon = 8 \text{ kJ mol}^{-1}$, the PC with the structure denoted as PN, the only structure that has no consecutive neutral beads, presents the least compact structure of the whole set. While PN5 with the lower charge density, and therefore no effect on PA compaction when considered alone, show in the ternary mixture the most compacted conformation of the whole set. This fact seems to be related with its higher capacity to chelate multivalent ions, due to the large number of consecutive neutral beads in the chain. In this respect, it was found experimentally, that DNA condensation and precipitation occurs at approximately the same N/P ratios (which can be roughly compared to the charge density), irrespectively of the chain size and architecture, branched or linear, presenting a slightly high efficiency for PEI of small chain length (see Figure 7.3). Also, the polyplex sizes were found to be comparable at Fe(III)/P values prior to aggregation, see Figure 5.5 Chapter 5.

7.4.2 Quantification of mi in PA-PC-mi complex

The quantification of trivalent ions surrounding the PA-PC complexes was also conducted. To determine the fraction of bounded metal ions, a method based on the probability density function for the nearest-neighbor mi-mi distribution, was used [313]. The integration of this function gives the ion cloud close to the complex. It further distinguishes between bulk and bound ions and gives some insight into the range of action of the PA chain over the neighboring ions. Table 7.4 gathers the quantities of trivalent ions for each system under study.

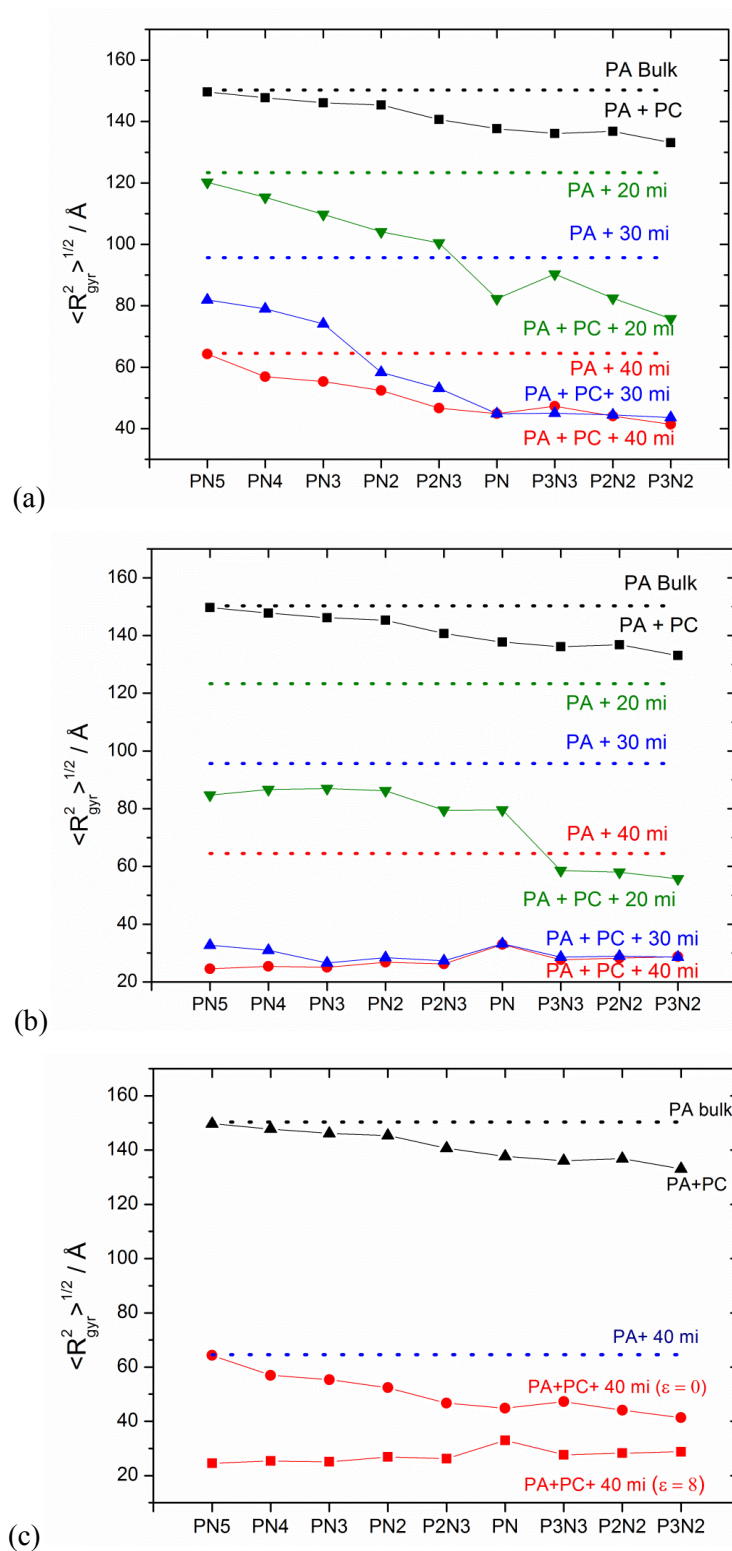


Figure 7.6. Effect of the charge density of the PC chains, number of trivalent ions, and the presence of a chelation on the rms radius of gyration, $\langle R_{gyr}^2 \rangle^{1/2}$, of the PA. Chelation between PC-mi is absent when $\epsilon = 0$ kJ mol⁻¹, panel (a) and present when $\epsilon = 8$ kJ mol⁻¹, panel (b). Panel (c) highlights the difference obtained for systems with 40 trivalent ions in the absence and presence of the chelation. Reference systems are also represented.

Table 7.4. Effect of the polycation architecture, multivalent ion concentration and PC-mi chelation on the number of trivalent ions condensed in the complex PA-PC-mi. The values were estimated through nearest neighbor analysis (mi-mi). N_{mi}^{nt} indicates the number of multivalent ions necessary to neutralize the system. The values of ϵ are given in kJ mol^{-1} .

PA-PC-mi systems							
PC	$N_{mi} = 40$		$N_{mi} = 30$		$N_{mi} = 20$		N_{mi}^{nt*}
	$\epsilon = 0$	$\epsilon = 8$	$\epsilon = 0$	$\epsilon = 8$	$\epsilon = 0$	$\epsilon = 8$	
PN5	34	34	29	30	20	20	37
PN4	33	34	29	30	20	20	36
PN3	32	33	29	30	20	20	35
PN2	31	31	28	29	20	20	33
P2N3	29	30	26	29	20	20	32
PN	28	28	27	27	20	20	30
P3N3	28	28	26	27	20	20	30
P2N2	27	27	26	27	20	20	30
P3N2	26	26	25	25	20	20	28

(*) N_{mi}^{nt} is calculated based on the unbalanced negative charge of PA left by PC following the equation, $N_{mi}^{nt} = \frac{(N_{seg,PA}) - (N_{PC} \cdot N_{+,PC})}{3}$.

The lowest mi concentration added, which corresponds to 20 trivalent ions (60 positive charges), contributes entirely to the neutralization of the residual PA-PC charge, irrespectively of the systems, and the whole set of mi is thus in the vicinity of the polyplex. For a higher number of added trivalent ions, there is still a higher probability for their fixation in the vicinity of PA-PC but differences arise with the architecture of the PC chains. The number of multivalent ions necessary to neutralize the PA-PC complex, N_{mi}^{nt} , is also shown in Table 7.4, and indicates that the amount of mi added to the last four systems of the table (higher PC charge density) is sufficient to neutralize the complexes. However, none of the complexes fully uptake the necessary mi. When an excess of mi is present, the number of condensed mi is slightly below that necessary to achieve full neutralization (typically 2 mi less), for all systems. Based on these results, it does seem that the number of positive trivalent ions, N_{mi} , attracted by the PC-PA complexes depends essentially on the complex charge, whereas chelation seems to be less significant. A dependence on the uptake of metal ions for PC efficiency to condense DNA is observed, which corroborates the experimental data (Figure 7.5).

7.4.3 Disposition of mi and PC in PA-PC-mi complexes

A contact analysis, describing the preferential position of PC monomers and mi along the PA chain, has been performed. The preferential disposition of the individual compacting agents along the PA chain, was firstly addressed. Two particles are considered to be in contact when the distance between their centers is shorter than 8 Å. The results of this analysis are depicted in Figure 7.7. Panel (a) presents the average number of PC monomers, corresponding to (two) PC chains with distinct charge densities that are in contact with the PA. For polycations possessing low charge densities, PN5, PN4 and PN3, the probability of contact with PA beads is low. Polycation chains seem to be evenly distributed along the PA, with some depletion close to its ends. As the charge density of the PC increases, the probability of finding a PC bead in contact with to the PA also rises, as expected. Beyond P2N3, the repulsion between the two PC chains is obvious, as indicated by the minimum in the curves at the center of the PA, as observed for the two fully charged PC chains [40].

It is clear from the results that systems P3N3 do not follow the general trend, showing a larger number of adsorbed monomers than system P2N2 that possesses a higher protonation degree. According to this, it is possible to conclude that the presence of a longer sequence of positive charges further increases the contact with PA. As such, PCs of the P3N_x type possess spots with more concentrated positive charge than PN_x or P2N_x, and the PC-PA interaction becomes stronger. In the case of trivalent ions alone, the distribution is homogeneous along the whole PA chain, Figure 7.6b. For higher concentrations of trivalent ions, the number of ions considered adsorbed onto the PA is, as expected, higher. Three systems were chosen to evaluate the disposition of the condensing agents in the ternary systems. Systems comprising low (PN5), intermediate (PN) and high (P3N2) protonation degree were selected. For each of these, the addition of 20 and 40 trivalent ions, as well as the absence and presence of the chelation, $\epsilon = 0$ and $\epsilon = 8 \text{ kJ mol}^{-1}$, was inspected. Analyses of the probability of contacts between PC-PA and mi-PA are provided in Figures 7.8, 7.9 and 7.10. Results of weakly protonated PC (PN5) are firstly considered (Figure 7.8).

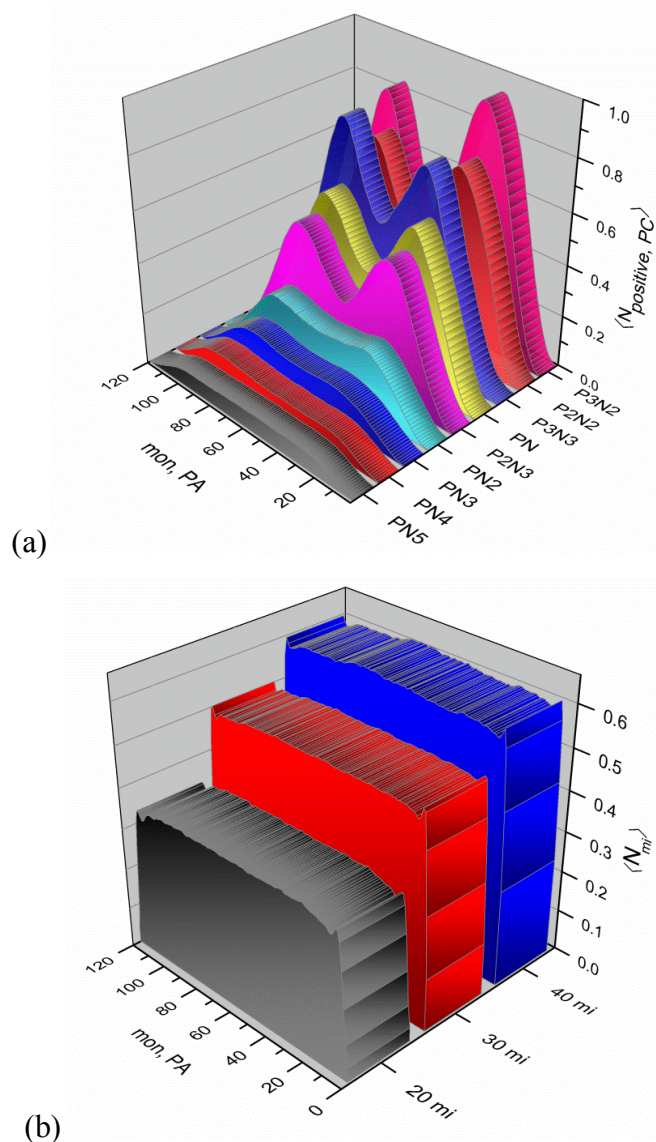


Figure 7.7. Contact analysis showing the preferential positioning of (a) PC chains with different architectures and (b) trivalent ions along the PA chain. A PC monomer or multivalent ion is considered to be in contact with PA monomers when the distance between them is lower than 8 Å. Systems contain only one condensing agent.

Considering the lower number of trivalent ions and no chelation interaction ($\epsilon = 0 \text{ kJ mol}^{-1}$), panel (a), it is observed that the probability of finding a PC in contact with the PA is very small, whereas the contact of trivalent ions with PA is more pronounced. It is, thus, clear that the interaction between PC and PA is quite weak, and trivalent ions adsorb more strongly onto the PA chain, being homogeneously distributed along PA and the charged segments of the PC are anchored in the spaces between the trivalent ions (see snapshot). When the number of trivalent

ions increase, panel (c), a larger concentration of mi is observed in the vicinity of the PA, as seen for the control systems, Figure 7.7b, and in good agreement with the data depicted in Table 7.4.

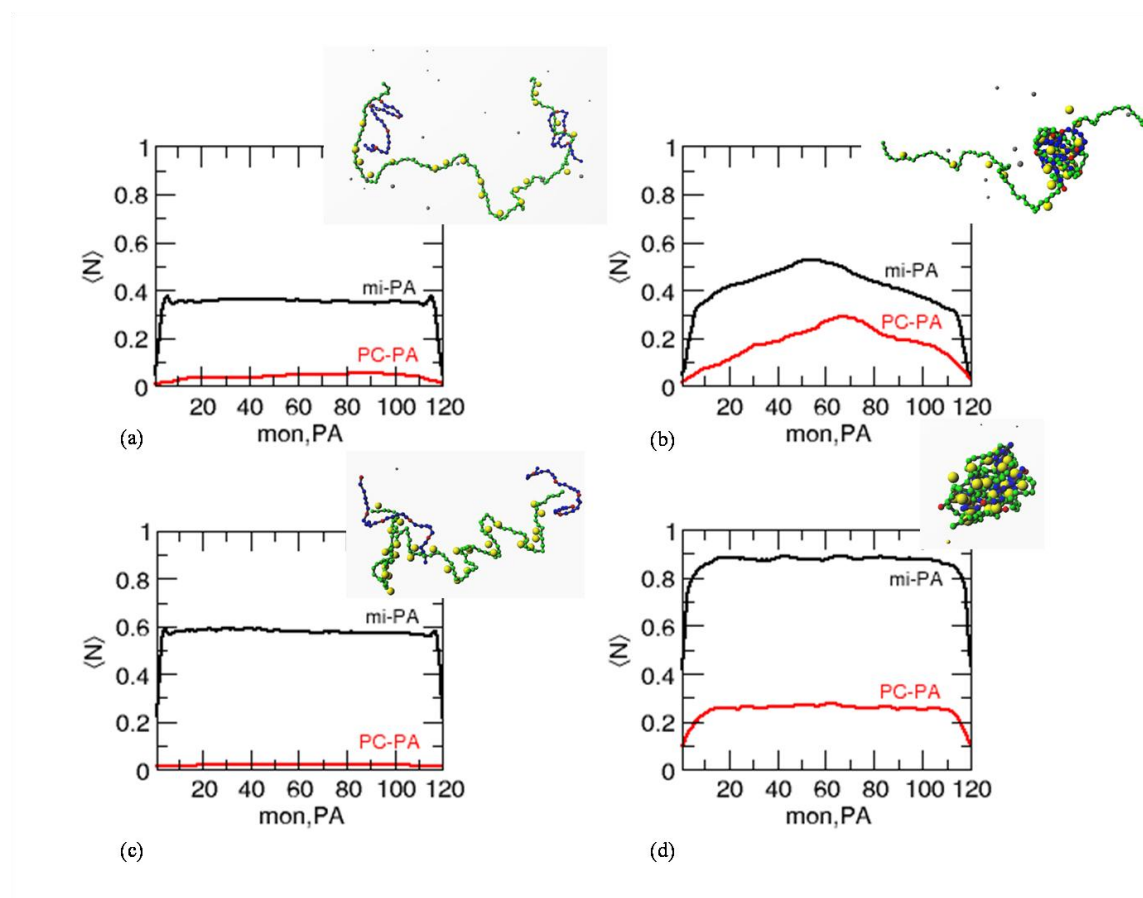


Figure 7.8. Contact analysis for PN5 systems with 20 trivalent ions at (a) $\varepsilon = 0$ and (b) $\varepsilon = 8 \text{ kJ mol}^{-1}$, and with 40 trivalent ions at (c) $\varepsilon = 0$ and (d) $\varepsilon = 8 \text{ kJ mol}^{-1}$. A representative snapshot of each system is also included. The PA segments are depicted in green, the neutral and positive segments of PC in blue and red, respectively, and the trivalent ions are presented in yellow.

This occurs at the expense of the PC binding, reflected in the decrease in the contact probability for PC monomers. The trivalent ions, in a higher number, fully cover the PA chain, diminishing the interaction with the PC. When chelation is promoted ($\varepsilon = 8 \text{ kJ mol}^{-1}$), the PC chains become more strongly bound to the PA, showing now a preferential positioning in the center of the PA. It is interesting to note that, even though the attraction of the PC chains to the PA increased and there is no visible repulsion between the PC chains along the PA, as observed for highly charged PC chains (Figure 7.7a). This suggests that the mi induce an association of the PC chains, probably as a consequence of the long sequences of neutral monomers. The trivalent ions accompany the trend followed by the PC, indicative of the association of both agents. An increase in the concentration of multivalent ions, Figure 7.8d, leads to the compaction of DNA and consequent loss of degrees of freedom. The probability of finding both condensing agents becomes thus, uniform along the PA chain, being also this one the system that shows a higher

concentration of agents close to PA. Hence, when PC-mi chelation is considered the interactions of both compacting agents with PA, is enhanced.

For an intermediately charged PC chain (PN), different contact profiles are obtained for most systems (Figure 7.9). The neat PA-PC systems (Figure 7.7) show that the increase in the number of charged groups in the PC promotes a stronger PA-PC contact. This is also observed in the presence of trivalent ions (Figure 7.9a).

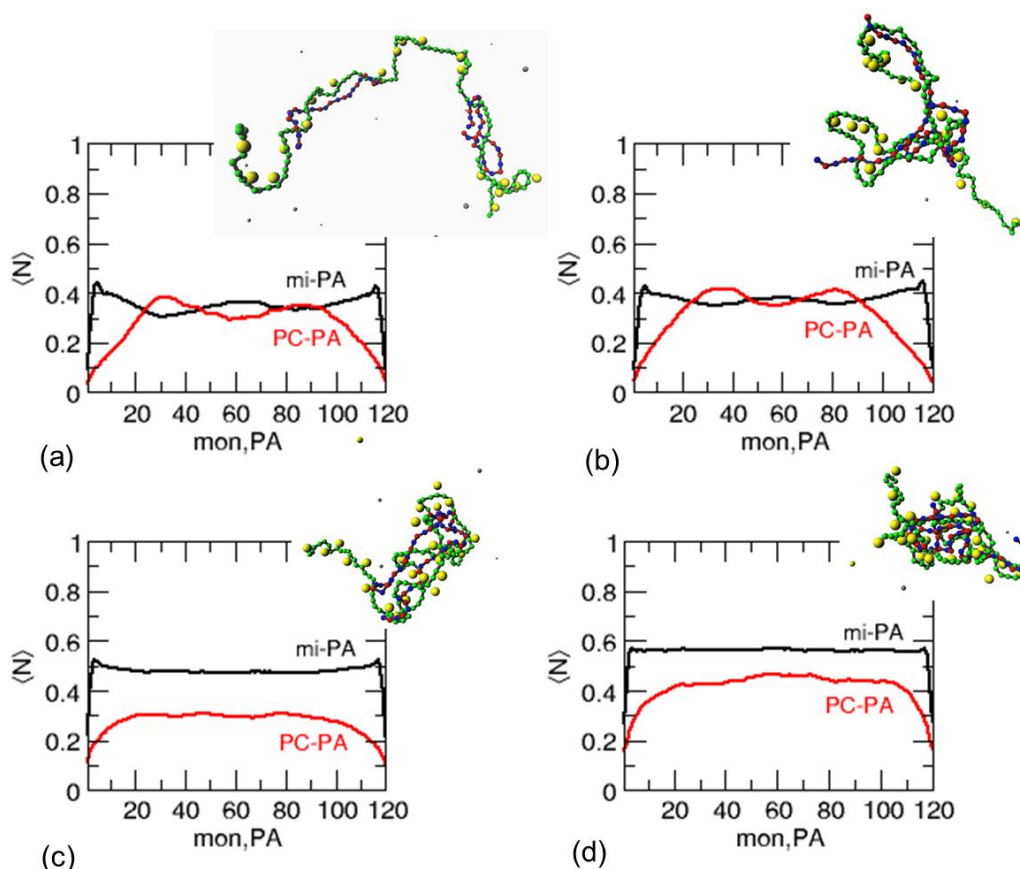


Figure 7.9. Contact analysis for PN systems with 20 trivalent ions at (a) $\epsilon = 0$ and (b) $\epsilon = 8 \text{ kJ mol}^{-1}$, and with 40 trivalent ions, at (c) $\epsilon = 0$ and (d) $\epsilon = 8 \text{ kJ mol}^{-1}$. A representative snapshot of each system is also included. The PA segments are depicted in green, the neutral and positive segments of PC in blue and red, respectively, and the trivalent ions are presented in yellow.

For this system, the PC chains reside preferentially in each half of the PA chain and the trivalent ions are now mostly excluded from the regions where the PC chains reside. This effect is partially lost when the number of trivalent ions is increased (panel c), probably due to the higher compaction degree of the PA. Interestingly, and contrarily to what was observed with PN5, the presence of PC-mi interaction does not affect the contact profiles significantly, except for a slight increase in the number of PC beads and trivalent ions that are in contact with the PA. We recall

that the values of $\langle R_{gyr}^2 \rangle^{1/2}$ obtained for these two systems PN plus 20 trivalents ($\epsilon = 0 \text{ kJ mol}^{-1}$) and ($\epsilon = 8 \text{ kJ mol}^{-1}$) are coincident, Figures 7.6a and b. Again, the presence of the chelation, leads to a higher proximity between the compacting agents and PA and to an increase of PA compaction, shown in the snapshot (panel d). The higher charge density of the PC, and the closeness of the charged beads makes it more difficult to accommodate trivalent ions, as it has been experimentally observed in binary mixtures of PC-mi [256, 281, 297, 312], which has consequences also in the ternary systems.

Finally, complexes formed with P3N2 PC were assessed and represented in Figure 7.10. This PC chain possesses the highest charge density of them all, which results in a stronger interaction with the PA chain, as observed above. In the first set, with 20 trivalent ions, panel (a) and (b), all trivalent ions are positioned close to the polypeplex, whereas in the set with 40 trivalent ions panels (c) and (d), 26 trivalent ions are found in the complex (Table 7.4). This difference has consequences in both PA compaction and contact profiles.

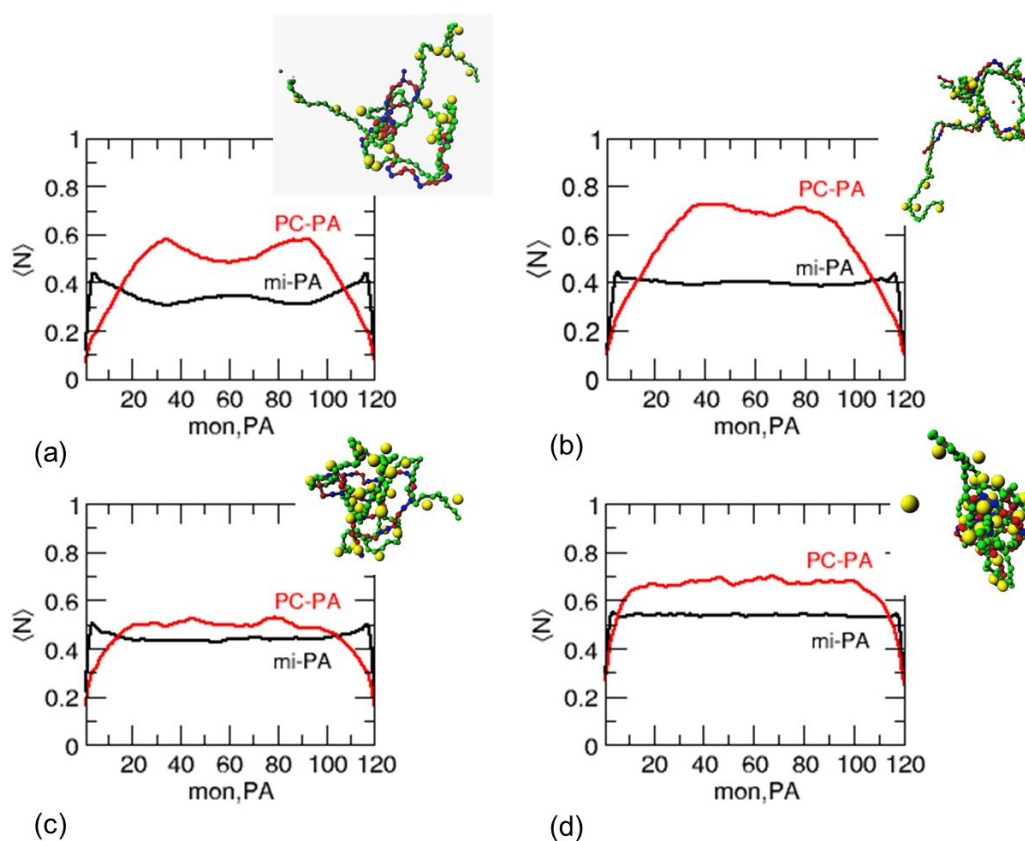


Figure 7.10. Contact analysis for P3N2 systems with 20 trivalent ions at (a) $\epsilon = 0 \text{ kJ mol}^{-1}$ and (b) $\epsilon = 8 \text{ kJ mol}^{-1}$, and with 40 trivalent ions, at (c) $\epsilon = 0 \text{ kJ mol}^{-1}$ and (d) $\epsilon = 8 \text{ kJ mol}^{-1}$. A representative snapshot of each system is also included. The PA segments are depicted in green, the neutral and positive segments of PC in blue and red, respectively, and the trivalent ions are presented in yellow.

The system of P3N2 with 20 mi, panel (a) and (b), shows the two PC chains preferentially separated along the PA, while trivalent ions are located between them and close to the ends of the PA. When chelation is considered, panel (c) and (d), the interaction between the condensing agents and PA increases but, interestingly, the effects are more pronounced than for system PN, even though the charge density of P3N2 is larger. The difference probably arises from the fact that systems P3N2 possess two consecutive neutral monomers, which seems to favor the PC-mi interaction in the presence of the chelation. As observed for PN5, the coexistence of mi and PC in the same position enhances PC contact, showing a cooperative effect.

To summarize, systems with PCs with a lower protonation degree, and hence, less effective condensing agents, are compensated by a stronger PC-mi interaction which ultimately leads to a comparable compaction in all systems when PC-mi chelation is considered.

7.5 Overview

From the present mechanistic study on DNA-PEI-Fe(III) complexes and previously published data, several conclusions can be drawn on the interactions governing these ternary mixtures. The addition of trivalent ions to DNA-PEI complexes results in an additional DNA compaction, observed both in experimental and theoretical data, in Chapter 4. The larger the concentration of PEI, the lower is the amount of Fe(III) necessary to induce reasonable degrees of DNA condensation and vice versa. Also, it was found that the positioning of Fe(III) along the PA chain is complementary to that of PC, and therefore mutual contact is avoided. In Chapter 5, different architectures of PEI, with different chain lengths displayed the same extend of DNA condensation at similar N/P and Fe(III)/P ratios, although slightly more pronounced for lower molecular weight PEI.

In this Chapter, new effects were investigated to further understand the interactions in ternary complex. As shown in the experimental part, the importance of chelation between PEI-Fe(III) was demonstrated, by both potentiometric and conductance measurements. Additional evidence of the chelation effect was attained by the retardation of DNA condensation when both condensing agents were mixed prior to the addition to DNA (see Figure 7.3). The premixing of the condensing agents reflects in a lower efficiency on DNA neutralization and a lower degree of compaction. Despite the coincident Fe(III)/P ratios of condensation, different concentrations of Fe(III) in the supernatant were quantified, pinpointing the influence of the PEI structural properties in the ternary mixture, with a larger removal of Fe(III) from the solution when bPEI10 is added (Figure 7.5). Generally, the profiles for both DNA condensation and Fe(III) fixation obtained are identical, irrespective the type of PEI used, which indicates that the chelation behavior characterized by potentiometry and conductance assays for bPEI1.2 may be extrapolated to other PEIs under study.

According to these new facts, systems were now modeled imposing differences in the linear charge density and in the disposition of positive and neutral monomers of the PC, as well as considering an attractive interaction between the neutral monomers of PC and trivalent ions, mimicking the chelation effect. The results obtained are schematically summarized in Figure 7.11.

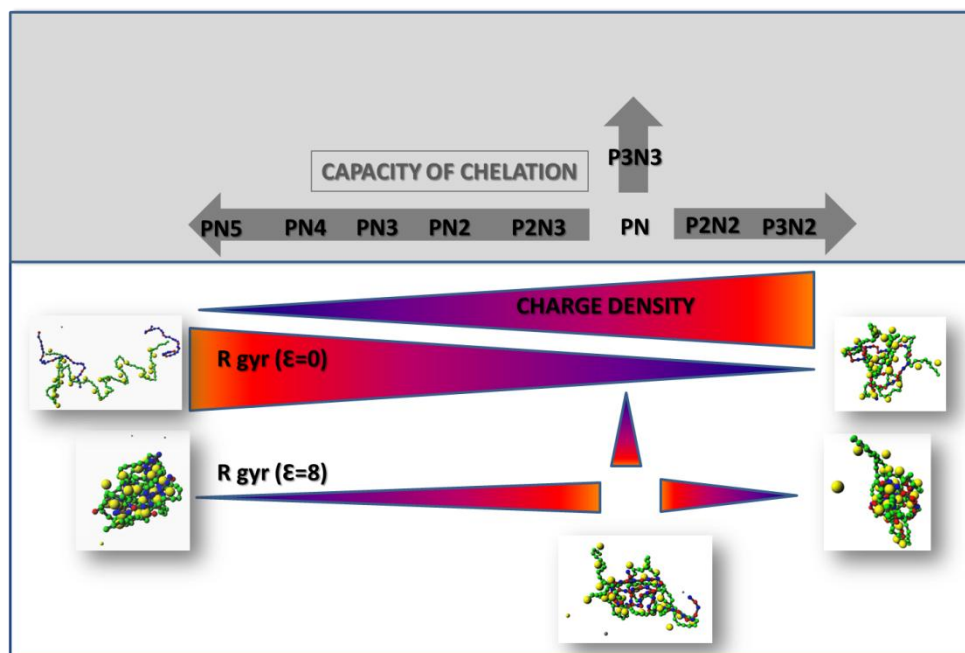


Figure 7.11. Schematic illustration of the general trends obtained by Monte Carlo simulations. Grey arrows represent the increase in the chelation capacity of PC chains (considering the number of consecutive neutral beads in PC), while the colored pointers represent the variation in charge density of the PC chains and radius of gyration of the PA (red regions correspond to higher values and blue ones to lower values). The values of ϵ are given in kJ mol^{-1} .

Two general aspects can be extracted from comparison of the systems with imposed chelation ($\epsilon = 8 \text{ kJ mol}^{-1}$), and in its absence ($\epsilon = 0 \text{ kJ mol}^{-1}$). At $\epsilon = 0 \text{ kJ mol}^{-1}$, the values of R_{gyr} are dependent on the charge density of the PC chains, presenting smaller values as the PC charge density is higher. The imposition of the chelation leads to a further decrease of the R_{gyr} for all studied systems, and the differences between systems become less noticeable, in good agreement with the experimental data in Chapter 5. In this case, PA compaction seems to be dictated by the capacity of chelation of PC and, even PC chains with a reasonably high degree of condensation can show chelating capacity provided they possess at least two consecutive neutral monomers. On the other hand, results show that the amount of trivalents in the surroundings of the PA-PC complex is very similar or equal for sets, suggesting that the imposed potential does not attract multivalent ions from the bulk. The mi concentration in each polyplex seems, to be governed by the unbalanced charge on the PA-PC complex. The main difference between the two sets of systems was found in

the distribution of the condensing agents. When chelation exists, contact analyses show overlap of the condensing agents. If chelation is hampered due to the proximity of positive charges, in the case of PN, an additional DNA compaction is less pronounced. On the other hand, in the lower charged polycation PN5, a large concentration of trivalent ions along the PC chain is possible.

7.6 Conclusions

This study was carried out to assess the mechanism behind the formation of DNA-PEI-Fe(III) complexes. Results from Monte Carlo simulations provide a rationale for the experimental data, obtained both in the present and previous Chapters. A synergistic effect resulting from the induced chelation between PEI-Fe(III) was observed. Fe(III) ions are able to equalize all the systems into a significant extent of compaction when PEI-Fe(III) interactions are considered. The rationalization of the behavior of these ternary mixtures allows enlarging the possibilities of optimization of their use as gene delivery vectors.

CHAPTER 8

PEI and Fe(III) mediating transfection

8.1 Introduction

The improvement and evaluation of different non-viral formulations such as polymer-based pDNA complexes (polyplexes) has been largely based on transfection measurements. Hitherto, among the cationic polymers, linear polyethylenimine (IPEI) is the most effective polycationic transfection agent, known as a golden standard for polymeric gene delivery [72, 102, 314]. In this final task the influence of the combination of Fe(III) with pDNA-IPEI22 complexes on the diverse multisteps followed until gene expression is evaluated. The conditions are selected to ensure a good performance of transfection, including the use of the more common used buffers and relevant simultaneously, the optimization of the polyplexes in the acetate buffer.

Thus, the interaction between mixing components is modulated by inducing systematic changes in buffer composition and ionic strength, using 4-(2-hydroxyethyl)-1-piperazineethanesulfonic acid (Hepes) and acetate buffer at physiological salt conditions and lower, and analyzed their repercussion. A collection of techniques was employed to elucidate the physicochemical properties and biological activity of the pDNA-IPEI22 and pDNA-IPEI22-Fe(III) complexes over a range of N/P and Fe(III)/P ratios.

8.2 Materials and Methods

8.2.1 Materials

Plasmid pCMVLuc (Photinus pyralis luciferase under control of CMV enhancer/promoter) described in Plank et al [315] was purified with the EndoFree Plasmid Kit from Qiagen (Hilden, Germany). Linear PEI (22 kDa) was synthesized by acid-catalyzed deprotection of poly(2-ethyl-2-oxazoline) (50kDa, Aldrich) as describe in Brissault et al [316]. Ferric chloride hexahydrate was purchased to Sigma-Aldrich (Germany). Cell culture media, glutamine, antibiotics and fetal calf serum (FCS) were purchased from Invitrogen GmbH (Karlsruhe, Germany). Cy5-labeling kit for pDNA was obtained from Mirus Bio (Madison, WI, USA). GelRed was obtained from Biotium (Hayward, USA). Glucose was purchased from Merck (Darmstadt, Germany), Hepes from Biomol GmbH (Hamburg, Germany) and sodium chloride from Prolabo (Haasrode, Belgium). Dilutions were prepared in, i) 20 mM Hepes buffered 150 mM NaCl (HBS) pH 7.4, ii) 20 mM Hepes buffered 5% glucose (HBG) pH 7.4, and iii) 30 mM acetate buffer (1.6 mM CH₃COOH, 28.4 mM NaCH₃COO.3H₂O) (Ac30) pH 6.0, iv) 50 mM acetate buffer (2.7 mM CH₃COOH, 47.3 mM NaCH₃COO.3H₂O) (Ac50) pH 6.0 and v) 100 mM acetate buffer (5 mM CH₃COOH, 95 mM NaCH₃COO.3H₂O) (Ac100) pH 6.0. Luciferase for cell culture lysis reagent, and D-luciferin sodium salt were obtained from Promega (Mannheim, Germany).

8.2.2 Complex formation

For gel shift, transfection and metabolic activity assays, DNA-IPEI and DNA-IPEI-Fe(III) complexes were prepared as follows. A fixed volume of PEI solution (4.5 μ L) with variable concentrations was added to 200 ng of pCMVLuc DNA solution (15 μ L) and rapidly mixed by pipetting. The final concentration of DNA in solution is 10 μ g mL⁻¹. The trivalent salt solutions were always freshly prepared and added directly to the DNA-PEI mixture 15 min after mixture equilibration, at a fixed volume (0.5 μ L), and mixed by pipetting once again. Polyplexes were allowed to equilibrate for 40 min at room temperature before use. Throughout this Chapter specific N/P ratios were determined, considering the mass of 330 g mol⁻¹ correspondent to one phosphate group on DNA. In PEI, the mass of 43 g mol⁻¹ corresponds to one amine group. The same calculation was performed considering now the molar concentration of positive charges for the Fe(III) in solution and represented as the Fe(III)/P ratio. The charge ratio between the condensing agents, PEI:Fe(III), in these studies was 2:1 and 1:1 in the complex. It should be noted that both the N/P and Fe(III)/P ratios are established on the basis of the amounts of PEI and DNA, and Fe(III) and DNA added to the solution. They do not necessarily reflect actual charge ratios.

In the case of polyplexes prepared to flow cytometry assays, the same aforementioned procedure but now the final concentration of DNA in solution is $50 \mu\text{g mL}^{-1}$ in a total volume of $100 \mu\text{L}$. Further details are given in the corresponding sections.

For size and zeta potential measurements, the concentration of plasmid DNA was the same $10 \mu\text{g mL}^{-1}$, but a larger volume sample of the polyplex mixture ($1000 \mu\text{L}$) was prepared according to the same proportions and procedure described previously.

8.2.3 Gel shift assay

DNA complexes (200 ng of pCMVLuc DNA in $20 \mu\text{L}$) with loading buffer (prepared from 6 mL of glycerine, 1.2 mL of 0.5 M EDTA, 2.8 mL of H_2O , 0.02 g bromophenol blue) were loaded into the wells of a 1% agarose gel in TBE buffer (Trizma base 10.8 g , boric acid 5.5 g , disodium EDTA 0.75 g , in 1 L of water) containing GelRed™ for DNA detection. The gel was run at 80 V for 80 minutes and then photographed under UV light.

8.2.4 Particle size and zeta-potential

Hydrodynamic radius and zeta potential of DNA-PEI and DNA-PEI-Fe(III) complexes were assessed by dynamic light scattering in a Delsa Nano C Submicron (Beckman Coulter, Krefeld, Germany). Samples were prepared, equilibrated and measured in triplicate at $25 \text{ }^\circ\text{C}$ with a detection angle of 160° . In the case of size measurements, the correlation functions were fitted by non-negative least squares (NNLS) and the distribution of particle sizes recorded.

8.2.5 Cell culture

HUH-7 hepatocellular carcinoma cells (JCRB 0403; Tokyo, Japan) were cultured in Dulbecco's modified Eagle's medium (DMEM) containing 2 mM glutamine, supplemented with 10% FBS. HeLa cells (human cervical carcinoma cells, ATCC CCL-2) were grown in DMEM supplemented with 10% FBS. All cultured cells were grown at $37 \text{ }^\circ\text{C}$ in 5% CO_2 humidified atmosphere.

8.2.6 Cell transfection

In vitro pCMVLuc DNA transfection efficiency was assessed in HUH-7 and HeLa cells. Measurements were performed in 96-well plates (TPP, Trasadingen, Switzerland) at a density of 1×10^5 cells/well, for both cell lines. Before transfection, medium was replaced with $80 \mu\text{L}$ of fresh growth medium, thereafter, the complexes in $20 \mu\text{L}$ were added to each well and incubated at $37 \text{ }^\circ\text{C}$. After 24 hours of transfection, the remaining medium in each well was removed by suction and cells were treated with $100 \mu\text{L}$ cell lysis buffer (25 mM Tris pH 7.8 , 2 mM

cyclohexylenedinitrilotetraacetate (CDTA), 2mM Dithiothreitol (DTT), 10% glycerol, 1% Triton[®] X-100). Luciferase activity in 35 μ L cell lysate was assessed in white 96 well plates using a luciferase assay kit (100 μ L Luciferase assay buffer, Promega, Mannheim, Germany) and measured on a luminometer for 10 s (Centro LB 960 instrument, Berthold, Bad Wildbad, Germany). All complexes were analyzed in at least triplicate. In assays performed with addition of chloroquine, a concentration of 100 μ M was added to the buffer solutions in which complexes were prepared, and then 4 hours post-transfection the medium was replaced by fresh growth medium to avoid cell damage.

8.2.7 Fluorescence activated cell sorting (FACS)

To assess the level of internalization of DNA-PEI and DNA-PEI-Fe(III) complexes the following procedure was conducted in HUH-7 cell line. Cells were seeded in 24 well plates at a density of 5×10^5 cells/well in 500 μ L medium 24 hours prior to transfection. Before transfection, medium was replaced with 400 μ L of fresh growth medium. An amount of 100 μ L polyplex solution with 1 μ g of pCMVLuc DNA containing Cy5-labeled DNA (20%) was added to the cells. Four hours after polyplexes addition, the cells were washed once with phosphate buffer saline (PBS) and treated with 100 IU/mL heparin to remove extracellularly bound complexes. Afterwards, the cells were harvested by treatment with trypsin/EDTA solution (Invitrogen GmbH, Karlsruhe, Germany). Trypsin was inactivated with medium (PBS) and cells were centrifuged (2000 rpm; 5 min). The remaining supernatant was removed and the pellet resuspended in 500 μ L PBS and analyzed using a Cyan[™] ADP flow cytometer (Dako, Hamburg, Germany). To discriminate between viable and dead cells, cells incorporating high levels of DAPI and showing a reduction in forward scattering as a measure of cell size were excluded from further analysis. Samples were analyzed using Flow Jo software (Treestar, Inc., San Carlos, USA). Experiments were performed in duplicate.

8.2.8 Metabolic activity assay

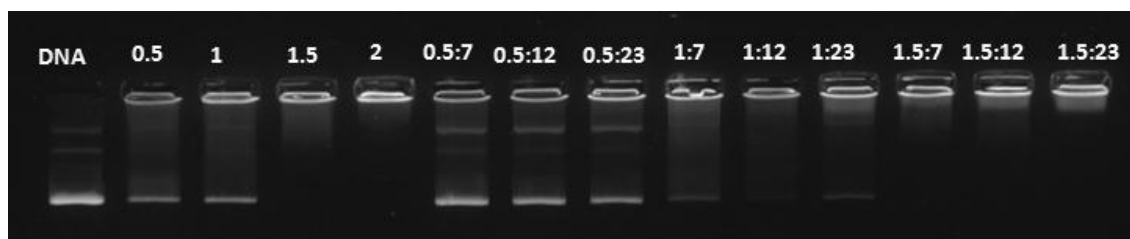
Metabolic activity was analyzed 48 h after transfection using the CellTiter-Glo[™] luminescent cell viability assay (Promega, Mannheim, Germany) according to the manufacturer's instructions. The assay is based on the quantitative measurement of the cellular ATP content. A volume of 50 μ L was removed from each well of the transfection plate and was mixed with 50 μ L of CellTiter-Glo[™] reagent. The plate was shaken for 2 minutes to induce cell lysis and allowed to incubate at room temperature for 15 min. Luciferase activity in 70 μ L cell lysate was measured in white 96 well plates using a luciferase assay kit (100 μ L Luciferase Assay buffer, Promega, Mannheim, Germany) on a luminometer (Centro LB 960 instrument, Berthold, Bad Wildbad, Germany). Untreated control cells correspond to 100% metabolic activity.

8.3 Results

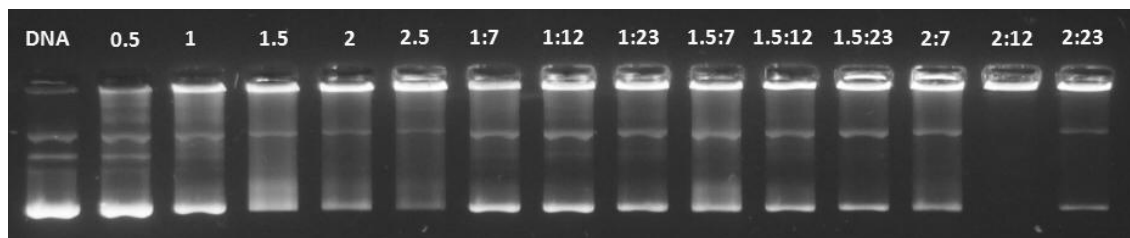
8.3.1 Gel shift assay

The spontaneous association of polyanion with polycations on aqueous media is a result of a strong electrostatic interaction, and therefore, the use of different biological buffers may influence the association of components of the ternary mixture [67]. Firstly, the properties of polyplexes prepared with Hepes and acetate buffers with different ionic strengths, Hepes with no extra addition of salt (HBG) and in the presence of salt (150 mM) and acetate buffer from 30-100 mM, were examined. The Hepes buffer is designated as a Good buffer [317] being generally considered to be a buffer with excellent buffering capacity over the required pH range, and additionally, possessing poor ability for metal complexation. Previously, it was reported efficient incorporation of DNA in DNA-PEI-Fe(III) polyplexes using acetate buffer at 150 mM [308], however, in the present study, acetate buffer over the range of 30-100 mM was used instead.

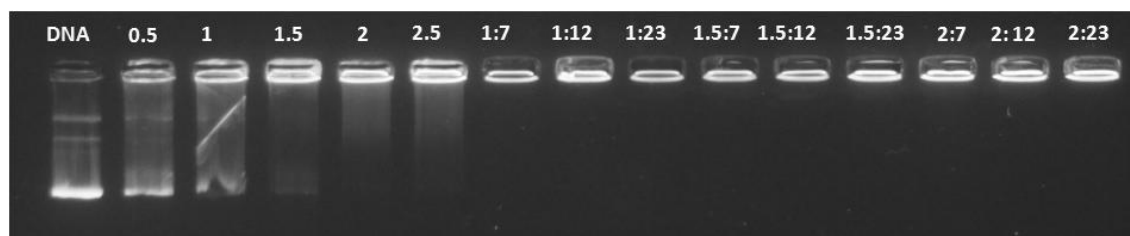
In Figure 8.1 are depicted results of agarose gel electrophoresis, displaying the electrophoretic mobility of DNA in polyplexes made of IPEI22 alone or IPEI22 in combination with Fe(III), and prepared in four different media. As expected, the addition of IPEI22 results in a decrease of the migration of DNA through the gel, indicating DNA neutralization. The addition of the second condensing agent, Fe(III), induces DNA condensation at an even lower N/P ratio, which is consistent with our earlier findings, Chapter 4 and 5. These observations are independent of the buffers used. However, and as expected, the comparison between panels (a) and (b) reveals a lower retention of DNA in the wells, i.e., lower DNA condensation, when solutions are prepared in a buffer with high ionic strength (HBS), and this fact is observed for both DNA-PEI and DNA-PEI-Fe(III) complexes. The same trend is observed for DNA-PEI and DNA-PEI-Fe(III) complexes prepared in acetate buffers, Ac30 and Ac100, see panels (c) and (d). This complexation delay obtained by high salt concentration is a strong indication of the predominant electrostatic nature of polyplex formation. Furthermore, differences in polyplex mobility are visible between the two different buffers used. Thus, DNA-PEI complexes prepared in acetate buffer neutralize at low N/P ratio, panel (c), similarly to the results found to HBG, in panel (a), whereas in the presence of Fe(III), more marked DNA retention is observed to complexes prepared in acetate buffer. For high ionic strength buffers, panels (b) and (d), the inhibition on the DNA neutralization is more evident in the case of complexes prepared with HBS than with Ac100. These divergences detected between Hepes and acetate buffers might be explained by the difference in the pH of the media, since a lower pH increases the protonation of PEI [244, 286]. Despite different abilities, all the systems are able to incorporate DNA and the synergy of PEI-Fe(III) is clearly observed, whatever the media employed.



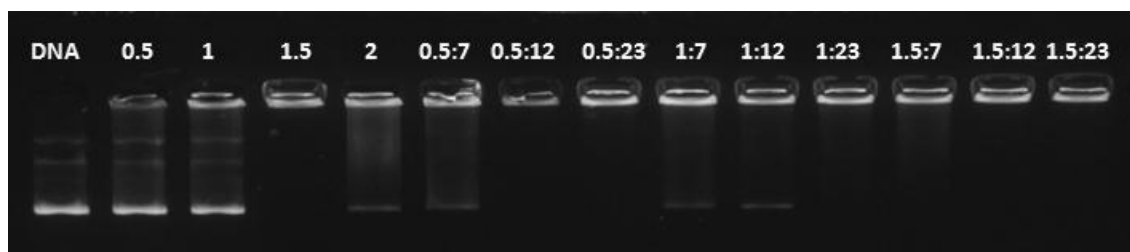
(a) HBG, pH 7.4



(b) HBS, pH 7.4



(c) Ac30, pH 6.0



(d) Ac100, pH 6.0

Figure 8.1. DNA binding assay by IPEI22 and the combination of IPEI22 and Fe(III), at different N/P and N/P:Fe(III)/P ratios, respectively. The polyplexes were prepared in Hepes and acetate buffers at different ionic strengths. The first lane of the gel corresponds to DNA in the absence of condensing agents. DNA concentration is $10 \mu\text{g mL}^{-1}$ in each sample.

8.3.2 DLS measurements

In order to monitor the effect of the addition of Fe(III) to DNA-PEI polyplexes in aqueous buffer solutions, dynamic light scattering (DLS) was used. Figure 8.2 shows the intensity distribution graphs of DNA-PEI and DNA-PEI-Fe(III) complexes generated in HBG and HBS, at N/P ratios similar to those later used in transfection assays. DNA-PEI complexes at N/P = 6 in

HBG, Figure 8.2a, were found to have a bimodal distribution with the strongest intensity belonging to complexes with roughly 100 nm, and a second population at larger sizes (ca. 1316 nm) with lesser intensity. Increasing N/P ratio leads to a reduction of the particle size, now with 70.4 ± 0.549 nm, in concordance with data reported in literature [83, 318].

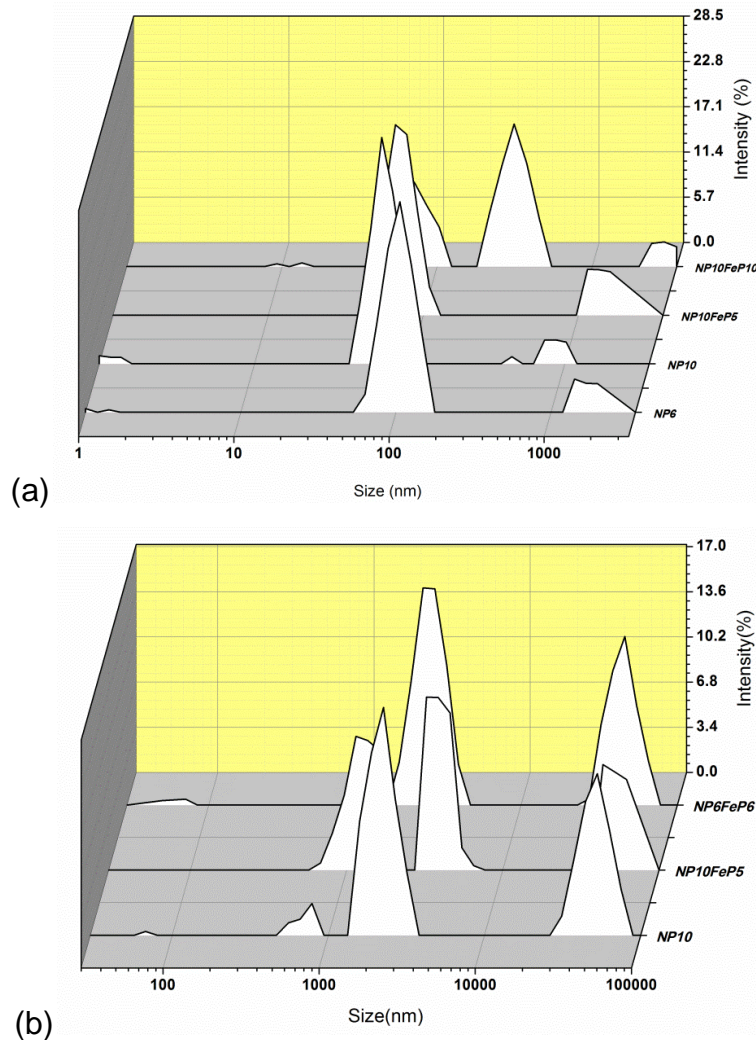


Figure 8.2. DLS curves of intensity size distribution for complexes prepared in biological buffers, (a) HBG and (b) HBS.

The addition of Fe(III) ions, on the other hand, leads to an increase in the size of the complexes from approximately 70 to 100 nm, at Fe(III)/P ratio of 5. At N/P:Fe(III) = 10:10, the intensity distribution graphs shows the appearance of a third peak at intermediate values around 220 nm arising possibly from the promotion of complexes aggregation, and/or from some expansion of the DNA-PEI complexes. In the case of complexes prepared in HBS, Figure 8.2b, larger particles are observed as expected. It has already been observed that, at physiological conditions, polyplexes with IPEI22 have an inherent tendency to aggregate that evolves with the time, conversely to what occurs with branched PEI chains with 25 and 800 kDa [83, 159, 318]. At higher ionic strength, the effective charge of the free polymer segments are reduced and,

consequently, also that of the complexes, which reduces the electrostatic stabilization of the particles and leading to high levels of aggregation [319]. Therefore, at $N/P = 10$, three different populations are observed displaying a large range of sizes. The presence of Fe(III) influences the populations differently; the peak corresponding to the population of smaller sizes becomes more intense, but, no significant differences are found for the larger populations when compared with analogous polyplex in the absence of Fe(III). Furthermore, the complexes prepared at lower N/P ratio, $N/P = 6$, even in the presence of Fe(III) attain larger sizes than those at $N/P = 10$. This fact corroborates with the fact that higher N/P ratios are more efficient in the control of the size of polyplexes [83].

The distribution of sizes for DNA-PEI and DNA-PEI-Fe(III) complexes prepared in Ac50 was further assessed at N/P values typically used in transfection, see Figure 8.3a. Complexes at $N/P = 5$ present a distribution shifted to higher values when compared to $N/P = 6$, with two populations distributed at lower sizes, with an average value of ca. 757.2 nm and the other corresponding to larger sizes ca. 1119.7 nm. In the case of complexes prepared at $N/P = 6$, again two peaks are clearly distinguishable, but this time for lower values, one population of small values ca. 180 nm and the other to larger sizes ca. 720 nm. Fe(III) contributes to reduce the size of DNA-PEI complexes, similarly to what was observed using HBS (Figure 8.2a), and the complexes prepared with $N/P:Fe(III)/P = 5:10$ show roughly the same distribution as those of $N/P = 6$, with a first population at ca. 225 nm and a second one to larger sizes (ca. 964.5 nm). Considering these data, it is concluded that Fe(III) reduces the size of polyplexes prepared at high or moderate ionic strength. This contrasts with the results obtained for the complexes prepared in HBG. As it is observed in DNA incorporation assays, Figure 8.1 panel (a) and (c), a low concentration of PEI is able to efficiently condense DNA when in conjunction with Fe(III) at low salt conditions. However, at high N/P ratio, the addition of the extra condensing agent seems to destabilize the complexes. For high salt conditions (HBS and Ac50), the presence of the extra condensing agent offers both stabilization and compaction of the complex.

In an attempt to understand the behavior of ternary polyplexes as a function of the ionic strength of the buffer, four acetate buffer solutions at different ionic strength ranging from 30 to 100 mM were used to prepare the polyplexes. The results of the average size and zeta potential obtained for ternary complexes, of low N/P ratio, are gathered in Figure 8.3a. The reduction of salt concentration in the media leads to the formation of smaller and more positively charged polyplexes. At low N/P ratios using Ac30, it is possible to attain small complexes with 261 ± 4 nm that possess, simultaneously, a high surface charge.

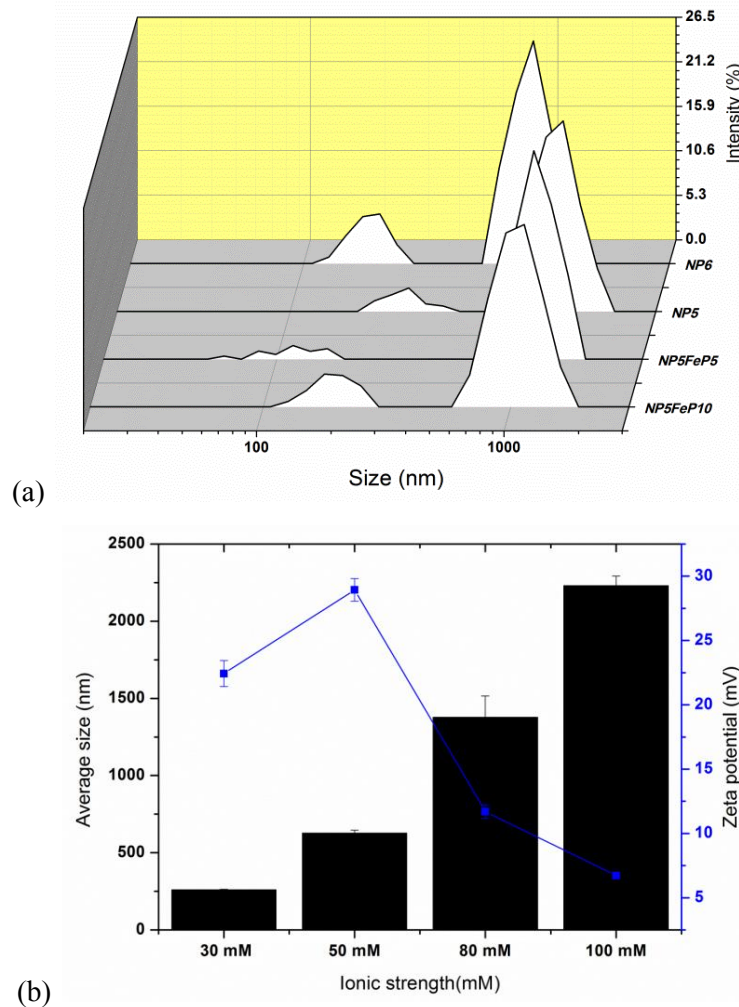


Figure 8.3. In panel (a) are represented the DLS curves of intensity size distribution for complexes prepared in Ac50. And, in panel (b) average size and zeta potential versus acetate buffer ionic strength of complexes at N/P:Fe(III)/P = 3:12.

8.3.3 Gene expression of DNA-PEI-Fe(III)

i. DNA-PEI-Fe(III) complexes prepared in HBS and HBG

The effect of the addition of Fe(III) to the DNA-PEI complexes on the reporter gene expression was determined using two different cell lines, HUH-7 and HeLa. Transfection efficiency was analyzed for polyplexes formed under low salt conditions, HBG, and under higher salt conditions, HBS (Figure 8.4). The trends attained are comparable for both cell lines, but polyplexes prepared in HBG show lower *in vitro* transfection efficiencies when compared to HBS, in agreement with the literature [83, 159]. Generally, it is observed that for complexes formed in HBG the addition of Fe (III) reduces their transfection efficiency, panels (a)-(d), being

directly correlated to the Fe(III)/P ratio, i.e., the larger the amount of Fe(III) added, the larger is the reduction on transfection efficiency. In the case of complexes prepared in HBS, with N/P=6, the higher concentration of Fe(III) maintained the transfection efficiency, in HeLa cell line, panel (b). In the case of the HUH-7 cell line, approximately 5-fold higher transfection efficiency, panel (a) is found. For N/P = 10 in HBS, in both cell lines, the gene uptake is almost preserved at the lowest Fe(III)/P = 5, but is reduced for higher Fe(III) concentrations, panel (c) and (d). These differences found in the optimal concentration of Fe(III) for complexes at N/P = 6 and N/P = 10 suggest the importance of the regulation of the additional complex charge provided by metal ions for transfection efficiency.

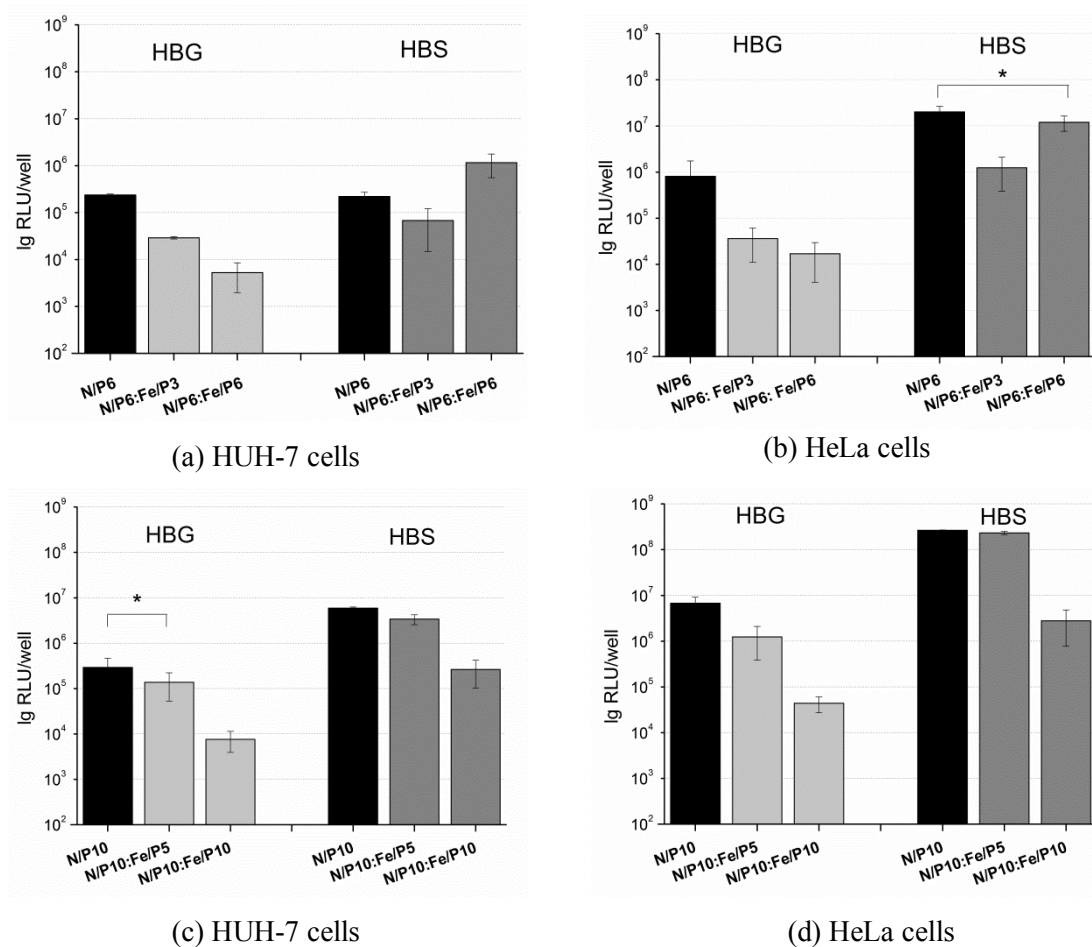


Figure 8.4. Reporter gene transfection of DNA-PEI and DNA-PEI-Fe(III) polyplexes on HUH-7 and HeLa cell lines. Complexes of DNA-PEI-Fe(III) were mixed in HBG and HBS at N/P ratios of 6 (a, b) and 10 (c, d), and compared to standard PEI complexes at the same N/P ratios. Luciferase activity is presented as mean values \pm SD of triplicates. A Student's t-test was performed to assess statistical significance between each sample and the reference N/P = 6 and N/P = 10 (HBG or HBS) (ns = not significant; * $p < 0.05$).

ii. DNA-PEI-Fe(III) complexes prepared in acetate buffers

The same analyses were conducted in systems prepared in acetate buffer, with increasing ionic strength, as shown in Figure 8.5. Here, the reference samples prepared in identical acetate buffer are also represented, for an easily comparison. Also represented are reference samples prepared in HBG or HBS, according to the similarity of the sizes of complexes. Results confirm the effect of the ionic strength of medium on transfection efficiency, as observed previously, yielding an increase in transfection efficiency in both cell lines when high ionic strength buffer is used to prepare the polyplexes. The influence of the addition of Fe(III) on transfection efficiency seems to be correlated also with this property. Complexes prepared in low concentrated buffer (Ac30), panels (a) and (b), in the presence of the metal ions show a decrease in gene expression in HUH-7 cells, whereas in HeLa, a sharp reduction is only observed for complexes at N/P:Fe(III)/P = 6:6. In the case of complexes at N/P:Fe(III)/P = 6:3 there is a slight increase of the transfection efficiency when compared with an analogous N/P = 6 in Ac30. The same is observed for those prepared in HBG.

As the ionic strength is increased (Ac50), panels (c) and (d), higher values of gene transfer are attained. The differences observed between DNA-PEI and DNA-PEI-Fe(III) complexes followed exactly the same trend as found before, in panels (a) and (b), but now the values become approximately equal to those of the reference samples. Recalling that the ionic strength of the medium influences considerably the size of the polyplexes (Figures 8.2 and 8.3b) this suggests that larger particles are more efficient in gene transfection *in vitro*, as expected. From the analysis of the complex sizes, the typical average size for a complex prepared at (Ac30) in the range of N/P ratios tested in the transfection assays is below 100 nm, while, in more concentrated buffer, ≥ 50 mM, larger complexes are formed with diameters including values above 500 nm (Figure 8.3a). The latter seem to be more prone to interact with the cell surface, and also to release from the endosome probably because of highly PEI concentration [83]. For the highest concentrated buffer (Ac100), panel (e) and (f), the addition of Fe(III) is less noticeable. The ternary complexes prepared in (Ac100) present values of reporter gene transfer higher than those in HBS but quite similar to their analogues in the absence of salt and in the same buffer. Note that, at this stage aggregation is very pronounced which consequently leads a high *in vitro* transfection.

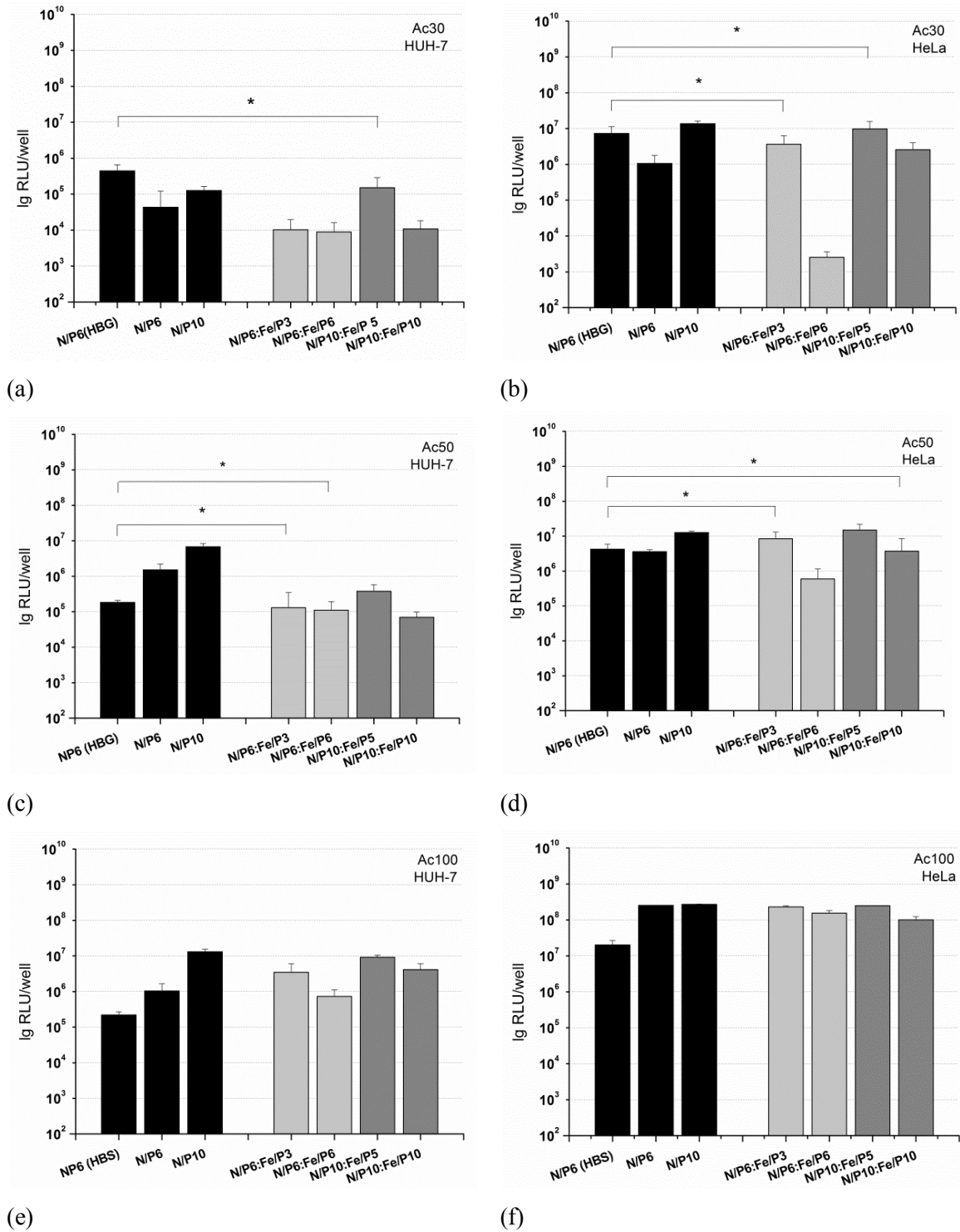


Figure 8.5. Reporter gene transfection of DNA-PEI and DNA-PEI-Fe(III) polyplexes on HUH-7 and HeLa cell lines. Complexes of DNA-PEI and DNA-PEI-Fe(III) were mixed in acetate buffers with different ionic strength, (a), (b) 30 mM (Ac30), (c), (d) 50 mM (Ac50), and (e), (f) 100 mM (Ac100), and then compared to standard PEI complexes at the same N/P ratios in the absence of Fe(III), and with analogue polyplexes prepared in HBG or HBS. Luciferase activity is presented as mean values \pm SD of triplicates. A Student's t-test was performed to assess statistical significance between each sample and the reference N/P = 6 (HBG or HBS) (ns = not significant; * $p < 0.05$).

iii. ***DNA-PEI-Fe(III) complexes prepared at low N/P ratios***

A factor of paramount importance in the use of PEI is the control of its intrinsic cytotoxicity. A proposed strategy to improve the biocompatibility of DNA-PEI complexes consists in reducing the concentration of PEI by replacement with Fe(III) attaining stable and positive complexes, according with trends shown in Chapter 5. Typically, the values of the N/P ratios used to form the complexes for transfection assays are equal or higher than 5 [320]. However, in high salt conditions the complexes formed at lower N/P tend to present larger sizes. Herein, the replacement of PEI by Fe(III) in complexes prepared at low N/P ratios is evaluated. The values of the N/P ratios were decreased towards N/P = 4 and 5, while the previously Fe(III)/P ratios were maintained. Intermediate acetate buffer Ac50 and Ac100 were chosen to form the complexes. The results of gene transfer for these ternary complexes are depicted in Figure 8.6.

Comparing the transfection efficiencies obtained in both cell lines, a marked dependence on cell type is clearly observed, especially in the case of Ac50, panel (c). Reporter gene expression values for complexes at lower N/P ratios present higher transfection efficiency values than those prepared at N/P = 6 [83]. The addition of Fe(III), in agreement with previous observations reduces the transfection efficiency when compared with related complexes in the absence of metal ions, in both cell lines. Nevertheless, the transfection of complexes DNA-PEI-Fe(III) at low N/P warrant the same transfection as the N/P = 6 ratio (HBS), in HUH-7 cells (panel a). In the case of Hela cells, complexes at low concentration of PEI combined with Fe(III) show a steep decrease in the transfection efficiency, panel (c). As expected, the increase of salt content, panel (d), is reflected rising values of the transfection obtained, but the same overall trends are observed.

Panel (e) gathers the results of transfection of the relevant complexes, including reference complexes, as well as the respective average sizes. The first point that should be made is the similarity of the values of transfection efficiency between N/P = 6 in HBG and HBS besides the marked difference between the sizes of these polyplexes. Moreover, for complexes prepared in Ac50 for a low N/P ratio of 5, the size of the polyplexes is very large, ca. 1123 nm, and so is the value of transfection attained. As the concentration of condensing agent is increased to N/P = 6, higher compaction of DNA is visible attaining values of roughly 544.2 nm with a consequent reduction in transfection efficiency. The primary effect of the addition of Fe(III) to complexes at N/P = 5 seems to be the narrowing of polyplex distribution, now with an average size of 890.7 nm. This happens by an increase in the percentage of small polyplexes, and the overall shift of the higher sizes to lower values, see Figure 8.3a. Nevertheless, the addition of metal ions allows to reduce the size of the complexes with a penalty in transfection efficiency (compared to N/P = 5 and in Ac50), but latter is close to those obtained for the reference systems N/P = 6 in HBG and HBS.

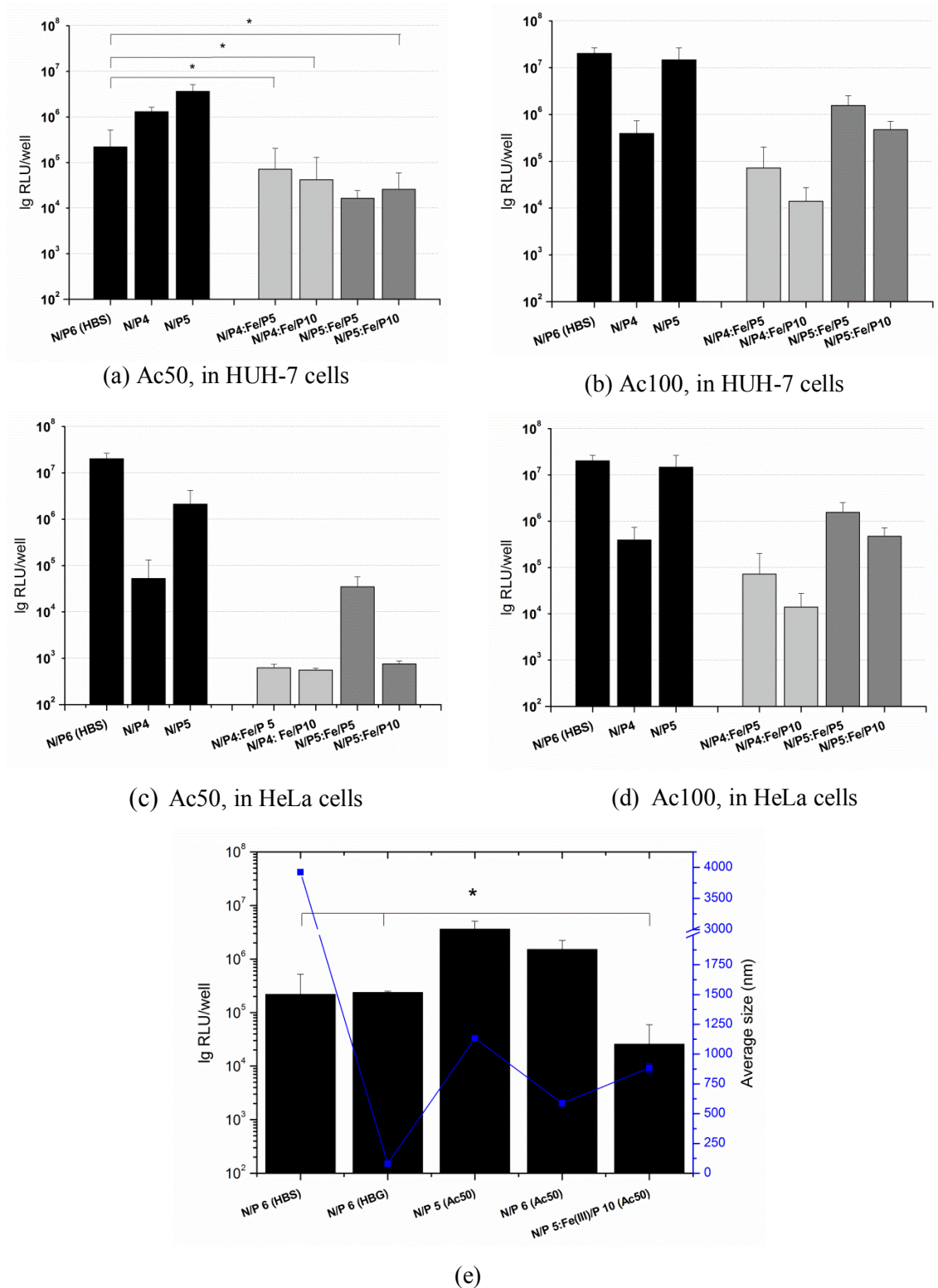


Figure 8.6. Reporter gene transfection of DNA-PEI and DNA-PEI-Fe(III) polyplexes applied on (a, b) HUH-7 and (c, d) HeLa cells. Polyplexes prepared in Ac50 and Ac100, at low values of N/P ratios are depicted and compared with reference systems. In panel is represented (e) size versus transfection of DNA-PEI compared with DNA-PEI-Fe(III) complexes in HUH-7. A Student's t-test was performed to assess statistical significance (ns = not significant; *p<0.05).

8.3.4 Effect of Fe(III) on DNA-PEI-Fe(III) cytotoxicity

To investigate the influence of the presence of Fe(III) in the complexes formed in HBG and HBS in the cytotoxicity of HUH-7 cells, adenosine triphosphate (ATP) which is present in metabolically active cells, was determined by bioluminescent assays. HeLa cells were also analyzed using this assay but no cytotoxicity to the cells was found within the tested conditions (data not shown). The complexes formed at N/P = 6 show minimal cytotoxicity (>80%) under conditions used, in both buffers (Figure 8.7). Increasing the concentration of PEI at N/P = 10 leads to higher levels of cell damage, as expected. However, the addition of Fe(III) to the complex N/P = 10 in HBG shows a slight increase in the biocompatibility of the complex, Figure 8.7a, whereas, in the case of complexes formed in HBS, the ternary complexes are found to be equally cytotoxic as DNA-PEI at N/P = 6, Figure 8.7b. A possible explanation is that the chelation between the amine groups and Fe(III) converts toxic PEI concentrated complexes (N/P = 10), into more tolerable complexes with cell viability close to that of complexes at N/P = 6. This fact has been previously observed by the increase of the half maximal metabolic inhibitory concentration, IC_{50} , for binary mixtures PEI-Fe(III) in comparison with the ones obtained for PEI alone, in Chapter 6.

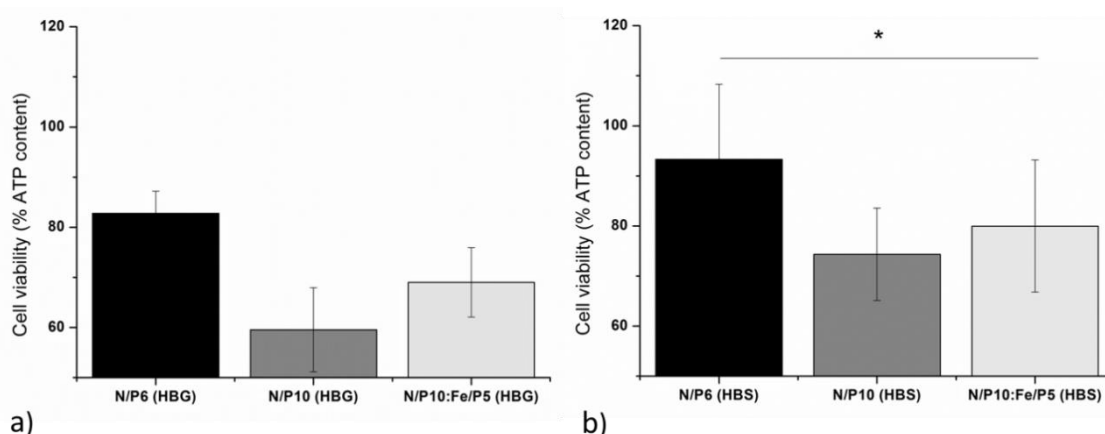


Figure 8.7. Cell viability was determined by a CellTiter Glo assay. Experiments were done in triplicates. A student's t-test was performed to assess statistical significance. (ns = not significant; * $p < 0.05$) DNA concentration is $10 \mu\text{g mL}^{-1}$ in each sample.

8.3.5 Effect of Fe(III) in endosome release and cellular association

In order to assess the impact of metal ions in the process of gene delivery, further studies were conducted. Chloroquine is a weak base which easily transposes the cell membrane and accumulates in endosomes promoting the endo/lysosomal release. The influence of this promoter in polyplex mediated transfection was tested in complexes prepared under low and high ionic strength, HBG and HBS (Figure 8.8). The presence of chloroquine has been showed to increase

the transfection efficiency by roughly 10-fold when prepared in HBG and presenting small sizes [83]. Contrarily, polyplexes prepared in HBS have shown no significant changes. Our results corroborate with these findings, showing an increase on the transfection efficiency when polyplexes are prepared in the HBG, panel (a), and no variation of those prepared in HBS, panel (b). This is again related with the sizes of the complexes, showing that the endosome escape is not a critical point for larger polyplexes, but reduces the transfection ability of smaller complexes, here enhanced with the help of the chloroquine. The presence of the second condensing agent, Fe(III), does not lead to significant changes in the transfection efficiency when HBG buffer is considered, panel (a). In this specific case, the increase of polyplex size, see Figure 8.2a, may also reduce the possible enhancement in gene expression mediated by chloroquine. Hence, for polyplexes at N/P:Fe(III)/P = 10:5 this explanation is not valid. Thus, the presence of Fe(III) inhibits the enhancer effect of chloroquine.

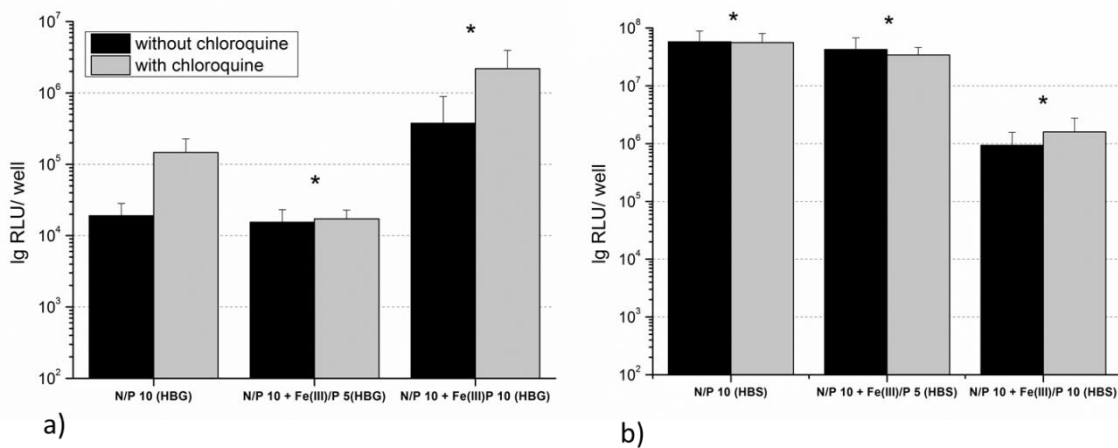
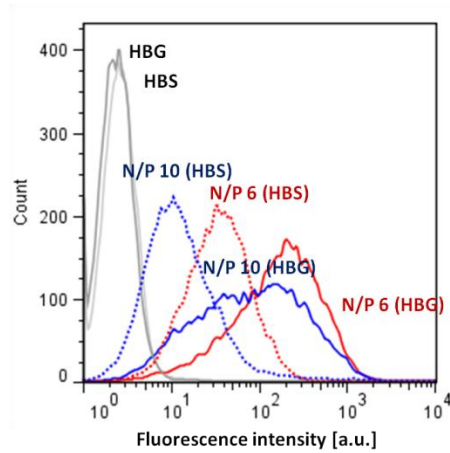


Figure 8.8. The effect of the addition of chloroquine to the medium during transfection assays in HeLa cells. Luciferase activity is presented as mean values \pm SD of triplicates. A Student's t-test was performed to assess statistical significance between samples with and without chloroquine (ns = not significant; * $p < 0.05$).

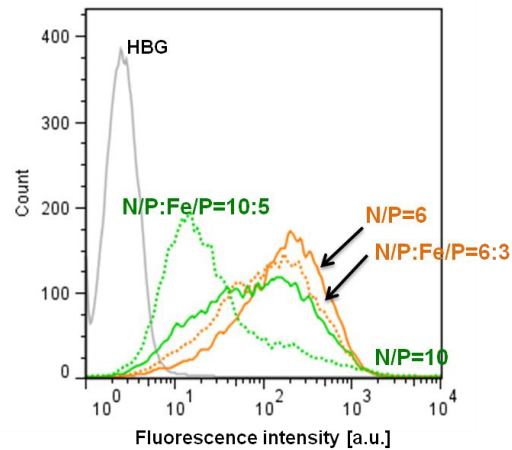
Moreover, fluorescence activated cell sorting (FACS) analysis were performed on HUH-7 transfected cells to inspect whether differences detected between DNA-PEI and DNA-PEI-Fe(III) complexes arise from the step of internalization. The uptake of DNA complexes into the cells was quantified by measuring the emission of Cy5 dye attached to plasmid, that according with the experimental procedure followed should only be detected those that internalized the cells. The distribution of fluorescence intensities for each DNA complex tested is depicted in Figure 8.9.

Firstly the internalization of reference complexes prepared at N/P = 6 and 10, in HBG and HBS, panel (a), was analyzed. In both buffers, a higher degree of internalization is observed for complexes formed at N/P = 6 than for those at N/P = 10. This observation must be addressed

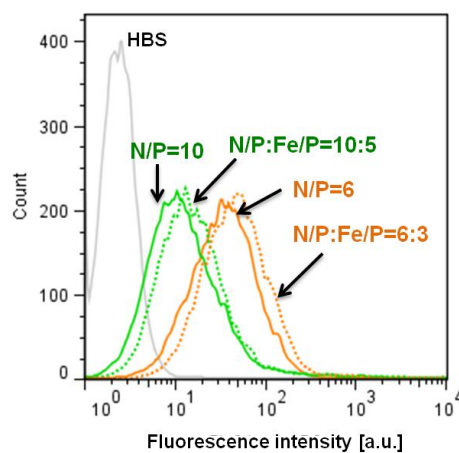
considering the higher amount of free PEI molecules in the latter, that have been considered responsible for reducing cellular association [165].



(a) HBG and HBS



(b) HBG



(c) HBS

Figure 8.9. DNA complexes cellular uptake in HUH-7 cells represented in flow cytometry histograms. In panel (a) are represented the DNA-PEI complexes at $N/P = 6$ and $N/P = 10$ in both, HBG and HBS; panel (b) are represented DNA-PEI and DNA-PEI-Fe(III) at charge ratios indicated in HBG and panel (c) are

represented DNA-PEI and DNA-PEI-Fe(III) at charge ratios indicated in HBS. In all histograms are represented the negative control (unstained cells) in HBS or HBG for comparison.

Particularly, complexes formed in HBS revealed a moderate degree of binding which is somewhat surprising due to their larger size. However, it should be noted here that, complexes formed in a medium with high ionic strength have a tendency to exhibit a lower surface charge than those prepared at low ionic strength, see Figure 8.3 panel (b). Figure 8.9, panels (b) and (c), gathers the results obtained for complexes with and without Fe(III) for a clearer comparison, formed in HBG and HBS. The Fe(III)/P ratios used in these assays were chosen according to the best transfection efficiency results obtained (see Figure 8.4).

The binding efficiency of DNA-PEI-Fe(III) complexes prepared in HBG is lower than that attained for DNA-PEI complexes. This difference is more evident in system N/P:Fe(III)/P = 10:5 than N/P:Fe(III)/P = 6:3. However, this detrimental effect did not affect the transfection efficiency of the complexes in N/P:Fe(III)/P = 10:5 (Figure 8.4c), contrarily to what is observed in complexes prepared in N/P:Fe(III)/P = 6:3, (Figure 8.4a). In the case of polyplexes prepared in HBS, panel (c), the curves obtained show a slightly beneficial effect in the cell entry stage, which can be ascribed to the presence of Fe(III). This happens to the same extent for both N/P ratios tested. As observed in Figure 8.4a, DNA-PEI-Fe(III) at N/P:Fe(III)/P = 6:6 showed a roughly 5.3-fold higher cell transfection than in the absence of Fe(III). At N/P:Fe(III)/P = 10:5, in Figure 8.3c, the transfection efficiency is nearly the same as that obtained for DNA-PEI complexes.

8.4 Discussion

The condensation of DNA with Fe(III) has been observed experimentally, but, the degree of condensation and stabilization of the complex is limited [27, 30]. On the other hand, PEI is known as one of the most efficient non-viral vector, but possesses a main drawback, its high cytotoxicity. Fe(III) on its own is also harmful to the cells, but this property suggests the opportunity of an iron-mediated oxidative attack to vulnerable cancer cells, that are commonly deficient in antioxidant enzymes, as a mechanism to recede tumors [191, 192, 321]. It has been observed that Fe(III) acts as a promoter of DNA condensation in DNA-PEI complexes, Chapter 3. Furthermore, the stable polyplex prepared with lower concentration of PEI resulted in more efficient polyplex decondensation, as well as in a higher biocompatibility, in Chapter 6.

The functional effect that Fe(III) ions have on the properties of DNA-PEI complexes generated in different buffer conditions was investigated and how, in turn, this affects their biological activity. It is well known that the formation of polyplexes is highly influenced by the chosen solution properties, including the nature of buffer used and the ionic strength of the solution [63, 67], which modulates the physical properties of the resulting complexes, such as the extent of condensation, size and charge [83, 272]. In this current chapter, the formation of DNA-PEI and DNA-PEI-Fe(III) complexes was investigated under different ionic strengths, ranging

from the physiologically relevant (100-150 mM) to low (30-50 mM) and more indicated to obtain suitable DNA complexes for gene delivery. The addition of Fe(III) to DNA-PEI polyplexes showed an enhancement on the condensation of DNA, independently of the buffer used. However, and due to the screening of electrostatic interactions in the presence of salt, the condensation of DNA was delayed to larger N/P and Fe(III)/P values (Figure 8.1). As expected, larger complexes were obtained at high N/P ratios and under high ionic strength (HBS), contrarily to what observed at low salt conditions (HBG) (Figure 8.2 a and b). Two distinct behaviors were discerned after metal addition to highly charged complexes: (i) at low salt conditions (HBG), the presence of Fe(III) favors an increase in the size of the complexes, whereas (ii) at high and intermediate salt conditions (HBS and Ac50), a reduction occurs (Figures 8.2 and 8.3). According to the core-shell model [319], the excess of charge in overcharged complexes is accommodated in the form of positively charged polymer “tails” protruding from the complex, which produces an electrostatically stabilizing shell around the particle avoiding interpolymer interactions and, thus, aggregation. At high ionic strength, the repulsion between the shells of two neighbor particles is screened, and aggregation may take place. A possibility is that the presence of Fe(III) acts as destabilizer of this shell in low salt concentrations, and as a stabilizer in the opposite conditions.

The transfection efficiency of DNA-PEI complexes was found to increase generally with the size of the particles, in both HUH-7 and HeLa cell lines, in good agreement with literature [83]. It should be noted that polyplexes with large sizes are generally less successful for *in vivo* gene delivery [86]. It is, therefore highly recommended to prepare complexes in low salt conditions to attain small size particles. However, *in vivo* studies also suggest that, somehow, complex aggregation should occur before their entry into the cell so as to reach efficient gene delivery [159, 322]. Thus, it is still of great interest to study the aggregate properties of polyplexes and its influence on the process of transfection.

In general, the addition of Fe(III) to DNA-PEI complexes leads to an equal or lower gene transfer efficiency, being the inhibitor effect more evident for polyplexes prepared at low ionic strength buffers (Figures 8.4 and 8.5 panels (a), (b)). At high salt conditions, the inhibition of transfection efficiency is less evident and, particularly in the case of polyplexes prepared at N/P:Fe(III)/P = 6:6 in HBS, there is an increase in transfection efficiency of 5.3 times compared to the analogous DNA-PEI complex in the absence of metal ions, in the HUH-7 cell line (see Figure 8.4a). Since the average size of the complexes is smaller in the presence of Fe(III), size cannot account for this increase. The effect of the metal ions in complexes formed in acetate buffers at intermediate (Ac50) and high ionic strength (Ac100) is less or not noticeable, respectively, Figure 8.5 b and c. This which may suggest that the main hurdle to overcome by DNA-PEI-Fe(III) complexes is the endosomal release, since larger complexes overcome this obstacle more easily. In the previous Chapter, we have concluded that chelation of Fe(III) with

the amine groups of PEI is of paramount importance to the final complex conformation. This property is fundamental to produce a high condensation of DNA, and to reduce the size of the DNA-PEI-Fe(III) complexes. However, the complexation of the amine groups by the metal ions may represent a problem to transfection efficiency, due to the possible decrease in the buffering capacity of PEI and, concomitantly, determines a decrease in the escape of the complex from the endosome. Note that Fe(III) is a very versatile metal, extremely efficient in acid-base reactions, which is able to chelate to Lewis bases. Upon chelation, it is difficult to reverse the process, considering that this interaction is very strong even at low pH [323]. Note that the most acidic endosome environment attains values of pH in the range of pH 5.7-7.8. This correlates well with the fact that chloroquine itself could not promote the release of DNA-PEI-Fe(III) complexes from the endosome, as it did with the DNA-PEI analogue, probably due to some interference of Fe(III). Some studies indicate that chelation between amine groups and metal species is dependent on the salt content of the medium [324, 325], and this fact may be an important feature in some systems, but further studies are needed.

The reinforcement of the positive charge of the PEI chains by the chelation of Fe(III) is likely to improve the interaction between the polyplex and the negatively charged cell membrane, improving the uptake of the cells. However, this is observed solely in the case of complexes prepared at high ionic strength media, HBS (Figure 8.9c), but does not occur in complexes prepared at low ionic strength conditions, with HBG (Figure 8.9b). This enhancement in the membrane interaction seems to indicate a higher positive charge in the surface of the DNA-PEI-Fe(III) complexes, in good agreement with our previous results on complexes prepared under high ionic strength conditions (Chapter 5).

Furthermore, cytotoxicity assays were performed to elucidate the impact of the addition of Fe(III) to the complexes used in transfection. We found that the addition of Fe(III) to the complexes and their chelation to positive amine groups reduces the harmful effect of PEI in the cells (Figure 8.8), corroborating prior results (Chapter 6). As proposed before, an additional attempt to reduce the cytotoxicity of DNA-PEI polyplexes resides in the reduction of the number of PEI by replacement with Fe(III). The selected complexes to test this hypothesis were those prepared at intermediary ionic strength (Ac50). From analysis of the results, it can be seen that the decrease of the N/P ratio is not relevant to the DNA-PEI efficacy *in vitro*, but this may be related with the increase in the size of complexes, Figure 8.3a. Systems in which Fe(III) is added, maintained the same levels of transfection efficiency as the reference (N/P = 6 in HBG and HBS), using N/P = 4 and 5, and at the same time allowed to control, to some extent, the size of complex, Figure 8.6e. The use of Fe(III) proved to be a valuable strategy to regulate the properties of the complex, including complex size and also, polyplex biocompatibility.

8.5 Conclusions

The large interest of Fe(III) ions in biomedical applications may anticipate the potential of its combination with efficient DNA-PEI polyplexes. The present study presents a comparative study of the physicochemical properties and transfection efficiencies of DNA-PEI and DNA-PEI-Fe(III) complexes generated in different biological buffers, ranging from low to high salt concentration regimes. Results have show that the effect of Fe(III) ions in properties and transfection activity of polyplexes is strongly dependent on the ionic strength of the buffer. At high ionic strength, Fe(III) enhances DNA-PEI condensation, reduces the complex size, increases the cell uptake and shows less perturbation of the transfection efficiency when compared with reference systems. On the other hand, at low salt content, the metal also enhances the DNA condensation but leads to some increase in the size of the complexes and to a reduction of their cellular uptake and transfection activity. Moreover, the interaction of Fe(III) with amines of PEI reflects in a mitigation of polycation cytotoxicity. In this context, the decrease in the number of PEI molecules in the complexes formed at intermediary ionic strength, leads to a small decrease in the transfection efficiency but still keeps values compared with those of reference complexes, while simultaneously allowing the regulation of the complex size. This study serve to highlight some of the aspects that govern in vitro transfection, and simultaneously, should help to elucidate the benefits of the incorporation of the versatile Fe(III) in a gene delivery system.

CHAPTER 9

Concluding remarks

The present work aimed at unraveling the parameters that modulate the physicochemical properties of efficient gene delivery DNA-PEI complexes, and assessing the effect of the addition of a second condensing agent with interesting properties, Fe(III), to DNA-PEI complexes, thus obtaining a ternary complex. The study was supported on a complete set of techniques, involving an experimental framework combined with Monte Carlo simulation. The combination of these two approaches, each with its inherent limitations and capabilities, results in a valuable methodology that allows strengthening the value of information that comes from each approach individually.

In the development of an efficient gene vector, the study of the overall properties of DNA complexes, such as complex charge and size, condensation and decondensation ability and toxicity, play paramount roles in the ultimate goal, gene expression. The present work encompasses a fundamental study of these properties evaluated under different conditions, imposing variations in the pH and ionic strength of the media, concentration of each condensing agent (N/P and Fe(III)/P ratios) and architecture and molecular weight of PEI chains. A comprehensive optimization was accomplished with a stepwise characterization of both DNA-PEI and DNA-PEI-Fe(III) complexes.

Firstly, the variation of pH on DNA-PEI complexes formation promotes nonmonotonic and nontrivial trends in the DNA precipitation behavior, electrophoretic mobility, and size of the complexes. At lower pH values, DNA and PEI interact more strongly and form complexes with larger mean sizes, which suggests disproportionation. On the other hand, complexes prepared at pH 8 show a weaker binding between DNA and PEI, forming smaller aggregates, and possibly a more uniform population. Some positive complexes are detected by electrophoresis, especially

those prepared at pH 6. Based on these results, an intermediate pH medium to pursue our work was selected.

In what concerns the effect of Fe(III) ions upon DNA-PEI complexes, it was found that it enhances the condensation of DNA in DNA-PEI mixtures. The combination of both condensing agents at $\beta_{\text{PEI/DNA}} < 1$, attained a degree of DNA condensation, higher than that found for $\beta_{\text{PEI/DNA}} = 1$, in the absence of the metal ions. The macroscopic behavior, monitored using UV spectrophotometry and gel electrophoresis, was qualitatively the same as that observed for single-molecule experiments, via fluorescence microscopy. In parallel MC simulations were performed. A rationale emerged from theoretical data, in which it is suggested that trivalent ions occupy, preferentially, the areas of the polyanion that are less populated by the polycation chains. Therefore, trivalent ions enhance the degree of compaction by inducing a local folding of the longer chain, allowing thus, to extend the range of action of the polycations, and leading to a narrowing of the size distribution. Furthermore, both experimental results and MC simulations proved that the use of a mixture of cationic agents facilitates DNA decondensation.

In order to investigate the influence of different architectures of PEI on DNA ternary complexes, branched and linear PEIs in conjunction with Fe(III) were studied. Firstly, it was found that the different PEIs, on their own, possess different efficiencies as condensing agents. Interestingly, the addition of Fe(III) to DNA-PEI systems tended to equalize the action of these different agents. PEIs with shorter chains (bPEI1.2 and lPEI2.5) are the most efficient in the presence of Fe(III). The addition of Fe(III) to the negative DNA-PEI polyplexes leads to the charge reversal of the complexes, which is an important factor to improve their interaction with the cell membranes. Additionally, polyplexes in solution at low N/P ratios are smaller in the presence of Fe(III), corroborating what was found using fluorescence microscopy, but their neutralization promotes aggregation, which is enhanced by high ionic strength conditions. Studies of cytotoxicity and hemolysis revealed a clear dependence on PEI concentration, molecular weight and degree of branching. Dependence was also found on the pH of the medium, leading to a high toxicity at lower pH. Results of cytotoxicity assays indicated that these features influence directly the interaction with the mitochondria and cell membrane damage. The saturation of the amine groups of PEI by Fe(III) ions reduced the PEI harmful effects upon the cells. In polyplexes, the substitution of PEI molecules by Fe(III) resulted in an enhancement of biocompatibility, when compared to DNA-PEI complexes with the same degree of condensation and complex surface charge. These results reinforce the possibility of producing polyplexes with a high degree of condensation and stability, and low cytotoxicity, which are desirable features for cell administration.

Further studies were carried out to shed light on the mechanism of interaction in the ternary complexes, taking in account the interaction between both condensing agents. Experimental evidence of the importance of the chelation effect was obtained by potentiometric

and conductance measurements. A delay in DNA condensation with respect to the concentration of condensing agents was observed when PEI and Fe(III) were pre-mixed, and then added to DNA. At a comparable DNA condensation degree, different concentrations of Fe(III) ions in the supernatant were quantified, with a larger removal of Fe(III) ions from the solution when bPEI10 is added. Overall, a coherent picture in which Fe(III) compensates for PEI, probably modulating the respective charge, emerges. According to these new findings, systems were modeled imposing a chelation effect and also varying the polycation architecture. The imposition of the chelation leads to a pronounced polyanion compaction for all the studied systems, and the differences between systems become less noticeable, in good agreement with what was obtained experimentally. Contact analyses revealed an overlap of the condensing agents. If chelation is hampered due to the proximity of positive charges, DNA compaction is less pronounced. Once again, it is shown that the disposition of trivalent ions along the polyanion is of extreme importance, in particular, their overlap with the polycation chains which reinforces the polycation linear charge density.

Finally, a comparative study of transfection efficiencies of DNA-PEI and DNA-PEI-Fe(III) complexes formed in different biological buffers at low, intermediate and high salt concentration regimes was conducted. Results show that the effect of Fe(III) in polyplex properties and transfection activity is strongly dependent on the ionic concentration of the buffer. At high ionic strength, Fe(III) enhances DNA-PEI condensation, reduces the complexes size, increases the cell uptake and shows less perturbation of transfection efficiency when compared with reference systems. Complexes formed in high ionic strength medium a N/P:Fe(III)/P = 6, the addition of Fe(III) shows to increase roughly 5-fold the transfection efficiency. On the other hand, at low salt content, the metal also enhances DNA condensation but leads to some expansion of the complexes and to a reduction of their cellular uptake and transfection activity. Moreover, the addition of Fe(III) to polyplexes used in transfection assays showed to decrease their cytotoxicity. In the same context, the decrease of PEI concentration in complexes formed at intermediary ionic strength induces a decrease in their transfection efficiency, but still values comparable to those of reference complexes are attained, while, simultaneously, allows regulating the complex size.

This study gathers valuable material for the understanding of the combination of polyamines and inorganic compounds in the condensation of DNA. Insights obtained should help to elucidate the benefits of the incorporation of the versatile Fe(III) ions in a gene delivery system, as well as assist new strategies based on the combination of condensing agents.

Bibliography

1. Besteman, K., et al., *Direct Observation of Charge Inversion by Multivalent Ions as a Universal Electrostatic Phenomenon*. Physical Review Letters, 2004. **93**(17): p. 170802.
2. Besteman, K., M.A.G. Zevenbergen, and S.G. Lemay, *Charge inversion by multivalent ions: Dependence on dielectric constant and surface-charge density*. Physical Review E, 2005. **72**(6).
3. Fielden, M.L., R.A. Hayes, and J. Ralston, *Oscillatory and ion-correlation forces observed in direct force measurements between silica surfaces in concentrated CaCl₂ solutions*. Physical Chemistry Chemical Physics, 2000. **2**(11): p. 2623-2628.
4. Considine, R.F., R.A. Hayes, and R.G. Horn, *Forces measured between latex spheres in aqueous electrolyte: Non-DLVO behavior and sensitivity to dissolved gas*. Langmuir, 1999. **15**(5): p. 1657-1659.
5. Kekicheff, P., et al., *Charge reversal seen in electrical double-layer interaction of surfaces immersed in 2-1 calcium electrolyte*. Journal of Chemical Physics, 1993. **99**(8): p. 6098-6113.
6. Guldbbrand, L., et al., *Electrical double-layer forces - A Monte Carlo study*. Journal of Chemical Physics, 1984. **80**(5): p. 2221-2228.
7. Valleau, J.P., R. Ivkov, and G.M. Torrie, *Colloid stability - The forces between charged surfaces in an electrolyte*. Journal of Chemical Physics, 1991. **95**(1): p. 520-532.
8. Watson, J.D. and F.H. Crick, *Molecular structure of nucleic acids*. Nature, 1953. **171**(4356): p. 737-738.
9. Dias, R. and B. Lindman, *DNA Interactions with Polymers and Surfactants*, in *DNA Interactions with Polymers and Surfactants*, R. Dias and B. Lindman, Editors. 2007, John Wiley & Sons, Inc.: Hoboken, New Jersey.
10. Mel'nikova, Y.S. and B. Lindman, *pH-Controlled DNA Condensation in the Presence of Dodecyltrimethylamine Oxide*. Langmuir, 2000. **16**(14): p. 5871-5878.
11. Bloomfield, V.A., D.M. Crothers, and I. Tinoco, *Nucleic Acids: Structures, Properties, and Functions*. 2000: University Science Books.
12. Franklin, R.E. and R.G. Gosling, *The structure of sodium thymonucleate fibres. I. The influence of water content*. Acta Crystallographica, 1953. **6**(8-9): p. 673-677.
13. Rothenburg, S., et al., *A PKR-like eukaryotic initiation factor 2 α kinase from zebrafish contains Z-DNA binding domains instead of dsRNA binding domains*. Proceedings of the National Academy of Sciences of the United States of America, 2005. **102**(5): p. 1602-1607.
14. Schiessel, H., *The physics of chromatin*. Journal of Physics: Condensed Matter, 2003. **15**(19): p. R699.
15. Thoma, F., T. Koller, and A. Klug, *Involvement of histone H1 in the organization of the nucleosome and of the salt-dependent superstructures of chromatin*. The Journal of Cell Biology, 1979. **83**(2): p. 403-427.
16. Watanabe, K. and K. Iso, *Magnesium Binding and Conformational Change of DNA in Chromatin*. Biochemistry, 1984. **23**(7): p. 1376-1383.
17. Gosule, L.C. and J.A. Schellman, *Compact form of DNA induced by spermidine*. 1976.
18. Maniatis, T., J.H. Venable Jr, and L.S. Lerman, *The structure of ψ DNA*. Journal of Molecular Biology, 1974. **84**(1): p. 37-64.
19. Lerman, L.S., *A Transition to a Compact Form of DNA in Polymer Solutions*. Proceedings of the National Academy of Sciences, 1971. **68**(8): p. 1886-1890.

20. Bloomfield, V.A., *DNA condensation by multivalent cations*. Biopolymers, 1997. **44**(3): p. 269-282.
21. Ueda, M. and K. Yoshikawa, *Phase Transition and Phase Segregation in a Single Double-Stranded DNA Molecule*. Physical Review Letters, 1996. **77**(10): p. 2133-2136.
22. Osica, V., et al., *Preliminary morphological and X-ray diffraction studies of the crystals of the DNA cetyltrimethylammonium salt*. Nucleic acids research, 1977. **4**(4): p. 1083-1096.
23. Bloomfield, V.A., R.W. Wilson, and D.C. Rau, *Polyelectrolyte effects in DNA condensation by polyamines*. Biophysical chemistry, 1980. **11**(3): p. 339-343.
24. Wilson, R.W. and V.A. Bloomfield, *Counterion-induced condensation of deoxyribonucleic acid. A light-scattering study*. Biochemistry, 1979. **18**(11): p. 2192-2196.
25. Widom, J. and R.L. Baldwin, *Monomolecular condensation of λ -DNA induced by cobalt hexamine*. Biopolymers, 1983. **22**(6): p. 1595-1620.
26. Bloomfield, V.A., *DNA condensation*. Curr Opin Struc Biol, 1996. **6**(3): p. 334-341.
27. Yamasaki, Y. and K. Yoshikawa, *Higher Order Structure of DNA Controlled by the Redox State of Fe^{2+}/Fe^{3+}* . Journal of the American Chemical Society, 1997. **119**(44): p. 10573-10578.
28. Kankia, B.I., V. Buckin, and V.A. Bloomfield, *Hexamminecobalt (III)-induced condensation of calf thymus DNA: circular dichroism and hydration measurements*. Nucleic acids research, 2001. **29**(13): p. 2795-2801.
29. Plum, G.E., P.G. Arscott, and V.A. Bloomfield, *Condensation of DNA by trivalent cations. 2. Effects of cation structure*. Biopolymers, 1990. **30**(5-6): p. 631-643.
30. Gawęda, S., et al., *Cationic agents for DNA compaction*. Journal of Colloid and Interface Science, 2008. **323**(1): p. 75-83.
31. Ainalem, M.-L., et al., *Condensing DNA with poly(amido amine) dendrimers of different generations: means of controlling aggregate morphology*. Soft Matter, 2009. **5**(11): p. 2310-2320.
32. Zinchenko, A.A., et al., *Controlling the Intrachain Segregation on a Single DNA Molecule*. Journal of the American Chemical Society, 2003. **125**(15): p. 4414-4415.
33. Raspaud, E., et al., *Solubility and charge inversion of complexes of DNA and basic proteins*. Physical review letters, 2006. **97**(6): p. 068103.
34. Balhorn, R., *The protamine family of sperm nuclear proteins*. Genome Biology, 2007. **8**(9): p. 227.
35. Kim, H.H., et al., *Basic peptide system for efficient delivery of foreign genes*. Biochimica et Biophysica Acta (BBA)-Molecular Cell Research, 2003. **1640**(2): p. 129-136.
36. Männistö, M., et al., *Structure-activity relationships of poly(L-lysines): effects of pegylation and molecular shape on physicochemical and biological properties in gene delivery*. Journal of Controlled Release, 2002. **83**(1): p. 169-182.
37. Miguel, M.G., et al., *DNA-cationic amphiphile interactions*. Colloids and Surfaces A: Physicochemical and Engineering Aspects, 2003. **228**(1-3): p. 43-55.
38. Lindman, B., et al., *DNA-lipid systems. An amphiphile self-assembly and polymer-surfactant perspective*, in *Lipid and Polymer-Lipid Systems*, T. Nylander and B. Lindman, Editors. 2002, Springer Berlin Heidelberg. p. 52-63.
39. Yoshikawa, K., et al., *Large discrete transition in a single DNA molecule appears continuous in the ensemble*. Physical review letters, 1996. **76**(16): p. 3029.
40. Jorge, A.F., et al., *Polyelectrolyte compaction by pH-responsive agents*. Physical Chemistry Chemical Physics, 2009. **11**(46): p. 10890-10898.
41. Dias, R.S., et al., *Modeling of DNA compaction by polycations*. The Journal of Chemical Physics, 2003. **119**(15): p. 8150-8157.
42. Iwaki, T. and K. Yoshikawa, *Competition between interchain and intrachain phase segregation*. Physical Review E, 2003. **68**(3): p. 031902.
43. Philippova, O.E., et al., *Salt-controlled intrachain/interchain segregation in DNA complexed with polycation of natural origin*. Macromolecules, 2005. **38**(22): p. 9359-9365.

44. Pinto, M.F., et al., *Controlling the morphology in DNA condensation and precipitation*. *Biomacromolecules*, 2009. **10**(6): p. 1319-23.
45. Zinchenko, A.A., et al., *DNA compaction by divalent cations: Structural specificity revealed by the potentiality of designed quaternary diammonium salts*. *ChemBioChem*, 2004. **5**(3): p. 360-368.
46. Trejo-Ramos, M.A., et al., *Structure of polyelectrolyte complexes by Brownian dynamics simulation: Effects of the bond length asymmetry of the polyelectrolytes*. *The Journal of Chemical Physics*, 2007. **126**(1): p. 014901.
47. Levin, Y. and J.J. Arenzon, *Kinetics of charge inversion*. *Journal of Physics A: Mathematical and General*, 2003. **36**(22): p. 5857.
48. Post, C.B. and B.H. Zimm, *Internal condensation of a single DNA molecule*. *Biopolymers*, 1979. **18**(6): p. 1487-1501.
49. Post, C.B. and B.H. Zimm, *Theory of DNA condensation: collapse versus aggregation*. *Biopolymers*, 1982. **21**(11): p. 2123-2137.
50. Yoshikawa, K. and Y. Matsuzawa, *Nucleation and growth in single DNA molecules*. *Journal of the American Chemical Society*, 1996. **118**(4): p. 929-930.
51. Park, S.Y., D. Harries, and W.M. Gelbart, *Topological Defects and the Optimum Size of DNA Condensates*. *Biophysical Journal*, 1998. **75**(2): p. 714-720.
52. Vasilevskaya, V.V., et al., *Structure of collapsed persistent macromolecule: Toroid vs. spherical globule*. *Biopolymers*, 1997. **41**(1): p. 51-60.
53. Schnurr, B., F. MacKintosh, and D. Williams, *Dynamical intermediates in the collapse of semiflexible polymers in poor solvents*. *EPL (Europhysics Letters)*, 2000. **51**(3): p. 279.
54. Noguchi, H. and K. Yoshikawa, *Folding path in a semiflexible homopolymer chain: A Brownian dynamics simulation*. *The Journal of Chemical Physics*, 2000. **113**: p. 854.
55. Arscott, P.G., A.Z. Li, and V.A. Bloomfield, *Condensation of DNA by trivalent cations. 1. Effects of DNA length and topology on the size and shape of condensed particles*. *Biopolymers*, 1990. **30**(5-6): p. 619-630.
56. Hibino, K., et al., *Na⁺ more strongly inhibits DNA compaction by spermidine (3⁺) than K⁺*. *Chemical Physics Letters*, 2006. **426**(4-6): p. 405-409.
57. Köping-Höggård, M., et al., *Improved chitosan-mediated gene delivery based on easily dissociated chitosan polyplexes of highly defined chitosan oligomers*. *Gene therapy*, 2004. **11**(19): p. 1441-1452.
58. González-Pérez, A., et al., *Cyclodextrin–Surfactant Complex: A New Route in DNA Decomposition*. *Biomacromolecules*, 2008. **9**(3): p. 772-775.
59. Makita, N. and K. Yoshikawa, *Proton concentration (pH) switches the higher-order structure of DNA in the presence of spermine*. *Biophysical chemistry*, 2002. **99**(1): p. 43-53.
60. Pavlov, G., et al., *Conformation of heparin studied with macromolecular hydrodynamic methods and X-ray scattering*. *European Biophysics Journal*, 2003. **32**(5): p. 437-449.
61. Burma, N.J. and I. Haq, *Advances in the analysis of isothermal titration calorimetry data for ligand–DNA interactions*. *Methods*, 2007. **42**(2): p. 162-172.
62. Ou, Z. and M. Muthukumar, *Entropy and enthalpy of polyelectrolyte complexation: Langevin dynamics simulations*. *The Journal of chemical physics*, 2006. **124**: p. 154902.
63. Ehtezazi, T., U. Rungsardthong, and S. Stolnik, *Thermodynamic analysis of polycation-DNA interaction applying titration microcalorimetry*. *Langmuir*, 2003. **19**(22): p. 9387-9394.
64. Matulis, D., I. Rouzina, and V.A. Bloomfield, *Thermodynamics of DNA binding and condensation: isothermal titration calorimetry and electrostatic mechanism*. *Journal of molecular biology*, 2000. **296**(4): p. 1053-1063.
65. Prevette, L.E., et al., *Deciphering the role of hydrogen bonding in enhancing pDNA-polycation interactions*. *Langmuir*, 2007. **23**(19): p. 9773-9784.
66. Rungsardthong, U., et al., *Effect of Polymer Ionization on the Interaction with DNA in Nonviral Gene Delivery Systems*. *Biomacromolecules*, 2003. **4**(3): p. 683-690.
67. Ma, P.L., et al., *New Insights into Chitosan–DNA Interactions Using Isothermal Titration Microcalorimetry*. *Biomacromolecules*, 2009. **10**(6): p. 1490-1499.

68. Pack, D.W., et al., *Design and development of polymers for gene delivery*. Nature Reviews Drug Discovery, 2005. **4**(7): p. 581-593.
69. Ashtari, M., et al., *The human visual cortex responds to gene therapy-mediated recovery of retinal function*. The Journal of clinical investigation, 2011. **121**(6): p. 2160.
70. Cavazzana-Calvo, M. and A. Fischer, *Gene therapy for severe combined immunodeficiency: are we there yet?* Journal of Clinical Investigation, 2007. **117**(6): p. 1456-1465.
71. Morille, M., et al., *Progress in developing cationic vectors for non-viral systemic gene therapy against cancer*. Biomaterials, 2008. **29**(24): p. 3477-3496.
72. Mintzer, M.A. and E.E. Simanek, *Nonviral Vectors for Gene Delivery*. Chemical Reviews, 2008. **109**(2): p. 259-302.
73. Sunshine, J.C., C.J. Bishop, and J.J. Green, *Advances in polymeric and inorganic vectors for nonviral nucleic acid delivery*. Therapeutic Delivery, 2011. **2**(4): p. 493-521.
74. Whitehead, K.A., et al., *In vitro-in vivo translation of lipid nanoparticles for hepatocellular siRNA delivery*. ACS nano, 2012. **6**(8): p. 6922-6929.
75. *Non-viral nanovectors for gene delivery: factors that govern successful therapeutics*. Expert Opinion on Drug Delivery, 2010. **7**(6): p. 721-735.
76. Verbaan, F., et al., *The fate of poly (2-dimethyl amino ethyl) methacrylate-based polyplexes after intravenous administration*. International journal of pharmaceutics, 2001. **214**(1): p. 99-101.
77. Robbens, J., et al., *Eco-, geno- and human toxicology of bio-active nanoparticles for biomedical applications*. Toxicology, 2010. **269**(2-3): p. 170-181.
78. Yousefi, A., et al., *Trends in polymeric delivery of nucleic acids to tumors*. Journal of Controlled Release, 2013.
79. Mislick, K.A. and J.D. Baldeschwieler, *Evidence for the role of proteoglycans in cation-mediated gene transfer*. Proceedings of the National Academy of Sciences, 1996. **93**(22): p. 12349-12354.
80. Kopatz, I., J.S. Remy, and J.P. Behr, *A model for non-viral gene delivery: Through syndecan adhesion molecules and powered by actin*. The journal of gene medicine, 2004. **6**(7): p. 769-776.
81. Prabha, S., et al., *Size-dependency of nanoparticle-mediated gene transfection: studies with fractionated nanoparticles*. International journal of pharmaceutics, 2002. **244**(1): p. 105-115.
82. Rejman, J., et al., *Size-dependent internalization of particles via the pathways of clathrin- and caveolae-mediated endocytosis*. Biochemical Journal, 2004. **377**: p. 159-169.
83. Ogris, M., et al., *The size of DNA/transferrin-PEI complexes is an important factor for gene expression in cultured cells*. Gene Therapy, 1998. **5**(10): p. 1425-33.
84. Zuhorn, I.S., et al., *Interference of serum with lipoplex-cell interaction: modulation of intracellular processing*. Biochimica et Biophysica Acta (BBA)-Biomembranes, 2002. **1560**(1): p. 25-36.
85. Zuhorn, I.S., R. Kalicharan, and D. Hoekstra, *Lipoplex-mediated transfection of mammalian cells occurs through the cholesterol-dependent clathrin-mediated pathway of endocytosis*. Journal of Biological Chemistry, 2002. **277**(20): p. 18021-18028.
86. Chollet, P., et al., *Side-effects of a systemic injection of linear polyethylenimine-DNA complexes*. The Journal of Gene Medicine, 2002. **4**(1): p. 84-91.
87. Sharma, V.K., M. Thomas, and A.M. Klivanov, *Mechanistic studies on aggregation of polyethylenimine-DNA complexes and its prevention*. Biotechnology and Bioengineering, 2005. **90**(5): p. 614-620.
88. Ogris, M., et al., *PEGylated DNA/transferrin-PEI complexes: reduced interaction with blood components, extended circulation in blood and potential for systemic gene delivery*. Gene therapy, 1999. **6**(4): p. 595-605.
89. Harris, T.J., et al., *Tissue-specific gene delivery via nanoparticle coating*. Biomaterials, 2010. **31**(5): p. 998-1006.

90. Oupický, D., et al., *Steric stabilization of poly-L-Lysine/DNA complexes by the covalent attachment of semitelechelic poly [N-(2-hydroxypropyl) methacrylamide]*. *Bioconjugate chemistry*, 2000. **11**(4): p. 492-501.
91. Ruponen, M., et al., *Extracellular glycosaminoglycans modify cellular trafficking of lipoplexes and polyplexes*. *Journal of Biological Chemistry*, 2001. **276**(36): p. 33875-33880.
92. Dauty, E., et al., *Intracellular delivery of nanometric DNA particles via the folate receptor*. *Bioconjugate chemistry*, 2002. **13**(4): p. 831-839.
93. Hashida, M., et al., *Cell-specific delivery of genes with glycosylated carriers*. *Advanced drug delivery reviews*, 2001. **52**(3): p. 187-196.
94. Kunath, K., et al., *Integrin targeting using RGD-PEI conjugates for in vitro gene transfer*. *The journal of gene medicine*, 2003. **5**(7): p. 588-599.
95. Wang, J., et al., *A gene nanocomplex conjugated with monoclonal antibodies for targeted therapy of hepatocellular carcinoma*. *Biomaterials*, 2012. **33**(18): p. 4597-4607.
96. Elfinger, M., et al., *Self-Assembly of Ternary Insulin– Polyethylenimine (PEI)– DNA Nanoparticles for Enhanced Gene Delivery and Expression in Alveolar Epithelial Cells*. *Biomacromolecules*, 2009. **10**(10): p. 2912-2920.
97. Nie, Y., et al., *Dual-targeted polyplexes: one step towards a synthetic virus for cancer gene therapy*. *Journal of Controlled Release*, 2011. **152**(1): p. 127-134.
98. Bareford, L.M. and P.W. Swaan, *Endocytic mechanisms for targeted drug delivery*. *Advanced drug delivery reviews*, 2007. **59**(8): p. 748-758.
99. Mishra, S., P. Webster, and M.E. Davis, *PEGylation significantly affects cellular uptake and intracellular trafficking of non-viral gene delivery particles*. *European journal of cell biology*, 2004. **83**(3): p. 97-111.
100. Rejman, J., M. Conese, and D. Hoekstra, *Gene Transfer by Means of Lipo- and Polyplexes: Role of Clathrin and Caveolae-Mediated Endocytosis*. *Journal of Liposome Research*, 2006. **16**(3): p. 237-247.
101. von Gersdorff, K., et al., *The internalization route resulting in successful gene expression depends on both cell line and polyethylenimine polyplex type*. *Molecular Therapy*, 2006. **14**(5): p. 745-753.
102. Boussif, O., et al., *A versatile vector for gene and oligonucleotide transfer into cells in culture and in vivo: polyethylenimine*. *Proceedings of the National Academy of Sciences of the United States of America*, 1995. **92**(16): p. 7297-7301.
103. Behr, J.-P., *The proton sponge: a trick to enter cells the viruses did not exploit*. *CHIMIA International Journal for Chemistry*, 1997. **51**(1-2): p. 1-2.
104. Zhou, J., et al., *PAMAM dendrimers for efficient siRNA delivery and potent gene silencing*. *Chemical communications*, 2006(22): p. 2362-2364.
105. Yamashiro, D.J., S.R. Fluss, and F.R. Maxfield, *Acidification of endocytic vesicles by an ATP-dependent proton pump*. *The Journal of cell biology*, 1983. **97**(3): p. 929-934.
106. Maxfield, F.R. and D.J. Yamashiro, *Endosome acidification and the pathways of receptor-mediated endocytosis*, in *Immunobiology of Proteins and Peptides IV*. 1987, Springer. p. 189-198.
107. Sonawane, N.D., F.C. Szoka, and A. Verkman, *Chloride accumulation and swelling in endosomes enhances DNA transfer by polyamine-DNA polyplexes*. *Journal of Biological Chemistry*, 2003. **278**(45): p. 44826-44831.
108. Dos, A., et al., *Acid– Base Interactions and Secondary Structures of Poly-l-Lysine Probed by 15N and 13C Solid State NMR and Ab initio Model Calculations*. *The Journal of Physical Chemistry B*, 2008. **112**(49): p. 15604-15615.
109. Akinc, A., et al., *Exploring polyethylenimine-mediated DNA transfection and the proton sponge hypothesis*. *The journal of gene medicine*, 2005. **7**(5): p. 657-663.
110. Erbacher, P., et al., *Putative role of chloroquine in gene transfer into a human hepatoma cell line by DNA/lactosylated polylysine complexes*. *Experimental cell research*, 1996. **225**(1): p. 186-194.
111. Khalil, I.A., et al., *Uptake pathways and subsequent intracellular trafficking in nonviral gene delivery*. *Pharmacological reviews*, 2006. **58**(1): p. 32-45.

112. Cotten, M., et al., *Transferrin-polycation-mediated introduction of DNA into human leukemic cells: stimulation by agents that affect the survival of transfected DNA or modulate transferrin receptor levels*. Proceedings of the National Academy of Sciences, 1990. **87**(11): p. 4033-4037.
113. Legendre, J.-Y. and F.C. Szoka Jr, *Delivery of plasmid DNA into mammalian cell lines using pH-sensitive liposomes: comparison with cationic liposomes*. Pharmaceutical research, 1992. **9**(10): p. 1235-1242.
114. Haensler, J. and F.C. Szoka Jr, *Polyamidoamine cascade polymers mediate efficient transfection of cells in culture*. Bioconjugate chemistry, 1993. **4**(5): p. 372-379.
115. Midoux, P., et al., *Chemical vectors for gene delivery: a current review on polymers, peptides and lipids containing histidine or imidazole as nucleic acids carriers*. British journal of pharmacology, 2009. **157**(2): p. 166-178.
116. Pichon, C., C. Gonçalves, and P. Midoux, *Histidine-rich peptides and polymers for nucleic acids delivery*. Advanced drug delivery reviews, 2001. **53**(1): p. 75-94.
117. Mann, A., et al., *Structural rearrangements and chemical modifications in known cell penetrating peptide strongly enhance DNA delivery efficiency*. Journal of Controlled Release, 2012. **157**(2): p. 260-271.
118. Wagner, E., et al., *Influenza virus hemagglutinin HA-2 N-terminal fusogenic peptides augment gene transfer by transferrin-polylysine-DNA complexes: toward a synthetic virus-like gene-transfer vehicle*. Proceedings of the National Academy of Sciences, 1992. **89**(17): p. 7934-7938.
119. Suh, J., D. Wirtz, and J. Hanes, *Efficient active transport of gene nanocarriers to the cell nucleus*. Proceedings of the National Academy of Sciences, 2003. **100**(7): p. 3878-3882.
120. Itaka, K., et al., *In situ single cell observation by fluorescence resonance energy transfer reveals fast intra-cytoplasmic delivery and easy release of plasmid DNA complexed with linear polyethylenimine*. The Journal of Gene Medicine, 2004. **6**(1): p. 76-84.
121. Kim, S., et al., *Engineered polymers for advanced drug delivery*. European Journal of Pharmaceutics and Biopharmaceutics, 2009. **71**(3): p. 420-430.
122. Schmaljohann, D., *Thermo- and pH-responsive polymers in drug delivery*. Advanced drug delivery reviews, 2006. **58**(15): p. 1655-1670.
123. Ganta, S., et al., *A review of stimuli-responsive nanocarriers for drug and gene delivery*. Journal of Controlled Release, 2008. **126**(3): p. 187-204.
124. Lin, C. and J.F. Engbersen, *The role of the disulfide group in disulfide-based polymeric gene carriers*. Expert Opinion on Drug Delivery, 2009. **6**(4): p. 421-39.
125. Soundara Manickam, D. and D. Oupický, *Polyplex gene delivery modulated by redox potential gradients*. Journal of drug targeting, 2006. **14**(8): p. 519-526.
126. Lee, Y., et al., *Visualization of the Degradation of a Disulfide Polymer, Linear Poly(ethylenimine sulfide), for Gene Delivery*. Bioconjugate Chemistry, 2006. **18**(1): p. 13-18.
127. Blacklock, J., et al., *Gene delivery in vitro and in vivo from bioreducible multilayered polyelectrolyte films of plasmid DNA*. Biomaterials, 2009. **30**(5): p. 939-950.
128. Salcher, E.E., et al., *Sequence-defined four-arm oligo (ethanamino) amides for pDNA and siRNA delivery: Impact of building blocks on efficacy*. Journal of Controlled Release, 2012. **164**(3): p. 380-386.
129. Chen, J., C. Wu, and D. Oupický, *Bioreducible hyperbranched poly (amido amine) s for gene delivery*. Biomacromolecules, 2009. **10**(10): p. 2921-2927.
130. Lin, S., et al., *An Acid-Labile Block Copolymer of PDMAEMA and PEG as Potential Carrier for Intelligent Gene Delivery Systems*. Biomacromolecules, 2007. **9**(1): p. 109-115.
131. Panté, N. and M. Kann, *Nuclear pore complex is able to transport macromolecules with diameters of ~ 39 nm*. Molecular biology of the cell, 2002. **13**(2): p. 425-434.
132. Brunner, S., et al., *Cell cycle dependence of gene transfer by lipoplex, polyplex and recombinant adenovirus*. Gene therapy, 2000. **7**(5): p. 401-407.
133. Grosse, S., et al., *Which mechanism for nuclear import of plasmid DNA complexed with polyethylenimine derivatives? The journal of gene medicine, 2006. 8(7): p. 845-851.*

134. Ludtke, J.J., M.G. Sebestyén, and J.A. Wolff, *The effect of cell division on the cellular dynamics of microinjected DNA and dextran*. *Molecular Therapy*, 2002. **5**(5): p. 579-588.
135. Neu, M., D. Fischer, and T. Kissel, *Recent advances in rational gene transfer vector design based on poly (ethylene imine) and its derivatives*. *The journal of gene medicine*, 2005. **7**(8): p. 992-1009.
136. Blagbrough, I.S., A.A. Metwally, and A.J. Geall, *Measurement of Polyamine pK a Values*, in *Polyamines*. 2011, Springer. p. 493-503.
137. Bencini, A., et al., *Proton coordination by polyamine compounds in aqueous solution*. *Coordination chemistry reviews*, 1999. **188**(1): p. 97-156.
138. Bastardo, L., et al., *Deuterium isotope effects on the interaction between hyperbranched polyethylene imine and an anionic surfactant*. *The Journal of Physical Chemistry B*, 2005. **109**(33): p. 16196-16202.
139. Von Zelewsky, A., L. Barbosa, and C. Schläpfer, *Poly (ethylenimines) as Brønsted bases and as ligands for metal ions*. *Coordination chemistry reviews*, 1993. **123**(1): p. 229-246.
140. Koper, G.J., et al., *Synthesis and protonation behavior of comblike poly (ethyleneimine)*. *Macromolecules*, 2003. **36**(7): p. 2500-2507.
141. Koper, G.J.M. and M. Borkovec, *Proton binding by linear, branched, and hyperbranched polyelectrolytes*. *Polymer*, 2010. **51**(24): p. 5649-5662.
142. Ziebarth, J.D. and Y. Wang, *Understanding the protonation behavior of linear polyethylenimine in solutions through Monte Carlo simulations*. *Biomacromolecules*, 2009. **11**(1): p. 29-38.
143. Borkovec, M., J. Daicic, and G.J. Koper, *On the difference in ionization properties between planar interfaces and linear polyelectrolytes*. *Proceedings of the National Academy of Sciences*, 1997. **94**(8): p. 3499-3503.
144. Borkovec, M., J. Daicic, and G.J.M. Koper, *Ionization properties of interfaces and linear polyelectrolytes: a discrete charge Ising model*. *Physica A: Statistical Mechanics and its Applications*, 2001. **298**(1-2): p. 1-23.
145. Blagbrough, I., A. Metwally, and A. Geall, *Measurement of Polyamine pK a Values*, in *Polyamines*, A.E. Pegg and J.R.A. Casero, Editors. 2011, Humana Press. p. 493-503.
146. Smits, R.G., G.J.M. Koper, and M. Mandel, *The influence of nearest- and next-nearest-neighbor interactions on the potentiometric titration of linear poly(ethylenimine)*. *The Journal of Physical Chemistry*, 1993. **97**(21): p. 5745-5751.
147. Borkovec, M. and G.J. Koper, *Proton binding characteristics of branched polyelectrolytes*. *Macromolecules*, 1997. **30**(7): p. 2151-2158.
148. Kobayashi, S., et al., *Chelating properties of linear and branched poly(ethylenimines)*. *Macromolecules*, 1987. **20**(7): p. 1496-1500.
149. Meier, U. and C.W. Schläpfer, *Interaction between Cl⁻ and linear and branched polyethylenimine in aqueous solution studied by ³⁵Cl- and ³⁷Cl-NMR*. *Berichte der Bunsengesellschaft für physikalische Chemie*, 1998. **102**(8): p. 1011-1018.
150. Suh, J., H.J. Paik, and B.K. Hwang, *Ionization of Poly(ethylenimine) and Poly(allylamine) at Various pH's*. *Bioorganic Chemistry*, 1994. **22**(3): p. 318-327.
151. Nagaya, J., et al., *Relationship between protonation and ion condensation for branched poly (ethylenimine)*. *Biophysical chemistry*, 1996. **60**(1): p. 45-51.
152. Choosakoonkriang, S., et al., *Biophysical characterization of PEI/DNA complexes*. *Journal of Pharmaceutical Sciences*, 2003. **92**(8): p. 1710-1722.
153. von Harpe, A., et al., *Characterization of commercially available and synthesized polyethylenimines for gene delivery*. *Journal of Controlled Release*, 2000. **69**(2): p. 309-322.
154. Hague, D.N. and A.D. Moreton, *Protonation sequence of linear aliphatic polyamines by ¹³C NMR spectroscopy*. *J. Chem. Soc., Perkin Trans. 2*, 1994(2): p. 265-270.
155. Fischer, D., et al., *In vitro cytotoxicity testing of polycations: influence of polymer structure on cell viability and hemolysis*. *Biomaterials*, 2003. **24**(7): p. 1121-1131.
156. Fischer, D., et al., *A Novel Non-Viral Vector for DNA Delivery Based on Low Molecular Weight, Branched Polyethylenimine: Effect of Molecular Weight on Transfection Efficiency and Cytotoxicity*. *Pharmaceutical Research*, 1999. **16**(8): p. 1273-1279.

157. Hong, S., et al., *Interaction of Polycationic Polymers with Supported Lipid Bilayers and Cells: Nanoscale Hole Formation and Enhanced Membrane Permeability*. *Bioconjugate Chemistry*, 2006. **17**(3): p. 728-734.
158. Kwok, A. and S.L. Hart, *Comparative structural and functional studies of nanoparticle formulations for DNA and siRNA delivery*. *Nanomedicine: Nanotechnology, Biology and Medicine*, 2011. **7**(2): p. 210-219.
159. Wightman, L., et al., *Different behavior of branched and linear polyethylenimine for gene delivery in vitro and in vivo*. *The Journal of Gene Medicine*, 2001. **3**(4): p. 362-372.
160. Zintchenko, A., et al., *Simple modifications of branched PEI lead to highly efficient siRNA carriers with low toxicity*. *Bioconjugate chemistry*, 2008. **19**(7): p. 1448-1455.
161. Tang, M. and F. Szoka, *The influence of polymer structure on the interactions of cationic polymers with DNA and morphology of the resulting complexes*. *Gene therapy*, 1997. **4**(8): p. 823-832.
162. Kunath, K., et al., *Low-molecular-weight polyethylenimine as a non-viral vector for DNA delivery: comparison of physicochemical properties, transfection efficiency and in vivo distribution with high-molecular-weight polyethylenimine*. *Journal of Controlled Release*, 2003. **89**(1): p. 113-125.
163. Petersen, H., et al., *Polyethylenimine-graft-poly (ethylene glycol) copolymers: influence of copolymer block structure on DNA complexation and biological activities as gene delivery system*. *Bioconjugate chemistry*, 2002. **13**(4): p. 845-854.
164. Clamme, J.P., J. Azoulay, and Y. Mély, *Monitoring of the formation and dissociation of polyethylenimine/DNA complexes by two photon fluorescence correlation spectroscopy*. *Biophysical journal*, 2003. **84**(3): p. 1960-1968.
165. Boeckle, S., et al., *Purification of polyethylenimine polyplexes highlights the role of free polycations in gene transfer*. *The Journal of Gene Medicine*, 2004. **6**(10): p. 1102-1111.
166. Fahrmeir, J., et al., *Electrophoretic purification of tumor-targeted polyethylenimine-based polyplexes reduces toxic side effects in vivo*. *Journal of Controlled Release*, 2007. **122**(3): p. 236-245.
167. Dai, Z., et al., *Elucidating the interplay between DNA-condensing and free polycations in gene transfection through a mechanistic study of linear and branched PEI*. *Biomaterials*, 2011. **32**(33): p. 8626-8634.
168. Yue, Y., et al., *Revisit complexation between DNA and polyethylenimine—effect of uncomplexed chains free in the solution mixture on gene transfection*. *Journal of Controlled Release*, 2011. **155**(1): p. 67-76.
169. Petersen, H., et al., *Synthesis, Characterization, and Biocompatibility of Polyethylenimine-graft-poly (ethylene glycol) Block Copolymers*. *Macromolecules*, 2002. **35**(18): p. 6867-6874.
170. Kircheis, R., et al., *Polycation-based DNA complexes for tumor-targeted gene delivery in vivo*. *The journal of gene medicine*, 1999. **1**(2): p. 111-120.
171. Erbacher, P., et al., *Transfection and physical properties of various saccharide, poly (ethylene glycol), and antibody-derivatized polyethylenimines (PEI)*. *The Journal of Gene Medicine*, 1999. **1**(3): p. 210-222.
172. Kurs, M., et al., *Novel Shielded Transferrin–Polyethylene Glycol–Polyethylenimine/DNA Complexes for Systemic Tumor-Targeted Gene Transfer*. *Bioconjugate Chemistry*, 2002. **14**(1): p. 222-231.
173. Ogris, M., et al., *Tumor-targeted gene therapy: strategies for the preparation of ligand–polyethylene glycol–polyethylenimine/DNA complexes*. *Journal of Controlled Release*, 2003. **91**(1–2): p. 173-181.
174. Jere, D., et al., *Degradable polyethylenimines as DNA and small interfering RNA carriers*. 2009.
175. Cho, C.-S., *Design and Development of Degradable Polyethylenimines for Delivery of DNA and Small Interfering RNA: An Updated Review*. *ISRN Materials Science*, 2012. **2012**: p. 24.

176. Deng, R., et al., *Revisit the complexation of PEI and DNA—How to make low cytotoxic and highly efficient PEI gene transfection non-viral vectors with a controllable chain length and structure?* Journal of Controlled Release, 2009. **140**(1): p. 40-46.
177. Dehshahri, A., et al., *Gene transfer efficiency of high primary amine content, hydrophobic, alkyl-oligoamine derivatives of polyethylenimine.* Biomaterials, 2009. **30**(25): p. 4187-4194.
178. Thomas, M. and A.M. Klibanov, *Enhancing polyethylenimine's delivery of plasmid DNA into mammalian cells.* Proceedings of the National Academy of Sciences, 2002. **99**(23): p. 14640-14645.
179. Crichton, R., *Solution Chemistry of Iron in Biological Media*, in *Inorganic Biochemistry of Iron Metabolism*. 2002, John Wiley & Sons, Ltd. p. 1-15.
180. Jolivet, J.P., C. Chaneac, and E. Tronc, *Iron oxide chemistry. From molecular clusters to extended solid networks.* Chemical Communications, 2004(5): p. 481-487.
181. Das, S., M.J. Hendry, and J. Essilfie-Dughan, *Transformation of Two-Line Ferrihydrite to Goethite and Hematite as a Function of pH and Temperature.* Environmental Science & Technology, 2011. **45**(1): p. 268-275.
182. Stefánsson, A., *Iron(III) Hydrolysis and Solubility at 25 °C.* Environmental Science & Technology, 2007. **41**(17): p. 6117-6123.
183. Flynn, C.M., *Hydrolysis of inorganic iron(III) salts.* Chemical Reviews, 1984. **84**(1): p. 31-41.
184. Das, S., M.J. Hendry, and J. Essilfie-Dughan, *Transformation of Two-Line Ferrihydrite to Goethite and Hematite as a Function of pH and Temperature.* Environmental Science & Technology, 2010. **45**(1): p. 268-275.
185. Carmona, F., et al., *Ferritin iron uptake and release in the presence of metals and metalloproteins: Chemical implications in the brain.* Coordination chemistry reviews, 2013. **257**(19–20): p. 2752-2764.
186. Ponka, P., C. Beaumont, and D.R. Richardson. *Function and regulation of transferrin and ferritin.* in *Seminars in hematology*. 1998.
187. Aruoma, O., et al., *The mechanism of initiation of lipid peroxidation. Evidence against a requirement for an iron (II)-iron (III) complex.* Biochemical Journal, 1989. **258**: p. 617-620.
188. Barnham, K.J., C.L. Masters, and A.I. Bush, *Neurodegenerative diseases and oxidative stress.* Nature Reviews Drug Discovery, 2004. **3**(3): p. 205-214.
189. Tam, T.F., et al., *Iron chelator research: Past, present, and future.* Current Medicinal Chemistry, 2003. **10**(12): p. 983-995.
190. Kalinowski, D.S. and D.R. Richardson, *The evolution of iron chelators for the treatment of iron overload disease and cancer.* Pharmacological Reviews, 2005. **57**(4): p. 547-583.
191. Foy, S.P. and V. Labhasetwar, *Oh the irony: Iron as a cancer cause or cure?* Biomaterials, 2011. **32**(35): p. 9155-9158.
192. Kiessling, M.K., et al., *Inhibition of Constitutively Activated Nuclear Factor- κ B Induces Reactive Oxygen Species- and Iron-Dependent Cell Death in Cutaneous T-Cell Lymphoma.* Cancer Research, 2009. **69**(6): p. 2365-2374.
193. Brigger, I., C. Dubernet, and P. Couvreur, *Nanoparticles in cancer therapy and diagnosis.* Advanced Drug Delivery Reviews, 2012. **64**(0): p. 24-36.
194. *Superparamagnetic Agents in Magnetic Resonance Imaging: Physicochemical Characteristics and Clinical Applications A Review.* Journal of Drug Targeting, 1998. **6**(3): p. 167-174.
195. Mahmoudi, M., et al., *Superparamagnetic iron oxide nanoparticles (SPIONs): Development, surface modification and applications in chemotherapy.* Advanced Drug Delivery Reviews, 2011. **63**(1–2): p. 24-46.
196. Sun, S.-L., et al., *Hybrid Polyethylenimine and Polyacrylic Acid-Bound Iron Oxide as a Magnetoplex for Gene Delivery.* Langmuir, 2012. **28**(7): p. 3542-3552.
197. Arsianti, M., et al., *Polyethylenimine Based Magnetic Iron-Oxide Vector: The Effect of Vector Component Assembly on Cellular Entry Mechanism, Intracellular Localization, and Cellular Viability.* Biomacromolecules, 2010. **11**(9): p. 2521-2531.

198. Mailänder, V., et al., *Carboxylated superparamagnetic iron oxide particles label cells intracellularly without transfection agents*. *Molecular imaging and biology*, 2008. **10**(3): p. 138-146.
199. Mahmoudi, M., et al., *Cell toxicity of superparamagnetic iron oxide nanoparticles*. *Journal of colloid and interface science*, 2009. **336**(2): p. 510-518.
200. Bulte, J.W., *In vivo MRI cell tracking: clinical studies*. *American Journal of Roentgenology*, 2009. **193**(2): p. 314-325.
201. Huang, D.-M., et al., *The promotion of human mesenchymal stem cell proliferation by superparamagnetic iron oxide nanoparticles*. *Biomaterials*, 2009. **30**(22): p. 3645-3651.
202. Mahmoudi, M., A. Simchi, and M. Imani, *Cytotoxicity of uncoated and polyvinyl alcohol coated superparamagnetic iron oxide nanoparticles*. *The Journal of Physical Chemistry C*, 2009. **113**(22): p. 9573-9580.
203. Metropolis, N., et al., *Equation of state calculations by fast computing machines*. *The Journal of Chemical Physics*, 1953. **21**: p. 1087.
204. Allen, M.P. and D.J. Tildesley, *Computer simulation of liquids*. 1989: Oxford university press.
205. Christos, G.A. and S.L. Carnie, *Computer simulation of semi-dilute polyelectrolyte solutions*. *Chemical Physics Letters*, 1990. **172**(3): p. 249-253.
206. Stevens, M.J. and K. Kremer, *Structure of salt-free linear polyelectrolytes*. *Physical Review Letters*, 1993. **71**(14): p. 2228.
207. Stevens, M.J. and K. Kremer, *The nature of flexible linear polyelectrolytes in salt free solution: A molecular dynamics study*. *The Journal of Chemical Physics*, 1995. **103**: p. 1669.
208. Dias, R. and B. Lindman, *DNA interactions with polymers and surfactants*. 2008: Wiley.
209. Landau, D.P. and K. Binder, *A Guide to Monte Carlo Simulations in Statistical Physics*. 3rd ed. 2009: Cambridge University Press.
210. Brender, C. and M. Lax, *A Monte Carlo off lattice method: The slithering snake in a continuum* *The Journal of Chemical Physics*, 1983. **79**: p. 2423.
211. Linse, P., *Simulation of charged colloids in solution*, in *Advanced Computer Simulation Approaches For Soft Matter Sciences II*. 2005, Springer. p. 111-162.
212. Kelly, S.M., T.J. Jess, and N.C. Price, *How to study proteins by circular dichroism*. *Biochimica et Biophysica Acta (BBA) - Proteins & Proteomics*, 2005. **1751**(2): p. 119-139.
213. *Zetasizer Nano ZS* Available from: http://www.malvern.com/labeng/technology/dynamic_light_scattering/dynamic_light_scattering.htm, accessed on 28/04/2013.
214. *Zeta Potential: A Complete Course in 5 Minutes*. Available from: <http://www.zeta-meter.com/5min.pdf> accessed on 26-09-2013.
215. White, H., et al., *GelStar® nucleic acid gel stain: high sensitivity detection in gels*. *Biotechniques*, 1999. **26**(5): p. 984-988.
216. *Introduction to fluorescence microscopy-Olympus*. Available from: <http://www.olympusmicro.com/primer/techniques/fluorescence/fluorhome.html> accessed on 26/09/2013.
217. Tarnowski, B.I., F.G. Spinale, and J.H. Nicholson, *DAPI as a Useful Stain for Nuclear Quantitation*. *Biotechnic & Histochemistry*, 1991. **66**(6): p. 296-302.
218. Kapuściński, J. and K. Yanagi, *Selective staining by 4', 6-diamidine-2-phenylindole of nanogram quantities of DNA in the presence of RNA on gels*. *Nucleic acids research*, 1979. **6**(11): p. 3535-3542.
219. Mosmann, T., *Rapid colorimetric assay for cellular growth and survival: Application to proliferation and cytotoxicity assays*. *Journal of Immunological Methods*, 1983. **65**(1-2): p. 55-63.
220. Sebaugh, J.L., *Guidelines for accurate EC50/IC50 estimation*. *Pharmaceutical Statistics*, 2011. **10**(2): p. 128-134.

221. Khinkis, L.A., et al., *Optimal design for estimating parameters of the 4-parameter hill model*. Nonlinearity in Biology, Toxicology, and Medicine, 2003. **1**(3): p. 363-377.
222. Parhamifar, L., H. Andersen, and S.M. Moghimi, *Lactate Dehydrogenase Assay for Assessment of Polycation Cytotoxicity*, in *Nanotechnology for Nucleic Acid Delivery*, M. Ogris and D. Oupicky, Editors. 2013, Humana Press. p. 13-22.
223. Kangas, L., M. Grönroos, and A. Nieminen, *Bioluminescence of cellular ATP: a new method for evaluating cytotoxic agents in vitro*. Medical biology, 1984. **62**(6): p. 338.
224. Fraga, H., *Firefly luminescence: A historical perspective and recent developments*. Photochemical & Photobiological Sciences, 2008. **7**(2): p. 146-158.
225. *CellTiter-Glo® Luminescent Cell Viability Assay*. Available from: <https://www.promega.com/~media/Files/Resources/Protocols/Technical%20Bulletins/0/CellTiter%20Glo%20Luminescent%20Cell%20Viability%20Assay%20Protocol.pdf> accessed on 30/09/2013.
226. Petty, R.D., et al., *Comparison of MTT and ATP-based assays for the measurement of viable cell number*. Journal of bioluminescence and chemiluminescence, 1995. **10**(1): p. 29-34.
227. Weyermann, J., D. Lochmann, and A. Zimmer, *A practical note on the use of cytotoxicity assays*. International journal of pharmaceutics, 2005. **288**(2): p. 369-376.
228. *Guidance for Industry Nonclinical Studies for the Safety Evaluation of Pharmaceutical Excipients*, U.F.a.D. Administration, Editor. 2005.
229. Zauner, W., N.A. Farrow, and A.M.R. Haines, *In vitro uptake of polystyrene microspheres: effect of particle size, cell line and cell density*. Journal of Controlled Release, 2001. **71**(1): p. 39-51.
230. Reibetanz, U., et al., *Flow Cytometry of HEK 293T Cells Interacting with Polyelectrolyte Multilayer Capsules Containing Fluorescein-Labeled Poly(acrylic acid) as a pH Sensor*. Biomacromolecules, 2007. **8**(6): p. 1927-1933.
231. Heller, D., *A Review and Applications of Flow Cytometry*. 2004.
232. Plank, C., et al., *Gene transfer into hepatocytes using asialoglycoprotein receptor mediated endocytosis of DNA complexed with an artificial tetra-antennary galactose ligand*. Bioconjugate chemistry, 1992. **3**(6): p. 533-539.
233. Shovskiy, A., et al., *Formation and Stability of Water-Soluble, Molecular Polyelectrolyte Complexes: Effects of Charge Density, Mixing Ratio, and Polyelectrolyte Concentration*. Langmuir, 2009. **25**(11): p. 6113-6121.
234. Strand, S.P., et al., *Influence of Chitosan Structure on the Formation and Stability of DNA-Chitosan Polyelectrolyte Complexes*. Biomacromolecules, 2005. **6**(6): p. 3357-3366.
235. Ma, P.L., et al., *New Insights into chitosan-DNA interactions using isothermal titration microcalorimetry*. Biomacromolecules, 2009. **10**(6): p. 1490-1499.
236. Rojas, O.J., et al., *Effect of Polyelectrolyte Charge Density on the Adsorption and Desorption Behavior on Mica*. Langmuir, 2002. **18**(5): p. 1604-1612.
237. Hayashi, Y., M. Ullner, and P. Linse, *A Monte Carlo study of solutions of oppositely charged polyelectrolytes*. The Journal of Chemical Physics, 2002. **116**(15): p. 6836-6845.
238. Dale, J.W. and M. von Schantz, *From Genes to Genomes: Concepts and Applications of DNA Technology*. 2nd ed. 2007, West Sussex: John Wiley & Sons.
239. Buck, R., et al., *Measurement of pH. Definition, standards, and procedures (IUPAC Recommendations 2002)*. Pure and applied chemistry, 2002. **74**(11): p. 2169-2200.
240. Crea, F., et al., *Thermodynamic study for the protonation of branched poly(ethylenimine) in NaCl (aq) and its dependence on ionic strength*. Journal of Chemical & Engineering Data, 2007. **52**(1): p. 279-285.
241. Braun, C.S., et al., *The structure of DNA within cationic lipid/DNA complexes*. Biophysical journal, 2003. **84**(2): p. 1114-1123.
242. Muntean, C.M., et al., *DNA structure at low pH values, in the presence of Mn²⁺ ions: a Raman study*. Journal of Raman Spectroscopy, 2005. **36**(11): p. 1047-1051.

243. Sukhanova, A., et al., *Human DNA topoisomerase I inhibitory activities of synthetic polyamines: relation to DNA aggregation*. *Bioorganic & Medicinal Chemistry*, 2001. **9**(5): p. 1255-1268.
244. Maurstad, G., S. Danielsen, and B.T. Stokke, *The Influence of Charge Density of Chitosan in the Compaction of the Polyanions DNA and Xanthan*. *Biomacromolecules*, 2007. **8**(4): p. 1124-1130.
245. Bronich, T.K., et al., *Recognition of DNA Topology in Reactions between Plasmid DNA and Cationic Copolymers*. *Journal of the American Chemical Society*, 2000. **122**(35): p. 8339-8343.
246. Cárdenas, M., et al., *DNA Compaction by cationic surfactant in solution and at polystyrene particle solution interfaces: a dynamic light scattering study*. *Physical Chemistry Chemical Physics*, 2004. **6**(7): p. 1603-1607.
247. Shovskiy, A.V., et al., *Formation and Stability of Soluble Stoichiometric Polyelectrolyte Complexes: Effects of Charge Density and Polyelectrolyte Concentration*. *Journal of Dispersion Science and Technology*, 2009. **30**(6): p. 980-988.
248. Hillaireau, H. and P. Couvreur, *Nanocarriers' entry into the cell: relevance to drug delivery*. *Cellular and Molecular Life Sciences*, 2009. **66**(17): p. 2873-2896.
249. Viola, J.R., et al., *Non-viral nanovectors for gene delivery: factors that govern successful therapeutics*. *Expert opinion on drug delivery*, 2010. **7**(6): p. 721-735.
250. Stellwagen, N.C., *Agarose gel pore radii are not dependent on the casting buffer*. *Electrophoresis*, 1992. **13**(1): p. 601-603.
251. Marcus, Y., *Thermodynamics of solvation of ions. Part 5.—Gibbs free energy of hydration at 298.15 K*. *Journal of the Chemical Society, Faraday Transactions*, 1991. **87**(18): p. 2995-2999.
252. Linse, P., *Molsim*. 2004: Lund University, Sweden.
253. Brender, C. and M. Lax, *A Monte Carlo off-lattice method: The slithering snake in a continuum*. *The Journal of Chemical Physics*, 1983. **79**: p. 2423.
254. Rivas, B. and K. Geckeler, *Synthesis and metal complexation of poly(ethyleneimine) and derivatives*, in *Polymer Synthesis Oxidation Processes*. 1992, Springer Berlin Heidelberg. p. 171-188.
255. Dias, R.S., P. Linse, and A.A.C.C. Pais, *Stepwise disproportionation in polyelectrolyte complexes*. *Journal of Computational Chemistry*, 2011. **32**(12): p. 2697-2707.
256. von Zelewsky, A., L. Barbosa, and C.W. Schlöpfer, *Poly(ethylenimines) as Brønsted bases and as ligands for metal ions*. *Coordination Chemistry Reviews*, 1993. **123**(1-2): p. 229-246.
257. Laatikainen, M., K. Sirola, and E. Paatero, *Binding of transition metals by soluble and silica-bound branched poly(ethyleneimine): Part I: Competitive binding equilibria*. *Colloids and Surfaces A: Physicochemical and Engineering Aspects*, 2007. **296**(1): p. 191-205.
258. Rivas, B.L., G.V. Seguel, and K.E. Geckeler, *Synthesis and properties of transition metal complexes with branched poly(ethyleneimine)*. *Die Angewandte Makromolekulare Chemie*, 1996. **238**(1): p. 1-10.
259. Angelescu, D.G. and P. Linse, *Monte Carlo simulation of the mean force between two like-charged macroions with simple 1: 3 salt added*. *Langmuir*, 2003. **19**(23): p. 9661-9668.
260. Godbey, W.T., K.K. Wu, and A.G. Mikos, *Size matters: Molecular weight affects the efficiency of poly(ethyleneimine) as a gene delivery vehicle*. *Journal of Biomedical Materials Research*, 1999. **45**(3): p. 268-275.
261. Kunath, K., et al., *The structure of PEG-modified poly(ethylene imines) influences biodistribution and pharmacokinetics of their complexes with NF- κ B decoy in mice*. *Pharmaceutical research*, 2002. **19**(6): p. 810-817.
262. Moghimi, S.M., et al., *A two-stage poly(ethyleneimine)-mediated cytotoxicity: implications for gene transfer/therapy*. *Molecular Therapy*, 2005. **11**(6): p. 990-995.
263. Leroueil, P.R., et al., *Wide Varieties of Cationic Nanoparticles Induce Defects in Supported Lipid Bilayers*. *Nano Letters*, 2008. **8**(2): p. 420-424.

264. Kircheis, R., L. Wightman, and E. Wagner, *Design and gene delivery activity of modified polyethylenimines*. *Advanced drug delivery reviews*, 2001. **53**(3): p. 341-358.
265. Morán, M.C., et al., *Counter-ion effect on surfactant-DNA gel particles as controlled DNA delivery systems*. *Soft Matter*, 2012. **8**(11): p. 3200-3211.
266. Morán, M.C., et al., *DNA gel particles: An overview*. *Advances in Colloid and Interface Science*. pii: **S0001-8686**(13): p. 00101-2.
267. Rao, S.B. and C.P. Sharma, *Use of chitosan as a biomaterial: studies on its safety and hemostatic potential*. *Journal of biomedical materials research*, 1997. **34**(1): p. 21-28.
268. Venkatesan, P., et al., *The potential of celecoxib-loaded hydroxyapatite-chitosan nanocomposite for the treatment of colon cancer*. *Biomaterials*, 2011. **32**(15): p. 3794-3806.
269. Zhao, Z.-X., et al., *Self-assembly nanomicelles based on cationic mPEG-PLA-*b*-Polyarginine (R_{15}) triblock copolymer for siRNA delivery*. *Biomaterials*, 2012. **33**(28): p. 6793-6807.
270. Colomer, A., et al., *pH-Sensitive Surfactants from Lysine: Assessment of Their Cytotoxicity and Environmental Behavior*. *Langmuir*, 2012. **28**(14): p. 5900-5912.
271. Gebhart, C.L. and A.V. Kabanov, *Evaluation of polyplexes as gene transfer agents*. *Journal of Controlled Release*, 2001. **73**(2): p. 401-416.
272. Russ, V., et al., *Oligoethylenimine-grafted polypropylenimine dendrimers as degradable and biocompatible synthetic vectors for gene delivery*. *Journal of Controlled Release*, 2008. **132**(2): p. 131-140.
273. Kostura, L., et al., *Feridex labeling of mesenchymal stem cells inhibits chondrogenesis but not adipogenesis or osteogenesis*. *NMR in Biomedicine*, 2004. **17**(7): p. 513-517.
274. Szalay, B., et al., *Potential toxic effects of iron oxide nanoparticles in in vivo and in vitro experiments*. *Journal of Applied Toxicology*, 2012. **32**(6): p. 446-453.
275. Godbey, W., K.K. Wu, and A.G. Mikos, *Poly(ethylenimine) and its role in gene delivery*. *Journal of Controlled Release*, 1999. **60**(2): p. 149-160.
276. Bieber, T. and H.-P. Elsässer, *Preparation of a low molecular weight polyethylenimine for efficient cell transfection*. *Biotechniques*, 2001. **30**(1): p. 74-7, 80-1.
277. Parhamifar, L., et al., *Polycation cytotoxicity: a delicate matter for nucleic acid therapy-focus on polyethylenimine*. *Soft Matter*, 2010. **6**(17): p. 4001-4009.
278. Burke, R.S. and S.H. Pun, *Extracellular Barriers to in Vivo PEI and PEGylated PEI Polyplex-Mediated Gene Delivery to the Liver*. *Bioconjugate chemistry*, 2008. **19**(3): p. 693-704.
279. Buyens, K., et al., *Monitoring the disassembly of siRNA polyplexes in serum is crucial for predicting their biological efficacy*. *Journal of Controlled Release*, 2010. **141**(1): p. 38-41.
280. Yue, Y., et al., *Revisit complexation between DNA and polyethylenimine — Effect of uncomplexed chains free in the solution mixture on gene transfection*. *Journal of Controlled Release*, 2011. **155**(1): p. 67-76.
281. Guibal, E., *Interactions of metal ions with chitosan-based sorbents: a review*. *Sep Purif Technol*, 2004. **38**(1): p. 43-74.
282. Kislenco, V.N. and L.P. Oliynyk, *Complex formation of polyethyleneimine with copper(II), nickel(II), and cobalt(II) ions*. *Journal of Polymer Science Part A: Polymer Chemistry*, 2002. **40**(7): p. 914-922.
283. Takagishi, T., et al., *Binding of metal ions by polyethylenimine and its derivatives*. *J Polym Sci Pol Chem* 1985. **23**(8): p. 2109-2116.
284. Fujimori, K., *Complexation of poly(ethyleneimine) with copper(II) and nickel(II) ions in 0.5 M KNO₃ solution*. *Journal of Polymer Science Part A: Polymer Chemistry*, 1985. **23**(1): p. 169-174.
285. Thiele, V.H. and K.-H. Gronau, *Kupfer- und Nickelkomplexe von Polyäthylenimin*. *Makromol Chem*, 1963. **59**(1): p. 207-221.
286. Jorge, A.F., et al., *DNA Condensation by pH-Responsive Polycations*. *Biomacromolecules*, 2010. **11**(9): p. 2399-2406.
287. Baes, C.F. and R.E. Mesmer, *The Hydrolysis of Cations*. 1976, New York: Wiley.

288. Raymond, K.N. and C.J. Carrano, *Coordination chemistry and microbial iron transport*. Accounts of Chemical Research, 1979. **12**(5): p. 183-190.
289. Jeong, J.H., et al., *DNA transfection using linear poly(ethylenimine) prepared by controlled acid hydrolysis of poly(2-ethyl-2-oxazoline)*. Journal of Controlled Release, 2001. **73**(2-3): p. 391-399.
290. Kabanov, N.M., et al., *Study of the structure of a polyacrylic acid-polyethyleneimine-copper (II) ternary polymer-metal complex*. Polymer Science U.S.S.R., 1979. **21**(1): p. 230-240.
291. Ribeiro, A.C.F., et al., *Interactions of vanadates with carbohydrates in aqueous solutions*. Journal of Molecular Structure, 2004. **703**(1-3): p. 93-101.
292. Barthel, J., et al., *Calibration of conductance cells at various temperatures*. Journal of Solution Chemistry, 1980. **9**(3): p. 209-219.
293. Marcus, Y., *Thermodynamics of solvation of ions. Part 5.-Gibbs free energy of hydration at 298.15 K*. Journal of the Chemical Society, Faraday Transactions, 1991. **87**(18): p. 2995-2999.
294. Dot, K., *Thermometric studies on the Fe(III)—EDTA chelate*. Talanta, 1978. **25**(2): p. 97-101.
295. Gordon, H.L. and J.P. Valleau, *A partially clothed pivot algorithm for model polyelectrolyte solutions*. Molecular Simulation, 1995. **14**(6): p. 361-379.
296. Sarraguça, J.M.G., et al., *Structure of polyelectrolytes in 3 : 1 salt solutions*. Journal of Chemical Physics, 2003. **119**(23): p. 12621-12628.
297. Krishnapriya, K.R. and M. Kandaswamy, *A new chitosan biopolymer derivative as metal-complexing agent: synthesis, characterization, and metal(II) ion adsorption studies*. Carbohydrate Research, 2010. **345**(14): p. 2013-2022.
298. Pereira, R.F.P., et al., *What drives the precipitation of long-chain calcium carboxylates (soaps) in aqueous solution?* Phys Chem Chem Phys, 2012. **14**(20): p. 7517-7527.
299. Valente, A.J.M., et al., *Effect of Europium(III) Chloride on the Aggregation Behavior of Sodium Dodecyl Sulfate*. Langmuir, 2006. **22**(13): p. 5625-5629.
300. Pereira, R.F., A.J. Valente, and H.D. Burrows, *Thermodynamic analysis of the interaction between trivalent metal ions and sodium dodecyl sulfate: An electrical conductance study*. J Mol Liq, 2010. **156**(1): p. 109-114.
301. Rivas, B.L., G.V. Seguel, and K.E. Geckeler, *Synthesis and properties of transition metal complexes with branched poly(ethyleneimine)*. Angewandte Makromolekulare Chemie, 1996. **238**(1): p. 1-10.
302. Baba, Y., K. Masaaki, and Y. Kawano, *Synthesis of a chitosan derivative recognizing planar metal ion and its selective adsorption equilibria of copper(II) over iron(III)*. Reactive and Functional Polymers, 1998. **36**(2): p. 167-172.
303. Conwell, C.C., I.D. Vilfan, and N.V. Hud, *Controlling the size of nanoscale toroidal DNA condensates with static curvature and ionic strength*. Proceedings of the National Academy of Sciences of the United States of America, 2003. **100**(16): p. 9296-301.
304. Conwell, C.C. and N.V. Hud, *Evidence that both kinetic and thermodynamic factors govern DNA toroid dimensions: effects of magnesium(II) on DNA condensation by hexammine cobalt(III)*. Biochemistry, 2004. **43**(18): p. 5380-7.
305. Akinchina, A. and P. Linse, *Diblock polyampholytes grafted onto spherical particles: effect of stiffness, charge density, and grafting density*. Langmuir, 2007. **23**(3): p. 1465-72.
306. Shovskiy, A., et al., *Formation and Stability of Water-Soluble, Molecular Polyelectrolyte Complexes: Effects of Charge Density, Mixing Ratio, and Polyelectrolyte Concentration*. Langmuir, 2009. **25**(11): p. 6113-6121.
307. Dias, R.S., et al., *Modeling of DNA compaction by polycations*. The Journal of Chemical Physics, 2003. **119**(15): p. 8150-8157.
308. Jorge, A.F., R.S. Dias, and A.A.C.C. Pais, *Enhanced Condensation and Facilitated Release of DNA Using Mixed Cationic Agents: A Combined Experimental and Monte Carlo Study*. Biomacromolecules, 2012. **13**(10): p. 3151-3161.

309. Ouameur, A.A., et al., *A comparative study of Fe(II) and Fe(III) interactions with DNA duplex: Major and minor grooves bindings*. DNA Cell Biology, 2005. **24**(6): p. 394-401.
310. Netto, L.E.S., A.M.D. Ferreira, and O. Augusto, *Iron(III) binding in DNA solutions - Complex formation and catalytic activity in the oxidation of hydrazine derivatives*. Chemico-Biological Interactions, 1991. **79**(1): p. 1-14.
311. Jorge, A.F., et al., *Ternary complexes DNA-Polyethylenimine-Fe(III) with linear and branched polycations: Implications on condensation, size, charge and in vitro biocompatibility*. Soft Matter 2013. **9**(45): p. 10799-10810.
312. Yang, Z., et al., *Preparation and adsorption behavior for metal ions of cyclic polyamine derivative of chitosan*. Journal of Applied Polymer Science, 2006. **100**(4): p. 3018-3023.
313. Sarraguça, J.M.G. and A.A.C.C. Pais, *Simulation of polyelectrolyte solutions. The density of bound ions*. Chemical Physics Letters, 2004. **398**(1-3): p. 140-145.
314. Pathak, A., S. Patnaik, and K.C. Gupta, *Recent trends in non-viral vector-mediated gene delivery*. Biotechnology Journal, 2009. **4**(11): p. 1559-1572.
315. Plank, C., et al., *Gene transfer into hepatocytes using asialoglycoprotein receptor mediated endocytosis of DNA complexed with an artificial tetra-antennary galactose ligand*. Bioconjugate Chemistry, 1992. **3**(6): p. 533-539.
316. Brissault, B., et al., *Synthesis of Linear Polyethylenimine Derivatives for DNA Transfection*. Bioconjugate Chemistry, 2003. **14**(3): p. 581-587.
317. Good, N.E., et al., *Hydrogen Ion Buffers for Biological Research*. Biochemistry, 1966. **5**(2): p. 467-477.
318. Tang, M.X. and F.C. Szoka, *The influence of polymer structure on the interactions of cationic polymers with DNA and morphology of the resulting complexes*. Gene Therapy, 1997. **4**(8): p. 823-832.
319. Dautzenberg, H., *Polyelectrolyte Complex Formation in Highly Aggregating Systems. 1. Effect of Salt: Polyelectrolyte Complex Formation in the Presence of NaCl*. Macromolecules, 1997. **30**(25): p. 7810-7815.
320. Wagner, E., C. Culmsee, and S. Boeckle, *Targeting of polyplexes: toward synthetic virus vector systems*. Advances in genetics, 2005. **53**: p. 333-354.
321. McCarty, M.F., J. Barroso-Aranda, and F. Contreras, *Oxidative stress therapy for solid tumors – A proposal*. Medical Hypotheses, 2010. **74**(6): p. 1052-1054.
322. Brissault, B., et al., *Linear Topology Confers in Vivo Gene Transfer Activity to Polyethylenimines*. Bioconjugate Chemistry, 2006. **17**(3): p. 759-765.
323. Gao, C., et al., *Designable Coordination Bonding in Mesopores as a pH-Responsive Release System*. Chemistry of Materials, 2010. **22**(19): p. 5437-5444.
324. Sengupta, A.K. and Y. Zhu, *Metals sorption by chelating polymers: A unique role of ionic strength*. AIChE Journal, 1992. **38**(1): p. 153-157.
325. Zachariou, M. and M.T. Hearn, *Application of immobilized metal ion chelate complexes as pseudocation exchange adsorbents for protein separation*. Biochemistry, 1996. **35**(1): p. 202-211.